Contributions à la modélisation mathématique et numérique de problèmes issus de la biologie : applications aux Prions et à la maladie d'Alzheimer

Erwan Hingant

Université Claude bernard Lyon 1
Institut Camille Jordan
UMR 5208 CNRS-UCBL

Thèse de doctorat
N° d'ordre: 2012-135

Contributions à la modélisation mathématique et numérique de problèmes issus de la biologie

Applications aux Prions et à la maladie d'Alzheimer

THÈSE

présentée et soutenue publiquement le 17 septembre 2012

pour l'obtention du diplôme de

Doctorat de l'Université Claude Bernard Lyon 1

(Spécialité Mathématiques Appliquées)

par

Erwan Hingant

sous la direction de

Ionel S. Ciuperca, Jean-Pierre Liautard & Laurent Pujo-Menjouet

Devant le jury composé de:

Mostafa Adimy	Directeur de Recherches à l'INRIA	Examinateur
Ionel S. Ciuperca	Maître de Conférence à l'Université Lyon 1	Directeur de thèse
Pierre Degond	Professeur à l'Université Paul Sabatier	Rapporteur
Marie Doumic	Chargé de Recherches à l'INRIA	Examinatrice
Jean-Pierre Liautard	Directeur de Recherches INSERM	Directeur de thèse
Stéphane Mischler	Professeur à l'Université Paris-Dauphine	Rapporteur
Laurent Pujo-Menjouet	Maître de Conférence à l'Université Lyon 1	Directeur de thèse

---

Ecole Doctorale Informatique et Mathématiques - EDA 512

Résumé

L'objectif de cette thèse est d'étudier, sous divers aspects, le processus de formation d'amyloide à partir de la polymérisation de protéines. Ces phénomènes, aussi bien *in vitro* que *in vivo*, posent des questions de modélisation mathématique. Il s'agit ensuite de conduire une analyse des modèles obtenus.

Dans la première partie nous présentons des travaux effectués en collaboration avec une équipe de biologistes. Deux modèles sont introduits, basés sur la théorie en vigueur du phénomène Prions, que nous ajustons aux conditions expérimentales. Ces modèles nous permettent d'analyser les données obtenues à partir d'expériences conduites en laboratoire. Cependant celles-ci soulèvent certains phénomènes encore inexpliqués par la théorie actuelle. Nous proposons donc un autre modèle qui corrobore les données et donne une nouvelle approche de la formation d'amyloide dans le cas du Prion. Nous terminons cette partie par l'analyse mathématique de ce système composé d'une infinité d'équations différentielles. Ce dernier consiste en un couplage entre un système de type Becker-Döring et un système de polymérisation-fragmentation discrète.

La seconde partie s'attache à l'analyse d'un nouveau modèle pour la polymérisation de protéines dont la fragmentation est sujette aux variations du fluide environnant. L'idée est de décrire au plus près les conditions expérimentales mais aussi d'introduire de nouvelles quantités macroscopiques mesurables pour l'étude de la polymérisation. Le premier chapitre de cette partie présente une description stochastique du problème. On y établit les équations du mouvement des polymères et des monomères (de type Langevin) ainsi que le formalisme pour l'étude du problème limite en grand nombre. Le deuxième chapitre pose le cadre fonctionnel et l'existence de solutions pour l'équation de Fokker-Planck-Smoluchowski décrivant la densité de configuration des polymères, elle-même couplée à une équation de diffusion pour les monomères. Le dernier chapitre propose une méthode numérique pour traiter ce problème.

On s'intéresse dans la dernière partie à la modélisation de la maladie d'Alzheimer. On construit un modèle qui décrit d'une part la formation de plaque amyloide *in vivo*, et d'autre part les interactions entre les oligomères d'Aβet la protéine prion qui induiraient la perte de mémoire. On mène l'analyse mathématique de ce modèle dans un cas particulier puis dans un cas plus général où le taux de polymérisation est une loi de puissance.

Abstract

The aim of this thesis is to study, under several aspects, the formation of amyloids from proteins polymerization. The mathematical modelling of these phenomena in the case of *in vitro* or *in vivo* polymerisation remains questioned. We then propose here several models, which are also investigated from theoritical and numerical point of view.

In the first part we present works done in collaboration with biologists. We propose two models based on the current theory on Prion phenomena that are designed for specific experimental conditions. These models allow us to analyse the experimental data obtained in laboratory and raise phenomena that remain unexplained by the theory. Then, from these results and biophysical considerations, we introduce a model which corroborates with data and provides a new approach on the amyloid formation in the particular case of Prion. This part is ended by the mathematical analysis of the model consisting of an infinite set of differentials equations. The system analysed is a Becker-Döring system coupled to a discrete growth-fragmentation system.

The second part is dedicated to the analysis of a new model for polymerization of proteins with fragmentation subject to the surrounding variations of the fluid. Thus, we propose a model which is close to the experimental conditions and introduce new measurable macroscopic quantities to study the polymerization. The first introductory chapter states the stochastic description of the problem. We give the equations of motion for each polymers and monomers as well as a general formalism to study the limit in large number. Next, we give the mathematical framework and prove the existence of solutions to the Fokker-Planck-Smoluchowski equation for the configurational density of polymers coupled to the diffusion equation for monomers. The last chapter provides a numerical method adapted to this problem with numerical simulations

In the last part, we are interested in modelling Alzheimer's disease. We introduce a model that describes the formation of amyloids plaques in the brain and the interactions between Aβ-oligomers and Prion proteins which might be responsible of the memory impairment. We carry out the mathematical analysis of the model. Namely, for a constant polymerization rate, we provide existence and uniqueness together with stability of the equilibrium. Finally we study the existence in a more general and biological relevant case, that is when the polymerization depends on the size of the amyloid.

Contents

Liste des travaux

Articles publiés

I. S. Ciuperca, E. H., L. I. Palade and L. Pujo-Menjouet, Fragmentation and monomers lengthening of rod-like polymers, a relevant model for prion proliferation, *Discrete and Continuous Dynamical Systems - Series B*, vol. 17 (3), pp. 775–799, 2012. [Chapitre 4]

M. T. Alvarez-Martinez, P. Fontes, V. Zomosa-Signoret, J. D. Arnaud, E. H., L. Pujo-Menjouet and J. P. Liautard, Dynamics of polymerization shed light on the mechanisms that lead to multiple amyloid structures of the prion protein, *Biochimica et Biophysica Acta (BBA) - Proteins & Proteomics*, vol. 1814 (10), pp. 1305–1317, 2011. [Chapitre 1]

Articles soumis

A numerical scheme for rod-like polymers with fragmentation and monomers lengthening. [Chapitre 6]

Travaux en cours

A micellar on-pathway intermediate step explains the kinetics of prion amyloid formation, avec P. Fontes, T. Alvarez-Martinez, J. D. Arnaud, J. P. Liautard et L. Pujo-Menjouet. [Chapitre 2]

Configurational polymers with fragmentation and monomers lengthening: limit from individual-discrete to population-continuous, avec R. Yvinec. [Chapitre 5]

A Discrete polymerization-fragmentation system with cluster pathway. [Chapitre 3]

A mathematical model including the role of the prion protein into Alzheimer's disease, avec M. Helal [Chapitre 7]

Introduction générale

Dans ce premier chapitre, nous introduisons les éléments de biologie, de modélisation et de mathématiques qui motivent les travaux de cette thèse et en facilitent la lecture. Dans un premier temps, nous rappelons des notions de biologie cellulaire et de modélisation du prion et de la maladie d'Alzheimer. Ensuite, nous présentons les prototypes d'équations de polymérisation-fragmentation qui sont à la base de nos modèles ainsi que leur cadre analytique qui permet de les étudier. Enfin nous présentons les travaux sur les polymères dans un fluide, de l'approche individu-discret à l'équation continue sur la densité et une méthode de résolution numérique.

---

1 Introduction biologique

Nous commençons cette partie en rappelant quelques éléments de biologie cellulaire et notamment certaines notions sur le rôle, la production et la structure des protéines. Celles-ci jouant un rôle particulier dans les maladies à prion et celle d'Alzheimer, qui nous intéresseront dans la suite de ce travail. Il est donc primordial d'en comprendre le fonctionnement.

1.1 Les protéines

Le rôle des protéines.

Les protéines sont des composants essentiels à la vie cellulaire. Elles représentent, suivant les tissus considérés, entre 55 et 85% de la matière sèche de notre organisme, les protéines constituent une famille de macromolécules majeure du vivant. On se référera en particulier au livre de Robert & Vian [189] pour se familiariser avec la biologie cellulaire. Les mécanismes biologiques dans lesquels sont impliqués les protéines, tant au niveau intracellulaire qu'extra-cellulaire, sont d'une grande diversité comme on peut le lire dans l'introduction de McCammon [154].

Il existe des protéines dont le rôle est structural; par exemple les collagènes structurant la peau, les tendons, les os ou le cartilage; l'actine qui constitue le cytosquelette des cellules et les fibres musculaires ou encore la kératine que l'on retrouve dans les ongles et les poils.

D'autres protéines jouent un rôle fonctionnel, par exemple l'hémoglobine qui permet le transport du dioxygène ou les anticorps qui sont des protéines intervenant dans le système immunitaire pour contrôler les infections. Il y a surtout des protéines qui assurent les principales fonctions des organismes telles les réactions biochimiques, ce sont les enzymes.

Enfin il y a les protéines régulatrices, telles les hormones qui transmettent l'information à travers l'organisme, par exemple l'insuline qui régule l'utilisation des sucres ou l'hormone de croissance qui, entre autres fonctions, stimule la division cellulaire.

Cette grande diversité de protéines est encodée dans le génome du noyau cellulaire. Nous allons examiner dans la section suivante comment les protéines sont produites.

La production des protéines.

La production de protéine est codée dans l'acide désoxyribonucléique ou ADN. L'ADN est une macromolécule de taille considérable localisée dans le noyau cellulaire des cellules eucaryotes tels que l'on rencontre chez les mammifères, les levures, etc. C'est la molécule qui renferme toute l'information génétique de l'organisme vivant. La molécule d'ADN est formée d'un double brin sur lesquels sont insérés les bases, au nombre de 4, formant ainsi un polymère. Un polymère est une succession de molécules formant une structure linéaire dont les sous unités constitutives sont appelés monomères. L'enchaînement des 4 bases définit le code génétique. La première phase de production d'une protéine est la lecture de ce code via des enzymes qui permettent de transcrire celui-ci en acide ribonucléique messager (ARN messager). L'ARN messager est aussi un polymère garant du transfert de l'information contenu dans l'ADN aux *usines* fabricant les protéines. Alors que l'ADN reste inchangé dans le noyau cellulaire, l'ARN messager va être transmis au cytoplasme (intérieur de la cellule) où il rencontrera les ribosomes qui fabriqueront la protéine selon un mécanisme complexe appelé transcription.

Les ribosomes produisent les protéines qui sont constitués d'acides aminés. Ces derniers forme une famille de 20 molécules composées de carbone, d'hydrogène, d'oxygène et d'azote. La séquence des acides aminés mise en place lors de la transcription se fait en fonction de l'information transmise par la séquence de l'ARN messager. Une protéine peut contenir de quelques dizaines d'acides aminés à plusieurs centaines et cette succession est appelée structure primaire de la protéine. Cette structure est solidarisée par des liaisons peptidiques, liaisons covalentes formées entre un carboxyle d'un acide aminé et l'amine d'un autre.

La structure primaire caractérise une protéine mais n'est pas suffisante pour la rendre fonctionnelle dans l'organisme. A cette fin la protéine passe par différentes étapes de structuration que l'on présente dans la section suivante.

La structure des protéines.

Nous venons de voir qu'une protéine est constituée d'une structure primaire ou séquence résultant de la transcription. Afin que la protéine soit fonctionnelle il est nécessaire qu'elle acquiert une structure tri-dimensionnelle complète. Pour cela elle prendra tout d'abord une structure locale dite secondaire puis une structure par interactions à longue distance

dite tertiaire et enfin, dans certains cas, une structure formée par l'interaction avec différente protéine (ou sous-unités) dite quaternaire qui lui conférera sa fonction complète.

La structure secondaire existe sous deux formes: les hélices α et les feuillets β. La première est un enroulement de certaines parties de la chaîne peptidique le long de son axe, formant une hélice stabilisée par des liaisons hydrogènes. La deuxième résulte d'un agencement parallèle de certaines parties de la chaînes formant ainsi un feuillet lié par des liaisons hydrogènes. Les structures secondaires s'assemblent pour former sa structure tertiaire.

En général, les protéines fibreuses sont composées essentiellement soit d'hélice α, soit de feuillets β. Les protéines globulaires, solubles, formeront une structure tertiaire autonome en assemblant des hélices α et feuillets β. Une dernière structure, la quaternaire est différente selon le cas. Les protéines fibreuse vont agencer leur structure tertiaire entre-elles pour former des fibres. Dans le cas de grosse protéines globulaire, c'est l'agencement des différents motifs tertiaire, qui vont donner la structure finale à la protéine, voir la Figure 1.

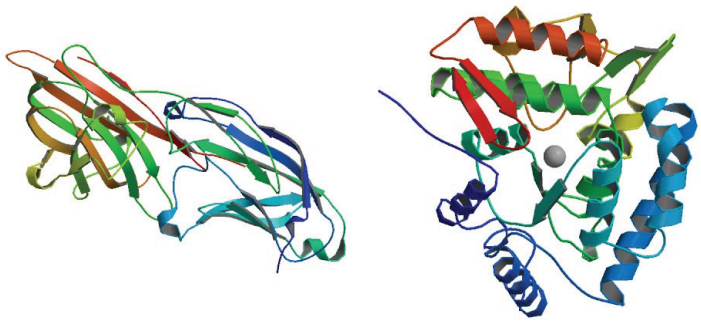

Figure 1: A gauche la protéine fibreuse Kératine et à droite la globulaire phénylalanine. La structure secondaire est donnée par les flèches pour les parties en feuillets β et les hélices α sont en cylindre. Les images proviennent de la base de données ouverte: Protein Data Bank.

La structure finale, qu'elle soit tertiaire ou quaternaire, correspond à la disposition énergétiquement la plus favorable donnant une forme spécifique à la protéine, responsable de son activité. La stabilité de l'ensemble de la protéine dépend du nombre de liaisons et de l'entropie de l'ensemble. Théoriquement la structure spatiale se forment naturellement et la protéine se replie sans apport d'énergie. Cependant, dans certains cas, il est nécessaire qu'une autre protéine soit présente pour favoriser la formation de ces liaisons. On appelle ces protéines des chaperonnes, elles interviennent dans le repliement pour l'optimiser mais ne font pas partie de configuration finale.

Les protéines forment une famille de molécules très diverse, tant par leur fonction que par leur structure tri-dimensionnelle. Deux d'entre elles nous intéresseront dans la suite: la protéine prion (PrP) et la protéine précurseur de l'amyloide (APP).

1.2 Les encéphalopathies spongiformes transmissibles et le prion

Les encéphalopathies spongiformes transmissibles

La problématique biologique qui motive l'essentiel des travaux de cette thèse, est l'étude des encéphalopathies spongiformes transmissibles (EST). Depuis près de 40 ans, la connaissance de ces maladies s'est considérablement développée. Une rétrospective de l'histoire des EST ainsi qu'un état de l'art est donnée par P. Beauvais dans [17]. L'apparition de la Maladie de Creutzfeldt-Jakob (MCJ) chez de jeunes enfants ayant reçu par injection de l'hormone de croissance ainsi que l'épidémie d'encéphalopathie spongiforme bovine connue sous le nom de *vache folle* dans les années 1990, ont notamment conduit la recherche à obtenir des avancées notoires dans ce domaine.

La première EST décrite le fut au XVIIIème siècle. A cette époque certains moutons étaient victimes de tremblements et de trouble du comportement entraînant inéluctablement leur mort, ce qui lui valu le nom de tremblante du mouton. Au XIXème siècle l'idée que cette maladie était de nature infectieuse apparut et certains s'essayèrent à inoculer la maladie, sans succès (voir P. Beauvais [17]). Quelques décennies plus tard, au XXème siècle les premières inoculations de la tremblante réussirent, puis la barrière d'espèces fut franchie en transmettant la maladie aux chèvres puis aux hamsters, permettant ainsi de simplifier les protocoles expérimentaux, Kimberlin [114].

Au début du XXème siècle furent découverts les premiers cas d'EST chez l'homme. D'abord par H.-G. Creutzeldt et ensuite A. Jakob, tous deux relevèrent des cas de démences avec troubles neurologiques et pertes neuronales dont l'issue en était fatale. Les premières publications eurent peu d'échos au sein de la communauté scientifique. En effet, seuls les élèves de A. Jakob continuaient de travailler sur ces cas. En revanche en 1955, V. Zigas découvrit le Kuru, cette maladie sévissait dans une tribu cannibale de Nouvelle-Guinée. L'ingestion rituelle du cerveau des morts transmettait la maladie. Les symptômes comparable à la tremblante du mouton furent rapidement remarqués. L'inoculation aux chimpanzés du Kuru termina de convaincre du caractère infectieux de cette maladie. De là naquirent les EST, dans une publication de Gajdusek en 1973, voir [82], l'auteur regroupait la tremblante, la MCJ et le Kuru pour définir une nouvelle famille de maladie dont le caractère infectieux et transmissible furent établis.

D'autres maladies furent ensuite classées parmi les EST (voir la Table 1). Certaines ayant des origines familiales ou génétiques; d'autres sporadiques ou encore acquises comme dans le cas des hormones de croissance ou de la variante de la MCJ par ingestion de bœuf contaminé. Toutes ont en commun certains signes cliniques, la transmissibilité et le caractère infectieux.

Il n'en restait pas moins que l'agent infectieux lui-même n'avait pu être isolé; ce fut le défi de la deuxième moitié du XXème siècle.

La théorie du prion

A cette époque, l'existence d'un agent infectieux a donc été mise en évidence. Cependant, ce dernier n'était alors identifié ni comme une bactérie, ni un virus ou tout autre pathogène

EST	Humaines	Animales
Sporadiques	MCJ* sporadique Insomnie fatale sporadique	Tremblante du mouton Encéphalopathie bovine naturelle Maladie du dépérissement chronique des ruminants sauvages Encéphalopathie des ovidés sauvages
Génétiques	MCJ familiales Syndrome de Gerstmann-Straüssler-Scheinker Insomnie fatale familiale	
Acquises	Kuru MCJ iatrogènes** variante de la MCJ	Encéphalopathie du vison Encéphalopathie bovine Encéphalopathie féline

*Maladie de Creutzfeldt-Jakob

**Par voie de transplantation, transfusion

Table 1: Classification non exhaustive des Encéphalopathies Spongiformes Transmissibles (EST).

connu. Il fallut attendre le début des années 1980 pour que soit isolé cet agent, il s'agissait de la protéine prion pour "proteinaceous infectious particle" ou PrP. Le groupe de S. Prusiner réussit à isoler cette protéine à partir de cerveaux de hamsters purifiés, après leur avoir inoculé la tremblante du mouton , Prusiner [182]. La protéine contenue dans les dépôts amyloides[1] suite à l'infection par la tremblante du mouton fut alors séquencée et baptisée PrP^{Sc} pour *scrapie*. En parallèle une protéine PrP soluble ayant le même séquençage est découverte dans des tissus sains, elle fut nommé PrP^{C} pour *cellular*. Ainsi coexistaient deux formes d'une même protéine, l'une dans les tissus sains et l'autre dans les cerveaux atteins d'EST.

La protéine présente dans les dépôts amyloides se revela être l'agent infectieux: une première dans l'histoire de la biologie qui valut le prix Nobel à S. Prusiner en 1998. Ainsi deux formes de la protéine coexistaient, l'une infectieuse et l'autre normalement produite par les cellules. Ces deux protéines ayant le même séquençage, qu'est-ce qui les différencie? La protéine est codée par le même gène et donc possède la même structure primaire. La réponse tient dans la structure secondaire de la protéine infectieuse PrP^{Sc} qui est enrichie en feuillets β en comparaison à la forme cellulaire, PrP^{C}. Les deux protéines ont donc deux structures secondaires différentes ce qui conduit l'une à agréger et former des fibres se déposant en amyloides dans le cerveau et l'autre à rester soluble dans la cellule.

Les deux formes co-existant, comment la forme infectieuse PrP^{Sc} entraîne-elle la PrP^{C} à changer de conformation? C'est la théorie du prion qui à ce jour préserve encore certains

[1]Accumulation de protéines sous forme insoluble

secrets. La théorie du prion est basée sur le fait que seule la protéine prion est responsable de la maladie, sans aucune autre intervention extérieure (virus, bactérie, etc). Ceci implique l'existence d'un mécanisme propre aux deux protéines qui entraîne la conversion de la PrP^{C} en PrP^{Sc}. Cette étape peut être vue comme une réaction catalytique: la présence d'une protéine de PrP^{C} près d'une fibre de PrP^{Sc} entraîne son changement de structure en s'attachant à la fibre. Ce processus a été proposé en 1967 par Griffith [92] pour expliquer la polymérisation de protéine avant même que le prion soit découvert. En revanche cette étape n'explique pas le phénomène de nucléation, c'est à dire l'apparition spontanée (appelée aussi sporadique) de la maladie.

Plusieurs explications ont été avancées, pour l'apparition des maladies à prion. D'une part, la PrP^{C} pourrait être une protéine auto-chaperone, c'est-à-dire qu'elle permettrait de modifier la structuration de la PrP^{C} en présence d'une de ses congénères, Liautard [141]. Puis celle de Lansbury basée sur l'existence d'une barrière énergétique: l'interaction de plusieurs monomères de PrP^{C} atteignant un seuil critique d'énergie engendre une transconformation de ces derniers et donne naissance à la PrP^{Sc}, voir les publications de Lansbury *et al.* [55, 108] .

L'hypothèse de Lansbury a été retenue pour la construction de différents modèles de prolifération du prion. Cependant, ce modèle n'apparaît pas être satisfaisant en l'état, pour expliquer les résultats *in vivo* obtenue. En effet, le phénomène de nucléation (formation du premier polymère) définit un Lag time (ou temps d'attente) qui est caractéristique dans les expériences effectués par l'équipe de J.-P. Liautard et détaillée au Chapitre 1. Ce temps ne semble pas corroboré avec les modèles existant. Dans le Chapitre 2, nous proposerons une nouvelle explication, soutenue par un modèle que nous avons développé.

Mais avant tout, dans la section suivante nous présentons les modèles classique de prolifération du prion qui serviront de références tout au long de cette thèse.

2 Modélisation de la prolifération de protéines

2.1 Les modèles pour le prion

La modélisation du prion a intéressé, non seulement la communauté des biophysiciens et des biologistes, mais aussi celle des mathématiciens. Tous cherchent à produire des modèles qui permettent d'interpréter les observations expérimentales. En effet, le mécanisme de prolifération du prion est encore mal connu du fait de la complexité des interactions moléculaires mises en cause et de la difficulté de les observer car elles se forment à une échelle microscopique. Pour cette raison, la modélisation est un outil incontournable qui permet de soutenir ou d'éliminer des hypothèses théoriques en confrontant les observations expérimentales aux prédictions des modèles. Dans la thèse de N. Lenuzza [139] on trouve un état de l'art très complet des modèles existants, nous en retiendrons deux qui ont servi de point de départ à nos travaux.

Un des premiers modèles construit pour modéliser la formation d'amyloides prion *in vivo* a été introduit par Masel *et al.* en 1999, [153]. Celui-ci modélise l'évolution de la concentration de protéine prion cellulaire PrP^{C} et de fibres amyloides PrP^{Sc} suivant leur

taille. Détaillons ce modèle et ses hypothèses. Il est supposé que les protéines de $\mathrm{PrP^C}$, données par la concentration $v(t) \geq 0$ au temps $t \geq 0$, sont produites dans le système à un taux constant $\lambda > 0$ et dégradées suivant une probabilité constante $\gamma > 0$ par unité de temps. D'autre part, les polymères de $\mathrm{PrP^{Sc}}$ sont décris suivant la concentration $p_i(t)$ au temps $t \geq 0$ pour chaque i représentant le nombre de monomères qui les composent (ou taille du polymères). Ceux-ci ne sont pas produits naturellement dans l'organisme, il n'y a donc pas de taux de production. En revanche, ils peuvent être dégradés suivant une probabilité μ_i par unité de temps qui dépend de leur taille. Le modèle rend alors compte de deux phénomènes qui sont à l'origine de la prolifération de la $\mathrm{PrP^{Sc}}$.

Le premier phénomène est la polymérisation. Les protéines de $\mathrm{PrP^C}$ s'agrègent avec les polymères, ainsi un polymère de taille i s'allonge en assimilant une nouvelle protéine et forme un nouveau polymère de taille $i+1$. L'élongation se produit suivant un coefficient τ_i dépendant de la taille du polymère et rendant compte de la réaction entre le monomère et le polymère (phénomène de diffusion, probabilité de s'attacher au polymère, etc). Ainsi le taux d'élongation d'un polymère de taille i est donnée par $\tau_i v(t)$ qui dépend de la concentration de monomères.

Le second processus est la fragmentation. En effet, la structure des fibres de $\mathrm{PrP^{Sc}}$ est supposée avoir une certaine fragilité qui dépend de sa taille. Par conséquent, elles peuvent se fragmenter en deux fibres plus petites. La probabilité qu'une fibre de taille i se scinde en deux est donnée par la probabilité β_i par unité de temps. On voit alors apparaître deux nouveaux polymères, l'un de taille $j \leq i$ et l'autre de taille $i-j$ suivant un noyau de probabilité $\kappa_{i,j}$.

Enfin, une conséquence de la théorie de Lansbury présentée à la section précédente est l'existence d'une taille critique de polymères, donnée par $n_0 > 0$. En dessous de cette taille il n'existe pas de polymères de $\mathrm{PrP^{Sc}}$. De ce fait, ce modèle suppose que si un polymère de taille i se fragmente et donc donne un polymère de taille $j < n_0$, alors celui-ci se décompose instantanément en j monomères.

En prenant en compte toutes ces remarques, le modèle construit s'écrit alors comme suit

$$\begin{cases} \dfrac{dv}{dt} &= \lambda - \gamma v - \displaystyle\sum_{i \geq n_0} \tau_i v p_i + 2 \sum_{j \geq n_0} \sum_{i < n_0} i \beta_j \kappa_{i,j} p_j \\ \dfrac{dp_i}{dt} &= -\mu_i p_i - (\tau_i v p_i - \tau_{i-1} v p_{i-1}) - \beta_i p_i + 2 \displaystyle\sum_{j \geq i+1} \beta_j \kappa_{i,j} p_j, \quad \text{for } i \geq n_0. \end{cases} \tag{1}$$

La version présentée ci-dessus est une généralisation du modèle initial de Masel *et al.* [153]. Ce système correspond à celui étudié mathématiquement par Doumic *et al.* [65]. A l'origine, le modèle est établi avec un taux constant de dégradation des polymères donné par μ, et un taux constant de polymérisation τ. De plus, la fragmentation est considérée proportionnelle à la taille c'est-à-dire que la probabilité de se fragmenter est donnée par $\beta_i = \beta(i-1)$ où $\beta > 0$ est une constante. Enfin, le noyau de fragmentation suit une loi uniforme, $\kappa_{i,j} = 1/(i-1)$ pour tout $j < i$. Ces hypothèses permettent alors de simplifier

le modèle, le rendant plus facile à étudier afin de le comparer aux données expérimentales. On le retrouvera dans les travaux suivant de Masel *et al.* [151, 152, 153].

Une limite de ce modèle *in vivo* est qu'il ne prend pas en compte la formation de polymères de taille n_0. Il représente donc l'évolution de la maladie dans le cas où il y a initialement des polymères, par exemple après inoculation ou infection. Il ne peut donc rendre compte de l'apparition spontanée de la maladie,*i.e.* du phénomène de nucléation (formation du premier polymère). D'autres modèles discrets (en taille) comme celui-ci ont été introduit, on citera par exemple les travaux de Ferrone [74], Lee *et al.* [135] ou encore Powers & Powers [179].

Dans les Chapitres 1 et 2 nous nous inspirons de ces modèles discrets. Cependant, nous modélisons le phénomène *in vitro* afin de comprendre les données expérimentales obtenues dans ces conditions. De plus, nous nous intéressons à la partie nucléation, ce qui nécessite un modèle décrivant la formation de polymères de taille n_0 en plus de la dynamique globale de polymérisation et de fragmentation des polymères.

En 2006, suite aux travaux de Masel *et al.* [153], l'article de Greer *et al.* [90] propose une version continue du système (1). Cela signifie que les polymères peuvent atteindre un continuum de taille. En effet, dans le problème précédent, l'unité de mesure des polymères est la taille du monomère (on ajoute 1 à chaque étape de polymérisation). Ici on considère le monomère comme infiniment petit, l'échelle d'étude est donc différente. La taille des polymères est alors donnée par une variable continue $x \in (x_0, +\infty)$, où $x_0 > 0$ est l'analogue de la taille critique n_0 dans ce dimensionnement.

L'objet qui permet maintenant de décrire l'évolution des polymères, est une fonction $(t, x) \mapsto p(t, x)$, qui représente la densité de polymères de taille x au temps $t \geq 0$. Le modèle de Greer *et al.* est construit suivant les mêmes hypothèses que le modèle discret. Cependant les coefficients de polymérisation et de fragmentation ainsi que le noyau de fragmentation ne sont plus des suites mais des fonctions, respectivement donnés par $\tau, \beta : \mathbb{R}_+ \mapsto \mathbb{R}_+$ et $\kappa : \mathbb{R}_+ \times \mathbb{R}_+ \mapsto \mathbb{R}_+$. Le terme de fragmentation est alors remplacé par un opérateur intégrale afin de prendre en compte toutes les tailles possibles. Quant à la partie polymérisation, elle est modélisée par un transport qui se produit à une vitesse donnée par $\tau(x)v(t)$. Le transport est une dérivée en x qui représente une élongation infinitésimale du polymère à chaque assimilation d'un monomère. La concentration de monomères, quant à elle, est toujours donnée par la fonction du temps v. On obtient alors le système d'équations

$$\begin{cases} \dfrac{dv}{dt} &= \lambda - \gamma v(t) - v(t) \displaystyle\int_{x_0}^{+\infty} \tau(x) p(t,x) dx + 2 \int_{x_0}^{+\infty} \int_0^{x_0} x \beta(y) \kappa(x,y) p(t,y) dx dy \\ \dfrac{\partial p}{\partial t} &= -\mu(x) p(t,x) - v(t) \dfrac{\partial}{\partial x} \left(\tau(x) p(t,x) \right) - \beta(x) p(t,x) \\ & \qquad + 2 \displaystyle\int_x^{+\infty} \beta(y) \kappa(x,y) p(t,y) dy, \quad \text{for } x \geq x_0. \end{cases} \tag{2}$$

Ce modèle présente, d'une part un intérêt mathématique (voir les travaux de Engler *et al.* [68] et Prüss *et al.* [184]), d'autre part il se justifie lorsque l'on étudie de grands polymères, par exemple lors d'un stade avancé de la maladie. Ainsi l'étude du modèle continue permet de comprendre l'évolution de la distribution en taille des grands polymères, permettant ainsi de caractériser les différentes souches de prions, Calvez *et al.* [29, 31].

Remarquons un fait important, relatif à ces deux modèles. Le travail de Doumic *et al.* [65] démontre rigoureusement le lien entre les deux modèles. En opérant un redimmensionnement des équations (1) selon un petit paramètre représentant la taille d'un monomère, ils obtiennent par passage à la limite le modèle (2). Cette étude mathématique permet ainsi de déterminer les échelles de grandeurs justifiant le modèle continu, celles-ci ayant été vérifiées expérimentalement (voir Lenuzza [139]). Notons aussi qu'il est discuté, dans ce travail, de la taille critique x_0 des polymères. En effet, cette dernière étant de l'ordre de quelques monomères, x_0 devrait être supposé nul.

Ces modèles pour le prion ne prennent pas en compte l'espace. Ce sont ce que l'on peut appeler des équations moyennées et supposent donc un environnement homogène. On verra par la suite que l'on peut prendre en compte l'environnement, notamment le solvant servant aux expérimentations. En effet, dans le Chapitre 4, on représentera la distribution de polymères selon une variable continue en taille avec $x_0 = 0$ ainsi qu'une variable de configuration et d'espace. Comme on le verra par la suite, le modèle considéré dans ce chapitre sera une généralisation de (2) sous certaines hypothèses d'homogénéité spatiale.

2.2 Les modèles pour Alzheimer

Au Chapitre 7, nous traitons du problème de la maladie d'Alzheimer. Un phénomène notoire de cette maladie est la formation de plaques amyloides dans le cerveau. Aussi appelées β-amyloides, ces dépôts sont issus de la polymérisation d'un peptide Aβ, *i.e.* un morceau de protéine (quelques acides aminées). L'APP est une protéine trans-membranaire, *i.e.* qui se trouve à la surface des cellules avec une partie de sa structure qui se trouve à l'intérieure de la cellule et l'autre en dehors, celle-ci est responsable de la formation du peptide Aβ. On pourra se référer à [96] et ses références.

Le mécanisme de prolifération des plaques amyloides dans la maladie d'Alzheimer peut être assimilé à celle du prion. C'est pourquoi les modèles pour la formation de β-amyloides sont de la même nature que ceux proposé ci-dessus, systèmes (1) et (2). On peut citer par exemple les travaux de Craft *et al.* [56, 57]. Dans les travaux effectués au Chapitre 7 nous prenons en compte la formation de ces plaques β-amyloides par une équation de transport (structurée en taille continue), tout comme dans le modèle (2).

Les deux modèles présentés dans la section 2.1 font partie d'une famille très vaste, celle des équations de polymérisation-fragmentation et de coagulation-fragmentation. Afin de remettre dans leur contexte mathématique ces équations et pour une meilleure lecture de la suite de cette thèse, nous présentons de manière très générale, dans la section suivante, les modèles discrets et continus de polymérisation et de fragmentation.

3 Les équations de polymérisation et de fragmentation

Nous avons présenté dans la section précédente deux modèles pour la prolifération du prion. Ces équations sont à l'origine de celles étudiées dans les travaux qui suivront. Afin de replacer ces modèles dans un cadre plus général, nous allons présenter certains modèles discrets puis continus des équations de polymérisation-fragmentation qui permettent de mieux appréhender ce type d'équations. Nous donnerons un bref état de l'art de ces modèles et évoquerons les différences avec les systèmes proposés dans cette thèse. Par ailleurs nous introduirons le cadre théorique et les outils analytiques utiles à leur étude mathématique.

3.1 Les versions discrètes

Les équations de polymérisation-fragmentation permettent de décrire l'évolution d'une population de clusters[2] caractérisés par leur taille (pouvant être par exemple des polymères). La dynamique de ces clusters est entraînée par les phénomènes; d'une part la polymérisation qui accroît la masse du cluster par assimilation d'un monomère[3]; d'autre part la fragmentation qui est la formation de clusters plus petits lorsque l'un d'entre eux se scinde. De manière plus générale, on parle de coagulation ou agrégation à la place de polymérisation lorsque deux clusters de tailles différentes peuvent s'associer. On retrouve de tels phénomènes par exemple en astrophysique pour représenter la formation de galaxies mais aussi en physique de l'atmosphère, pour la formation de goutte d'eau, du brouillard ou encore dans les aérosols. On a aussi de tels modèles en biologie pour représenter les phénomènes de formation de micelles[4] qui apparaissent par interaction hydrophobique de molécules en solution, par exemple les lipides. Enfin, en physique des polymères on retrouve très fréquemment ces équations et en biologie comme on a pu le voir dans la section précédente. Nous utiliseront de telles équations dans la partie I de cette thèse.

Nous nous concentrons maintenant sur les équations elles-mêmes, sans se soucier du phénomène physique ou biologique modélisé. Nous en présentons leur mécanismes à travers une revue de modèles classiques.

Débutons en introduisant ce qui est sûrement le premier modèle de cette famille et introduit par Becker et Döring dans [18]. Il consiste à décrire l'évolution de clusters par addition et dissociation un à un de monomères, c'est-à-dire l'unité de référence pour mesurer la taille des agrégats et noté C_1. On peut schématiser la réaction de polymérisation comme suit

$$C_i + C_1 \xrightarrow{a_i} C_{i+1}$$

ou C_i est un cluster contenant i élément C_1. D'autre par la dissociation s'écrit

$$C_{i+1} \xrightarrow{b_{i+1}} C_1 + C_i.$$

[2] On utilise cet anglicisme qui signifie grappe pour définir un amas ou agrégat composé de plusieurs fois la même entité élémentaire, par exemple le polymère qui se compose de monomères.

[3] Sous-unité élémentaire pouvant être une protéine par exemple.

[4] Cluster sphérique ou cylindrique

Les taux de réaction sont respectivement donnés par a_i pour la polymérisation et b_i la dissociation. De ces schémas cinétiques nous pouvons écrire, par la loi de l'action de masse, les flux de chaque agrégat de tailles i et donner ainsi l'équation d'évolution des concentrations pour chaque taille. Le système de Becker-Döring (BD) s'écrit ainsi

$$\textbf{(BD)} \qquad \begin{cases} \dfrac{dc_1}{dt} = -2J_1 - \displaystyle\sum_{i=2}^{+\infty} J_i, \\ \\ \dfrac{dc_i}{dt} = J_{i-1} - J_i, \ \forall i \geq 2. \end{cases}$$

avec les flux donnés pour tout $i \geq 1$ par

$$J_i = a_i c_i c_1 - b_{i+1} c_{i+1}.$$

Cette modélisation des concentrations de clusters implique que la quantité de clusters est supposée très grande mais de taille discrète. Nous n'avons donc pas d'information sur la taille maximale que peut atteindre un cluster, c'est pourquoi le système est constitué d'une infinité d'équations. On utilisera ce modèle dans les Chapitres 2 et 3 pour représenter la formation de micelles, on peut aussi se référer à Neu *et al.* [162] pour la modélisation de telles structures.

Dans la modélisation de la prolifération du prion que nous introduirons aux chapitres 2 et 3, on considère non seulement la formation de micelles mais aussi celle des polymères. Tout comme dans le modèle (1) nous considérons la fragmentation c'est-à-dire qu'un cluster de taille i peut se scinder pour former plusieurs clusters de tailles inférieures et pas seulement perdre un unique élément comme dans (BD). Ainsi on introduit le noyau $k_{i,j}$ de fragmentation qui donne le nombre moyen de clusters de taille j obtenus par fragmentation d'un cluster plus grand de taille i, à savoir dans le cas d'une fragmentation dite binaire[5]

$$C_j \xrightarrow{b_i k_{i,j}} C_j + C_{i-j}.$$

Le taux b_i est désormais interprété comme celui de la fragmentation. On notera que le noyau de fragmentation doit respecter la conservation de la masse c'est-à-dire que la somme des tailles issues de la fragmentation doit être la même que celle du cluster d'origine. Cela se traduit par la condition sur $k_{i,j}$ suivante: $\sum_{j=1}^{i-1} j k_{i,j} = i$. On obtient alors le système de polymérisation-fragmentation discret (PFD) suivant

$$\textbf{(PFD)} \qquad \begin{cases} \dfrac{dc_1}{dt} = -2a_1 c_1 c_1 - \displaystyle\sum_{j=2}^{+\infty} a_j c_j c_1 + \sum_{j=2}^{+\infty} b_j k_{j,1} c_j, \\ \\ \dfrac{dc_i}{dt} = -(a_i c_i c_1 - a_{i-1} c_{i-1} c_1) - b_i c_i + \displaystyle\sum_{j=i+1}^{+\infty} b_j k_{j,i} c_j, \ \forall i \geq 2, \end{cases}$$

[5]Un cluster qui se casse en deux

La formation de plus de deux clusters par fragmentation est autorisée par un tel choix de noyau. Dans certain modèles, comme celui présenté auparavant (1) et dans les Chapitres 2 et 3 de cette thèse, on considère une fragmentation binaire. Le noyau de fragmentation s'écrit alors à partir d'un noyau de probabilité symétrique $\kappa_{i,j}$, ce qui donne $k_{i,j} = 2\kappa_{i,j}$ de tel sorte que $\sum_{j=1}^{i-1} \kappa_{i,j} = 1$ et $\kappa_{i,j} = \kappa_{i,i-j}$ pour la symétrie, voir par exemple Doumic *et al.* [65]. Le système (BD) s'obtient à partir de (PFD) en prenant $k_{i+1,i} = 1$ pour tout $i \geq 1$, $k_{1,1} = 2$ et $k_{i,j} = 0$ sinon. Ces deux modèles sont donc intimement liés.

On peut encore généraliser quelque peu ces équations pour en donner un prototype qui va nous permettre de poser le cadre d'étude de ces modèles. Ce dernier est le système de coagulation-fragmentation discrète (CFD) qui s'obtient en supposant que toutes les associations s'opèrent, en d'autres termes tous les clusters peuvent coalescer. On a donc les réactions suivantes

$$C_i + C_j \xrightarrow{\phi_{i,j}} C_{i+j}$$

où $\phi_{i,j}$ est le taux de coagulation d'un cluster de taille i avec un cluster de taille j qui conduit à un cluster de taille $i + j$. Le système CFD s'écrit alors sous la forme suivante:

$$\textbf{(CFD)} \qquad \frac{dc_i}{dt} = \frac{1}{2}\sum_{j=1}^{i-1} \phi_{j,i-j} c_j c_{i-j} - \sum_{j=1}^{+\infty} \phi_{i,j} c_i c_j - b_i c_i + \sum_{j=i+1}^{+\infty} b_j k_{j,i} c_j, \ \forall i \geq 1,$$

en prenant $b_1 = 0$ (le monomère ne se fragmente pas). L'hypothèse naturelle sur ce taux de coagulation est la symétrie, on suppose que $\phi_{i,j} = \phi_{j,i}$. Une fois de plus on peut faire le lien avec (PFD) en prenant

$$\begin{cases} \phi_{i,1} = \phi_{1,i} = \tau_i, \ \forall i \geq 2 \text{ et } \phi_{1,1} = 2\tau_1, \\ \\ \phi_{i,j} = 0, \text{ sinon} \end{cases}$$

Ces modèles sont construis de telle sorte que la masse totale du système soit conservée. C'est pourquoi nous faisons l'hypothèse de conservation sur $k_{i,j}$ et de symétrie sur $\phi_{i,j}$, ainsi on obtient par sommation puis par l'interversion formelle des sommes et en intégrant en temps, la relation pour tout temps t d'existence des solutions

$$\sum_{i\geq 1} i c_i(t) = \sum_{i \geq 1} i c_i^{in},$$

où c^{in} est la donnée initiale. On retrouve formellement cette relation dans les trois modèles présentés ci-avant. En effet, n'ayant aucune dégradation ni production de clusters dans ces équations on s'attend donc à ce que les solutions satisfassent cette équation obtenue formellement. Il apparaît donc naturelle de considérer l'espace mathématique

$$X = \left\{ (x_i)_{i\geq 1} \in \mathbb{R}^{\mathbb{N}^*} \ : \ \sum_{i \geq 1} i|x_i| < \infty \right\},$$

dans lequel vivront les suites de concentrations c_i de clusters de taille $i \geq 1$. On cherchera donc des solutions $c = (c_i)_{i\geq 1}$ à valeur dans X pour tout temps d'existence de la solution. La condition la plus faible requise sur la condition initiale (hors positivité) est que son premier moment soit fini, *i.e.* que $c^{in} \in X$ pour s'assurer qu'elle soit de masse finie. Cet espace est utilisé notamment par Ball *et al.* dans [10] pour (BD) et dans [9] pour (CFD) ainsi que Laurençot dans [129] pour (CFD).

Il n'est pas possible de démontrer en toute généralité l'existence de solution qui préserve la masse constante. En effet, on obtient un défaut de conservation dans certains cas lorsque le coefficient de coagulation vérifie $\phi_{i,j} > K(i+j)$ tout du moins pour i et j grand et une certaine constante $K > 0$, voir par exemple Hendriks *et al.* dans [99]. On peut voir ce phénomène, dit de gélation, comme une transition de phase lorsqu'il y a formation de particule infiniment grande. En revanche dans le cas où la vitesse de coagulation est contrôlée, l'existence de solutions qui préserve la masse a été établie. On se réfèrera encore une fois aux articles de Ball *et al.* suivant: [10] pour (BD) et [9] pour (CFD). Dans l'article de Laurençot [129] pour (CFD), est proposée une démonstration alternative qui permet d'étendre le résultat en donnant un résultat supplémentaire sur la propagation des moments. C'est cette méthode que nous utilisons dans le Chapitre 3 pour conduire l'analyse d'un modèle pour le prion qui couple deux modèles, l'un de type (PFD) et l'autre de type (BD).

Le traitement de l'unicité est proposé selon deux alternatives. Soit en faisant une hypothèse plus restrictive sur la condition initiale, dans [9, 129] est fait l'hypothèse qu'un moment d'ordre plus grand que un soit contrôlé. Soit de restreindre l'hypothèse sur le taux de coagulation, par exemple dans [9, 10]. Ces deux pistes sont des perspectives à court terme pour donner suite au Chapitre 3. De la même manière l'asymptotique de ces problèmes a été étudié, notamment dans le cas où il y a une analogue de la *Maxwellienne* pour les équations de Boltzmann, ce qui s'appelle aussi *detailed balance*, c'est-à-dire qu'il existe M_i tel quelque

$$\phi_{i,j} M_i M_j = b_{i+j} k_{i+j,j} M_{i+j}.$$

Cette condition assure la réversibilité du processus et la convergence vers l'équilibre est donnée par des arguments d'entropie. On citera les travaux de Ball *et al.* dans [8, 10] et de Slemrod dans [198] pour (BD) ainsi que Cañizo dans [27] et Jabin & Niethammer dans [105]. Aussi, la vitesse de convergence vers l'équilibre a été levé, notamment dans le travail de Fournier & Mischler [80] où la vitesse de convergence exponentielle est obtenue sans hypothèse de réversibilité. Toutes ces études sont autant de pistes pour poursuivre le travail débuté au Chapitre 3 et qui permettront de dégager le comportement asymptotique des solutions.

3.2 L'approche continue

Dans la section précédente nous avons présenté plusieurs modèles discrets de la famille des équations de coagulation-fragmentation. Une hypothèse sous-jacente dans ceux-ci est celle de *grandes populations*; pourtant, les tailles que peuvent atteindre les clusters sont

en quantité dénombrable. En effet, ces systèmes sont constitués d'une infinité d'équations pour chaque taille $i \geq 1$ de cluster, l'unité de référence de taille étant le monomère ou cluster de taille 1. Désormais, nous souhaitons modéliser ce type de problème à une échelle macroscopique (clusters éventuellement de très grandes tailles, vivant plutôt dans un continuum que dans $\mathbb{N}$). Dans cet objectif, il est intéressant de changer d'échelle dans les modèles discrets, afin de passer à la limite (dans un sens à définir) pour obtenir une version continue de ces modèles. Nous adoptons donc ici la vision de Neu *et al.* [162], ou encore de Laurençot & Mischler [131].

Dans la suite de cette section nous présentons certains de ces modèles continus, ainsi qu'un bref état de l'art sur la théorie de ces équations. Les outils introduits serviront de référence pour aborder les parties II et III, dans lesquelles ce point de vue continu est retenu.

Le premier modèle que l'on peut mentionner est celui qui fût introduit par Lifschitz & Slyozov [142]. Il est l'analogue du modèle de Becker-Döring pour modéliser l'évolution de clusters macroscopiques. L'évolution de ces clusters y est décrite par une équation d'évolution sur une fonction $(t,x) \mapsto f(t,x)$ représentant la densité de clusters de taille $x \in \mathbb{R}_+$ au temps $t \geq 0$, complétée par une contrainte sur la masse totale du système. Le problème s'écrit donc, pour tout $(x,t) \in \mathbb{R}_+^* \times \mathbb{R}_+$,

$$\textbf{(LS)} \qquad \begin{cases} \dfrac{\partial}{\partial t} f(x,t) + \dfrac{\partial}{\partial x}\left((a(x)u(t) - b(x))f(x,t)\right) = 0, \quad , \\ \\ u(t) + \displaystyle\int_0^\infty x f(x,t)dx = \rho, \quad \forall t \geq 0. \end{cases}$$

où $a(x)$ représente le taux de polymérisation, analogue continu de la suite $(a_i)_i$ de la section précédente, tandis que le taux de dé-polymérisation $b(x)$ est l'analogue de $(b_i)_i$. La fonction u quant à elle décrit la concentration de monomères au temps $t \geq 0$, *i.e* c_1 dans le modèle discret (BD), et la fonction $v(x,t) = a(x)u(t) - b(x)$ en facteur devant f exprime alors que la densité est modifiée soit suite à une polymérisation, soit suite à une fragmentation. Enfin, $\rho > 0$ est une constante qui vaut pour la masse totale système, conservée au cours du temps.

D'autre part le modèle de polymérisation-fragmentation discret (PFD) donne, en version continue, le modèle *had hoc* suivant, pour tout $(x,t) \in \mathbb{R}_+^* \times \mathbb{R}_+$,

$$\textbf{(PFC)} \qquad \begin{cases} \dfrac{\partial}{\partial t} f(x,t) + u(t)\dfrac{\partial}{\partial x}\left(a(x)f(x,t)\right) = -b(x)f(x,t) \\ \qquad\qquad\qquad\qquad + \displaystyle\int_0^\infty b(y)k(y,x)f(y,t)dy, \\ \\ \dfrac{d}{dt}u(t) = -u(t)\displaystyle\int_0^\infty a(x)f(x,t)dx, \quad \forall t \geq 0. \end{cases}$$

ou encore, par conservation de la masse, l'équation sur u peut être remplacée par la contrainte

$$u(t) + \int_0^\infty x f(x,t) dx = \rho,$$

la constante $\rho > 0$ étant la masse totale du système. Ce modèle de polymérisation-fragmentation, ainsi que la version (2), on été très largement étudiée par exemple dans la thèse de Gabriel [81]. Il existe également des applications de ce type d'équation pour la modélisation du cycle cellulaire, on pourra lire Perthame [175]. Aussi notons la similarité de (PFC) avec l'équation de Lifschitz-Slyozov, notamment le terme de transport et la contrainte de masse. D'ailleurs le modèle (LS) a été étendu à un système prenant en considération la coagulation, étudié par Collet & Goudon dans [49]. Dans ce système, la fragmentation est remplacée par un opérateur de coagulation:

$$Q(f,f)(x) = \frac{1}{2}\int_0^x \phi(y, x-y) f(y) f(x-y) dy - \int_0^{+\infty} \phi(x,y) f(x) f(y) dy,$$

où ϕ est le taux de coagulation. Cet opérateur est une version continue des termes de coagulation dans (CFD) de la section précédente et présente certaines similarités avec l'opérateur de collision de Boltzmann.

Le point de vue du modèle (LS) est celui qui sera adopté dans la Partie III pour modéliser la formation de plaques amyloides pour Alzheimer. Cependant la concentration u n'est pas donnée par une loi de conservation mais par un opérateur différentiel qui dépend d'autres quantités. Malgré cela l'étude du problème peut se faire de manière analogue à (LS). Dans les travaux de Collet & Goudon [49, 50], la méthode proposée est de prouver l'existence d'une solution au sens des caractéristiques pour le problème autonome, *i.e.* lorsque u est donnée, puis de donner l'existence d'une solution au problème entier par une méthode de point fixe. Tout comme dans les versions discrètes, on s'attend à ce que les solutions préservent la masse total. La densité f se doit de vivre dans l'espace des fonctions L^1 pour la mesure xdx soit

$$L^1(\mathbb{R}_+, xdx) := \left\{ f : \mathbb{R}_+ \mapsto \mathbb{R} \text{ mesurable } \middle|\ \int_0^{+\infty} x\,|f(x)|\,dx < \infty \right\}.$$

On retiendra cette méthode pour résoudre le problème qui fait l'objet de la Partie III. Cette technique est une première étape, elle requiert une régularité relativement contraignante sur les coefficients. Pour étendre ces résultats on utilise le principe de convergence faible en approchant par des solutions de coefficients réguliers pour obtenir à la limite une solution faible pour des coefficients plus généraux. Cette méthode a été utilisée dans les travaux de Laurençot [128, 130, 133] pour l'équation de Lifschitz-Slyozov, avec et sans coagulation.

Le modèle (PFC) qui représente l'évolution de polymères sujets à la polymérisation et fragmentation dans un système préservant la masse est le point de départ du modèle introduit au Chapitre 4. L'étude des modèles de polymérisation-fragmentation a donné lieu à plusieurs travaux, par exemple Simonett & Walker [197] puis Laurençot & Walker [132] et Walker [213] pour le modèle prion (2), et [28] pour le modèle linéaire (u constant).

Plus généralement la littérature traite des équations de coagulation-fragmentation, sans le terme de transport, ou remplacé par l'opérateur de coagulation, par exemple Stewart & Meister[202] et Laurençot [127]. Dans le Chapitre 4 où nous introduisons un terme de polymérisation et de fragmentation pour un modèle plus général nous avons fait le choix de faire l'étude dans un espace à poids, de type

$$L^2(\mathbb{R}_+, e^{\alpha x}dx), \qquad \alpha > 0.$$

On propose ainsi un espace plus restreint pour les solutions, et donc pour la condition initiale. Mais cette méthode a l'avantage de donner des solutions dont tous les moments sont contrôlés. Cet espace contrôle la décroissance à l'infini des solutions et permet de traiter différemment le terme de polymérisation. Il est justifié aussi par l'écriture de formulations variationelles du problème pour les autres variables du modèle qui seront détaillées dans la section suivante.

Nous ne pouvons terminer cette section sans noter les travaux qui ont permis de justifier rigoureusement le lien entre les modèles discrets et les équations continues. Citons par exemple l'article de Laurençot & Mischler [131] pour le passage de (BD) à (LS) et celui de Doumic *et al.* [65] pour le passage du modèle de Masel *et al.* (1) au modèle de Greer *et al.* (2). C'est aussi dans cette philosophie que s'inscrit le Chapitre 5. Nous en parlons dans la section suivante.

4 Les modèles de configuration des polymères dans un fluide.

L'étude des fluides polymériques a donné lieu à de nombreux travaux. Plusieurs modèles ont été proposés pour décrire les propriétés de ces fluides et des polymères évoluant en leur sein. Afin de comprendre les différents modèles et la théorie sur les fluides polymériques on pourra se référer par exemple à Bird *et al.* [23] ainsi que Doi & Edwards [64]. Dans la section suivante nous présentons le modèle étudié au Chapitre 4 basé sur une représentation des polymères par des tiges *rigides*. Dans la section suivante, nous introduisons le formalisme utilisé au Chapitre 5 qui permet de justifier un tel modèle à partir des équations individu-discret.

4.1 Equations de Fokker-Planck-Smoluchowsky

Il existe principalement deux modèles de polymères. Le premier décrit des polymères rigides (assimilés à des tiges) et est souvent appelé dans la littérature modèle *rod-like* ou *rigid rod*. Le second est utilisé pour des polymères extensibles et on le nomme FENE pour *Finitely Extensible Nonlinear Elastic*, il possède de nombreux dérivés. Dans ce contexte, on suppose que le polymère se comporte idéalement comme un ressort entre deux masses ou une chaîne de ressort, on pourra par exemple lire la thèse de Lelièvre [138]. Ici, nous restreignons au cas de polymères rigides.

Dans cette approche, nous décrivons l'évolution des polymères dans un fluide par une densité. Précisément, si l'on se place dans un domaine spatial $\Omega \in \mathbb{R}^3$, et que l'on

considère une population de polymères rigides de longueur fixée dans ce domaine, il s'agit alors d'étudier l'évolution la densité $f(t,x,\eta) \geq 0$ de polymères au point $x \in \Omega$, au temps $t \geq 0$ et dont la configuration est donnée par l'orientation $\eta \in \mathbb{S}^2$. On établit que cette densité est solution d'une équation de type *Fokker-Planck-Smoluchowsky*,

$$\frac{\partial}{\partial t} f + u \cdot \nabla_x f + \nabla_\eta \cdot \Big(P_{\eta^\perp} \left(\nabla_y u \; \eta \right) f - D \nabla_\eta f \Big) = 0, \tag{3}$$

où $u = u(t,x)$ est la vitesse du fluide environnant et D le coefficient de diffusion rotationnelle des polymères. De plus, pour $z \in \mathbb{R}^3$, $P_{\eta^\perp} z = z - (z \cdot \eta)\eta$ désignee la projection de z sur le plan orthogonal à η. Ce modèle est dérivé entre autres par Doi & Edwards [64], Bird *et al.* [23] et Kirkwood [116] en faisant l'hypothèse que les polymères ne diffusent pas en espace et que la solution (le fluide environnant) est suffisamment diluée pour qu'il n'y ait pas de potentiel d'interaction, autre que les forces browniennes, entre les polymères.

Le champ de vitesse du fluide u est soit imposé, soit solution d'un système de type Stokes ou Navier-Stokes. Dans ce dernier cas on obtient un système couplé entre l'équation sur f et celles sur u. En effet, la densité de polymères joue alors un rôle dans l'équation d'évolution du fluide *via* une contribution au tenseur des contraintes $\boldsymbol{\tau}$ (voir Doi & Edwards [64], Bird *et al.* [23] et Otto & Tzavaras [169], Degond *et al.* [59]), de la forme

$$\boldsymbol{\tau} \propto \int_{\mathbb{S}^2} (3\eta \otimes \eta - Id) f \, d\eta.$$

Dans cette thèse, afin de se rapprocher des résultats expérimentaux que nous avons observés, nous avons fait le choix de partir d'une description *rigid-rod* de polymères de protéines, au sein d'un fluide de champs de vitesse donné. Le choix du modèle rigide provient en effet des observations des biologistes sur les polymères formés par la protéine prion (voir le Chapitre 4). En revanche, à la différence du modèle de longueur fixe ci-dessus, ces polymères s'allongent par addition de monomères et se fragmentent. Nous avons donc fait le choix d'introduire la taille dans ces équations et de reprendre les phénomènes de polymérisation-fragmentation tels que proposés dans la section 2.1. Rappelons que dans ces modèles de polymérisation-fragmentation et coagulation-fragmentation, la dépendance en l'espace avait déjà été prise en compte, mais uniquement pour représenter des phénomènes de diffusions, sans interactions avec un fluide environnant (voir par exemple les travaux de Wrzosek [226] et Collet & Poupaud [51]). Ici, nous ajoutons l'interaction avec la solution, ce qui donne une autre dépendance en espace. Il est à noter que cette idée de modélisation que nous présentons ci-après pourrait fournir de nouvelles quantités mesurables, utiles à l'étude des propriétés de ces polymères. Indirectement, en effet, ce modèle pourra par exemple permettre de reconstruire des taux de polymérisations, d'étudier la rigidité des polymères et ainsi leur taux de fragmentation. Il existe des techniques permettant d'étudier les propriétés mécaniques de tels polymères en imposant un cisaillement au fluide, voir par exemple Smith *et al.* [199] et Perkins *et al.* [174]. Ceci vient en complément de l'étude de la valeur propre liée au problème de polymérisation-fragmentation, Gabriel [81], de l'étude de la distribution en taille, Calvez *et al.* [29] ou encore des méthodes de problème inverse pour la reconstruction des taux de polymérisation ou de fragmentation, Doumic *et al.* [65, 66].

Dans le chapitre 4 on introduit donc un modèle décrivant l'évolution au cours du temps de polymères rigides. Les inconnues sont $f(t,x,\eta,r)$, la densité de polymères en position $x \in \Omega$, au temps $t \geq 0$, d'orientation $\eta \in \mathbb{S}^2$ et de taille $r \in \mathbb{R}_+$ la taille; et la densité de monomères $\phi(t,x)$ en $x \in \Omega$ au temps $t \geq 0$. La version proposée au Chapitre 4 s'écrit, pour un champ de vitesse u donné, comme suit:

$$\frac{\partial f}{\partial t} + u \cdot \nabla_x f + \nabla_\eta \cdot \left[P_{\eta^\perp} \left(\nabla_y u \ \eta \right) f - D_1 \nabla_\eta f \right] + \nabla_r \cdot \left[\tau(\phi, u, x, \eta, r) f \right] = -\beta(u,x,\eta,r) f + 2 \int_r^{+\infty} \beta(u,x,\eta,r') \kappa(r',r) f(t,x,\eta,r') dr', \quad (4)$$

et

$$\frac{\partial \phi}{\partial t} + u \cdot \nabla_x \phi - D_2 \Delta \phi = - \int_{\mathbb{S}^2 \times \mathbb{R}_+} \tau(\phi, u, x, \eta, r) f(t,x,\eta,r) dr d\eta, \quad (5)$$

où τ et β sont respectivement les taux de polymérisation et de fragmentation, tous deux pouvant dépendre des variables de position x, d'orientation η, de la taille r mais aussi du champ de vitesse u. Plus généralement encore ils peuvent dépendre du gradient de vitesse ∇u. Enfin le taux de polymérisation τ est une fonction de la densité de monomères ϕ.

On remarquera que la fragmentation est similaire à celle considérée dans la section 2.1 et donc κ est un noyau de probabilité. Ce système est complété par des conditions initiales et des conditions aux bords discutées au Chapitre 4. On démontre dans ce même chapitre l'existence de solution à ce problème. Pour cela on s'inspire des travaux faits sur les modèles rigides et FENE, où la solution de (3) satisfait pour tout $T > 0$

$$f \in L^\infty(0,T; L^2(\Gamma \times \mathbb{S}^2)).$$

L'analyse se fait *via* une formulation variationnelle du problème. On citera par exemple les travaux de Barrett & Süli [14, 15], Otto & Tzavaras [169].

Pour le problème (4-5) on retiendra cette technique. Cependant nous n'emploierons pas la méthode classique de recherche des solutions au problème de polymérisation-fragmentation, dont l'espace naturellement associé est $L^1(\mathbb{R}_+, (1+r)dr)$. Cette méthode consiste en général à obtenir des solutions régulières puis par des principes de compacité faible d'obtenir des solutions L^1 pour des coefficients et des conditions initiales moins réguliers. Dans le Chapitre 4, nous avons fait le choix de rechercher des solutions dans

$$f \in L^\infty(0,T; L^2(\Omega \times \mathbb{S}^2 \times \mathbb{R}_+, e^{\alpha r} dr d\eta dx),$$

ce qui permet d'écrire la formulation variationnelle du problème. Notons pourtant que cela reste consistant avec la théorie L^1, car notre espace L^2 à poids, *i.e* pour la mesure $e^{\alpha r} dr$ avec $\alpha > 0$ s'injecte dans L^1. Notre étude demande tout de même une condition supplémentaire sur la condition initiale, qui correspond à un contrôle de la décroissance à l'infini de la queue de distribution en taille, soit un contrôle de tous les moments initiaux (pour la taille r).

Quelques mots sur les méthodes numériques liées à ce problème. Au Chapitre 6, nous proposons une méthode numérique pour le problème (4-5). La structure des équations

permet de décomposer la solution en harmoniques sphériques. C'est la méthode la plus utilisée pour les modèles FENE et rigiges, par exemple dans les travaux de Chauvière & Lozinski [42]. Par ailleurs, on mentionne les travaux sur les équations de renouvellement cellulaire par Angulo *et al.* [5, 6], qui permettent de résoudre numériquement les équations de fragmentation (voir Perthame [175] pour le lien avec les équations de renouvellement). Dans ce chapitre on combine ces deux méthodes. On notera qu'il existe d'autres méthodes pour résoudre les équations de fragmentation, notamment Filbet [75] et Bourgade & Filbet [25], qui propose une formulation basé sur une description conservative de la fragmentation et pourrait être une piste pour poursuivre les travaux proposés ici. Enfin il est possible de donner une description individu discrète de ce type de modèle, et ainsi obtenir des solutions numériques, Lelièvre [138]. Nous présentons ce point de vue à la section suivante.

4.2 Une description stochastique, individu-discrète

Dans cette section nous présentons ce qui fait l'objet du Chapitre 5, un modèle individu-discret pour le problème introduit, dans sa version continue, à la section précédente. Un tel modèle décrit l'ensemble des interactions pour un nombre fini de particules. Ainsi on écrit toutes les forces physiques qui s'appliquent au niveau microscopique sur chaque particule, dans le but ensuite de justifier les modèles continus, comme limites du problème discret. Cela conduit à un système d'équations décrivant le mouvement des monomères et des polymères dans un fluide donné par sa vitesse $u(t,x) \in \mathbb{R}^3$ au temps $t \geq$ et en $x \in \Gamma$, le domaine physique. Pour la dérivation de ces équations, nous utilisons les lois de la physique, on peut se référer par exemple à Doi & Edwrads [64], Kirkwood [116], Bird *et al.* [23], Degond *et al.* [60]. D'une part les monomères sont considérés comme des particules sphériques, d'autre part les polymères comme des tiges rigides. Le choix du modèle *rod-like* pour les polymères est issu des observations expérimentales, voir Chapitre 4.

Le monomère est idéalisé comme une bille, caractérisée par son centre de masse de trajectoire X_t, dans le domaine spatial Γ. La vitesse V_t, de telle sorte que $dX_t = V_t dt$, satisfait une équation de Langevin (Langevin [124]). Celle-ci s'écrit de la manière suivante:

$$m dV_t = \xi(u(t, X_t) - V_t)dt + \sigma dW_t,$$

où m est la masse du monomère, ξ le coefficient de frottement (force proportionnelle à la vitesse relative au fluide) et σ l'intensité du Brownien W_t, qui est un processus de Wiener de dimension 3. Ce dernier rend compte des forces aléatoires exercées par l'ensemble des autres particules du système. De la même manière, on écrit les équations sur les polymères, représentés par les trois quantités suivantes au temps $t \geq 0$

1. Son centre de masse $Y_t \in \mathbb{R}^3$ qui suit une trajectoire suivant le champ de vitesse u,
2. Son orientation $H_t \in \mathbb{S}^2$ dont les variations sont dérivées à partir du moment angulaire,
3. Sa taille $R_t \in \mathbb{R}_+$.

Ainsi, ces objets décrivant les monomères et les polymères sont des processus stochastiques. On pourra retrouver une telle approche dans les travaux sur les modèles FENE suivant: Jourdain *et al.* [112] et Lelièvre [138].

Maintenant, afin de prendre en compte l'élongation et la fragmentation, nous introduisons des taux de probabilités pour qu'un monomère s'attache à un polymère (élongation) ou qu'un polymère se scinde en deux (fragmentation). On obtient alors un système d'équations qui régit le mouvement de chaque particules (position et/ou configuration), soumis à des sauts qui rendent compte de ces deux phénomènes caractéristiques aux polymères formés de protéines. L'idée s'inspire des travaux déjà réalisés sur la coagulation et la fragmentation, par exemple: Wagner [211, 212], Hendriks [99], Lushnikov [149] et Marcus [150].

L'objet de cette étude est dans un premier temps, de décrire l'évolution des quantités mises en jeu. Pour cela on utilise un processus auxiliaire, la mesure empirique (voir par exemple les travaux de Fournier & Méléard [79] et Champagnat *et al.* [40]). Elle se décompose en deux mesures, l'une pour les monomères

$$\mu_t^m = \sum_{i=1}^{N_t^m} \delta_{X_t^i}, \tag{6}$$

où N_t^m est le nombre de monomères au temps t et X_t^i la position du monomère étiqueté par i, l'autre pour les polymères

$$\mu_t^p = \sum_{j=1}^{N_t^p} \delta_{(Y_t^j, H_t^j, R_t^j)}, \tag{7}$$

par analogie. Elles chargent l'espace *via* des mesures de Dirac dont l'évolution est donnée, d'une part par le mouvement continu et d'autres part, par les sauts, que l'on modélise par des processus de Poisson à valeurs mesures. On construit alors les équations différentielles stochastiques (EDS) correspondant à chacune de ces deux mesures empiriques. On obtient un système (couplé) de deux équations sur chacune de ces mesures, qui caractérise entièrement l'évolution du modèle.

Dans un second temps, nous nous attachons au redimensionnement des équations sur la mesure empirique. En introduisant un petit paramètre (ici la taille des monomères), on obtient alors un problème limite qui représente l'évolution du système à une échelle mésoscopique, intermédiaire entre le microscopique et l'échelle macroscopique. Ces méthodes proviennent des idées développées pour ce type de problèmes dans Prokhorov [181], Kurtz [121] et bien d'autres (voir introduction du Chapitre 5).

Dans le Chapitre 5, nous ne nous intéressons pas à la limite entièrement déterministe, qui se voudrait être le problème présenté à la section précédente (4-5). Mais, nous faisons un re-dimensionnement intermédiaire, pour obtenir ainsi une mesure déterministe pour les monomères (l'idée est de décrire cette population par une densité), tandis que celle des polymères reste un processus stochastique à valeur mesures. Ce choix réside dans

le fait que l'on considère toujours une population finie de polymères qui baigne dans un continuum de monomères. Nous pensons que cette échelle présente un intérêt pour les expériences biologiques où clairement le nombre de polymères est "dénombrable" alors que celui des monomères est très grand. Nous introduisons donc une alternative au problème entièrement déterministe (4-5), qui méritera par la suite d'être étudié qualitativement et comparé aux données expérimentales, notamment par des simulations numériques.

Part I

Modélisation de la prolifération *in vivo* de la protéine prion

Chapter 1

Multiple amyloid structures of the prion protein

Dans ce chapitre deux modèles sont étudiés, l'un pour la nucléation l'autre pour la polymérisation, dans le but de les comparer aux données expérimentales de polymérisation *in vitro* de la protéine prion. Les modèles introduits sont simplifiés de telle manière à ce que les paramètres puissent être identifiés. Chaque hypothèse est justifiée dans les conditions expérimentales de ce travail. L'analyse des données à partir de ces modèles démontre la nécessité d'une étape intermédiaire dans la polymérisation ayant lieu au tout début des expériences: cette étape étant à l'origine de l'hétérogénéité des structures d'amyloides observées expérimentalement. Ce travail est issus d'une collaboration avec l'équipe de J.-P. Liautard (INSERM) et publié en version intégrale dans *Biochimica et Biophysica Acta (BBA) - Proteins & Proteomics*, [3].

1.1 Introduction

Prions are the unconventional infectious agents responsible for transmissible spongiform encephalopathies. They appear to be composed mainly or exclusively of misfolded prion protein (PrP^{Sc}). Prion replication involves the conversion of the normal prion protein (PrP^{C}) into the misfolded isoform, catalyzed by tiny quantities of PrP^{Sc} present in the infectious material [183].

The mainstream molecular theory proposed to explain the prion phenomenon is the so-called amyloid formation introduced by Lansbury's team [55, 108]. It describes the formation of large aggregates of proteins ordered by specific contacts [74]. The model is based on nucleation-dependent protein polymerization that describes many well-characterized processes, including protein crystallization, microtubule assembly, flagellum assembly, sickle-cell hemoglobin fibril formation, bacteriophage procapsid assembly, and actin polymeriza-

tion as well as amyloid polymerization. Nucleus formation requires a series of association steps that are thermodynamically unfavorable ($K \ll 1$) and so the resultant intermolecular interactions do not outweigh the entropic cost of association [46]. Once the nucleus has been formed, further addition of monomers becomes thermodynamically favorable ($K \gg 1$) because monomers attach to the growing polymer, resulting in rapid polymerization/growth [74]. According to this theory, nucleus formation is the kinetic barrier to sporadic prion diseases that can be bypassed by infection. Nucleus formation is very slow at monomer concentrations slightly exceeding the critical concentration, whereas a small increase in PrP concentration would greatly increase the rate of nucleation [55, 108]. It is assumed that infection results from seeding of PrP polymerization, by preformed PrP^{Sc} nuclei.

Amyloids are fibrillar protein polymers with a cross-β structure [45]. Polymerization of proteins or peptides into amyloid fibrils occurs during a number of protein deposition diseases but also during the physiological assembly of several microbial proteins into cell surface structures. In the particular case of the prion proteins, amyloids or amyloid-like assemblies become self-perpetuating *in vivo* and thus turn into pathological infectious agents in mammals or protein-based genetic elements in yeast [34].

Amyloid formation appears to be the heart of prion propagation. The isomorphism between prion semiology and amyloid formation should be extended to the molecular mechanisms of strain formation and to molecular mechanisms of species barrier phenomenon. For several years, the existence of prion strains questioned the "protein only" hypothesis of prion diseases. Today, a number of experimental works have clearly demonstrated that structural differences correlate with biological strains [20, 53, 173, 206], see also [52, 72] for recent reviews. Furthermore, besides the natural biological strains discovered during purification of the infectious agent from the brain of infected animals or humans, new strains have been obtained by in vitro manipulation of recombinant or purified prion protein [48, 137]. However, the question of the molecular mechanisms at the origins of the strains is still unclear. In the present work, we show the appearance of heterogeneous structures during nucleation and their propagation during polymerization. This phenomenon suggests a critical sensitivity to the initial conditions that could explain both the *in vitro* creation of new strains and the stability of biological isolates. We show that this phenomenon takes place during the first step of the reaction, before nucleation.

1.2 Models

Protein amyloid polymerization is a complex feature that has received great attention and numerous models have been proposed [74, 90, 153, 179], a complete review of the models has been recently published [161]. However, the complexity of the models and the high number of independent parameters do not generally allow a complete identification of the theoretical parameters with those available by the experiments. But, the experimental methods used during this work render some simplifications available, first because of the reduced number of parameters, but also because some experimental results can be used to validate the choice of some simplifications and so reduce the complexity of more general

models. The purpose of this section is to propose and to justify simpler models where parameters can be experimentally determined and so to analyze the *in vitro* polymerization kinetics under the experimental conditions used during this work.

1.2.1 Analysis of nucleation without polymerization

We consider here a simplified theory, based on the *pre-equilibrium* assumption of Goldstein and Stryer [87], of the nucleation, see also [74, 168, 179]). Denoting by A_1 the concentration of monomers *i.e.* the $\mathrm{PrP}^{\mathrm{C}}$ and then by A_i, $i = 2, \ldots, n$ the concentration of oligomers, the size i corresponds to the number of monomers that forms it. The critical size n of oligomer stands for the nucleus size, after which the system becomes irreversible. Let consider the following nucleation system

$$\begin{cases} A_1 + A_1 \underset{k_-^2}{\overset{k_+^1}{\rightleftharpoons}} A_2, \\ \quad \vdots \\ A_1 + A_i \underset{k_-^{i+1}}{\overset{k_+^i}{\rightleftharpoons}} A_{i+1}, \qquad \text{for } 2 \leq i \leq n-3, \\ \quad \vdots \\ A_1 + A_{n-2} \underset{k_-^{n-1}}{\overset{k_+^{n-2}}{\rightleftharpoons}} A_{n-1}, \\ A_1 + A_{n-1} \xrightarrow{k_+^{n-1}} A_n, \end{cases}$$

with k_+^i and k_-^i are the reaction rates, respectively for addition and depletion of monomers, depending on the step. This system simulates the nucleus formation, noted A_n of size n which is the latter step, it is irreversible. At this point, we do not consider elongation after the nucleus formation. The dynamics is described by the following differential equations

$$\begin{cases} \dfrac{d}{dt} A_1 = -J_1 - \displaystyle\sum_{i=1}^{n-1} J_i, \\ \dfrac{d}{dt} A_i = J_{i-1} - J_i, \qquad \text{for } 2 \leq i \leq n-1, \\ \dfrac{d}{dt} A_n = J_{n-1}, \end{cases}$$

with $J_i = k_+^i A_1 A_i - k_-^{i+1} A_{i+1}$, for $i = 1, \ldots, n-2$ and $J_{n-1} = k_+^{n-1} A_1 A_{n-1}$.

Let us assume that the nucleation is well-balanced. This simplification is generally assumed by most of the models proposed [101, 168]. It could be challenged *in vivo* but the homogeneity of the *in vitro* system described here justifies this hypothesis. So, regarding the quantities $i = 1, \ldots, n-1$ at equilibrium (denoted by A_i^{eq}) we obtain from the above system that $J_i = J_{i-1}$, for $i = 2, \ldots, n-1$ and thus

$$-J_1 - \sum_{i=1}^{n-1} J_i = -nJ_1 \Rightarrow J_i = 0, \text{ for any } i = 1, \dots n-1.$$

From this, we can compute A_{n-1}^{eq} according to A_1^{eq}, which gives $A_{n-1}^{eq} = K {A_1^{eq}}^{n-1}$, where $K = \prod_{i=1}^{n-2} k_+^i / k_-^{i+1}$. If the monomer concentration is considered large enough, and the amount of monomers used for the nucleation steps is insignificant in comparison with the initial monomer concentration, then $A_1^{eq} \approx A_1(0) = M_0$, where M_0 is the initial monomer concentration. This assumption is quite straightforward under the conditions used because only some nuclei are necessary to start the polymerization that is afterward sustained by secondary nucleation highly dependent of the breaking of amyloid fibril during the vigorous stirring used during the *in vitro* polymerization. We now deduce an approximation of the time evolution of nucleus concentration, given by

$$\frac{d}{dt} A_n = k_+^{n-1} M_0^n$$

It is then possible to deduce a lag time of nucleation (T_{nlag}) defined such that

$$nA_n\left(T_{nlag}\right) = \varepsilon M_0,$$

where ε is a given fraction of the protein concentration (that can be arbitrary chosen in accordance with experimental measurement purposes) that stands for the proportion of monomers polymerized in nuclei. It needs to be small enough to be consistent with the hypothesis $A_1^{eq} \approx M_0$. Thus, T_{nlag} is given by the following expression

$$T_{nlag} = \frac{\varepsilon}{n k_+^{n-1} K M_0^{n-1}}.$$

A major characteristic of the nucleation theory is the strong dependence of the fibril formation rate on concentration which increases with the size of nucleus. This concentration dependence can be expressed in terms of T_{nlag} as follows:

$$\log\left(T_{nlag}\right) = -(n-1)\log\left(M_0\right) + C, \tag{1.1}$$

where $C = \log\left(\frac{\varepsilon}{n k_+^{n-1} K}\right)$ is a constant.

1.2.2 A polymerization model with constant mean length

Let us assume that polymers of size longer than n lengthen by adding one monomer after another. Let us denote by F_i the concentration of polymers of size i, and M the monomer concentration. The lengthening is considered as a constant irreversible process in agreement with the Dock–Lock mechanism discussed above [69, 85, 166] and can be given by

$$F_i + M \xrightarrow{k} F_{i+1}, \text{ for any } i \geq n.$$

By virtue of the Law of Mass Action, we deduce a differential equation on each concentrations of polymers of size i, that is for any $i > n$

$$\frac{d}{dt}F_i = kM(F_{i-1} - F_i), \text{ and } \frac{d}{dt}F_n = -kMF_n, \tag{1.2}$$

and an equation for the concentration of monomers

$$\frac{d}{dt}M = -kM\sum_{i\geq n} F_i. \tag{1.3}$$

In more general models [90, 118, 153] the secondary nucleation is inserted into the equations resulting from the possibility of splitting the polymer. This splitting rate is considered constant leading to a fibril length dependent of the monomer concentration [90, 118, 153] that gives a good representation of *in vivo* kinetics of prion infection [151] and some *in vitro* amyloid polymerization [118]. However, under the conditions used in the experiments described in our work, under vigorous shaking, polymer splitting cannot be considered as constant, it is rapid and leads to homogeneous length of the polymer. This was experimentally proven by the measurement of the mean length of the amyloid during polymerization when concentration varies from initial concentration to zero. Indeed, the lengths remain constant throughout the experiment (see Supplemental data [3, Figure S9]). Such a result was also obtained by Chatani *et al.* [41] using β2-microglobuline amyloid and ultrasonication. Thus we assume that the polymer fragmentation process occurs in such a way that it allows the fibrils to have a constant mean length N throughout the experiment. Such assumption directly leads to

$$m := \sum_{i\geq n} iF_i = N\sum_{i\geq n} F_i,$$

that is the mass of polymers m is equal to the total number of polymers times N the mean length of the polymers. Now summing (1.2) over $i \geq n$, we get the conservation equation

$$\frac{d}{dt}m + \frac{d}{dt}M = 0.$$

It follows that $M + m = \rho_0$ where $\rho_0 := m_0 + M_0$ the initial concentrations of the total mass. Now from the latter assumption on the constant mean length and the above conservation with (1.3), we have

$$\frac{d}{dt}m = \frac{1}{\tau}m(1 - \frac{m}{\rho_0}).$$

with $\tau = \frac{N}{k\rho_0}$. This equation is the well-known Verhulst model for logistic growth. Taking the initial condition $m(T_0) = m_0$ at time T_0, the unique solution is

$$m(t) = \frac{\rho_0}{1 + e^{-\frac{t-T_i}{\tau}}}, \tag{1.4}$$

where T_i the inflexion time defined by

$$T_i = T_0 + \tau \ln\left(M_0/m_0\right). \tag{1.5}$$

1.2.3 Methods

In order to understand what the T_{lag} consist of, we have performed seeded experiments that eliminate the part of the T_{lag} resulting from the formation of nucleus (*i.e.* T_{nlag}) as defined in Section 1.2.1. In seeded experiments, curves obtained (see Figures 1.1 and 1.2) by observing polymerization with fluorescent Thioflavin T[1] (ThT) given by $y(t)$ at time t are supposed to be linear according to the mass of amyloids. Thus from equation (1.4) and since $y(t) = am(t) + b$ with a, $b \geq 0$ we get

$$y(t) = b + \frac{a\rho_0}{1 + e^{-\frac{t-T_i}{\tau}}}. \tag{1.6}$$

This equation, independent of the amyloid protein type, fits the fibrillation data reasonably well and was shown to have real physical meanings [135]. T_i is the time at the inflexion point of the sigmoid and the slope $1/\tau$ of the sigmoid can be identified as a polymerization rate, see Figure 1.1. In order to minimize the participation of the polymerization rate in the determination of lag time, we define the lag time (T_{lag}) as proposed by many authors [135] as a function of T_i and τ.

$$T_{lag} = T_i - 2\tau. \tag{1.7}$$

It corresponds to 12% of the mass polymerized, since $m(T_{lag}) \simeq 0.12\rho_0$. The 4 parameters of the sigmoidal which are b, a, τ and T_i are obtained by fitting polymerization curves. It allows the calculation of the time at which polymerization truly begins T_0 with (1.5) and brings out a residual lag time $T_{rlag} = T_{lag} - T_0$ independent of the nucleation and of the autocatalytic characteristic of polymerization. The different parameters and lag times or summarize in Table 1.1.

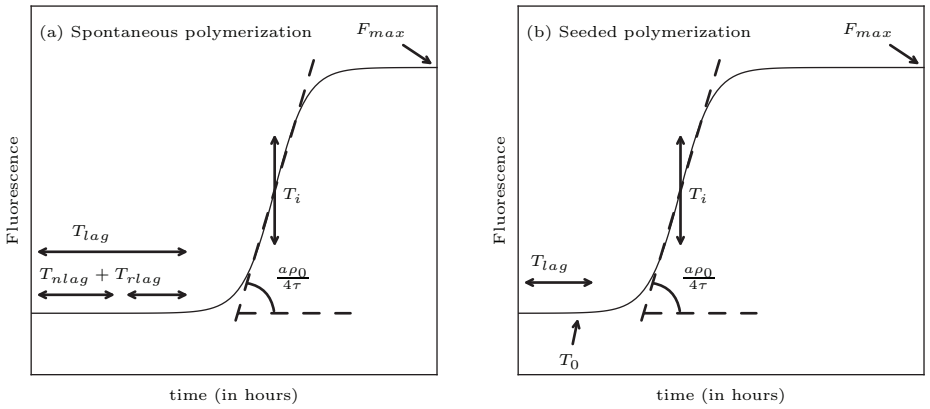

Figure 1.1: Schematic representation of the curves parameters obtained from regression analysis. The curves were obtained according to (1.6) for spontaneous polymerization and seeded polymerization. The meaning of the parameters is depicted on the figure and the different types of lag times are clarified.

[1]Thioflavin T is used to monitor and quantify the presence of protein aggregate with its red dye.

In spontaneous nucleation experiments, the experimental data are fitted with (1.6) too. Indeed, spontaneous experiment is a seeded experiment with seeds being the first nucleus occurring after a nucleation time T_{nlag}.

Parameters	
F_{max}	Complete polymerization measured as the maximum of fluorescence.
$1/\tau$	Rate of polymerization.
T_i	Inflexion time when polymerization is the fastest.

Lag times	
T_{lag}	Lag time, defined in equation (1.7).
T_0	Time at which polymerization starts.
T_{nlag}	Genuine lag time resulting from nucleation, defined in (1.1).
T_{rlag}	Residual lag time, experimentally shown to be T_0 in seeding experiments.

Table 1.1: Meaning of the parameters and the different types of lag times.

1.3 Results

1.3.1 Prion-amyloid formation under different incubation conditions follows similar dynamics

The goal of the present work was is to shed light on the mechanisms involved in the dynamic and the generation of heterogeneity during the formation of different structural types of amyloids of the prion protein rPrP[2]. Amyloids formation is obtained from partially unfolded proteins [113]. As a first approach, we took advantage of this observation to use three buffers A, B and C that induce different denaturation stages of the native prion protein. Analysis was performed by Circular Dichroism (CD), see Annex F. The secondary structure of the prion protein in buffer B is mainly under the α-helix conformation. The comparison of the CD spectrum obtained in buffer B with the one observed in benign buffer (*i.e.* PBS) shows that the prion protein conformation remains mainly under α-helix when transferred into this buffer B. On the other hand, the CD spectrum obtained in buffer A evidenced a major change in the secondary structure with a loss of α-helix and a dramatic increase of the random coiled proportion in the molecule [4]. To obtain amyloid formation we incubated the recombinant prion protein at different concentrations (0.1 mg/ml to 1.2 mg/ml) and different temperatures (between 20 $^\circ$C and 37 $^\circ$C), and in each buffer (*i.e.* in buffers A, B and C). Amyloid formation was monitored by thioflavin-T (ThT) fluorescence. The resultant curves were analyzed as described in Section 1.2.3 and parameters deduced are presented in Figure 1.1. Figure 1.2, on the left, shows some independent kinetics of the amyloid formation under buffer B at a concentration of 0.4 mg/ml. The kinetics of

[2]Recombinant 90-231 prion protein from Syrian hamster (Misocricetus auratus).

polymerization obtained under the different buffers conditions, *i.e.* buffers A and B, gave qualitative similar results, *i.e.* the experimental results can be well approximated by the sigmoidal curve of the equation (1.6) with correlation coefficient $R > 0.99$. (see Figure 1.1 for a definition of the geometrical representation of the parameters that were extracted from the experimental curves).

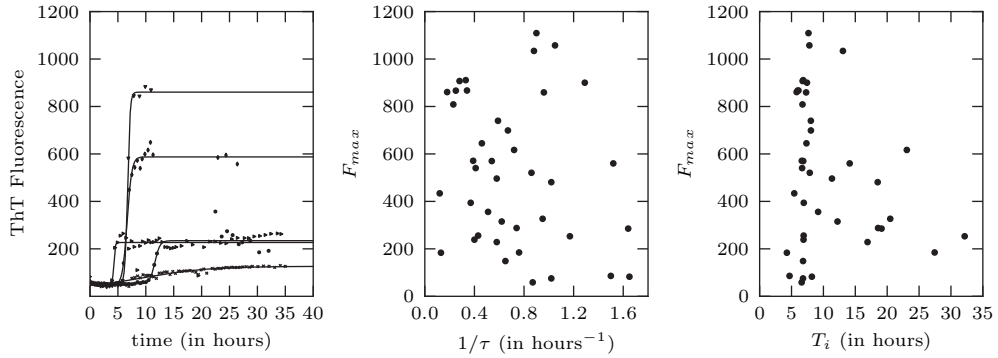

Figure 1.2: Heterogeneity of the kinetics of polymerization of rPrP. Samples containing 0.4 mg/ml of the rPrP were incubated upon continuous shaking in the same condition. The experimental points (on the left) were used to perform a non linear regression using (1.6). The results are representative of a great number (several dozen) of experiments. The maximum fluorescence, $F_{max} = b + a\rho_0$ according to (1.6), was plotted against $1/\tau$ (in the middle) and T_i (on the right) obtained from regression when using equation (1.6).

1.3.2 Polymerization dynamics reveal a highly stochastic mechanism originating from the heterogeneity of nucleation

The first observation that can be worked out from the kinetics curves obtained (Figure 1.2) is the heterogeneity of the maximum of fluorescence, in the middle and on the right. Maximum fluorescence varied in the range of five folds. It should be stressed that these values fluctuated in a single experiment between wells of the same plate and there is no correlation with the position on the plate. These observations can be interpreted in three ways:

1. either only a part of the monomers are polymerized
2. the existence of an irreversible off-pathway that extract the protein to an amorphous aggregate
3. the fluorescence of ThT differed from one preparation to another.

The first hypothesis was tested by measuring the quantity of monomers remaining in the supernatant after centrifugation of the aggregates. Although fine differences have been seen, no systematic differences can be correlated with the fluorescence (results not

shown), this hypothesis is rejected. A consequence of the second proposition would be the existence of a relation between the maximum of fluorescence (F_{max}) and the T_{lag} and/or τ, the irreversible off-pathway leading to an apparent decrease of the initial concentration thus increasing lag time. No such relations were observed in Figure 1.2. On the other hand, a FACS analysis (see Annex E) clearly showed that polymers can be differentiated by their ThT binding capacity as shown by the ratio between fluorescence and size of the amyloids, see Figure 1.3. We thus concluded that different polymers exhibiting different ThT binding properties could be spontaneously formed during *in vitro* polymerization.

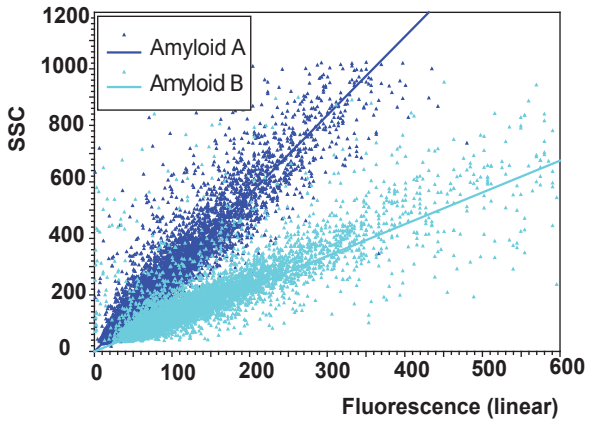

Figure 1.3: FACS analysis of the fibrils labeled with ThT. Two different preparations, of amyloids obtained in buffer A and buffer B, were analysed by FACS as described in Annex E. Each point is put on the figure as a function of size (SSC) and ThT fluorescence.

To confirm the reality of heterogeneity, we first analysed the dynamics of the polymerization. The characteristic sigmoid curve can be interpreted according to equation (1.6) to compute a lag time (T_{lag}) and a polymerization rate ($1/\tau$), see Section 1.2.3. A major observation of a systematic study of the T_{lag} is its heterogeneity both when different buffers are compared but also within a same buffer condition, see Figure 1.2. However, the lag time depends on the initial concentration of monomers and the apparent dispersion of the measurement decreases when concentration increases, see Figure 1.4 on the left. These two results seem qualitatively in agreement with a nucleation dependent mechanism of polymerization. In order to rationalize this observation, we decided to compute the number of monomers in the putative nucleus using the relation (1.1). Surprisingly the number of monomers determined according to this theory is only between 1.8 and 2.2, a result hardly consistent with the nucleation theory, particularly to explain the many years long incubation times observed in the sporadic forms of the Creutzfeldt-Jakob disease (CJD). Such an astonishing result has been previously observed by Baskakov and Bacharova [16] for mammalian prion protein, by Collins *et al.* [54] for yeast prion, by Chen *et al.* [43] for polyglutamine or Padrick and Miranker [170] for Islet Amyloid (IAPP). These observations were interpreted either as the existence of an off-pathway for the prion polymerization [16, 54] or as a more complex kinetics for IAPP [170]. Although, odd structures have been

observed with high resolution microscopy of prion amyloids [16], the existence of an off-pathway can only be ascertained by an analysis of the kinetic data. Three tests have been proposed to ascertain the existence of an off-pathway [180],

1. the dependency of the T_{lag} on initial concentration (Figure 1.4),

2. a fit obtained with light scattering (not feasible here),

3. the improvement of the fitting of the first part of the kinetic while initial concentration increases.

Thus we performed a study of the fitting of the first half part of the polymerization curve to the equation proposed by Powers et al. [180], $y(t) = at^2+bt+c$, where a, b, c are constants and y is the fluorescence measured at time t. We found that the correlation coefficient did not improve when higher concentration of monomers was used (see Supplementary data in [3, Figure S1]). This result, together with independence of T_{lag} to maximum fluorescence F_{max} (Figure 1.2 middle and right), seems to rule out the existence of an off-pathway under the conditions used during these experiments. However, due to the low sensitivity of this test, we decided to address this question by another way. Indeed, another approach to explain the relation between T_{lag} and the monomer concentration is to understand what the lag time consists of in our experiments. We thus decided a thorough analysis of the lag time.

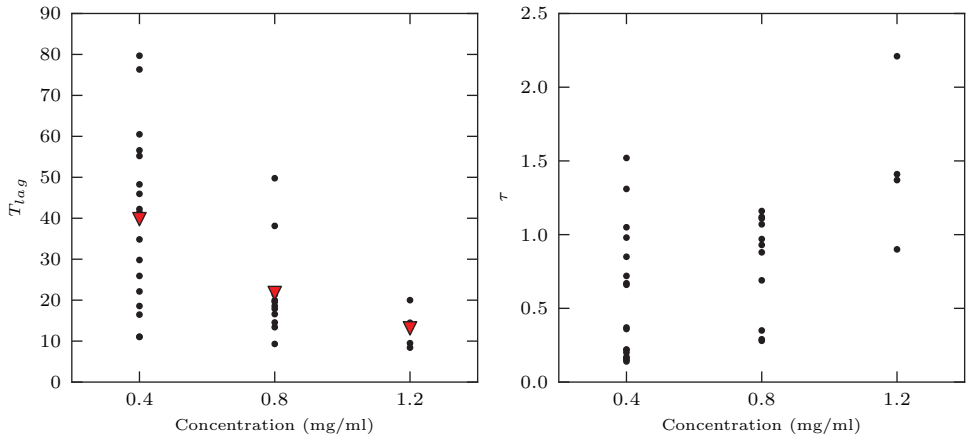

Figure 1.4: Lag time (T_{lag}) and rate (τ) dependency of the initial concentration of monomeric rPrP. Kinetics analyses were performed as described in Section 1.2.3. Kinetics of amyloid polymerization of rPrP at different concentrations in buffer B at room temperature was obtained in a single experiment (a 96-well plate). T_{lag} was calculated according to (1.7) (on the left) and τ was deduced directly from (1.6) (on the right).

1.3.3 What is the meaning of apparent T_{lag} in seeding experiments?

In order to investigate the nature of lag time, let us denote T_{lag} as the time before the beginning of observable polymerization according to (1.7). In seeding experiments, the T_{lag} does not depend on nucleation (this is clear precisely because of seeding) and thus, T_{lag} should reflect only the sigmoid kinetics that results from an autocatalytic reaction (see Section 1.4 and theory proposed in Section 1.2.2). As a consequence, increasing the quantity of seed should result in the complete disappearance of this lag time (T_{lag}). (See for instance [90, 118, 135]). This absence of lag time after seeding was observed with numerous proteins that undergo an amyloid polymerization, for instance insulin [102], the β-peptide of Alzheimer disease [71, 103] or the polyglutamine of Huntington disease [221].

In order to test this inference, we have performed an experiment by increasing the seed concentration. The results presented in Figure 1.5 (on the left) invalidate this hypothesis for *in vitro* prion polymerization. Indeed, even at very high concentration of seeds (*i.e.* greater than 10%) an apparent lag time is still obtained suggesting that another phenomenon is responsible for at least a part of this occurrence. As expected, from equation (1.5), the decrease of T_i is correctly approximated by a function of the logarithm of the seeding ratio, and the curve intersects the T_i axis around 3h (with a 95% probability to be between 2 and 4h) (see Figure 1.5, in the middle). This value could correspond to a residual lag time (T_{rlag}, see Figure 1.1) under the experimental conditions involved. In order to study the mechanisms responsible for this delay, we have developed a model of polymerization that allows us to identify the parameters of the equations obtained (see Sections 1.2.2 and 1.2.3). In equation (1.6), the contribution of seeding inside the delay time before polymerization is targeted. Indeed, as detailed in Section 1.2.2, T_0 is the time when seeded polymerization truly begins. Thus, when different from zero, T_0 is a residual lag time (T_{rlag}) not explained by polymerization kinetics. An analysis of the distribution of T_0 confirms that a residual lag time with a mean of 3.3 ± 0.15h was necessary before polymerization starts (see Figure 1.5, on the left). This value (3.3 ± 0.15h) is in good agreement with the one (3 ± 1h) found by an independent method described above and presented in Figure 1.5 (in the middle). This implies that a time dependent sufficiently long process (*i.e.* 3h under our experimental conditions) precedes the beginning of polymerization induced by seeding.

Many hypotheses can explain such a phenomenon; however, a simple one would be the existence of a conformational change (see Supplementary data [3, Figure S2] for a numerical simulation of this hypothesis). Consequently, we decided to test the possibility that a time dependent conformational change leading to an amyloid competent isoform is necessary to begin polymerization. We thus performed an experiment of a delayed seeding to test the possibility that this conformational change comes from the monomer. The results (here with buffer B) show that delayed seeding decreased the lag time but, as a surprise, did not result in its complete disappearance, see Figure 1.6 panels A and B. The time dependency of the T_{rlag} was well approximated by an exponential curve ($r > 0.98$) that leaves another residual lag time (T_{rrlag}) of 1.7 ± 0.3 h when seeding is performed at 1% and 1.10 ± 0.4h when seeding is performed at 10%, suggesting that a complex mechanism

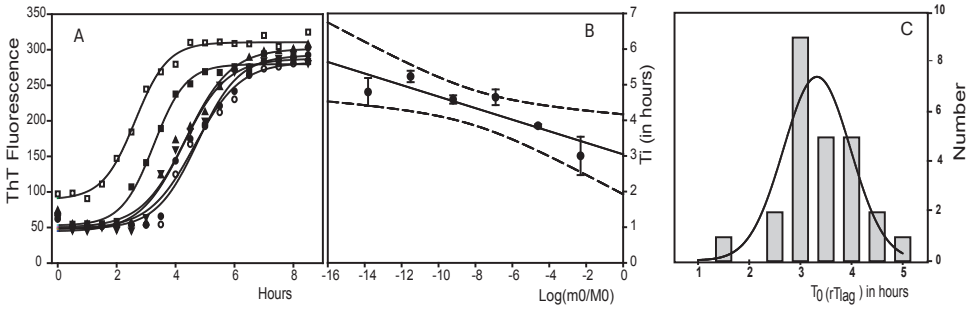

Figure 1.5: Lag time did not disappear when seed concentration increased. Kinetics analyses were performed as described in Section 1.2.3. Kinetics of amyloid polymerization of rPrP at 0.4 mg/ml in buffer B at room temperature was obtained in a 96-well plate after seeding with m_0 mg/ml of amyloid prepared as described in Annex B. T_i was obtained according to equation (1.6). Left panel represents one set of curves obtained among 3 in each experiment. Middle panel represents the dependency of T_i against seed quantities in case of polymerization induced by seeding. M_0 is the initial concentration of the monomer and m_0, is the concentration of monomers in the polymers added to seed the reaction. As a consequence, when $m_0 = M_0$, $\log(m_0/M_0) = 0$, thus the value of T_i obtained at this point represents the delay necessary to begin polymerization. Right panel shows the delay of polymerization measured by T_0 from (1.5) when seeding is performed with $m_0 = 0.004$ mg/ml of amyloid prepared in the same buffer.

was involved. Two hypotheses can be made to explain such a result:

1. either amyloid seeds undergo conformational changes,
2. monomer conformational change results from a complex mechanism involving many different steps during conformational changes and one of these steps needs interaction with amyloid.

We tested the first hypothesis: did the amyloid change its structure during the seeding process? In order to investigate this possibility, we decided to fix, with formaldehyde the amyloid before seeding. Fixation (*i.e.* chemical cross-linking) of the amyloid did not change the dynamics parameters of polymerization (see Supplementary data [3, Figure S3]). Thus, major structural changes of the seeds were not necessary to start polymerization, leaving as sole explanation a complex mechanism of polymerization that involved monomers. However, any mechanisms involving the monomer should be sensitive to concentration. To challenge this possibility, we decided to change the concentration of monomers (PrP^C) but kept the same quantity of seeds. A numerical simulation of this experiment, with the simple conformational change hypothesis (a change of conformation is necessary to incorporate monomers into polymers) shows that T_i and consequently T_{lag} should decrease when monomer concentration increase (see Supplementary data [3, Figure S4]). On the contrary, the experimental results shown in Figure 1.6 (panel C) clearly exhibit an increase of the apparent lag time with respect to the monomer concentration. Thus, a new hypothesis is needed to be added. We then propose that many conformations could co-exist. Some of them would interact with the amyloid polymers but could not

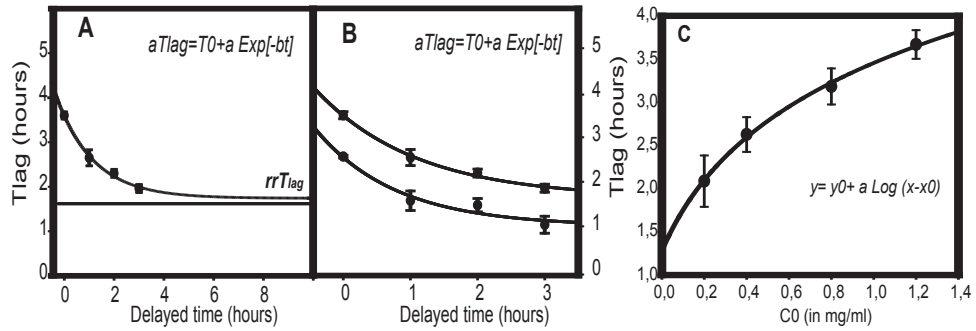

Figure 1.6: Panel A and B: Delayed seeding reduced apparent lag Time (T_{lag}) but did not conceal it. Kinetics of amyloid polymerization of rPrP at 0.4 mg/ml in buffer B at room temperature was obtained in a 96-well plate. Samples were incubated 0, 1, 2 or 3h before seeding with either 0.004 mg/ml (panels A and B) or 0.04 mg/ml (panel B) of amyloid prepared in the same buffer . We used an exponential function (see figure) to join the points ($r > 0.98$). Panel C: Increasing initial concentration of monomers while the concentration of seeding polymers was kept constant resulted in an increase of T_{lag}. Kinetics of amyloid polymerization of rPrP in buffer B at different concentration was obtained in a 96-well plate after seeding 0.004 mg/ml of amyloid prepared in the same buffer.

polymerize, see model Figure 1.11. In order to validate this model, we investigated the consequences of this proposition.

1.3.4 Heterogeneity of the nucleation process explains dynamics of polymerization

As a consequence of the model proposed above, the nucleation can start with different protein conformations. This hypothesis is sustained by the observation of the dispersion of the T_{lag} (see for example Figures 1.2 and 1.4) that suggests that the reaction is randomly sensitive to the initial conditions *i.e.* the first nucleus formed will dictate the dynamics and probably the polymers structure. As a consequence, various nuclei could be formed independently resulting in heterogeneity of different polymers (see Figures 1.2 and 1.3). This is also obvious when comparing parameters of the kinetics (*i.e.* T_{lag} and $1/\tau$) (see Figure 1.4). Figure 1.4 (on the right) shows that the apparent polymerization rate (τ) is widely dispersed not only between buffer conditions but also within the same buffer. Furthermore, the apparent rate of polymerization is totally independent of the initial concentration. This result can also be interpreted as heterogeneity of nucleation and subsequent polymer formation. It can be suggested that different nuclei generated structurally different polymers each exhibiting specific polymerization dynamics.

1.3.5 Electron microscopy analysis confirms heterogeneity of polymer structures

A straightforward consequence of the previous experiment suggested that structural differences in nucleus formed should lead to polymer heterogeneity. This latter effect should

then be observed by microscopy. The polymers, labeled with ThT, have been first observed by fluorescence microscopy. (Samples of the images are shown as Supplementary data [3, Figure S5]). Indeed very different aspects can be observed, from genuine individual fibrils to huge aggregates where no fibril can be individually distinguished. However, the resolution of optical microscopy, although allowing a large number of sample analyses, cannot distinguish fine structures of the polymers. We thus completed this study by electron microscopy analysis. Many individual experiments reveal specific type of structures even if in some cases the structures look alike, see Figure 1.7. Heterogeneity of the polymers, between the preparation and eventually between buffers is the main observation. A quantitative analysis of the polymers width clearly confirmed the dispersion of the parameters characterizing the structure of the polymers (Supplementary data [3, Figure S6]).

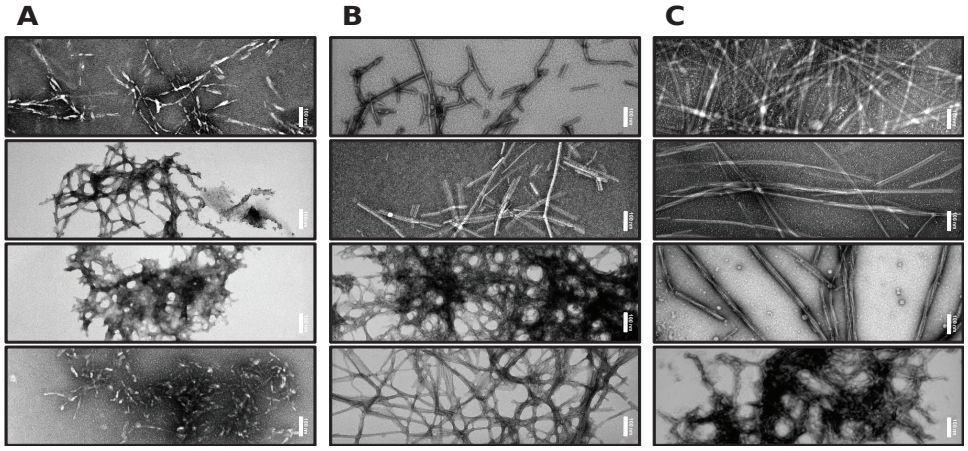

Figure 1.7: Electron microscopy analysis confirms the heterogeneity of the amyloid structures. Aliquots of sample obtained after polymerization in buffer A (panel A) or buffer B (panel B), or buffer C (panel C) were proceeded as described in Annex C for examination in negative stain by Electron microscopy. The images represent an arbitrary selection among many different structures that were observed during this work. Scale bars represent 100 nm.

1.3.6 Successive seeding allows the selection of more "efficient" amyloid strains

The existence of a structural heterogeneity and the corresponding dynamics parameters have numerous consequences that can be used to better characterize the mechanisms involved. For instance, the results presented above suggest that, in some cases, the apparent rate of polymerization is a mix of many independent rates resulting from the combination of structural and dynamical different amyloids, see Figure 1.7 and Supplementary data [3, Figure S6]. A question arises from this observation: What are the effects of repetitive seeding on this heterogeneous mix? After seeding a solution of monomers, two main parameters direct the polymerization dynamics: the number of nuclei and the polymerization rate ($1/\tau$) (sensitivity of the polymer to splitting is included in this parameter by the mean

length N, see Section 1.2.2. However, it is quite clear that repetitive seeding will favor the fastest polymerization structures (including true polymerization rate k, and sensitivity to splitting N, *i.e.* k/N) leading to a selection of the amyloid fittest to the buffer conditions and agitation used. We thus decided to produce prion-amyloid by repeating seeding and to analyze the kinetic characteristics of the polymerization.

We thus designed an experiment to test the effect of successive seeding on the kinetics of amyloid formation in buffer B. The results evidenced that successive seeding increased the polymerization rate and decreased the T_{lag} strengthening the hypothesis that a selection operates on a heterogeneous population, see Figure 1.8. According to Pedersen *et al.* [172], survival-of-the-fittest would be the mechanism causing the preferred amyloid molecular packing that correlates with the conditions present under fibril formation. However, an increase of polymerization rate could also reflect a mechanism of better packing, for instance by zipping a longer upbeta-core structure, a kind of adaptation.

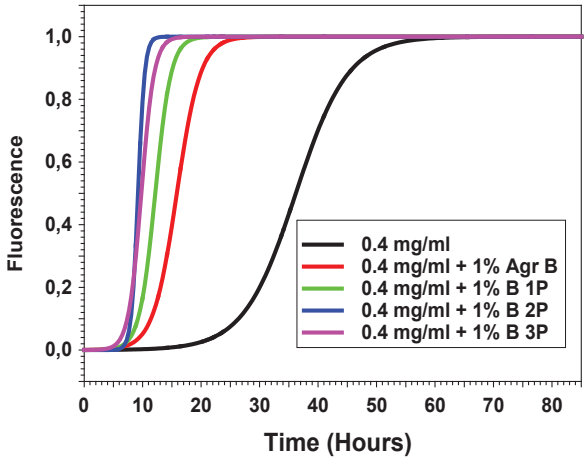

Figure 1.8: Repeated seeding leads to a decrease of T_{lag} and an increase of the apparent rate of polymerization ($1/\tau$). Kinetics of amyloid polymerization of the rPrP at 0.4 mg/ml in buffer B at room temperature was obtained in a 96-well plate. The experimental results were normalized in order to clearly evidence that the T_{lag} and speed polymerization. The first kinetic (black line) was obtained without seeding. All the other curves were obtained after seeding at 0.004 mg/ml using the previous amyloid as presented on the figure.

1.3.7 Successive seeding in the same buffer conserved the strain characteristics

Another consequence of the heterogeneity of the structure obtained would be the conservation of the nucleus structure during successive seeding. It should be pointed out that such a result would be in conflict with the thermodynamical hypothesis. Indeed, it was suggested by Pedersen *et al.* [171] using glucagon as model that, under specific conditions, the structure reached by the amyloid is always the same, the one of the minimal energy (a kind of generalization of the Anfinsen principle). This implied that the forma-

tion is thermodynamically driven. To decide between these two hypotheses, we selected two preparations that exhibit noticeably different parameters (*i.e.* ThT binding and dynamics characteristics) and we used these two samples to seed successively independent preparations. The results obtained with buffer B are presented in Figure 1.9, the kinetics characteristic (*i.e.* T_{lag}, τ and fluorescence) and the ThT binding properties remain approximately the same during three successive seedings. To confirm this observation, we have compared the amyloid structure by electron microscopy (see Supplementary data [3, Figure S7]). These results suggest that, at least for a few successive seedings, nucleation is predominant on determining the kind of structure that is selected and thus seeding conserved the specificities of the amyloid, something reminiscent of the strains phenomenon. However, due to the few number of successive seedings, these observations cannot rule out the thermodynamic fate of the system according "the Ostwald step rules" [207].

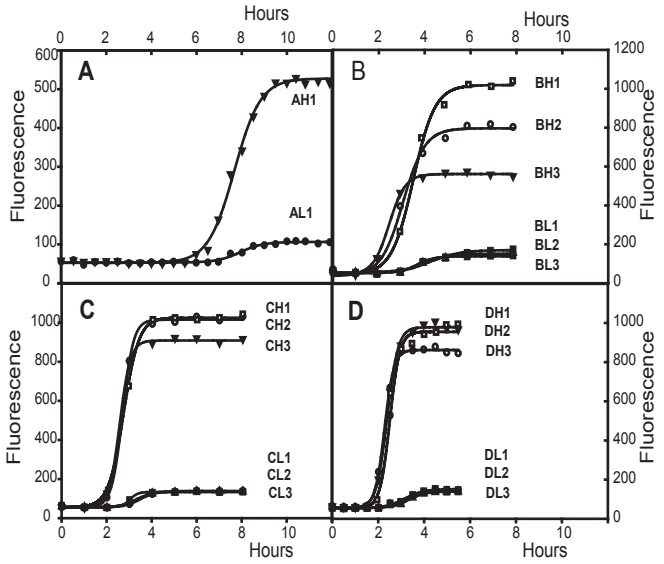

Figure 1.9: While decreasing T_{lag} and increasing apparent rate of polymerization ($1/\tau$), strains are maintained during repeated seeding. Successive seeding experiments were performed as follows: amyloid polymerizations of rPrP were obtained at 0.4 mg/ml in buffer B at room temperature in a 96-well plate. A set of polymerization was first performed without seeding and two preparations with very different characteristics (*i.e.* Maximum fluorescence, rate of polymerization and lag time) were selected (panel A). They were called AH1 (panel A, High fluorescence, sample 1) and AL1 (panel A, low fluorescence, sample 1).
Three aliquots of each were used to seed polymerizations with the same concentration of rPrP (0.4 mg/ml) in the same buffer B. Three independent seeding were done and presented in panel B. BH1, BH2 and BH3 were obtained by seeding with AH1 and BL1, BL2 and BL3 were obtained by seeding with AL1.
Experiments were carried on by seeding polymerization with preparation BH1 and BL1. The kinetics obtained is presented in panel C.
Finally preparation CH1 and CL1 were used to seed a last polymerization, the kinetics of which are presented in panel D.

1.3.8 For prion, fibril nucleation and elongation do not involve similar molecular mechanisms

A consequence of the predominance of the nucleus directed polymerization could be a discrepancy between kinetic parameters polymerization and nucleus formation dynamics. Previous studies of amyloid formation *in vitro* using insulin, glucagon, β2-microglobuline and different variants of Aβ (1-40) as model systems have shown that the length of the lag time and the elongation rate are correlated [73, 118, 177]. To determine whether this is the case for the rPrP used here, the elongation rate ($1/\tau$) and the lag time (T_{lag}) for individual samples of some variants studied were plotted in Figure 1.10. As expected from the model deduced from the previous experiments, the results revealed a complete absence of correlation between these two parameters, suggesting a predominance of nucleation parameters in the determination of T_{lag}. This observation indicates a different mechanism of trans-conformation of the monomer during fibril nucleation and elongation. This result seems completely different from those obtained with other peptides and proteins [73, 118, 177], suggesting that prion fibrillation takes a specific way not common to other amyloid formation. However, this is not a fundamental discrepancy but only a different experimental point of view (see Discussion below).

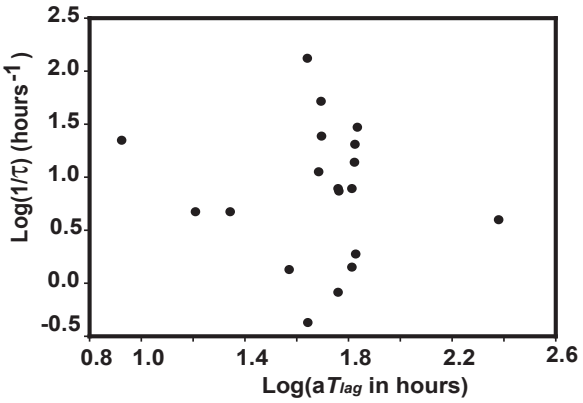

Figure 1.10: Under the experimental conditions used, no correlation between apparent rate of polymerization ($1/\tau$) and T_{lag} can be observed. Kinetics of amyloid polymerization of rPrP at 0.4 mg/ml in buffer A at room temperature was obtained in a 96-well plate.

1.4 Discussion

Although prion protein aggregation has been studied for quite a long time, a number of fallacies persist. Probably the most notable is the assumption that a lag time in the kinetics represents a nucleation phase and that the end of such a lag corresponds to cessation of nucleation. This idea was challenged by experimental results obtained by numerous authors that reveal a linear dependency of the T_{lag} with monomer concentration not exceeding a

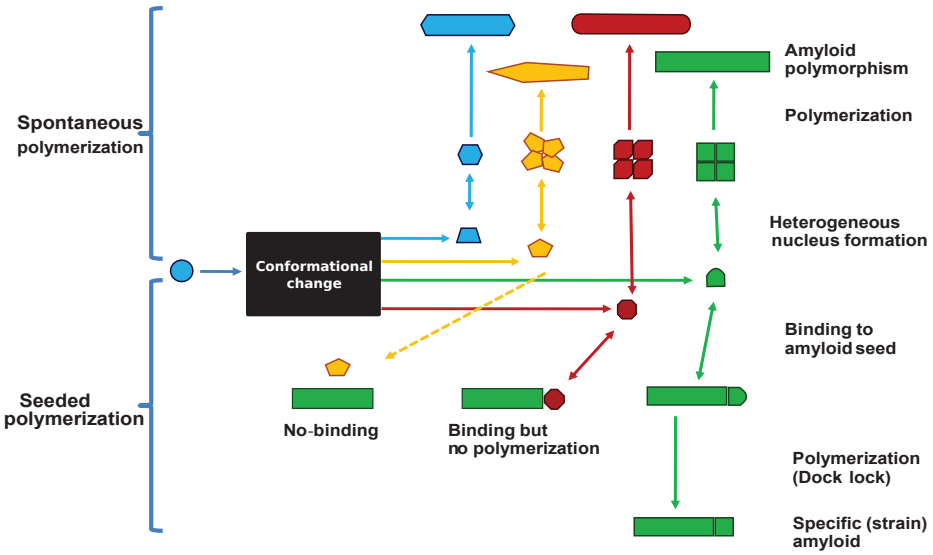

Figure 1.11: Model of prion amyloid formation. Amyloidogenesis of prion protein *in vitro* is a nucleation-dependent polymerization process. However, nucleation is not the main determinant of the lag time, another mechanism should be postulated to explain the weak dependency to the initial concentration of monomers and the residual lag time observed during seeded polymerization. This mechanism is symbolized by a black box and some hypotheses on its nature are proposed in the Discussion. The diversity of the amyloids obtained [207] with the same purified prion protein implies the genesis of different conformers of the monomer, but only the corresponding conformer can react with a precise amyloid used for seeding. This hypothesis would explain not only the heterogeneity of amyloids but also the perpetuation of the strains and results presented here (Figure 1.6 panel C) that has shown an inverse dependency of the lag time with initial concentration at constant seed.

nucleus size of $n \simeq 2$. This result, also found for some other amyloid-forming proteins, is challenging for the nucleation theory of prion that was introduced to explain very long delay before onset of the disease. *In vitro*, this low number of monomers found in the nucleus was generally attributed to an accumulation of large off-pathway species whose formation is competitive with the on-pathway processes that leads to amyloid [16, 186, 201]. However, in many cases off-pathway appears as an *ad hoc* hypothesis that was difficult to sustain by experimental results, the evidence of odd structures on electron microscopic image cannot be unambiguously interpreted as off-pathway. In some cases, a more complex pattern of the polymerization process was used to explain the complex dynamics of amyloid formation, as for instance the 'Nucleated Conformational Conversion' (NCC) of yeast prion element [PSI+] [196] or the dispersed phase-mediated fibrillogenesis (PMF) for amylin [170]. In the case of hamster rPrP polymerized *in vitro* , we found no kinetic evidence for an off-pathway, thus, we proposed that an additional path, on-pathway, is necessary to explain the results observed, see Figure 1.11 for a schematic representation. This is probably a first step, before nucleation, because we showed that seeded polymerization begins after a delay (3h when considering our experimental conditions) that can be interpreted as the generation of active monomers, resulting probably from a change in

spatial structure. Thus, the results presented here can be explained by a complex mechanism that directs conformational changes leading to structural competent monomers. Because the conformational change takes about 3h under the experimental conditions we used here; it cannot be a simple protein 'breathing' that needs only a small fraction of a second as for instance in polyglutamine [221]. In the model depicted in Figure 1.11, this step is symbolized by a black-box. Unconventional initiation steps of the reaction preceding polymerization have been proposed to explain complex behavior in amyloidogenesis. In the case of polyglutamine this was interpreted as a simple conformational change [221], but, in this model, seeding results in a complete disappearance of the T_{lag}. For α-synuclein the dynamics was interpreted as a fibrillation process in which oligomeric granular species turn into amyloid fibrils through concerted lateral association of the preformed granules [21], amylin polymerization was also shown by ATF microscopy to result from the association of oligomers [89]. Evidence of the existence of micelles during the fibrillogenesis of β-amyloid peptide has also been published [145, 192]. Taken into account the results we present, we suggest that the time before polymerization is linked to the production of multiple conformations. The molecular mechanisms that sustain this process in the case of hamster rPrP are under investigation.

Structural heterogeneity of the amyloid polymerized from a highly purified protein is a well-established fact [86, 88, 156, 176]. A cross-β sheet structure set up the core of amyloid protofilaments that represents the filamentous substructures of mature fibrils. Although the basic structural arrangement of the cross-β structure is conserved for different fibrils, there are different possibilities for them to pack into the three-dimensional fibril structure. Such variable protofilament arrangements can give rise to several distinct amyloid fibril morphologies that were recently unraveled at the atomic level [223]. Structurally polymorphic amyloid fibrils are not only reported for *in vitro* preparations. Examination of several tissue-extracted amyloid fibrils shows also significant structural polymorphism [110]. In prion diseases, the strain phenomenon has been correlated with difference in structure of the associated amyloid [20, 53, 173, 206], and it was recently demonstrated that *in vitro* built specific amyloid conformations sustained new phenotypic strains [48]. However, to generate these different structures, Colby et al. [48] used different conditions, decreasing urea, and/or temperature. But, we show here that structural diversity can also be generated under the same environmental conditions, a phenomenon already observed for some other amyloids [86, 156]. We made a link between the heterogeneity of structures and the polymerization dynamics. We propose that the different parameters (*i.e.* the polymerization rate and the sensitivity to agitation) are selected during nucleus formation. The important lag time heterogeneity observed (see Figure 1.4) suggests that the first nucleus formed determines the characteristics of the dynamics of polymerization that are encrypted in the amyloid structure. When built, the selected structure propagates because it overcomes nucleation, and then fibril morphology is propagated to daughter fibrils by a template dependent mechanism. Such self-propagating fibril structure represents the structural basis of multiple strains of mammalian prion diseases.

It was observed during serial passage that synthetic prion went to a gradual adaptation with decreasing incubation period [48, 137], and we observed a similar phenomenon by successive seeding that reduced T_{lag} and increased polymerization rate. Two interpretations

can be proposed:

1. selection of the best adapted structure, *i.e.* those that multiply the most rapidly under the buffer conditions used

2. an adaptation of the structure, for example by extending cross-β structure.

These two explanations are not mutually exclusive. Furthermore, the decrease in the lag phase during serial passaging clearly goes against the conformational change hypothesis and argues for simple nuclear heterogeneity. However, to explain the long incubation period, Colby et al. [48] suggested that infectious amyloid is "contaminated" by a so-called intermediate (rPrP*) unfolded protein. From our results it can be proposed that a mixture of "strains" was obtained reducing the quantity of the most infectious strain.

Under the experimental conditions used in this work, there is no evident correlation between lag time and maximal rate, see Figure 1.10. This observation appears in contradiction with previous reports [73, 118, 153, 228]. Indeed, these authors have observed that the lag time is generally well correlated with the inverse of the maximal growth rate. This correlation did not appear under the experimental conditions used in our work, but putting the experimental points we have obtained into a more general graph that takes into account many independent experimental works, our results are in agreement with the previous observations [73, 118] (see Supplementary data [3, Figure S8]). This means that, although our results are consistent with the general phenomenon, the specificities of our experiments shed light on a phenomenon not observable when more general aspects are taken into account. According to Knowles *et al.* [118], when secondary nucleation pathways are active, the experimental results are primarily determined by the exponential growth regime that takes place in the initial phase of the reaction. However, the magnitude of the noise on T_{lag} for the same rate of polymerization is a very important factor. If one selects a range of rate value of 2 the T_{lag} can vary as much as 100 times, and reciprocally if one select a small interval of T_{lag}. In other words: enough variability exists in the experimental results to hide important phenomena. This is the case in our experiments. The physico-chemical conditions of polymerization remain very close in the set of experiments we present, mainly if compared with the set of results compiled by Fandrich [73] or Knowles *et al.* [118]. Our experimental approach appears to be more adapted to reveal marginal phenomena while compilation of heterogeneous results evidence more general phenomena. However, this marginal phenomenon allows us to shed light on an important phenomenon of the prion diseases, the production of diversity from homogeneous conditions.

Interesting consequences can be proposed in light of this work:

1. The creation of infectious prions from the recombinant protein has been rather disappointing. Although important successes have been published [33, 48, 61, 137, 217], most of the trials have been unsuccessful, raising the question of the reality of this phenomenon. This suggests that only some preparations are infectious. We show here that different structures can be generated from a unique starting condition. If we accept that a relation exists between structures and strains, our results suggest that only some of

the structural strains are infectious, those presenting a set of dynamics parameters in accordance with the *in vivo* polymerization. Such a set has been theoretically predicted [90] and experimentally observed for yeast prion-like elements [205] and a marked structural difference has been evidenced between infectious and non infectious prion amyloids [222]. A question remains: what are the structural characteristics that lead to infectious amyloids and how to direct *in vitro* experiment to obtain them? Are there only dynamics as proposed [205] for yeast prion, or also structural as proposed for Podospora prion [188, 191].

2. The results presented here reveal that many different amyloid structures can be obtained with a highly purified prion protein. Changing polymerization conditions modifies the set of possible structures, and, under a single defined condition this set seems to be very large. This means that probably a huge amount of possibilities is open for new infectious amyloids emergence. As pointed out by C. Soto [200], the possibility that a new amyloid based plague could emerge, should be taken seriously into account.

Chapter 2

A micellar on-pathway intermediate step explains the kinetics of prion amyloid formation

Ce chapitre fait suite au précédent qui émet l'hypothèse de l'existence d'un intermédiaire dans la polymérisation *in vitro* de la protéine prion. Dans ce chapitre, cet intermédiaire est identifié expérimentalement comme une structure micellaire, génératrice de la trans-conformation de la protéine prion. On construit un modèle permettant de modéliser *a priori* cet intermédiaire ainsi que la polymérisation et la fragmentation des polymères. On compare ensuite le modèle ainsi construit avec des données expérimentales pour le valider. Ce travail est issus d'une collaboration avec l'équipe de J.-P. Liautard (INSERM) et sera prochainement soumis pour publication.

2.1 Introduction

Transmissible spongiform encephalopathies, or prion diseases, are a group of fatal neurodegenerative disorders of humans and animals. The pathogenic process is typically associated with conformational conversion of a cellular protein, called prion or PrP^{C}, to a misfolded isoform, called PrP^{Sc}. The 'protein-only' model asserts that this rogue PrP^{Sc}represents the infectious prion agent, self-propagating by binding $PrP^{C}$and inducing its conversion to the abnormal PrP^{Sc} [182, 183]. This scenario was quantitatively described as a nucleation-dependent amyloid polymerization [55, 153]. However, inconsistent results followed from this theory when compared to the *in vitro* polymerization experiments, see Chapter 1 and [16]. Indeed, although the dynamics of polymerization

resemble a simple nucleus-dependent fibrillogenesis, neither the initial concentration dependence nor off-pathway hypothesis fit completely experimental results when compared to theoretical models, refers to Chapter 1. In order to obtain consistency between the experimental results with the nucleus dependent polymerization, we postulate the existence of an on-pathway step, taking place before nucleation. Here we show that micelles are formed, leading to an amyloid competent isoform of the prion protein (denoted by PrP^*) a necessary step to induce nucleation and amyloid polymerization. To analyse the consequences of this hypothesis, we develop a quantitative model with an explicit description of the microscopic processes, and we compare experimental data with the results predicted by the model.

2.2 The context

It is now generally accepted that the prion phenomenon results from an amyloid polymerization after an initial nucleus formation in the very early phase of protein aggregation. Models based on nucleation-dependent polymerization [74, 135, 179] describe a molecular mechanism leading to the formation of large protein aggregates, first by involving thermodynamically unfavourable steps that become favourable when the nucleation kinetic barrier is reached. A striking consequence of these models, is the unfavourable first steps can be bypassed by seeding with preformed polymers. However, due to the transient nature of the initial nucleus, our knowledge of the interactions that form this initial structure is very sparse and, as a consequence, the understanding of species allowing the prion proteins to overcome the strong kinetic barrier to form a specific amyloid conformation is highly limited [196]. This may have led to one of the most notable persisting fallacy which claims that the lag phase of prion proliferation, defined as the required phase for the nucleus formation [55, 97], reflects the unfavourable nucleation phase. This idea was challenged by experimental results obtained by numerous authors who revealed a linear dependence of the lag time (denoted by T_{lag}) to monomer concentration not exceeding a nucleus size of about 2 monomers, see Chapter 1 and [16]. This result, also found for some other spontaneous amyloid-forming proteins [54], was generally attributed to an accumulation of large off-pathway species whose formation is competitive with the on-pathway processes that lead to amyloid [16, 180]. However, in the case of hamster rPrP[1] polymerized *in vitro*, we previously found no kinetic evidence for an off-pathway, see Chapter 1. Consequently, we propose that an additional on-pathway step is necessary to explain the results observed. We hypothesize that this new stage stands very likely for a first step. It would occur before nucleation, because experimentally, we were able to show that seeded polymerization always begins after a time delay that can be interpreted as the time needed to generate active monomers, see Chapter 1. In order to find out what types of structures could be involved, we have performed a time dependent electron microscopic analysis during polymerization of hamster rPrP. Few minutes after dilution into polymerization buffer, we observed spherical structures looking like rigid micelles, see Figure 2.1 panel A and 2.2). The size of these spheres was heterogeneous with a mean around 30

[1]Recombinant Syrian Hamster Prion Protein 90-231.

nm. The size distribution fit well with a log normal distribution, see Figure 2.1 panel B. A sphere of 30 nm diameter reaches a surface area of around 3000 nm^2, the rPrP have a width of about 1.5 to 2 nm^2 thus the sphere contains about 1000 proteins on its surface. In order to ensure that these structures are formed of rPrP, we decided to label them with antibodies. This method clearly identified spheres consisting of rPrP in Figure 2.3.

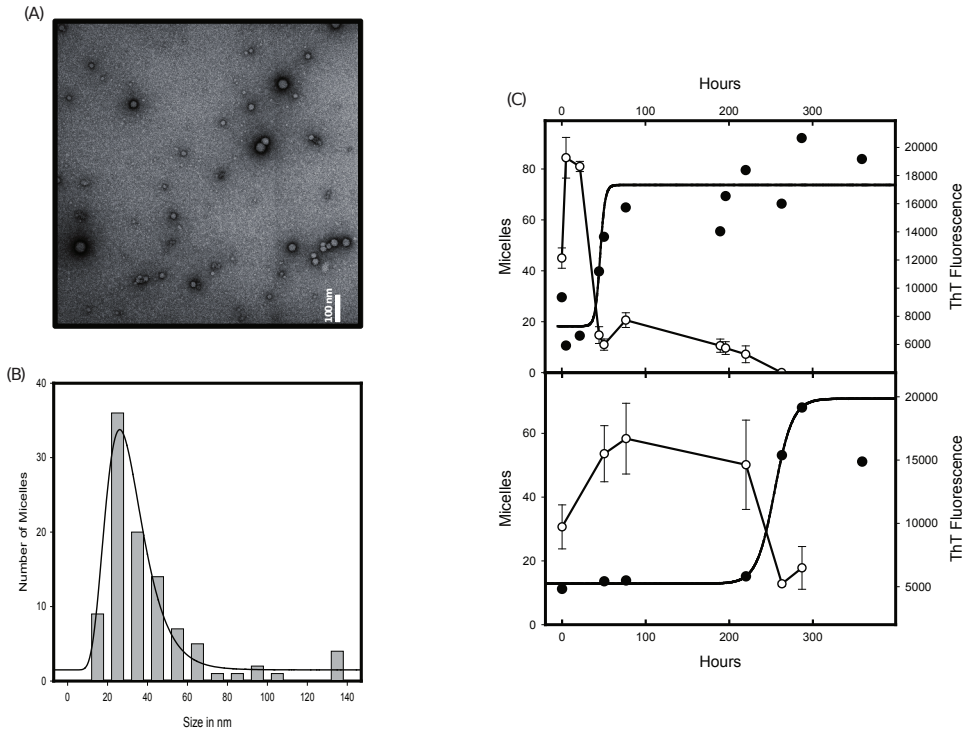

Figure 2.1: Micelle-like structures precede amyloid fibrilles formation. (A), Electron microscopy view of the rPrP^C few minutes after solubilisation in buffer B, see Annexes B and C. Samples were adsorbed on carbon/formvar film and negatively stained by 2% uranyl-acetate, and examined on a Jeol 1200 EX. (B), Diameter measurement of the micelles observed as described in item A. (C), Comparison of the dynamics of micelles and amyloids. Amyloid formation was measured by fluorescence of ThT and micelles number counted directly on arbitrarily selected grids observed at the same (top in buffer B and down in buffer C).

In chapter 1, we showed that polymerization kinetics could not be explained by the existence of an off-pathway. Thus an important question remains: what exactly is the role of micelles in the polymerization mechanism. Consequently, we decided to analyse the evolution of the micelle quantity during polymerization kinetics. Qualitative analysis using electron microscopy revealed that the number of micelles is important a few minutes after dilution into polymerization buffer, and then rapidly decreases when fibrils are formed, see

[2]Thanks to Protein Workshop v1.0 and PDB ID 1B10.

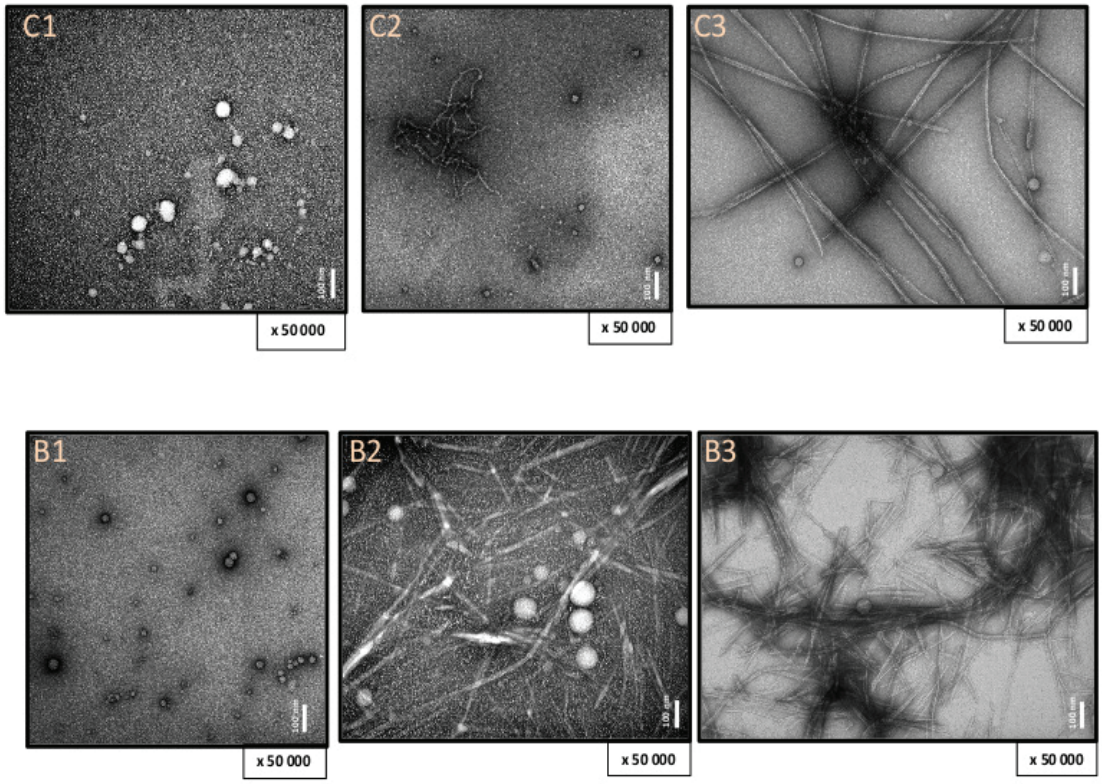

Figure 2.2: Transmission electron microscopy's views of the experiments at different times in two differents buffers, C and B. It clearly shows micelles (spherical structures) and fibrils of PrP^{Sc} (rod-like structures).

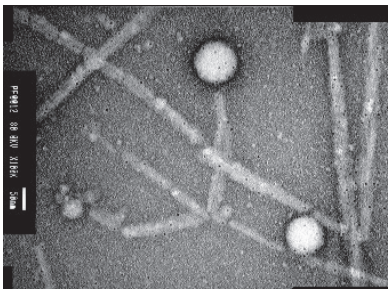

Figure 2.3: Characterization by anibodies of micelles (spherical structures).

Figure 2.1 panel C. A semi-quantitative analysis of the amount of round shape structures suggested a precursor relationship between the micelles and fibrils. This was established in two different buffers exhibiting very different lag phase and thus showing that it is very likely a common feature of *in vitro* prion polymerization.

2.3 The model

2.3.1 Quantitative model of polymerization including on-pathway micelles

To quantitatively analyse the consequences of an on-pathway micelle intermediate, we built an *a priori* model, describing the different steps of microscopic processes involved and their contributions to the reaction. From this microscopic model it is then possible to quantify macroscopic data, such as micelles, polymer and monomer concentration. The model can be detailed into four main parts.

1. The first phase is the formation of dependent PrP micelles through a growth phase with addition and loss of monomers as a cluster dynamic.
2. Second phase, micelles help the transition towards a new structure, denoted by PrP*, that is stabilized in the micelle itself and is released as an isoform monomer.
3. Third phase, this free isoform PrP* is able to nucleate.
4. Fourth phase, nucleation promotes polymerization of PrP$^{\mathrm{Sc}}$and fibrils break when size increases, leading to a rapid polymer growth phase.

The schematic representation of this model is summarized in Figure 2.4 in red box of the panel (a). The whole process, described above and the associate kinetic equations introduced in Table 2.1, can be translated into a mathematical model consisting of a system of ordinary differential equations. This system contains an infinite set of equations for each species, i.e. the two free monomers isoforms, PrP$^{\mathrm{C}}$and PrP*, then an equation for each size (that can theoretically reach infinity) of polymers and micelles. It is possible with this model to describe qualitatively and quantitatively the time evolution of each species, and also macroscopic quantity. In the next section we establish this model.

2.3.2 Micelle dynamics and PrP* monomer formation.

We propose a mathematical model that incorporates the micellar on-pathway intermediate step, presented in Figure 2.4 panel (a) and Table 2.1. We assume that micelles are formed following a cluster dynamics with conformational rearrangement which leads to PrP* isoforms. The PrP^C monomers interact with a micelle M_i of size i, by adding monomers into a micelle at a rate $a_i \geq 0$ depending on the number i of monomers in the micelle. On the other hand, a micelle releases PrP^C monomers at a depletion rate $b_i \geq 0$. The PrP* isoform monomers have the same dynamics as PrP^C, with a_i^* and b_i^* non negative reaction rates, respectively for addition and loss of transconform monomers in a micelle of size i. In the equations below, we denote by m_1 the concentration of PrP^C monomers and m_i the concentration of micelles of size i for $i \geq 2$, where 2 stands for the critical micelle size. Moreover, we denote by p_1 the concentration of PrP* isoform of the protein. The model deals with concentrations thus we consider an infinite number of monomers and

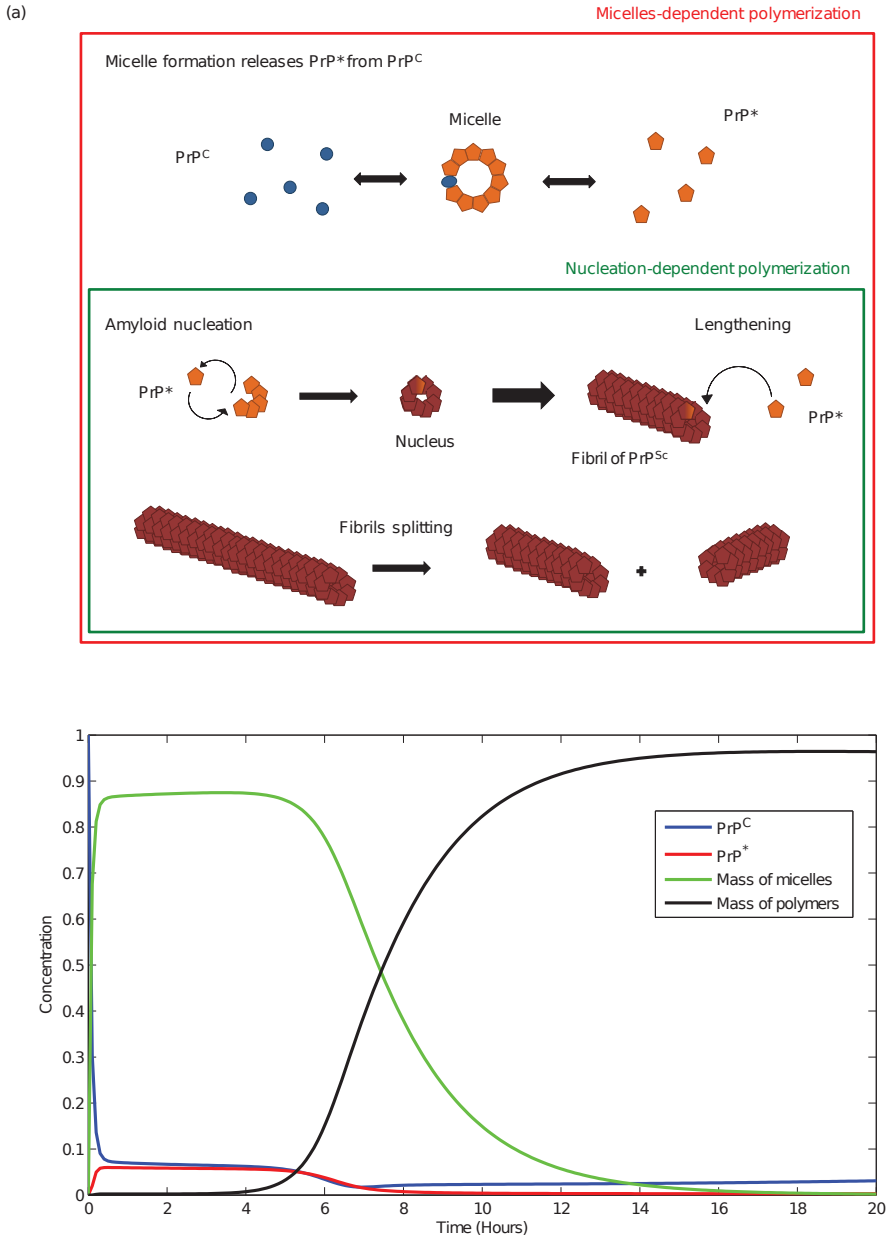

Figure 2.4: A mathematical model describing the micelle and amyloid dynamic. a, Schematic representation of the model associated to the kinetic equations in Table 1. The blue spheres represent the PrPC monomers. In yellow, the PrP* stabilized by micelles. In red, the PrPSc polymers, binding PrP* at its ends and are able to split. b, Qualitative normalized dynamics of the model.

Description	**Reaction scheme**	**Reaction fluxes**
Micelles formation	$M_1 + M_i \underset{b_{i+1}}{\overset{a_i}{\rightleftharpoons}} M_{i+1}$	$J_i = a_i M_1 M_i - b_{i+1} M_{i+1}$
and PrP* released	$M_{i+1} \underset{b^*_{i+1}}{\overset{a^*_i}{\rightleftharpoons}} M_i + P_1$	$J^*_i = a^*_i P_1 M_i - b^*_{i+1} M_{i+1}$
Amyloids polymerization	$P_1 + P_i \underset{k^-_{i+1}}{\overset{k^+_i}{\rightleftharpoons}} P_{i+1}$	$H_i = k^+_i P_1 P_i - k^-_{i+1} P_{i+1}$
Amyloids splitting	$P_i \xrightarrow{r_i \kappa_{i,j}} P_{i-j} + P_j$	$F_i = -r_i P_i + \sum_{j \geq i+1} r_j \kappa_{j,i} P_j$

Table 2.1: Hereinbefore, we used the following notations for species: M_1 stands for the $\mathrm{PrP^C}$monomers, then M_i is the micelles consisting of i monomers and P_1 for the $\mathrm{PrP^*}$, whereas P_i is the polymers of size i. Kinetic rates or defined in Sections 2.3.2 and 2.3.3. provide a polymer of size j and another of size $i - j$.

micelles (at least a very large number) thus we assume that the size of micelles could be infinitely large. These assumptions lead us to set an infinite system of ordinary differential equations over the size of micelles and monomers,

$$\begin{cases} \dfrac{dm_1}{dt} = -J_1 - \displaystyle\sum_{i \geq 1} J_i, \\ \dfrac{dm_i}{dt} = J_{i-1} - J_i + J^*_{i-1} - J^*_i, \qquad i \geq 2, \\ \dfrac{dp_1}{dt} = -J^*_1 - \displaystyle\sum_{i \geq 1} J^*_i, \end{cases} \tag{2.1}$$

where the flux J_i accounting for the PrP^C, and J^*_i for the $\mathrm{PrP^*}$, are given by

$$J_i = a_i m_1 m_i - b_{i+1} m_{i+1}, \quad \text{and} \quad J^*_i = a^*_i p_1 m_i - b^*_{i+1} m_{i+1}.$$

with $J^*_1 = a^*_1 p_1 p_1 - b^*_2 m_2$ and neglecting the $\mathrm{PrP^*}/\mathrm{PrP}^C$ interaction. Indeed, we suppose that in the free form, monomers are much more numerous in the PrP^C isoform than the $\mathrm{PrP^*}$ one.

2.3.3 $\mathrm{PrP^{Sc}}$ polymerization and the whole model.

Let us describe here the amyloid (or in other words polymer) dynamics. First, a growth phase is defined by polymerization of the $\mathrm{PrP^*}$ isoform with polymers of size i at a rate $k^+_i \geq 0$. Second, the depolymerization of $\mathrm{PrP^*}$ monomers from a polymer of size i happens at a rate $k^-_i \geq 0$. Finally, the fragmentation process involves at a non-negative splitting rate r_i. When it splits, a polymer of size $i \geq 2$ leads to two new polymers of size j and $i - j$ with a probability given by $\kappa_{j,i} \geq 0$. To be consistent with the fact that a polymer splits equally into two polymers and the preservation of the total number of monomers,

the $\kappa_{i,j}$'s have to satisfy $\kappa_{j,i} = \kappa_{i-j,i}$, moreover $\kappa_{j,i} = 0$ when $j \geq i$ and,

$$\sum_{j=0}^{i-1} \kappa_{j,i} = 1, \text{ for any } j \leq i.$$

Thus, the evolution equations on the concentrations p_i for each polymers of size $i \geq 2$ are given by

$$\frac{dp_i}{dt} = H_{i-1} - H_i - r_i p_i + 2 \sum_{j \geq i+1} r_j \kappa_{i,j} p_j,$$

with

$$H_i = k_i^+ p_1 p_i - k_{i+1}^- p_{i+1}, \qquad \text{for } i \geq 1.$$

The size of polymers can be infinitely large for the same reason as the micelles are. As a consequence of polymerization/depolymerization, equation on p_1 in (2.1) has to be modified and the system is complete with the equations on p_i which reads,

$$\begin{cases} \dfrac{dm_1}{dt} = -J_1 - \displaystyle\sum_{i \geq 1} J_i \ , \\ \dfrac{dm_i}{dt} = J_{i-1} - J_i + J_{i-1}^* - J_i^* \ , \quad \text{for any } i \geq 2, \\ \dfrac{dp_1}{dt} = -J_1^* - \displaystyle\sum_{i \geq 1} J_i^* - H_1 - \sum_{i \geq 1} H_i + 2 \sum_{j \geq 2} r_j \kappa_{1,j} p_j \ , \\ \dfrac{dp_i}{dt} = H_{i-1} - H_i - r_i p_i + 2 \displaystyle\sum_{j \geq i+1} r_j \kappa_{i,j} p_j \ , \quad \text{for any } i \geq 2. \end{cases} \tag{2.2}$$

with initial data,

$$m_i(0) = m_i^0 \geq 0 \ \text{ and } \ p_i(0) = p_i^0 \geq 0, \text{ for any } i \geq 1.$$

We consider a closed system, without degradation nor production of monomers, thus it is expected that the model preserves the total mass of monomers that reads,

$$\frac{d}{dt} \sum_{i \geq 1} i m_i(t) + \frac{d}{dt} \sum_{i \geq 1} i p_i(t) = 0, \text{ for any } t \geq 0,$$

which is formally satified. All the parameters of the system are summarize in Table 2.2.

2.3.4 General assumptions.

The model mentioned above is used to fit data, that is why we have to give assumptions on rates to obtain a physical and biological relevant model. In the case of micelles, we assume as in [22] that the assimilation rates a_i and a_i^* are constant for any $i \geq 1$ and we denote them by a and a^* respectively, both of them being positive constants. The depletion rate

Parameters	Description
m_1	Concentration of PrP^C monomers
m_i	Concentration of micelles of size $i \geq 2$
p_1	Concentration of PrP^* monomers
p_i	Concentration of polymers of size $i \geq 2$
a_i	Assimilation rate for PrP^C monomers into a micelle of size i
b_i	Depletion rate for PrP^C monomers by a micelle of size i
a_i^*	Assimilation rate for PrP^* monomers into a micelle of size i
b_i^*	Depletion rate for PrP^* monomers by a micelle of size i
n	Critical size of the stable nucleus for polymer
k_i^+	Elongation rate of a polymer of size i
k_i^-	Depolymerization rate of a polymer of size i
r_i	Fragmentation rate of a polymer of size i
$\kappa_{i,j}$	Size distribution kernel after splitting

Table 2.2: Overview of the parameters used in the model.

have to account for the spherical structure of a micelle, with its radius linked with the number of monomers that composes it. In [22], this term is given under the form

$$b_0 e^{Ai^{-1/3}+Bi^{1/3}}, \text{ for } i \geq 2,$$

which is derived from chemical potential for one species of monomers. For the sake of simplicity we interpret differently this form and adapt it to this model. First, we suppose that in the smallest size, micelles do not transconformed PrP^C monomers into amyloid competent isoform. We justify this assumption by thermodynamical constraints, assumed to be stronger in the greatest size. As the term in $i^{-1/3}$ is dominant for small micelles, we let

$$b_{i+1} = b_0 e^{Ai^{-1/3}}.$$

The term in $i^{1/3}$ is dominant in the greatest size, thus this part is taken into account for the depletion of PrP^*,

$$b_{i+1}^* = b_0^* e^{Bi^{1/3}}.$$

Now, for polymerization, we consider a constant polymerization rate $\tau > 0$, such that k_i^+ is equal to τ for any $i \geq 1$, and a depolymerization rate k_i^- equal to a constant $d > 0$ for $i < n$, where n is the nucleus size and equal to 0 for longer polymer, $i \geq n$, *i.e.* polymerization becomes an irreversible process after the nucleus is reached. Moreover, a linear splitting rate is taken, that is $r_i = \beta(i-1)$ with $\beta > 0$ and a uniform kernel given by

$$\kappa_{j,i} = \begin{cases} \frac{1}{i-1}, & \text{if } i > j > 0 \\ 0, & \text{otherwise.} \end{cases}$$

Thus the fluxes, in the whole system (2.2), read now

$$J_i = am_1m_i - b_0e^{Ai^{-1/3}}m_{i+1}, \quad \text{and} \quad J_i^* = a^*p_1m_i - b_0^*e^{Bi^{1/3}}m_{i+1}.$$

and

$$H_i = \tau p_1 p_i - dp_{i+1}, \text{ and } i < n, \quad \text{and} \quad H_i = \tau p_1 p_i, \text{ when } i \geq n.$$

with, the fragmentation term given by

$$F_i = -\beta(i-1)p_i + 2\beta \sum_{j \geq i+1} p_j.$$

2.4 Results

2.4.1 Analysis of the experimental results based on this model

A qualitative analysis of the dynamic of micelles and polymers given by the model (see Figure 2.4 at the bottom) corresponds to the one observed in experiments (see Figure 2.1). As expected, the correlation between polymers formation and the decreasing of micelles concentration is connected with the PrP^* formation. For this purpose, we assume in our simulations that PrP^* comes from micelles and does not exist before, *i.e.* its initial concentration is null. Furthermore, this model was built to analyse the lag phase and compares it to data. Several definitions of the T_{lag} exist but they are mostly related to the T_{50}, which is the time when half of the final polymerized mass is reached. One of the definitions links the T_{50} to the lag time by $T_{lag} = T_{50} - 2\tau$, with $1/\tau$ the maximal slope of the sigmoid [135]. This formula is true for a genuine sigmoidal equation, but here we cannot have any analytical solution to the model. Since the half time is better defined and more tractable on data, we used it to analyse results. We focus on three main results provided by the model:

1/ We perform an analysis of the delay before polymerization starts when the experiments are seeded with preformed PrP^{Sc} polymers at different concentrations, note that nucleation steps are bypassed in this case. Previous works [90, 153] predicted the disappearance of the lag phase (Figure 2.5) and expected the half time to go to zero. In Figure 2.6, we can see that these phenomena are absolutely not observed experimentally while, on the other hand, the model we introduced fits correctly the data. Moreover, as expected the half time computed in our model does not converge to zero when the seeding concentration of PrP^{Sc}polymers increases.

2/ Results in Figure 2.6 (at the top) show that the lag phase persists with an increasing concentration of PrP^{C}monomers considering the nucleation case (without seeding). The shape of dependency to the initial condition is preserved, *i.e.* a linear log-log shape, but it remains independent of the nucleus size, Figure 2.7.

3/ In the conventional model of nucleation, if the seeding is postponed, an increase of the T_{50} equal to the delay time before seeding should be observed (at least in the very first

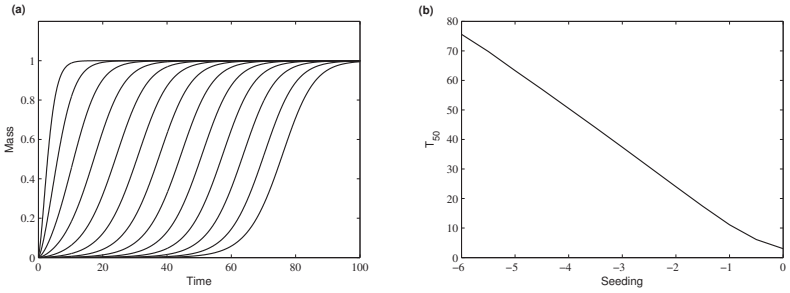

Figure 2.5: Numerical simulation of the model in [153] in *in vitro* conditions. **a,** The normalyzed polymerization shape for different seeding given by $m_0 = 10^{-k}C_0$, the concentration of polymers. Coefficient $k = 0$ varying from 0 to 6 with $C_0 = 0.4$mg/ml the initial concentration of PrP^C. **b,** T_{50} *vs.* seeding associate to the polymerization shape in (a).

hours when the experiment takes place far enough from the T_{lag}). However, this dependency was not observed experimentally and the T_{50} is less than the one expected. This suggests that a phenomenon occur during the early phase without seeding, which accelerates polymerization when nucleus is introduced. Our model explains this phenomenon by formation of the amyloid competent isoform and results are shown in Figure 2.8.

4/ In the next step, we analyse the shape of the maximal speed distribution of polymerization $1/\tau$ as a function of initial concentration. Our simulations appear to be consistent with the experimental data, see Figure 2.9. Taken together these four points, we can conclude that the experimental data corroborate the model. Furthermore, it suggests a simple explanation for the weak dependency of the lag time with initial concentration and it proposes a new interpretation of the overcoming kinetic barrier of the prion protein. *A posteriori*, the microscopic processes involving prion proliferation, built here, describe the observed macroscopic facts.

2.4.2 Evidences for the existence of micelle as an on-pathway

The existence of micelle as an on-pathway during the formation of amyloid *in vitro* leads then to the question of the existence of such intermediate *in vivo*. Indeed, the concentrations of rPrP used to study the *in vitro* polymerization are far above those observed *in vivo* and buffers involved are not compatible with life. But, in the view presented here, micelles play the important role to sustain the conformation that is eligible for the amyloid formation. This suggests that the PrP^Cshould reach a specific conformation to be able to polymerize into amyloid. What happens *in vivo*? It was recently shown

1. that the conformational structure and stability of the recombinant human PrP in a membrane environment are substantially different from those of the free protein in solution [160, 193],

2. that anionic lipids bicelles converted α-helix-rich rPrP to a β-sheet conformation [148],

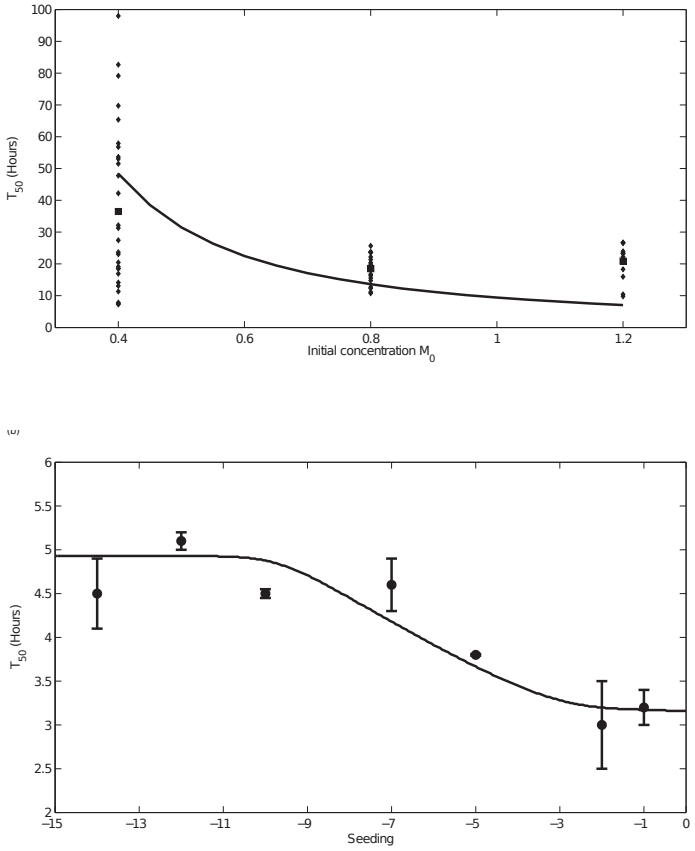

Figure 2.6: T_{50} correlation between the model and experimental results. At the top, diamonds are the T_{50} (in hours) obtain by fitting experimental data with a sigmoid as described in Chapter 1 for initial concentration of PrP^C equal to 0.4, 0.8 and 1.2 mg/ml. Squares are the mean value of the T_{50} while continuous line is the value obtain with the theoretical model. At the bottom, squares stand for the mean T_{50} (in hours) with standard errors obtained for a series of experiments with PrP^{Sc}seeding concentration equal to $10^{-k}M_0$ for k from 1 to 14, with $M_0 = 0.4$ mg/ml, the initial concentration of PrP^C. The continuous line corresponds to the simulations.

3. that lipid is necessary to convert PrP^C to infectious PrP^{Sc} under physiological conditions [217, 218],

4. that the hydrophobic highly conserved middle region of PrP is involved in the interaction with lipid membranes [216], and deletion in this part of the molecule impaired PrPSc induced conversion [219].

This phenomenon was also observed for other amyloid forming peptides [136, 209]. Thus our hypothesis is the formation of mixed-micelles containing phospholipids and rPrP reducing the concentration necessary to reach CMC (Critical Micellar Concentration) under physiological conditions.

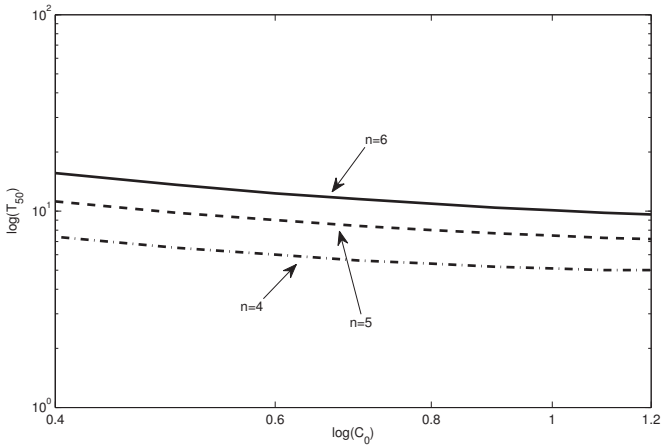

Figure 2.7: The half-time T_{50} *vs.* initial concentration of PrP^C, C_0. It appears that the decreasing rate in log scale of the half-time remains independent on the nucleus size n for the micelles-dependent model which is in opposition with the nucleation-dependent model.

The main characteristic of the *in vivo* formed amyloids is infectiosity and this property is related to the amyloid structure [44]. It is important to remind that most of the amyloids produced *in vitro* are not infectious. However, recently it was shown that addition of phospholipids [218] during *in vitro* polymerization leads consistently to infectious amyloids [61, 217]. Furthermore, it was demonstrated that rPrP proteins interact with membrane phospholipids [193] and this interaction precedes conformational changes [160], a phenomenon also observed for other amyloid forming peptides [136]. Thus our hypothesis is the formation of mixed-micelles containing phospholipids and rPrP, and in such mixed-micelles, as in pure prion micelles, the protein reaches the PrP* conformation competent to generate infectious amyloids.

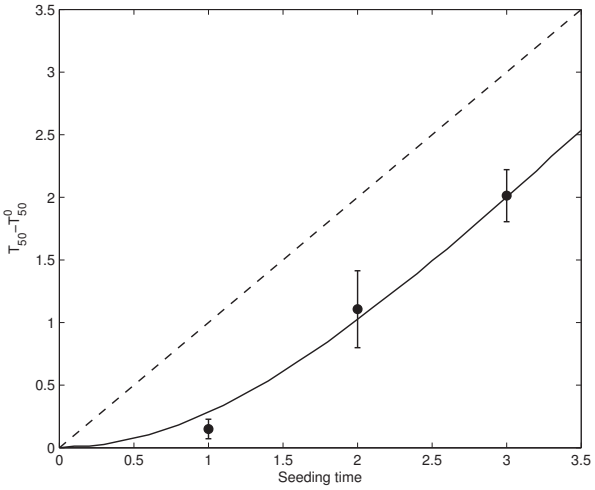

Figure 2.8: Dependency of the T_{50} according to the seeding time. Circle is the mean with standard deviation of the half-time over 3 experiments. Meanwhile, the solid line is the result provided by the model and the dashed line is the theoritical Half-time when pure nucleation-dependent polymerization is considered (without trans-conformation). This experiment is made up of 4 test tubes containing 0.4mg/ml of PrP^C monomers in the same buffer at time $t = 0$. Then, at $t = 0$ the first tube is seeded with preformed polymers this leads to a half-time set as the T^0_{50}. The second test tube is seeded 1 hour later (the seeding time) with the same concentration of polymers and so forth. The T_{50} is supposed to be linearly brought forward (dashed line) according to the seeding time, in the case where nothing happens between the beginning of the experiments and the time when polymers are introduced. Experimentally this time is less than the one expected (circle on the figure). The formation of micelles and trans-conformed monomers at the early phase explains this situation.

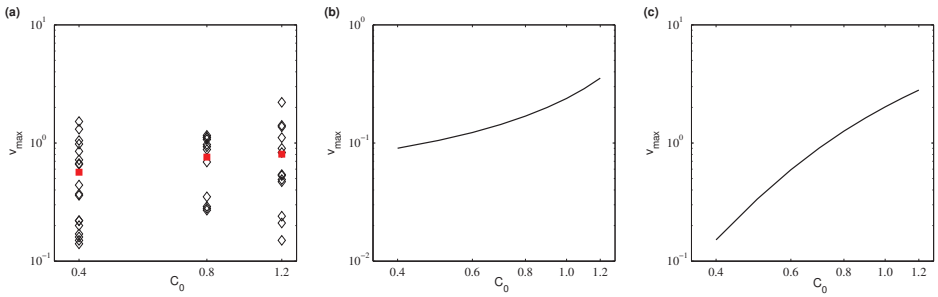

Figure 2.9: Dependency of v_{max} *vs.* C_0, comparison of the two models with experimental results. The greater slope, v_{max}, is the slope at the inflexion point and C_0 is the initial concentration of $\mathrm{PrP}^{\mathrm{C}}$. **a,** Experimental data obtained in different buffer, and the slope is obtained by fitting them with a sigmoidal shape. **b,** Result obtains with the nucleation-dependent model and **c,** with the micelles-dependent model.

Chapter 3

A Discrete Polymerization-Fragmentation Equations with Cluster Pathway

Dans ce chapitre on s'attache à l'analyse mathématique du modèle introduit au chapitre précédent. Celui-ci consiste en un système discret de polymérisation-fragmentation couplé avec un système de Becker-Döring qui décrit l'évolution de deux structures distinctes en compétition. On montre ici l'existence de solutions préservant la masse totale du système couplé, ainsi que la propagation des moments initiaux, suivant la méthode de [Laurençot, *Proc. Edim. Math. Soc. II*, 45 (2002)].

3.1 Introduction

The purpose of this study is to establish the well-posedness of a polymerization-fragmentation model with pathway. The origin of this model takes place in the modelling of prion proliferation. The prion protein is responsible of certain diseases like Creutzfeld-Jackob disease, Kuru or Bovine Spongiform Encephalopathy (Madcow). Classically, There are two known forms of the prion protein, the Prion Protein Cellular denoted PrP^C and the Prion Protein Scrapie, PrP^{Sc}. The monomeric form, PrP^C, is regularly produced in body cell and the pathological isoform PrP^{Sc} exists under polymer form. The PrP^{Sc} polymer is able to induce PrP^C by binding, and to replicate by splitting. This has been first modeled by Masel *et al.* [153] and by Greer *et al.* [90]. In Chapter 1, some inconsistency in the results are high lightened when this theory is confronted to *in vitro* experiments, so that in Chapter 2, we propose an intermediate step which forms an amyloid competent isoform, the PrP^*, of the PrP^C. This intermediate amyloid is able to nucleate and polymerize, leading

to PrP^{Sc} polymerization. Moreover, it can be described as a micelle structure (spherical structure) compared to a cluster, so that we have modeled its dynamic with a Becker-Döring model [10]. Combining these two models leads to the one presented hereinafter. The PrP^{C} monomers are denoted by C_1, the micelles composed of i monomers by C_i, the monomeric PrP^{*} by P_1 and PrP^{Sc} of size i by P_i. The main processes, schematized in figure 3.1, are

- The PrP^{C} forms micelles and is assimilated at a rate a_i in a micelle of size i and released at a rate b_i.
- The PrP^{*} is assimilated at a rate a_i^* in a micelle of size i and released at a rate b_i^*.
- The PrP^{*} forms polymers; the polimerization rate is given by k_i and the de-polymerization rate by d_i.
- The PrP^{Sc} splits at a rate r_i and leads to two polymers of size $i-j$ and j (binary splitting) with a probability $\kappa_{j,i}$.

Thus the model can be written in terms of an infinite system of ordinary differential equations,

$$\begin{cases} \dfrac{dc_1}{dt} = -J_1 - \displaystyle\sum_{i\geq 1} J_i, \\ \dfrac{dc_i}{dt} = J_{i-1} - J_i + J_{i-1}^* - J_i^*, \quad i \geq 2, \\ \dfrac{dp_1}{dt} = -J_1^* - \displaystyle\sum_{i\geq 1} J_i^* - H_1 - \sum_{i\geq 1} H_i + 2\sum_{j\geq 2} r_j \kappa_{1,j} p_j, \\ \dfrac{dp_i}{dt} = H_{i-1} - H_i - r_i p_i + 2\displaystyle\sum_{j\geq i+1} r_j \kappa_{i,j} p_j, \quad i \geq 2, \end{cases} \tag{3.1}$$

completed with given initial data,

$$c_i(0) = c_i^{in} \text{ and } p_i(0) = p_i^{in}. \tag{3.2}$$

The fluxes are defined for any $i \geq 2$ by

$$\begin{cases} J_i = a_i c_1 c_i - b_{i+1} c_{i+1}, \\ J_i^* = a_i^* p_1 c_i - b_{i+1}^* c_{i+1}, \\ H_i = k_i p_1 p_i - d_{i+1} p_i, \end{cases} \tag{3.3}$$

and noting that three reactions are possible to provide a cluster of size 2, we obtain for $i = 1$:

$$\begin{cases} J_1 = a_1 c_1 (c_1 + p_1) - b_2 c_2, \\ J_1^* = a_1^* p_1 (c_1 + p_1) - b_2^* c_2, \\ H_1 = k_1 p_1 p_1 - d_2 p_2. \end{cases} \tag{3.4}$$

Let us note that the problem has to be modeled with such infinite system, because we

Figure 3.1: Schematic representation of the model

do not know *a priori* the maximal size that can be reached by the polymers. Moreover an important fact is that this model could be applied to prion proliferation with an on-pathway, but also for an off-pathway, as the one proposed by Powers and Powers [180]. More generally it can be used for amyloid formation when a clustering pathway is assumed.

In the next section we first state the hypothesis and the main result of existence obtained in this work. Then, in section 3.3 we approach the problem by a finite system and provide some estimates. The last section is devoted to the proof of the main result. The method used here is an application to our model of a powerful method proposed by P. Laurençot in [129] in the context of coagulation-fragmentation equations.

3.2 Main results

We start by investigating the natural functional spaces in which we will search the solutions. First, the total mass of the system (3.1) given by

$$\rho(t) := \sum_{i=1}^{\infty} ic_i(t) + \sum_{i=1}^{\infty} ip_i(t),$$

is expected to be preserved in time, *i.e.* $\rho(t) = \rho(0)$ for any time $t \geq 0$, since there are neither production nor degradation of particles. In fact this is obtained from (3.1) when multiplying each equation by i and summing over i and interverting without justifications the sums. For this reason we want solutions with finite mass, thus we introduce the suitable Banach space

$$X = \left\{ x = (x_i)_{i\geq 1} \subset \mathbb{R} \ : \ \sum_{i=1}^{\infty} i|x_i| < \infty \right\},$$

equipped with the norm

$$\|x\|_X = \sum_{i=1}^{\infty} i|x_i|.$$

Also, we are interested in non-negative solutions. Then, we consider the non-negative cone of X that is the appropriate subset for relevant solutions, namely

$$X^+ = \{x \in X \ : \ \forall i \geq 1, \ x_i \geq 0\}.$$

It has been proved in classical coagulation-fragmentation models (see [99] and references in [129]) that under some coagulation rate the mass conservation breaks down in finite time, *i.e* it exists $t_c < +\infty$ such that $\rho(t_c) < \rho(0)$. This phenomenon is known as *gelation*. Here, this class of rates is avoided by assuming a constant $K > 0$ such that,

$$0 \leq a_i, a_i^*, k_i \leq Ki, \quad \forall i \geq 1. \tag{3.5}$$

Indeed, the gelation is not a relevant case in our biological interests.

Hypothesis on the de-polymerization and fragmentation rates. We assume some weak assumptions on *de-polymerization* rate and fragmentation rate, namely

$$b_i, b_i^*, d_i, r_i \geq 0, \quad \forall i \geq 2, \quad \text{and } r_1 = 0. \tag{3.6}$$

The size distribution kernel for a binary fragmentation has to respect the symmetry and the mass conservation, thus we require:

$$\begin{cases} \kappa_{j,i} \geq 0 \ \forall\, i, j\,, \quad \text{and } \kappa_{j,i} = 0, \forall\, j \geq i, \\ \kappa_{j,i} = \kappa_{i-j,i} \ \forall\, i,\, j, \\ \sum_{j=1}^{i-1} \kappa_{j,i} = 1 \ \forall\, i \geq 2. \end{cases} \tag{3.7}$$

Moreover, as remarked in [65], symmetry and conservation readily lead to

$$2\sum_{j=1}^{i-1} j\kappa_{j,i} = i. \tag{3.8}$$

Assumptions (3.5–3.7) are adapted from the ones made by Ball and Carr in [9, 10] and then by Laurençot in [129], to prove the existence of solution to coagulation-fragmentation model, without any constraint on fragmentation rate, belonging to X.

Definition of a solution. From this framework, we now define what we call a solution to (3.1–3.2).

Definition 3.1. Let $T > 0$ and $c^{in},\ p^{in}$ be two sequences of real numbers. A couple (c, p) is a solution to (3.1–3.2) on $[0, T]$, if $c = (c_i)_{i\geq 1}$ and $p = (p_i)_{i\geq 1}$ are two sequences of continuous functions on $[0, T]$ such that:

i) $\sum_{i\geq 1}(a_i + a_i^*)c_i$ and $\sum_{i\geq 1} k_i p_i$ belong $L^1(0, T)$,

ii) $\sum_{i\geq 2}(b_i + b_i^*)c_i$ and $\sum_{i\geq 2} d_i p_i$ belong $L^1(0, T)$,

iii) $\sum_{j\geq i+1} r_j \kappa_{i,j} p_j$ belong to $L^1(0, T)$ for any $i \geq 1$,

iv) and it holds for any $t \in [0, T]$:

$$\begin{cases} c_1(t) = c_1^{in} - \displaystyle\int_0^t \Big(J_1 + \sum_{i\geq 1} J_i\Big) ds, \\ c_i(t) = c_i^{in} + \displaystyle\int_0^t \left(J_{i-1} - J_i + J_{i-1}^* - J_i^*\right) ds, \quad i \geq 2, \\ p_1(t) = p_1^{in} - \displaystyle\int_0^t \Big(J_1^* + H_1 + \sum_{i\geq 1} (J_i^* + H_i) + \sum_{i\geq 2} r_i \kappa_{1,j} p_j(s)\Big) ds, \\ p_i(t) = p_i^{in} + \displaystyle\int_0^t \Big(H_{i-1} - H_i - r_i p_i(s) + \sum_{j\geq i+1} r_j \kappa_{i,j} p_j(s)\Big) ds, \ i \geq 2. \end{cases} \tag{3.9}$$

The points i)–iii) ensure that the righ-hand-side of (3.9) is well defined.

Existence of solutions. Before stating the main result, we need to introduce a class of functions U that enjoy some properties, namely:

$$(\mathrm{P}_1)\quad \left|\begin{array}{l} U \in \mathcal{C}^1([0,+\infty)) \cap W^{2,\infty}_{\mathrm{loc}}(0,+\infty) \text{ and,} \\ U \text{ is non-negative and convex with } U(0)=0, \\ U' \text{ is concave and } U'(0) \geq 0. \end{array}\right.$$

$$(\mathrm{P}_2)\quad \left|\begin{array}{l} U \in \mathcal{C}^2([0,+\infty)) \text{ and,} \\ U \text{ is non-negative and convex with } U(0)=0, \\ U' \text{ is convex with } U'(0)=0, \\ \text{It exists } k_U > 0, \text{ such that } \forall x \geq 0,\ U'(2x) \leq k_U U'(x). \end{array}\right.$$

$$(\mathrm{P}_\infty)\quad \left|\begin{array}{l} U \text{ satisfies } (\mathrm{P}_1) \text{ and,} \\ \lim\limits_{x\to+\infty} U'(x) = \lim\limits_{x\to+\infty} \dfrac{U(x)}{x} = +\infty. \end{array}\right.$$

Remark 3.1. We remark as in [129] that $U : x \mapsto x^\alpha$ satisfies (P_∞) when $\alpha \in (1,2]$ and (P_2) when $\alpha \geq 2$.

The existence of a solution reads:

Theorem 3.2 (Existence and moments conservation)**.** *Under hypothesis (3.5–3.7). If c^{in} and p^{in} both belong to X^+, then for any $T > 0$ there exists at least one couple (c,p) solution to (3.1–3.2) on $[0,T]$ in the sense of the definition 3.1, such that*

$$c \text{ and } p \in C([0,T];X^+)$$

and for any $t \in [0,T]$

$$\|c(t)+p(t)\|_X = \|c^0+p^0\|_X.$$

Finally, if there exists U satisfying (P_1) or (P_2) with $\sum_{i\geq 1} U(i)(c_i^{in}+p_i^{in}) < +\infty$ then

$$\sup_{t\in[0,T]} \sum_{i\geq 1} U(i)(c_i(t)+p_i(t)) < +\infty.$$

Remark 3.2. The last result in the above theorem states in other words that if the initial condition has a finite moment, the solution preserves this property.

Remark 3.3. This theorem is adapted from [129, Theorems 2.3 and 2.5] to our model. But in our result we have the continuity in time of c and p into X independently.

From now on we will assume that the different rates are given and enjoy properties (3.5–3.7). Also, we always refer to K for the constant given by (3.5). Moreover we assume that the initial condition c^{in} and p^{in} are fixed such that

$$(c^{in},p^{in}) \in X^+ \times X^+.$$

The next section is devoted to the study of a finite approximation system. We state existence and additional estimates on this approximate problem, before proving theorem 3.2 in the section right after, by passing to the limit in the size N of our approximation.

3.3 Finite approximation

As done naturally in [9, 10, 129], we first study the finite approximation of the system before going to the limit. Precisely, the system of size $N \geq 3$ is written as follow

$$\begin{cases} \dfrac{dc_1^N}{dt} = -J_1^N - \displaystyle\sum_{i=1}^{N-1} J_i^N, \\ \dfrac{dc_i^N}{dt} = J_{i-1}^N - J_i^N + J_{i-1}^{*\,N} - J_i^{*\,N}, \quad 2 \leq i \leq N-1, \\ \dfrac{dc_N^N}{dt} = J_{N-1}^N + J_{N-1}^{*\,N}, \\ \dfrac{dp_1^N}{dt} = -J_1^{*\,N} - \displaystyle\sum_{i=1}^{N-1} J_i^{*\,N} - H_1^N - \sum_{i=1}^{N-1} H_i^N + 2\sum_{j=2}^{N} r_j \kappa_{1,j} p_j^N, \\ \dfrac{dp_i^N}{dt} = H_{i-1}^N - H_i^N - r_i p_i^N + 2 \displaystyle\sum_{j=i+1}^{N} r_j \kappa_{i,j} p_j^N, \quad 2 \leq i \leq N-1, \\ \dfrac{dp_N^N}{dt} = H_{N-1}^N - r_N p_N^N, \end{cases} \tag{3.10}$$

with the initial condition given for $i = 1, \ldots, N$ by

$$c_i^N(0) = c_i^{in}, \text{ and } p_i^N(0) = p_i^{in}. \tag{3.11}$$

and where J_i^N, $J_i^{*\,N}$ and H_i^N are defined as in (3.3) and (3.4), replacing c_i and p_i by c_i^N and p_i^N. We now state a result of existence and uniqueness for system (3.10) - (3.11), with some useful properties for the next study.

Lemma 3.3. *Let $N \geq 3$, then there exists a couple (c^N, p^N) with $c^N = (c_i^N)_{1 \leq i \leq N}$ and $p^N = (p_i^N)_{1 \leq i \leq N}$ such that*

$$c^N \text{ and } p^N \text{ belong to } C^1\left([0,\infty), \mathbb{R}_+^N\right),$$

is the unique solution to (3.10) – (3.11)*. Moreover, for any $(\varphi_i)_i \in \mathbb{R}^N$ and $t \geq 0$ it holds*

$$\frac{d}{dt}\sum_{i=1}^{N} \varphi_i \left(c_i^N + p_i^N\right) = \sum_{i=1}^{N-1} \left(\varphi_{i+1} - \varphi_i - \varphi_1\right)\left(J_i^N + J_i^{*\,N} + H_i^N\right) + \sum_{i=2}^{N} \left(2\sum_{j=1}^{i-1} \varphi_j \kappa_{j,i} - \varphi_i\right) r_i p_i^N, \tag{3.12}$$

and

$$\sum_{i=1}^{N} i \left(c_i^N + p_i^N\right) = \sum_{i=1}^{N} i \left(c_i^{in} + p_i^{in}\right). \tag{3.13}$$

Proof. Existence, uniqueness and positivity of a local solution to the finite system follow from standards arguments in the theory of ordinary differential equations. Multiplying

each equation on i in the system (3.10) by φ_i and summing over i from 1 to N, the result (3.12) follows from reordering the finite sum. Equation (3.13) holds by taking $\varphi_i = i$ for any i in (3.12) and using (3.8). Global existence follows from the bound on c_i^N and p_i^N given by the conservation (3.13). □

In order to get the convergence of the finite approximation system towards a solution of the full problem, we need additional estimates, particularly on the time derivative of the solution to (3.10). Thus we state the following lemma.

Lemma 3.4. *Let $T > 0$ and $i \geq 1$. There exists a constant $C_i(T)$ depending on i, T, K and the initial datum (c^{in}, p^{in}), such that for any $N \geq i$ it holds*

$$\int_0^T \left| \frac{dc_i^N}{dt}(s) \right| + \left| \frac{dp_i^N}{dt}(s) \right| \, ds \leq C_i(T),$$

where (c^N, p^N) is the unique solution to (3.10–3.11) given by lemma 3.3.

Proof. From the mass conservation (3.13) we have for any $N \geq i$ that

$$c_i^N + p_i^N \leq \sum_{j=1}^{N} c_j^{in} + p_j^{in} \leq ||c^{in} + p^{in}||_X.$$

Using the above estimate and combining it with the equation on c_i^N in (3.10) for $i = 2, \ldots, N-1$ together with the definition of the fluxes (3.3-3.4) we get

$$\int_0^T \left| \frac{dc_i^N}{dt}(s) \right| ds \leq \gamma_i T ||c^{in} + p^{in}||_X, \tag{3.14}$$

where $\gamma_i = (a_{i-1} + a_i + a_{i-1}^* + a_i^*)||c^{in} + p^{in}||_X + (b_{i+1} + b_i + b_{i+1}^* + b_i^*)$. It is the same for p_N^N with $\gamma_N = (a_{N-1} + a_{N-1}^*)||c^{in} + p^{in}||_X + (b_N + b_N^*)$. Now remarking that

$$c_1^N(T) = c_1^{in} - \int_0^T \left(2J_1^N(s) + \sum_{i=2}^{N-1} J_i^N(s) \right) ds.$$

It implies by definition of the fluxes J_i, using the non-negativity of c_1^{in} and c_i^N together with (3.6), that

$$\left| 2b_2 c_2^N + \sum_{i=2}^{N-1} b_{i+1} c_{i+1}^N \right|_{L^1(0,T)} \leq c_1^N(T) + \int_0^T \left(2a_1(c_1^N + p_1^N)c_1^N + \sum_{i=2}^{N-1} a_i c_i^N c_1^N \right) dt.$$

The right hand side of the above estimate can be uniformly bounded according to N, using (3.5) and the conservation (3.13), namely:

$$\left| 2a_1(c_1^N + p_1^N)c_1^N + \sum_{i=2}^{N-1} a_i c_i^N c_N^1 \right|_{L^1(0,T)} \leq 2KT||c^{in} + p^{in}||_X^2,$$

where K is given by (3.5). These two last computations easily lead to

$$\int_0^T \left| \frac{dc_1^N}{dt}(s) \right| ds \leq ||c^{in} + p^{in}||_X + 4KT||c^{in} + p^{in}||_X^2, \tag{3.15}$$

when remarking that the c_i^N and the rates are non-negative. It remains now to find a bound on the p_i^N. Equations on p_i^N for $i = 2, \ldots, N-1$ in system (3.10) lead to

$$p_i^N(T) = p_i^{in} + \int_0^T \left(H_{i-1}^N(s) - H_i^N(s) - r_i p_i^N + 2 \sum_{j=i+1}^N r_j k_{i,j} p_j^N \right) ds.$$

As done before, it implies by definition of the fluxes when using the non-negativity of rates, the non-negativity of the p_i^N and (3.5) together with (3.13) that

$$\left| 2 \sum_{j=i+1}^N r_j k_{i,j} p_j^N \right|_{L^1(0,T)} \leq ||c^{in} + p^{in}||_X + \delta_i T||c^{in} + p^{in}||_X,$$

with $\delta_i = k_i||c^{in} + p^{in}||_X + d_i + r_i$. We conclude that

$$\int_0^T \left| \frac{dp_i^N}{dt}(s) \right| ds \leq ||c^{in} + p^{in}||_X + (\tilde{\delta}_i + \delta_i)||c^{in} + p^{in}||_X, \tag{3.16}$$

with $\tilde{\delta}_i = (k_{i-1} + k_i)||c^{in} + p^{in}||_X + (d_i + d_{i+1}) + r_i$. Let us end this proof by estimating the derivative of p_1. By the same arguments as above we get

$$\int_0^T \left| \frac{dp_i^N}{dt}(s) \right| ds \leq ||c^{in} + p^{in}||_X + 8KT||c^{in} + p^{in}||_X^2, \tag{3.17}$$

Estimates (3.14–3.17) readily follow and this ends the proof.

□

To end this section, we provide some additional uniform estimates, in order to pass to the limit when N tends to infinity, such as the control of the moments of the solution.

Lemma 3.5. *Let $T > 0$. Assume that U is a given function that fulfills the property (P_1) or (P_2), then there exists a constant $C_u(T)$ depending on T, U, K and the initial datum (c^{in}, p^{in}), such that for any $N \geq 3$ and $t \in [0, T]$ it holds,*

$$\sum_{i=1}^N U(i) \left(c_i^N + p_i^N \right) \leq C_u(T) \sum_{i=1}^N U(i) \left(c_i^{in} + p_i^{in} \right), \tag{3.18}$$

where (c^N, p^N) is the unique solution to (3.10–3.11) given by lemma 3.3. Futhermore, the following estimates hold true for any $N \geq 3$:

$$0 \leq \int_0^T \sum_{i=1}^{N-1} \left(U(i+1) - U(i) - U(1) \right) \left((b_{i+1} + b_{i+1}^*) c_{i+1}^N + d_{i+1} p_{i+1}^N \right) ds$$
$$\leq C_u(T) \sum_{i=1}^N U(i) \left(c_i^{in} + p_i^{in} \right), \tag{3.19}$$

and

$$0 \leq 2\int_0^T \sum_{i=1}^{N-1} i \sum_{j=i+1}^{N} \left(\frac{U(j)}{j} - \frac{U(i)}{i}\right) \kappa_{i,j} r_j p_j^N \leq C_u(T) \sum_{i=1}^{N} U(i) \left(c_i^{in} + p_i^{in}\right). \tag{3.20}$$

Proof. Let us fix $T > 0$ and U satisfying (P_1) or (P_2). Assume that (c^N, p^N) is the unique solution to (3.10–3.11), given by lemma 3.3. Taking $\varphi_i = U(i)$ for any $i = 1, \ldots, N$ in (3.12), we get

$$\begin{aligned}\frac{d}{dt}\sum_{i=1}^{N} U(i)\left(c_i^N + p_i^N\right) \;=\; & -\sum_{i=2}^{N}\left(U(i) - 2\sum_{j=1}^{i-1} U(j)\kappa_{j,i}\right) r_i p_i^N \\ & + \sum_{i=1}^{N-1} \left(U(i+1) - U(i) - U(1)\right)\left(J_i^N + J_i^{*\,N} + H_i^N\right). \end{aligned} \tag{3.21}$$

Let us recall then [129, Lemma 3.2] that this implies there exists a constant m_u depending only on U such that for any $i, j \geq 1$,

$$(i+j)\left(U(i+j) - U(i) - U(j)\right) \leq m_u \left(iU(j) + jU(i)\right). \tag{3.22}$$

By definition of the fluxes (3.3–3.4) and using (3.22) together with (3.21), it easily leads to

$$\begin{aligned}\frac{d}{dt}\sum_{i=1}^{N} U(i)\left(c_i^N + p_i^N\right) \leq & -\sum_{i=2}^{N}\left(U(i) - 2\sum_{j=1}^{i-1} U(j)\kappa_{j,i}\right) r_i p_i^N \\ & + m_u \sum_{i=2}^{N-1} \frac{U(i) + iU(1)}{i+1}\left(a_i c_1^N c_i^N + a_i^* p_1^N c_i^N + k_i p_1^N p_i^N\right) \\ & + m_u \frac{U(1) + 1U(1)}{2}\left(a_1(c_1^N + p_1^N)c_1^N + a_1^*(p_1^N + c_1^N)c_1^N + k_1 p_1^N p_1^N\right) \\ & - \sum_{i=1}^{N-1}\left(U(i+1) - U(i) - U(1)\right)\left((b_{i+1} + b_{i+1}^*)c_{i+1}^N + d_{i+1} p_i^N\right). \end{aligned} \tag{3.23}$$

Thus from (3.23), the fact that $U(1) \leq U(i)/i$ by property of U and hypothesis (3.5) it holds:

$$\begin{aligned}\frac{d}{dt}\sum_{i=1}^{N} U(i)\left(c_i^N + p_i^N\right) \leq & -\sum_{i=2}^{N}\left(U(i) - 2\sum_{j=1}^{i-1} U(j)\kappa_{j,i}\right) r_i p_i^N \\ & - \sum_{i=1}^{N-1}\left(U(i+1) - U(i) - U(1)\right)\left((b_{i+1} + b_{i+1}^*)c_{i+1}^N + d_{i+1} p_i^N\right) \\ & + 2m_u K \sum_{i=1}^{N-1} U(i)(c_1^N + p_1^N)(c_i^N + p_i^N). \end{aligned} \tag{3.24}$$

Let us remark that the convexity of U gives

$$\frac{U(i+1)-U(0)}{i+1} \leq \frac{U(i+1)-U(1)}{i} \Rightarrow \frac{U(i+1)}{i+1} - \frac{U(i)}{i} \leq \frac{U(i+1)-U(i)-U(1)}{i},$$

and from the fact that $U(0)=0$, we have $x \mapsto U(x)/x$ is an increasing function, thus

$$U(i+1)-U(i)-U(1) \geq 0.$$

Also, from (3.8) we remark that

$$2\sum_{j=1}^{i-1} U(j)\kappa_{j,i} = 2\sum_{j=1}^{i-1} j\frac{U(j)}{j}\kappa_{j,i} \leq U(i), \tag{3.25}$$

and thus, combining (3.3), (3.25) with (3.24) and (3.13) we get

$$\frac{d}{dt}\sum_{i=1}^{N} U(i)\left(c_i^N + p_i^N\right) \leq 2m_u K||c^{in}+p^{in}||_X \sum_{i=1}^{N-1} U(i)(c_i^N + p_i^N).$$

By Gronwall's lemma it exists $C_u(T)$ such that (3.18) holds true. Now from (3.18) we go back to (3.24) and integrate over $(0,T)$, it gives (3.19). Finally, we remark that by hypothesis (3.8) to get

$$U(i) - 2\sum_{j=1}^{i-1} U(j)\kappa_{j,i} = 2\sum_{j=1}^{i-1}\left(j\frac{U(i)}{i} - U(j)\right)\kappa_{j,i} = 2\sum_{j=1}^{i-1} j\left(\frac{U(i)}{i} - \frac{U(j)}{j}\right)\kappa_{j,i},$$

and thus

$$\sum_{i=2}^{N} U(i) - 2\sum_{j=1}^{i-1} U(j)\kappa_{j,i} = 2\sum_{i=1}^{N-1}\sum_{j=i+1}^{N} i\left(\frac{U(j)}{j} - \frac{U(i)}{i}\right)\kappa_{i,j}.$$

Using this above equality, again with (3.18) we go back to (3.24) and integrate over $(0,T)$ to obtain (3.20). □

We are now ready to prove the existence of a solution to the problem (3.1–3.2).

3.4 Existence of solutions with moments propagation

This section is devoted to the proof of theorem 3.2. From the previous section we know that for any finite approximation we have a solution that fulfills some properties. It allows us to construct a sequence of solutions, indexed by N. The key ingredient to prove the result is a version of the De La Vallée-Poussin theorem for integrable functions mentioned by P. Laurençot in [129, Theorem 4.1]. We recall it below.

Theorem 3.6 (de la Vallée-Poussin theorem)**.** *Let $(\Omega, \mathcal{B}, \mu)$ be a measured space and consider a function $\omega \in L^1(\Omega, \mathcal{B}, \mu)$. Then there exists a function V satisfying (P_∞) such that*

$$V(|\omega|) \in L^1(\Omega, \mathcal{B}, \mu).$$

We apply this theorem as in [129]. Let $(\mathbb{N}^*, \mathcal{P}(\mathbb{N}^*))$ equipped with the measure

$$\mu(I) = \sum_{i \in I} c_i^{in} + p_i^{in}, \ I \in \mathcal{P}(\mathbb{N}^*).$$

Since c^0 and p^0 belong to X^+, the identity function $Id : x \to x$ satisfies $Id \in L^1(\mathbb{N}^*, \mathcal{P}(\mathbb{N}^*), \mu)$. Thus by theorem 3.6, there exists U_0 satisfying (P_∞) such that

$$\sum_{i \geq 1} U_0(i)(c_i^{in} + p_i^{in}) < \infty.$$

This estimate is crucial for the following. It state that if we control the first moment of the initial data, *i.e.* c_i^{in}, $p_i^{in} \in X^+$, we actually control a little more that the first moment, that is with some weight function U_0 enjoying property (P_∞).

The sketch of the proof of theorem 3.2 is as follows. In the first step we prove that up to a subsequence the sequence of approximated solutions is converging. The step 2 concerns some estimations on this limit which are necessary to get the convergence of all the terms needed in the step 3. Finally step 4 ends the proof.

Let us fix $T > 0$ in the following.

Step 1. Extraction of a subsequence. In the previous section we stated the existence, in lemma 3.3, of a global solution to the finite approximating sytem. By virtue of this lemma we are therefore able to construct for any $i \geq 1$ two sequences, $(c_i^N)_{N \geq i \wedge 3}$ and $(p_i^N)_{N \geq i \wedge 3}$. Moreover, from the conservation (3.13) in lemma 3.3 and with lemma 3.4, it holds that $(c_i^N)_{N \geq i \wedge 3}$ and $(p_i^N)_{N \geq i \wedge 3}$ are bounded, uniformly with respect to N, in $L^\infty([0,T]) \cap W^{1,1}([0,T])$. We now infer from the Helly selection principle [119, Sec. 36.5], there exists two functions c_i and p_i such that, up to a subsequence still indexed by N, for any $t \in [0,T]$ it holds

$$c_i^N(t) \underset{N \to \infty}{\longrightarrow} c_i(t) \text{ and } p_i^N(t) \underset{N \to \infty}{\longrightarrow} p_i(t). \tag{3.26}$$

Moreover c_i and p_i are two functions of bounded variation on $[0,T]$. Taking the limit implies that both c_i and p_i are non-negative functions. Let now $M \geq 3$ and $N \geq M$. With the conservation (3.13) we get for any $t \in [0,T]$

$$\sum_{i=1}^{M} i(c_i^N(t) + p_i^N(t)) \leq ||c^{in} + p^{in}||_X.$$

Taking the limit $N \to +\infty$ it holds that for any $M \geq 3$,

$$\sum_{i=1}^{M} i(c_i(t) + p_i(t)) \leq ||c^{in} + p^{in}||_X.$$

This is a bounded series of non-negative functions thus it is a converging series. It infers that $c = (c_i)_{i \geq 1}$ and $p = (p_i)_{i \geq 1}$ belong to X^+ with

$$||c_i(t) + p_i(t)||_X \leq ||c^{in} + p^{in}||_X \text{ for any } t \in [0,T]. \tag{3.27}$$

We have now a limit candidate to be a solution to the infinite system. We have to check that the couple (c, p) is a solution.

Step 2. Additional estimates. Here we show several estimations that will allow us to pass to the limit. For this step we assume that it exists U satisfying (P_1) or (P_2) such that

$$\sum_{i\geq 1} U(i)(c_i^{in} + p_i^{in}) < +\infty. \tag{3.28}$$

Using lemma 3.5, for $M \geq 3$ and $N \geq M$ we get for any $t \in [0, T]$

$$\sum_{i=1}^{M} U(i)(c_i^N + p_i^N) \leq C(T),$$

$$0 \leq \int_0^T \sum_{i=1}^{M} (U(i+1) - U(i) - U(1)) \left((b_{i+1} + b_{i+1}^*)c_{i+1}^N + d_{i+1}p_{i+1}^N\right)\, ds \leq C(T),$$

and

$$0 \leq 2\int_0^T \sum_{i=1}^{M-1} i \sum_{j=i+1}^{M} \left(\frac{U(j)}{j} - \frac{U(i)}{i}\right) \kappa_{i,j} r_j p_j^N \leq C(T),$$

where $C(T)$ is a constant depending on T, U, K and the couple (c^{in}, p^{in}). Let us now take the limit $N \to +\infty$: the above inequalities still hold true with c_i^N and p_i^N replaced by c_i and p_i. Furthermore, since U satisfies (P_1) or (P_2), as mentioned before, it follows that each term in the sums is non-negative and hence the series are converging. It allows us to take the limit $M \to +\infty$ and we have for any $t \in [0, T]$

$$\sum_{i\geq 1} U(i)(c_i + p_i) \leq C(T), \tag{3.29}$$

$$0 \leq \int_0^T \sum_{i\geq 1} (U(i+1) - U(i) - U(1)) \left((b_{i+1} + b_{i+1}^*)c_{i+1} + d_{i+1}p_{i+1}\right)\, ds \leq C(T),$$

and

$$0 \leq 2\int_0^T \sum_{i\geq 1} i \sum_{j\geq i+1} \left(\frac{U(j)}{j} - \frac{U(i)}{i}\right) \kappa_{i,j} r_j p_j \leq C(T).$$

Moreover, if we assume that U satisfies (P_∞), let $\varepsilon > 0$. It exists M such that

$$\forall i \geq M,\ U(i+1) - U(i) \geq \int_i^{i+1} U'(x)dx \geq \frac{1}{\varepsilon} + U(1),$$

thus for any $N > M$, it holds for all $t \in [0, T]$

$$\int_0^T \sum_{i=M+1}^{N} \left((b_{i+1} + b_{i+1}^*)c_{i+1}^N + d_{i+1}p_{i+1}^N\right)\, ds \leq \varepsilon C(T), \tag{3.30}$$

and also

$$0 \leq \int_0^T \sum_{i \geq M+1} \left((b_{i+1} + b^*_{i+1}) c_{i+1} + d_{i+1} p_{i+1} \right) \, ds \leq \varepsilon C(T). \tag{3.31}$$

Furthermore, for any $i \geq 1$ it exists $M \geq i$ such that

$$\forall j \geq M, \frac{U(j)}{j} \geq \frac{1}{\varepsilon} + \frac{U(i)}{i},$$

thus for any $N > M$, it holds for all $t \in [0, T]$

$$0 \leq \int_0^T \sum_{j=M+1}^{N} \kappa_{i,j} r_j p_j^N \leq \frac{\varepsilon}{2} C(T), \tag{3.32}$$

and also

$$0 \leq \int_0^T \sum_{j \geq M+1} \kappa_{i,j} r_j p_j \leq \frac{\varepsilon}{2} C(T). \tag{3.33}$$

Step 3. Convergence. From theorem 3.6, it exists U_0 satisfying (P_∞) such that

$$\sum_{i \geq 1} U_0(i)(c_i^{in} + p_i^{in}) < +\infty.$$

Thus, estimations in Step 2. remain true without any additional assumptions than c^{in} and p^{in} belonging to X^+. Now we are in position to prove that the terms needed converge as required. Indeed, from the Lebesgue-dominated convergence theorem we readily obtain that for any $i \geq 1$

$$J_i^N, \ J_i^{*\,N}, \ H_i^N \underset{N \to \infty}{\longrightarrow} J_i, \ J_i^*, \ H_i \text{ respectively in } L^1(0,T),$$

and

$$r_i p_i^N \underset{N \to \infty}{\longrightarrow} r_i p_i \text{ in } L^1(0,T).$$

Then we have to verify that

$$\sum_{i=2}^{N} J_i^N, \ \sum_{i=2}^{N} J_i^{*\,N}, \ \sum_{i=2}^{N} H_i^N \underset{N \to \infty}{\longrightarrow} \sum_{i \geq 2} J_i, \ \sum_{i \geq 2} J_i^*, \ \sum_{i \geq 2} H_i \text{ respectively in } L^1(0,T),$$

and

$$\sum_{j=i+1}^{N} \kappa_{i,j} r_j p_j^N \underset{N \to \infty}{\longrightarrow} \sum_{j \geq i+1} \kappa_{i,j} r_j p_j \text{ in } L^1(0,T).$$

The proof follows the one proposed in [129]. For sake of clarity we only give the details for $\sum_{i=2}^{N} J_i^N$, since the other convergences are obtained in the same way. Namely, we will prove that:

$$\left\| \sum_{i=2}^{N-1} a_i c_1^N c_i^N - \sum_{i=2}^{\infty} a_i c_1 c_i \right\|_{L^1(0,T)} \underset{N \to \infty}{\longrightarrow} 0, \tag{3.34}$$

and

$$\left\| \sum_{j=2}^{N} b_{i+1} c_{i+1}^N - \sum_{j\geq 2} b_{i+1} c_{i+1} \right\|_{L^1(0,T)} \underset{N\to\infty}{\longrightarrow} 0. \tag{3.35}$$

First, let us prove (3.34). For $M \geq 2$, with the help of (3.5), (3.26) and (3.13), by virtue of the Lebesgue-dominated convergence theorem, it holds

$$\lim_{N\to\infty} \left| \sum_{i=2}^{M} a_i c_1^N c_i^N - \sum_{i=2}^{M} a_i c_1 c_i \right|_{L^1(0,T)} = 0. \tag{3.36}$$

Furthermore, with (3.5), (3.13), (3.18) and the fact that U_0 satisfies (P_∞), for $N \geq M+2$, we have:

$$\begin{aligned} 0 \leq \left| \sum_{i=M+1}^{N-1} a_i c_1^N c_i^N \right|_{L^1(0,T)} &\leq K||c^{in} + p^{in}||_X \left\| \sum_{i=M+1}^{N-1} \frac{i}{U_0(i)} U_0(i) c_i^N \right\|_{L^1(0,T)} \\ &\leq C(T) \sup_{i\geq M} \frac{i}{U_0(i)}. \end{aligned} \tag{3.37}$$

Similarly, since (3.29) holds with U_0,

$$0 \leq \left\| \sum_{i=M+1}^{\infty} a_i c_1 c_i \right\|_{L^1(0,T)} \leq C(T) \sup_{i\geq M} \frac{i}{U_0(i)}. \tag{3.38}$$

Thus, by virtue of (3.36–3.38), for any $M \geq 2$,

$$\limsup_{N\to\infty} \left\| \sum_{i=2}^{N} a_i c_1^N c_i^N - \sum_{i=2}^{\infty} a_i c_1 c_i \right\|_{L^1(0,T)} \leq C(T) \sup_{i\geq M} \frac{i}{U_0(i)}. \tag{3.39}$$

By definition of U_0, the right hand side of inequality (3.39) goes to 0 as M goes to infinity and (3.34) holds true.

It remains to prove (3.35). First, with the help of (3.26), (3.13) and by virtue of the Lebesgue-dominated convergence theorem, it holds for any $M \geq 2$

$$\lim_{N\to+\infty} \left\| \sum_{j=2}^{M} b_{i+1} c_{i+1}^N - \sum_{j=2}^{M} b_{i+1} c_{i+1} \right\|_{L^1(0,T)} = 0. \tag{3.40}$$

Thus, from with (3.40) and (3.30-(3.31)), for any $\varepsilon > 0$

$$\limsup_{N\to\infty} \left\| \sum_{j=2}^{N} b_{i+1} c_{i+1}^N - \sum_{j\geq 2} b_{i+1} c_{i+1} \right\|_{L^1(0,T)} \leq 2\varepsilon C(T).$$

Let ε goes to 0 and (3.35) holds true.

Step 4. Final stage. We are in position to pass to the limit in the approximating system and we obtain that (c, p) is a solution to (3.1–3.2). Indeed, points i) to iii) are satisfied and all the terms are converging. The continuity of each c_i and p_i follows since every terms in the integral are $L^1(0,T)$. The propagation of the moments is obtained since we have proved that (3.28) implies (3.29). It remains to prove that $c \in C([0,T], X)$. Let $t \in [0,T)$, $h > 0$ and $M \geq 1$ we get

$$\begin{aligned}
||c(t+h) - c(t)||_X &= \sum_{i=1}^{M} i|c_i(t+h) - c_i(t)| + \sum_{i \geq M+1} i|c_i(t+h) - c_i(t)| \\
&\leq \sum_{i=1}^{M} i|c_i(t+h) - c_i(t)| \\
&\quad + \sup_{i \geq M} \frac{i}{U_0(i)} \sum_{i \geq M+1} U_0(i)(|c_i(t+h)| + |c_i(t)|) \\
&\leq \sum_{i=1}^{M} i|c_i(t+h) - c_i(t)| \\
&\quad + 2C_u(T) \sup_{i \geq M} \frac{i}{U_0(i)} \sum_{i \geq 1} U_0(i)(c_i^{in} + p_i^{in}).
\end{aligned}$$

Thus, let $h \to 0$ the first sum in the last inequality goes to zero by continuity of the c_i and then taking $M \to +\infty$, because U_0 satisfies (P_∞) we get

$$\lim_{h \to 0} ||c(t+h) - c(t)||_X = 0.$$

For the same reason its holds true when $t \in (0,T]$ and $h < 0$. Moreover, we can proceed as above and we get $p \in C([0,T], X)$. To end, we prove that the total mass is constant.

Let $t \geq 0$,

$$\begin{aligned}
\Big| \|p+c\|_X - \|p^0+c^0\|_X \Big| \leq & \left| \sum_{i=1}^{N} i(p_i+c_i) - \sum_{i=1}^{N} i(p_i^{in}+c_i^{in}) \right| \\
& + \left| \sum_{i=N+1}^{\infty} i(p_i+c_i) - \sum_{i=N+1}^{\infty} i(p_i^{in}+c_i^{in}) \right| \\
\underset{(3.13)}{\leq} & \sum_{i=1}^{N} i \left| p_i + c_i - p_i^N - c_i^N \right| + \sum_{i=N+1}^{\infty} i \left| p_i + c_i \right| \\
& + \sum_{i=N+1}^{\infty} i \left| p_i^{in} + c_i^{in} \right| \\
\leq & \sum_{i=1}^{M} i \left| p_i + c_i - p_i^N - c_i^N \right| + \sum_{i=M+1}^{N} i \left| p_i^N + c_i^N \right| \\
& + \sum_{i=M+1}^{\infty} i \left| p_i + c_i \right| + \sum_{i=N+1}^{\infty} i \left| p_i^{in} + c_i^{in} \right| \\
\underset{(3.18)-(3.29)}{\leq} & \sum_{i=1}^{M} i \left| p_i + c_i - p_i^N - c_i^N \right| \\
& + \sum_{i=N+1}^{\infty} i \left| p_i^{in} + c_i^{in} \right| + C(T) \sup_{i \geq M} \frac{i}{U_0(i)} .
\end{aligned} \tag{3.41}$$

By (3.26) and noting that p^0 and c^0 belong X^+, it follows by passing to the limit in $N \to +\infty$, that:

$$\Big| \|p+c\|_X - \|p^0+c^0\|_X \Big| \leq C(T) \sup_{i \geq M} \frac{i}{U_0(i)}. \tag{3.42}$$

We get the conservation by taking the limit $M \to +\infty$. This ends the proof of theorem 3.2. □

3.5 Concluding remarks

In this work we provided an existence result for a model of polymerization-fragmentation with pathway, written under the form of an infinite system of ordinary differential equations. We extend to this problem the proof of Laurençot [129] which provide a powerful mehtod to prove existence of solutions to dicrete coagulation-fragmentation equations with moments propagation. Moreover, we deduce the continuity in time of solutions into X, that have not been mentionned in [129].

The main advantage of the problem investigated here is that it can be used for various applications, an then furnish an interesting prototype to study. However, the result obtained only concerns existence of solutions, without any clue on uniqueness. This question

may require more restrictive assumptions and should be studied further as in the works of Ball *et al.* [9, 10] and Laurençot [129].

Annexe

Experimental procedures for prion proliferation measurements

A Expression and purification of recombinant prion protein

Recombinant 90-231 prion protein (rPrP) from Syrian hamster (Misocricetus auratus) provided by S. B. Prusiner was produced as described previously [4]. Protein concentrations were determined spectrophotometrically (Beckman spectrophometer) using an extinction coefficient of 25327 $M^{-1} \cdot cm^{-1}$ at 278 nm and a molecular mass of 16.227 kDa. Purity of the protein preparation was assessed by phase reverse HPLC. The protein was stored lyophilised at $-80\,^{\circ}$C.

B Preparative *in vitro* polymerization

Samples containing 0.4 to 1.2 mg/ml of the oxidized form of HaPrP90-231 (rPrP) were incubated for 1-5 days with 50 mM sodium acetate, pH 4.0, 0.5 MGdnHCl (Buffer A) or pH 6.8 in phosphate-buffered saline (PBS), 1 M GdnHCl, 2.44 M urea, 150 mM NaCl (Buffer B), or 50 mM MES, pH 6.0, 2MGdnHCl (Buffer C) [16]. The rPrP spontaneously converted into the fibrillar isoform upon continuous shaking at 250 rpm in conical plastic tubes (Eppendorf) in a reaction volume 1.3 ml at 37 $^{\circ}$C (lying down Tube). In somecases, polymerization was obtained upon continuous shaking at 600 rpm using a Thermomixer comfort (Eppendorf) in conical plastic tubes (Eppendorf) in a reaction volume 0.4 ml at 37 $^{\circ}$C (upright Tube). Tomonitor the kinetics of fibril formation aliquots were withdrawn and diluted 100-fold into PBS to a final concentration of rPrP of 4 µg/ml. After the addition of thioflavin T (ThT) (Sigma) to a final concentration 10 µM for 5 min. the fluorescence measurements were performed at room temperature with a FluoroMax-2 fluorimeter (Jobin Yvon-Spex, Tokyo, Japan) with a 10.4 mm path length rectangular cuvette. ThT emission spectra were recorded after excitation at 450 nm (excitation and emission slit widths, 4 nm), each emission spectrum (slit width, 4 nm) was the average of three scans.

C Transmission electron microscopy

Samples were absorbed on carbon / formvar-coated copper grids (300 mesh) (Agar scientific, Saclay, France) and stained by negative contrast with 2% (w/v) uranyl acetate for 1 min. Labeled samples are observed after negative contrast with uranyl acetate 2% on a JEOL 1200 EX II transmission electron microscope (Service commun de microscopie électronique de l'université Montpellier II, Montpellier, France) at 80 kV of voltage. Length and width of fibrils were measured with ImageJ software (`http://rsbweb.nih.gov/ij/`).

D Fluorescence microscopy

Samples were diluted in sodium acetate 50 mM buffer pH5 containing 10 µM Thioflavin T (ThT). Images acquisition was performed on an inverted Leica DM IRB microscope equipped with a Leica DFC350 FX digital camera at gross x945. Images were analyzed with Adobe Photoshop and ImageJ software.

E FACS analysis

Flow cytometric analysis of aggregates was performed as described [214]. Measurements were made using a FACScalibur (Becton Dickinson) with Cell Quest software. 1 ml of a fibril suspension at 2.4 μM final and placed in the flow cytometer; 10,000 data points were acquired for subsequent analysis. The thioflavin-T, assays were performed by adding a freshly prepared stock solution to the protein samples to final thioflavin-T concentration of 10 μM. Samples were allowed to reach equilibrium for 5 min before data collection. The fluorescence intensity of ThT (FL1), collected during the second acquisition, was then plotted versus particle size measured by side scattering (SSC).

F FTIR and CD analysis

CD spectra were recorded at ambient conditions using a J810 spectropolarimeter (Jasco). A 0.1 cm optical path length quartz cell was used to record spectra of proteins in the far UV region (190-260 nm). Protein concentration and buffers were those used in the UV absorbance experiments. Baseline corrected CD spectra were acquired at a scan speed of 20 nm $\cdot$ min^{-1}, a 1 nm bandwidth, and a response time of 1 s. The sample compartment was purged with pure dry nitrogen. Spectra were signal-averaged over four scans.

The IR spectra were obtained with a Bruker (Ettlingen, Germany) Vertex 80v FTIR spectrometer equipped with a liquid-nitrogen-cooled, broad-band, mercury-cadmium telluride solid-state detector. The spectra (100 scan accumulation) were co-added after registration at a spectral resolution of 2 cm^{-1} and analyzed with the Opus 6.0 program. For comparison of soluble and aggregated protein, all spectra were recorded with dry samples. After the isolation of aggregates by centrifugation (22 psi $\approx$ 127,000 g for 60 min, airfuge air-driven Microultracentrifuge Beckman Coulter), and suspension in corresponding buffer, the sample was deposited onto a CaF2 plate, and the solvent was allowed to

evaporate overnight at room temperature. To compare qualitatively the spectra of different samples, each spectrum was normalized with respect to the integrated intensity of the entire spectrum.

G Kinetic measurements of polymerization

The kinetics of amyloid formation was monitored in SpectraMax Gemini XS (Molecular Devices). Samples containing 0.1 to 1.2 mg/ml of the oxidized form of HaPrP90-231 (rPrP) were incubated in Buffer A, Buffer B or Buffer C upon continuous shaking at 1350 rpm in 96-well plate and in the presence of ThT (10 μM). The kinetics was monitored by bottom-reading of fluorescence intensity using 445 nm excitation and 485 and 500 nm emission. Every set of measurements was performed in triplicates, and the results were averaged. Seeding was performed by adding a percentage of previously prepared amyloid and the w/w percent was calculated assuming that suspension was homogeneous.

Part II

Modélisation de la polymérisation-fragmentation dans un fluide

Chapter 4

Fragmentation and monomer lengthening of rod-like polymers, a relevant model for prion proliferation

Dans ce chapitre nous introduisons un modèle pour des polymères rigides soumis à un fluide. Nous intégrons dans les équations la configuration des polymères ainsi que leur taille soumise au processus d'élongation par monomères et de fragmentation. On démontre ensuite l'existence de solutions dans un espace L^2 à poids préservant ainsi tous les moments de la solution. Le résultat est donné par construction, le problème semi-discrétisé en temps et l'espace L^2 nous permet d'écrire une formulation variationnelle à chaque pas de temps, construisant ainsi une solution par morceau. Le passage à la limite est obtenu par des arguments de compacité. Ce chapitre est le résultat d'une collaboration avec I. S. Ciuperca, L. I. Palade et L. Pujo-Menjouet publié dans *Discrete and Continuous Dynamical Systems - Series B*, [47].

4.1 Introduction

In 1999, Masel *et al.* [153] introduced a new model of polymerization in order to quantify some kinetic parameters of prion replication. This work was based on a deterministic discrete model developed into an infinite system of ordinary differential equations, one for each possible fibril length. In 2006, Greer *et al.* in [90] modified this model to create a continuum of possible fibril lengths described by a partial differential equation coupled with an ordinary differential equation. This approach appeared to be "conceptually more accessible and mathematically more tractable with only six parameters, each of which having a

biological interpretation" [90]. However, based on discussions with biologists, it appeared that these models were not well adapted for *in vitro* experiments. In these experiments, proteins are put in tubes and shaken permanently throughout the experiment to induce an artificial splitting in order to accelerate the polymerization-fragmentation mechanism. To the best of our knowledge, dependence of polymer and monomer interaction on the shaking orientation and strength, space competition and fluid viscosity had never been taken into account until now. Thus, it seemed natural to propose a model generalizing the Greer model and adapt it to the specific expectations of the biologists. We therefore introduce a new model of polymer and monomer interacting in a fluid, with the whole system subjected to motion. A large range of *in vitro* experiments involving this protein refers to this protocol in order to accelerate the polymerization-fragmentation process. Moreover, even as our model could be well adapted to other polymer-monomer interaction studies, we give here a specific application to prion dynamics to make an interesting link with the previous Masel *et al.* [153] and Greer *et al.* [90] modelsMaria-Teresa Alvarez-Martinez and Pascaline Fontes and Viviana Zomosa-Signoret and Jacques-Damien Arnaud and Erwan Hingant and Laurent Pujo-Menjouet and Jean-Pierre Liautard. On the other hand, due to the complexity of the model, any mathematical analysis becomes a challenge. We adapt here a technique of semi-discretization in time for proving the main result of existence of positive solutions, we also provide the basis for the numerical approximation of the problem. The mathematical novelty of this chapter resides in the choice of the *ad hoc* function spaces and the appropiate modification of the existing techniques to this new type of problem. Also this work presents an alternative way for proving the existence of positive solutions as compared to the one given by Engler *et al.* in [68], Laurençot and Walker in [132] and Simonett and Walker in [197]. It is then useful to those who consider which techniques to use when proving the existence of positive solutions of this class of equations. The objective of this chapter is twofold: not only to make a step forward in mathematical modelling of a class of polymer-monomer interaction models, but also to propose, within a new framework, how to adapt an existing mathematical technique that will prove the existence of positive solutions to the problem. The biological implications (*e.g.* quantitative and qualitative comparison with experimental data) of this chapter model will be addressed in a subsequent work.

For the sake of clarity, we present several fundamental morphological features of prions with relevance to the mathematical modelling of this chapter (*i.e.* molecular dynamics of a low enough concentration prion solution).

Prions are responsible for several diseases such as *bovine spongiform encephalopathy* for animals, also *Creutzfeld-Jacob disease*, *Kuru* for humans, and it is now commonly accepted that prions are proteins [183]. There are two types of prions: the *Prion Protein Cellular* also called PrP^{C} and *Prion Protein Scrapie* denoted by PrP^{Sc}. It has been proven that PrP^{C} proteins are naturally synthesized by mammalian cells and consist only of monomers. On the other hand, the infectious PrP^{Sc} proteins are present only in pathologically altered cells and exist only in "polymer"-shape. The conversion process of a non-pathological into a pathologically modified one consists in attaching the former to an already existing polymer (for details see *e.g.* [125]). As a consequence, the polymers lengthen. However the

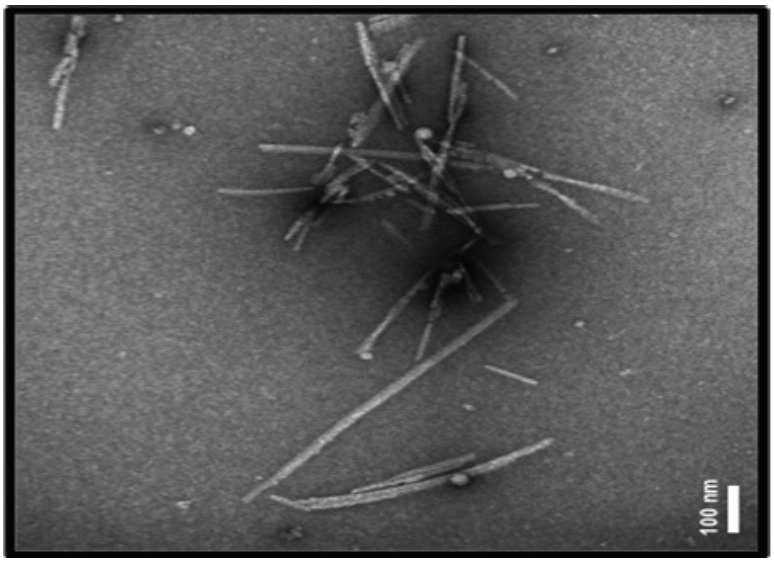

Figure 4.1: View of prion fibrils, Transmission Electron Microscopy image (Courtesy of Prof. J.-P. Liautard, INSERM Université Montpellier 2, France).

sized-up new polymers are fragile, and shorten down their size by splitting whenever the polymer solution is subjected to some flow conditions. The size lengthening/shortening process takes place continuously, its kinetics being dependent on monomer concentration, flow intensity, polymer size, etc. Polymers may be seen as string-like molecules [194]. When polymer proliferation occurs, they do interact to form fibrils; these latter exhibit a (physically speaking) more stable structure and appear as rod-like molecules; Figure 4.1. In this chapter we deal with idealized rod-like PrP^{Sc}, a realistic choice taking into account the flow-related experiments we investigate. We consider the presence of a finite amount of PrP^{C}(free monomers) and PrP^{Sc} proteins, as well as of "seeding" rod-like PrP^{Sc} at initial condition, and fibril lengthening/splitting (*i.e.* fragmentation). It is also important to note that our model is related to *in vitro* experiments: neither source terms of monomers and polymers nor degradation rates are taken into account. We propose a comprehensive molecular model that accounts for the flow behavior as observed in *in vitro* experiments, focusing on the dynamics of monomers and fibrils. A good deal of experimental laboratory work involves complex flows (*e.g.* diffusion, mixing, etc.). Raw data are provided by sensors designed to acquire macroscopically observable properties like stresses, flow rates, etc. The latter can strongly be influenced by the microscopic interactions. Our model does provide an understanding of how various polymers-monomer and polymer-solvent relationship result in a configurational probability diffusion equation, with the help of which one can investigate the stress tensor and related quantities. Therefore, it is of use for flow pattern monitoring sensors. The current approach is at an early stage of development. The scission (breakage) process - the most important mechanism in the *in vitro* development/proliferation of infectious proteins - is taken three-dimensionally. While

prior models such as those of [90, 153] (for mathematically in nature aspects related to, see [30, 68, 91, 132, 184, 194, 197, 213]) neglect the flow influence on prion dynamics, the one in [90] was rather succesful in predicting prion molecular dynamics in the *in vivo* rest state, and our model is a generalization of [90]. In order to consider the configuration of polymers in 3-dimensional space, the prion fiber are modelled as a rigid rod polymer molecule the length of which is time dependent; Figure 4.2. The dynamics of rigid rod molecular fluids

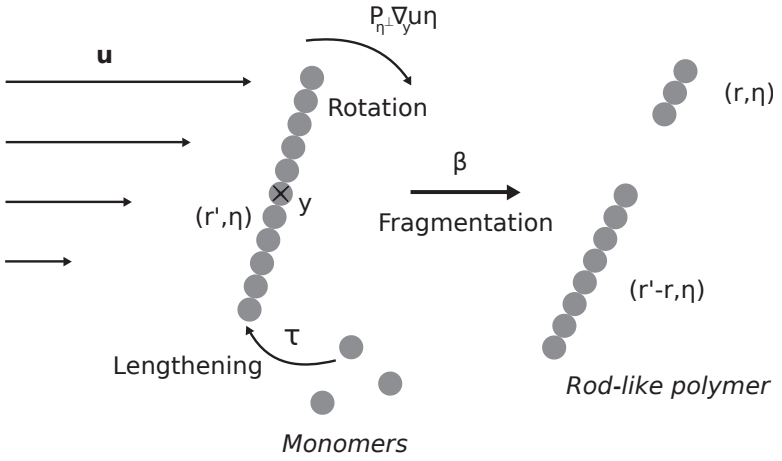

Figure 4.2: Prion fibril modelized as rigid rod polymer under flow.

has been initiated by Kirkwood [116] and significantly enriched and brought to fruition by Bird and his school [23] (see also [104] for a more succinct presentation). As in any kinetical theory, the cornerstone is the probability of the configurational diffusion equation, which is of a Fokker-Planck-Smoluchowski type. The latter is the key ingredient for calculating (the macroscopic) stress tensor and related quantities. In the following we shall derive a suitable generalization of equations 14.2-8 in [23] that account for prion dynamics as observed in experiments [35, 183, 229].

This chapter begins by first presenting the constitutive assumptions which later lead to the probability configurational diffusion equation in its general form. We give a mathematical conceptual framework and a presentation of the main result: the existence of global weak non-negative solution. To achieve this, we obtain a variational formulation of the corresponding boundary value problem, and the proof is based on a semi-discretization in time technique.

4.2 The general model

4.2.1 Polymers

Let a fiber be modeled as a rod-like molecule here represented by a vector in $\mathbb{R}^3$. For convenience, we use separate symbols for the length $r \in \mathbb{R}_+ = (0, +\infty)$, and for the angle-

vector $\eta \in \mathbb{S}^2$, with $\mathbb{S}^2$ being the unit sphere of $\mathbb{R}^3$. Contrary to the assumption made in [90] and for simplicity, we assume here that polymers could be arbitrary small, that is no critical (lower) length is considered (this assumption is explained in [65]). For technical reasons and without any loss of realistic assumptions, we suppose that fibers are contained in a bounded, smooth open set Ω in $\mathbb{R}^3$, and the position of each fiber center of mass is denoted by the vector $\mathbf{y}$. We assume a velocity vector field $\mathbf{u} : \Omega \times \mathbb{R}_+ \to \mathbb{R}^3$ such that

$$\nabla_{\mathbf{y}} \cdot \mathbf{u} = 0 \text{ in } \Omega, \text{ and } \mathbf{u} \cdot \vec{n} = 0 \text{ on } \partial\Omega. \tag{4.1}$$

with $\vec{n}$ the outward normal. The polymer configurational probability distribution function $\psi(r, \eta, \mathbf{y}, t)$, at any time $t > 0$, solves the following equation

$$\frac{\partial}{\partial t}\psi + \mathbf{u} \cdot \nabla_{\mathbf{y}}\psi + \frac{\partial}{\partial r}\left(\tau(\phi, \mathbf{u}, r, \eta)\psi\right) = \mathcal{B}\psi + \mathcal{F}\psi. \tag{4.2}$$

with $(r, \eta, \mathbf{y}) \in \mathbb{R}_+ \times \mathbb{S}^2 \times \Omega$. Fibers are transported by the velocity vector field $\mathbf{u}$ and lengthening occurs at a rate $\tau \geq 0$ that depends on the free monomers density, ϕ. In dilute regime, the microscopic hydrodynamics is accounted for by the term $\mathcal{B}$ as in [169] and defined by

$$\mathcal{B}[\psi](r, \eta, \mathbf{y}, t) = A(r)\ \nabla_\eta \cdot \Big[D_1 \nabla_\eta \psi - \mathrm{P}_{\eta^\perp}\left(\nabla_{\mathbf{y}}\mathbf{u}\ \eta\right)\ \psi\Big],$$

where ∇_η and $(\nabla_\eta \cdot)$ denote the gradient and divergence on $\mathbb{S}^2$. $A \geq 0$ is a weight function that accounts for the influence of the length increase upon the motion and $D_1 > 0$ the diffusion coefficient on the sphere. Moreover, the transport on the sphere due to the velocity field is given by $\mathrm{P}_{\eta^\perp}\left(\nabla_{\mathbf{y}}\mathbf{u}\ \eta\right)$, with $\mathrm{P}_{\eta^\perp}\mathbf{z} = \mathbf{z} - (\mathbf{z} \cdot \eta)\eta$, for all $\mathbf{z} \in \mathbb{R}^3$, denoting the projection of the vector $\mathbf{z}$ on the tangent space at η.
The fragmentation (scission) process takes place at rate $\beta(\nabla_{\mathbf{y}}\mathbf{u}, \mathbf{u}, r, \eta) \geq 0$ and is described by $\mathcal{F}$ following [90] and given by

$$\mathcal{F}[\psi](r, \eta, \mathbf{y}, t) = -\beta(\nabla_{\mathbf{y}}\mathbf{u}, \mathbf{u}, r, \eta)\psi(r, \eta, \mathbf{y}, t) + 2\int_r^\infty \beta(\nabla_{\mathbf{y}}\mathbf{u}, \mathbf{u}, r', \eta)\kappa(r, r')\psi(r', \eta, \mathbf{y}, t)\ dr'.$$

The size redistribution kernel κ accounts for the fact that a polymer breaks into smaller fibers. It is symmetric, since a polymer of size r' breaks with equal probability into a fiber of size $r' - r$ and r; moreover, the fragmentation/recombination is mass preserving process. We assume here that upon splitting, given the pecularity of the motion process, and its impact on the scission, the resulting clusters of fibrils have the same center of mass as the initial polymer. It seems reasonable to assume that the orientation remains unchanged right after the scission. Therefore: $\kappa(r, r') \geq 0$, $\kappa(r, r') = 0$ if $r > r'$, $\kappa(r' - r, r') = \kappa(r, r')$ and

$$\int_0^{r'} \kappa(r, r')\ dr = 1. \tag{4.3}$$

The probability configurational function ψ must be a non-negative solution, satisfying the non-zero size boundary condition

$$\psi(0, \eta, \mathbf{y}, t) = 0,$$

and the initial condition

$$\psi(r,\eta,\mathbf{y},0)=\psi^0(r,\eta,\mathbf{y}),$$

with ψ^0 a known non-negative initial probability.

4.2.2 Monomers

The concentration of free monomers, given by the distribution $\phi(\mathbf{y},t)$ at time $t>0$ at any $\mathbf{y}\in\Omega$, solves

$$\frac{\partial}{\partial t}\phi+\mathbf{u}\cdot\nabla_{\mathbf{y}}\phi-D_2\Delta\phi=-\int_{\mathbb{S}^2\times\mathbb{R}_+}\tau(\phi,\mathbf{u},r,\eta)\psi(r,\eta,\mathbf{y},t)\;dr\;d\eta, \tag{4.4}$$

with $D_2>0$ the diffusion coefficient. The integral term is due to polymerization of monomers, being transconformed (misfolded), into fibers. Moreover, monomer concentration ϕ must be a non-negative solution satisfying the (no transport across) boundary condition

$$\nabla_y\phi\cdot\vec{n}=0 \text{ on } \partial\Omega,$$

with $\vec{n}$ the outward normal vector on the boundary $\partial\Omega$, as well as the initial condition

$$\phi(\mathbf{y},0)=\phi^0(\mathbf{y}),$$

with ϕ^0 an initially non-negative given concentration. We adjoin to these equations the balance equation for the total number of monomers contained in the domain Ω:

$$\int_\Omega\left[\phi(\mathbf{y},t)+\int_{\mathbb{R}_+\times\mathbb{S}^2}r\;\psi(r,\eta,\mathbf{y},t)\;d\eta\;dr\right]\;d\mathbf{y}=\rho, \text{ for all } t\geq 0, \tag{4.5}$$

where ρ is (experimentally) known from the outset. The above balance equation is formally satisfied, as a consequence of equations (4.2)–(4.4) using also (4.1).

4.2.3 Velocity vector field

As an aside, notice the velocity vector field, $\mathbf{u}(t,\mathbf{y})\in\mathbb{R}^3$, for all $t>0$ and $\mathbf{y}\in\Omega$, satisfies the Navier-Stokes equations (for incompressible fluids)

$$\begin{aligned}&\frac{\partial}{\partial t}\mathbf{u}+(\mathbf{u}\cdot\nabla)\,\mathbf{u}=-\nabla p+\nu\Delta\mathbf{u}-\nabla\cdot\mathbf{S},\\&\nabla\cdot\mathbf{u}=0,\\&\mathbf{u}\cdot\vec{n}=0.\end{aligned}$$

p is the pressure , ν the viscosity of the Newtonian solvent within which the prions (*i.e.* rigid-rod molecules) are dissolved, and $\mathbf{S}$ is the non-Newtonian extra stress tensor contribution (to the total stress) due to the presence of rigid rods. The latter is given by [23] as

$$\mathbf{S}(\mathbf{y},t)=\int_{\mathbb{R}_+}r^2\int_{\mathbb{S}^2}\eta\otimes\eta\;\psi\;d\eta dr.$$

In the following, we suppose that $\mathbf{u}$ is given and the unknown functions are only ψ and ϕ. The existence and uniqueness of the solutions to the full system with the Navier-Stokes equations introduced above (that is $\mathbf{u}$, ψ and ϕ) will be the topic of a subsequent work.

4.3 Main result

4.3.1 Constitutive assumptions

Assume the velocity vector field satisfies the regularity

$$\mathbf{u} \in \mathcal{C}^1\left([0,\infty), W^{1,\infty}(\Omega)\right)$$

such that

$$\nabla_{\mathbf{y}} \cdot \mathbf{u} = 0 \ \text{ and } \ \mathbf{u} \cdot \vec{n} = 0 \text{ on } \partial\Omega. \tag{4.6}$$

Next, we adhere to the view on prion proliferation expressed in [90, 91, 153, 184]. The splitting (scission) rate of fibers, given by β, is assumed to be linear in r. Therefore let $g : M_3(\mathbb{R}) \times \mathbb{R}^3 \times \mathbb{S}^2 \to \mathbb{R}_+$ be continuous with respect to the first and second variable, such that $\beta(\sigma, \mathbf{v}, r, \eta) = g(\sigma, \mathbf{v}, \eta)\, r$, for all $\sigma \in M_3(\mathbb{R})$, $\mathbf{v} \in \mathbb{R}^3$, $r > 0$ and $\eta \in \mathbb{S}^2$. Moreover, we assume that for all bounded subsets $B \subset \mathbb{R}^3$ and $O \subset M_3(\mathbb{R})$ there exist positive constants $\overline{g}_{B,O} \geq \underline{g}_{B,O}$ such that

$$\underline{g}_{B,O} \leq g(\sigma, \mathbf{v}, \eta) \leq \ \overline{g}_{B,O}, \quad \text{for every } \ (\sigma, \mathbf{v}, \eta) \in O \times B \times \mathbb{S}^2.$$

Let $T > 0$ be fixed. Then, due to the smoothness of $\mathbf{u}$, there exists $\overline{g} \geq \underline{g} > 0$ such that

$$\underline{g} \leq g(\nabla_{\mathbf{y}}\mathbf{u}, \mathbf{u}, \eta) \leq \overline{g}, \quad \text{for every } \ (t, \mathbf{y}, \eta) \in [0, T] \times \Omega \times \mathbb{S}^2.$$

We consider the polymerization rate τ linear in (the free monomers density) ϕ, i.e. there exists $\tau_0 > 0$ such that

$$\tau(\phi, \mathbf{v}, r, \eta) = \tau_0 \phi.$$

This assumption had been already evoked by Greer *et al.* [90] and corresponds to a mass action binding. The splitting kernel κ accounts for the probability of a polymer with initial length r, to split into a polymer with a shorter length r' as described in [90], and is given by

$$\kappa(r, r') = \begin{cases} 1/r' & \text{if } 0 < \mathrm{r} \leq \mathrm{r}', \\ 0 & \text{else.} \end{cases}$$

This expression is compatible with (4.3) (and the conservation law (4.5)). Then the length weight function $A \geq 0$ is supposed to be in $L^\infty(\mathbb{R}_+)$ and there exists $C_A > 0$ such that

$$\|A\|_{L^\infty(\Omega)} = C_A < \infty \tag{4.7}$$

We remark that, by virtue of $\mathbf{u}$ being sufficiently smooth and for fixed $T > 0$, there exists $C_P > 0$ such that

$$\|\mathrm{P}_{\eta^\perp}\left(\nabla_{\mathbf{y}}\mathbf{u}\ \eta\right)\|_{\mathrm{L}^\infty([0,\mathrm{T}]\times\Omega\times\mathbb{S}^2)} = \mathrm{C_P} < \infty,$$

Using the result stated in the Appendix, there exists $C_D > 0$ such that

$$\|\nabla_\eta \cdot \mathrm{P}_{\eta^\perp}\left(\nabla_{\mathbf{y}}\mathbf{u}\ \eta\right)\|_{\mathrm{L}^\infty([0,\mathrm{T}]\times\Omega\times\mathbb{S}^2)} = \mathrm{C_D} < \infty. \tag{4.8}$$

Thanks to the assumptions given in this section, the problem can be re-written as:

$$\begin{aligned}\frac{\partial}{\partial t}\psi + \mathbf{u}\cdot\nabla_{\mathbf{y}}\psi + \tau_0\phi\frac{\partial}{\partial r}\psi - A(r)\ \nabla_\eta\cdot\left[D_1\nabla_\eta\psi - \mathrm{P}_{\eta^\perp}\left(\nabla_{\mathbf{y}}\mathbf{u}\ \eta\right)\ \psi\right] \\ = -g(\nabla_{\mathbf{y}}\mathbf{u},\mathbf{u},\eta)r\psi + 2g(\nabla_{\mathbf{y}}\mathbf{u},\mathbf{u},\eta)\int_r^\infty \psi(r',\eta,\mathbf{y},t)\ dr',\end{aligned} \tag{4.9a}$$

$$\frac{\partial}{\partial t}\phi + \mathbf{u}\cdot\nabla_{\mathbf{y}}\phi - D_2\Delta\phi = -\tau_0\phi\int_{\mathbb{S}^2\times\mathbb{R}_+}\psi(r,\eta,\mathbf{y},t)\ dr\ d\eta, \tag{4.9b}$$

$$\psi(r=0,\eta,\mathbf{y},t) = 0, \tag{4.9c}$$

$$\nabla_y\phi\cdot\vec{n} = 0, \quad \text{on } \partial\Omega \tag{4.9d}$$

$$\psi(t=0) = \psi^0 \text{ and } \phi(t=0) = \phi^0, \tag{4.9e}$$

Remark 4.1 (Particular case: Zero velocity field, as in the Greer's model). Consider $\mathbf{u} = 0$, and assume that g is such that $g(0,\eta) = g_0$, a constant, for any η. In fact, even in the absence of flow the prion-fibrils can undergo scission and re-combination. Suppose that ϕ is independent of y, then let $f(t,r) = \frac{1}{|\Omega|}\int_{\Omega\times\mathbb{S}^2}\psi(r,\eta,\mathbf{y},t)\ d\eta d\mathbf{y}$ be the average of ψ. Integrating equations (4.9) leads to

$$\begin{aligned}&\frac{\partial}{\partial t}f + \tau_0\phi(t)\frac{\partial}{\partial r}f + g_0 r f = 2\underline{g}\int_r^\infty f(r',t)\ dr' \text{ over } (\mathrm{t},\mathrm{r})\in\mathbb{R}^2_+,\\ &\frac{d}{dt}\phi(t) = -\tau_0\phi(t)\int_{\mathbb{R}_+} f(r,t)\ dr,\\ &f(0,t) = 0.\end{aligned}$$

Note that the above system of equations is the one proposed in [90] where it was produced under the assumption of prion conservation mass (no protein synthesis, no metabolic degradation).

4.3.2 Functional framework

In this section we present the functional framework one of the main mathematical novelty of this chapter, next the definition of weak solutions to the system (4.9).

Let $a:\mathbb{R}_+\to\mathbb{R}_+$ be defined by $a(r) = \mathrm{e}^{\alpha r}$ for a $\alpha > 0$. Denote $Q = \mathbb{S}^2\times\mathbb{R}_+$ and $d\mathbf{q} = a(r)drd\eta$. Let the following Hilbert spaces be defined as

$$L^2_\alpha = \left\{\psi\in L^1_{loc}\left(\Omega\times Q\right),\ \int_{\Omega\times Q}\psi^2\ d\mathbf{q}d\mathbf{y} < \infty\right\}.$$

Then,

$$V = \left\{\psi\in L^1_{loc}\left(\Omega\times Q\right),\ \int_{\Omega\times Q}\left(A(r)|\nabla_\eta\psi|^2 + (1+r)\psi^2\right)\ d\mathbf{q}d\mathbf{y} < \infty\right\},$$

and

$$V_1 = \Big\{ \psi \in L^1_{loc}(\Omega \times Q), \\ \int_{\Omega\times Q} \left(\left| \frac{\partial}{\partial r}\psi \right|^2 + A(r)|\nabla_\eta \psi|^2 + (1+r)\psi^2 \right) \, d\mathbf{q}d\mathbf{y} < \infty \Big\}.$$

Recall the Sobolev space $H^1(\Omega)$ endowed with the norm

$$\|\phi\|_{H^1} = \|\phi\|_{L^2(\Omega)} + \|\nabla_y \phi\|_{L^2(\Omega)}.$$

We also use the canonical embedding

$$V_1 \subset V \subset L^2_\alpha = (L^2_\alpha)' \subset V' \subset (V_1)'.$$

For any $\theta \in \mathbb{R}$, let $L^1_\theta = \Big\{ \psi \in L^1_{loc}(\Omega \times Q), \ \int_{\Omega\times Q} |\psi| \ r^\theta dr d\eta d\mathbf{y} < \infty \Big\}$. Then we have the canonical embedding

$$L^2_\alpha \subset L^1_\theta, \quad \text{for any } \ \alpha > 0 \ \text{ and } \ \theta \geq 0,$$

which makes sense in regard to the mass conservation and the total quantity of polymers when $\theta = 0$ or $\theta = 1$.

4.3.3 Variational formulation

To begin with, we introduce test function spaces. Let $T > 0$. First, for the polymer ψ-equation, let $\mathcal{X}_1$ be the completion of
$\mathcal{C}^\infty_c((-T,T) \times \overline{\Omega} \times \mathbb{S}^2 \times [0,+\infty))$ with respect to the norm $\| \cdot \|_{\mathcal{X}_1}$

$$\|\widetilde{\psi}\|_{\mathcal{X}_1} = \int_0^T \left(\left\| \frac{\partial}{\partial t}\widetilde{\psi} \right\|^2_{L^2_\alpha} + \|\nabla_{\mathbf{y}} \widetilde{\psi}\|^2_{L^2_\alpha} + \|\widetilde{\psi}\|^2_{V_1} \right) \, dt$$

In particular, this implies that, if $\widetilde{\psi} \in \mathcal{X}_1$, then $\widetilde{\psi}(t = T) = 0$. Second, the test functions for the ϕ-equation are elements of $\mathcal{X}_2$, the latter space being the completion of $\mathcal{C}^\infty_c((-T,T)\times\overline{\Omega})$ with respect to the norm $H^1((0,T) \times \Omega)$. In particular this implies that if $\widetilde{\phi} \in \mathcal{X}_2$, then $\widetilde{\phi}(t = T) = 0$. In order to obtain a variational formulation of (4.9) we first assume that we have a strong solution which is smooth enough. Then we multiply (4.9a) by $\widetilde{\psi}(r, \eta, \mathbf{y}, t)a(r)$, with $\widetilde{\psi} \in \mathcal{X}_1$, and integrate over $(0,T) \times \Omega \times Q$, next we multiply (4.9b) by $\widetilde{\phi} \in \mathcal{X}_2$ and integrate over $(0,T) \times \Omega$. We note

$$\begin{aligned} \int_{\mathbb{R}_+} \tau_0 \phi \frac{\partial}{\partial r}\psi \ \widetilde{\psi} \ a(r)dr &= -\int_{\mathbb{R}_+} \tau_0 \phi\psi \ \frac{\partial}{\partial r}\left(\widetilde{\psi} a(r)\right) \ dr, \\ &= -\int_{\mathbb{R}_+} \tau_0 \phi\psi \ \left(\frac{\partial}{\partial r}\widetilde{\psi} + \alpha\widetilde{\psi} \right) \ a(r)dr, \end{aligned}$$

since $\widetilde{\psi} \in \mathcal{X}_1$. One also has:

$$\int_{\mathbb{S}^2} \nabla_\eta \cdot (D_1 \nabla_\eta \psi) \, \widetilde{\psi} \ d\eta = -\int_{\mathbb{S}^2} D_1 \nabla_\eta \psi \cdot \left(\nabla_\eta \widetilde{\psi} - 2\eta\widetilde{\psi} \right) \ d\eta,$$

and

$$\int_{\mathbb{S}^2} \nabla_\eta \cdot \left(\mathrm{P}_{\eta^\perp} \left(\nabla_{\mathbf{y}} \mathbf{u} \; \eta \right) \psi \right) \widetilde{\psi} \; d\eta = - \int_{\mathbb{S}^2} \mathrm{P}_{\eta^\perp} \left(\nabla_{\mathbf{y}} \mathbf{u} \; \eta \right) \psi \cdot \left(\nabla_\eta \widetilde{\psi} - 2\eta \widetilde{\psi} \right) \; \mathrm{d}\eta,$$
$$= - \int_{\mathbb{S}^2} \mathrm{P}_{\eta^\perp} \left(\nabla_{\mathbf{y}} \mathbf{u} \; \eta \right) \psi \cdot \nabla_\eta \widetilde{\psi} \; \mathrm{d}\eta,$$

since $\mathrm{P}_{\eta^\perp} \left(\nabla_{\mathbf{y}} \mathbf{u} \; \eta \right) \cdot \eta = 0$ (see for instance Appendix II in [169] for calculation details on the sphere). Moreover, by assumption (4.6) on $\mathbf{u}$,

$$\int_\Omega \left(\mathbf{u} \cdot \nabla_{\mathbf{y}} \psi \right) \widetilde{\psi} \; d\mathbf{y} = - \int_\Omega \psi \left(\mathbf{u} \cdot \nabla_{\mathbf{y}} \widetilde{\psi} \right) \; d\mathbf{y},$$

and

$$\int_\Omega \left(\mathbf{u} \cdot \nabla_{\mathbf{y}} \phi \right) \widetilde{\phi} \; d\mathbf{y} = - \int_\Omega \phi \left(\mathbf{u} \cdot \nabla_{\mathbf{y}} \widetilde{\phi} \right) \; d\mathbf{y}.$$

Then a variational formulation of (4.9a) is

$$\begin{aligned} &- \int_{\Omega \times Q} \psi^0 \; \widetilde{\psi}(t=0) \; d\mathbf{q} d\mathbf{y} - \int_0^T \int_{\Omega \times Q} \psi \left(\frac{\partial}{\partial t} \widetilde{\psi} + \mathbf{u} \cdot \nabla_{\mathbf{y}} \widetilde{\psi} \right) \; d\mathbf{q} d\mathbf{y} \; dt \\ &+ \int_0^T \int_{\Omega \times Q} A(r) \left(D_1 \nabla_\eta \psi \left(\nabla_\eta \widetilde{\psi} - 2\eta \widetilde{\psi} \right) - \mathrm{P}_{\eta^\perp} \left(\nabla_{\mathbf{y}} \mathbf{u} \; \eta \right) \psi \cdot \nabla_\eta \widetilde{\psi} \right) \; d\mathbf{q} d\mathbf{y} \; dt \\ &+ \int_0^T \int_{\Omega \times Q} \psi \left(g(\nabla_{\mathbf{y}} \mathbf{u}, \mathbf{u}, \eta) r \widetilde{\psi} - \tau_0 \phi \left(\frac{\partial}{\partial r} \widetilde{\psi} + \alpha \widetilde{\psi} \right) \right) \; d\mathbf{q} d\mathbf{y} \; dt \\ &\qquad = 2 \int_0^T \int_{\Omega \times Q} g(\nabla_{\mathbf{y}} \mathbf{u}, \mathbf{u}, \eta) \left(\int_r^\infty \psi \; dr' \right) \widetilde{\psi} \; d\mathbf{q} d\mathbf{y} \; dt, \end{aligned} \tag{4.10}$$

for any $\widetilde{\psi} \in \mathcal{X}_1$ and for (4.9b),

$$\begin{aligned} &- \int_\Omega \phi^0 \; \widetilde{\phi}(t=0) \; d\mathbf{y} - \int_0^T \int_\Omega \phi \; \left(\frac{\partial}{\partial t} \widetilde{\phi} + \mathbf{u} \cdot \nabla_{\mathbf{y}} \widetilde{\phi} \right) \; d\mathbf{y} \; dt + \\ &\qquad + \int_0^T \int_\Omega \left[D_2 \; \nabla_{\mathbf{y}} \phi \cdot \nabla_{\mathbf{y}} \widetilde{\phi} + \tau_0 \phi \; \widetilde{\phi} \left(\int_{\mathbb{S}^2 \times \mathbb{R}_+} \psi \; dr d\eta \right) \right] \; d\mathbf{y} \; dt = 0, \end{aligned} \tag{4.11}$$

for any $\widetilde{\phi} \in \mathcal{X}_2$.

4.3.4 Theorem of existence

At this point we are prepared to introduce our main result. It gives the existence of non-negative weak solution to our problem under the general assumptions of section 4.3.1.

Theorem 4.1 (**Main result**). *Let $\phi^0 \in L^\infty(\Omega)$ be non-negative and $\psi^0 \in L^2_\alpha$ non-negative such that there exists a constant $C_0 > 0$ with*

$$\psi^0 \leq C_0 e^{-\alpha r}.$$

Then, for any $T > 0$, there exists at least one solution (ψ, ϕ) to the weak formulation (4.10)-(4.11) of the problem (4.9), with ψ and ϕ non-negative. Moreover we have $\psi \in L^\infty(0,T; L^2_\alpha) \cap L^2(0,T;V)$ and $\phi \in L^\infty(0,T; L^2(\Omega)) \cap L^2(0,T; H^1(\Omega))$.

Remark 4.2. Proving the uniqueness of the solution is a rather lengthy undertaking and will be done in a follow up work.

Remark 4.3. Weak solutions to the above variational formulation with stronger regularity than the one implied by the theorem above satisfy the problem (4.9) in a strong sense. Moreover, this variational formulation complies weakly with the mass conservation principle. Therefore, let $\varphi \in H^1(0,T)$, with $\varphi(t=T)=0$, and take $\widetilde{\psi}(r,\eta,\mathbf{y},t) = re^{-\alpha r}\varphi(t) \in \mathcal{X}_1$ and $\widetilde{\phi}(t,\mathbf{y}) = \varphi(t) \in \mathcal{X}_2$ in the variational formulations. Using the fact that, for any real value function f

$$\int_{\mathbb{S}^2} \eta \cdot \nabla_\eta f \; d\eta = 0.$$

we obtain

$$-\varphi(t=0)\int_\Omega \left[\phi^0 + \int_{\mathbb{R}_+\times\mathbb{S}^2} r\ \psi^0\ d\eta\ dr\right] d\mathbf{y} \\ - \int_0^T \frac{d}{dt}\varphi(t)\ \int_\Omega \left[\phi + \int_{\mathbb{R}_+\times\mathbb{S}^2} r\ \psi\ d\eta\ dr\right] d\mathbf{y}\ dt = 0.$$

If the solution is smooth enough we have then the mass conservation result

$$\frac{d}{dt}\int_\Omega \left[\phi + \int_{\mathbb{R}_+\times\mathbb{S}^2} r\ \psi\ d\eta\ dr\right]\ d\mathbf{y} = 0.$$

4.4 Proof of the main result

The proof consists of three main steps. First (subsection 3.1), a semi-discretization in time of the problem to obtain an approximation of the solution. Second, we get appropriate estimates (subsection 3.2), and third we obtain a solution by passing to the limit (subsection 3.3).

4.4.1 Semi-discretization in time

Let $N > 0$ and $\{t_n\}_{n=0}^N$ a subdivision of $[0,T]$ such that $t_0 = 0$, $t_N = T$ and $t_n - t_{n-1} = \Delta t > 0$. We denote by ψ^n and ϕ^n the approximations of ψ and ϕ at t_n. Denote $\mathbf{u}^n(\mathbf{y}) = \mathbf{u}(t_n,\mathbf{y})$. First, for any $s \in [0,T]$, consider the following problem on $[0,T]$:

$$\begin{cases} \dfrac{d}{dt}\chi^n(t) = \mathbf{u}^n(\chi^n(t)), \\ \chi(s) = \mathbf{y}. \end{cases}$$

We recall that the regularity of $\mathbf{u}$ is $\mathcal{C}^1(0,T;W^{1,\infty})$, therefore $\mathbf{u}^n \in W^{1,\infty}(\Omega)$ so that there exists a unique solution χ^n which will be denoted in the following by $\chi^n(t;s,\mathbf{y})$. The map $\mathbf{y} \to \chi^n(t;s,\mathbf{y})$ is a homeomorphism from Ω onto Ω, and since $\mathbf{u}$ is divergence-free, we have

$$\det \nabla_y \chi^n(t;s,\cdot) = 1, \text{ a.e. in } \Omega \times [0,T].$$

Define the function

$$x_n : \Omega \to \Omega, \text{ by } x_n(\mathbf{y}) = \chi^n(t_n; t_{n-1}, \mathbf{y}).$$

This map x_n is invertible. Let us denote z_n as its inverse. We remark that

$$z_n(\mathbf{y}) = \chi^n(t_{n-1}; t_n, \mathbf{y}).$$

Assume now that $\psi^{n-1} \in V$ and $\phi^{n-1} \in H^1$ are known. We consider two problems: find $\psi^n \in V$ such that

$$\begin{aligned}
&\int_{\Omega\times Q} \frac{\psi^n(r,\eta,\mathbf{y}) - \psi^{n-1}(r,\eta,z_n(\mathbf{y}))}{\Delta t}\ \widehat{\psi}\ d\mathbf{q}d\mathbf{y} \\
&\quad + \int_{\Omega\times Q} A(r)\left(D_1\nabla_\eta\psi^n \cdot \left(\nabla_\eta\widehat{\psi} - 2\eta\widehat{\psi}\right) - \mathrm{P}_{\eta^\perp}\left(\nabla_{\mathbf{y}}\mathbf{u}^n\eta\right)\psi^n \cdot \nabla_\eta\widehat{\psi}\right)\ d\mathbf{q}d\mathbf{y} \\
&\quad + \int_{\Omega\times Q} \psi^n\left(g(\nabla_{\mathbf{y}}\mathbf{u}^n, \mathbf{u}^n, \eta) r\widehat{\psi} - \tau_0\phi^{n-1}\left(\frac{\partial}{\partial r}\widehat{\psi} + \alpha\widehat{\psi}\right)\right)\ d\mathbf{q}d\mathbf{y} \\
&\qquad\qquad = 2\int_{\Omega\times Q} g(\nabla_{\mathbf{y}}\mathbf{u}^n, \mathbf{u}^n, \eta)\left(\int_r^\infty \psi^{n-1}\ dr'\right)\widehat{\psi}\ a(r) dr d\eta d\mathbf{y}, \quad (4.12)
\end{aligned}$$

for any $\widehat{\psi} \in V_1$, and find $\phi^n \in H^1$ such that

$$\begin{aligned}
&\int_\Omega \left(\frac{\phi^n(\mathbf{y}) - \phi^{n-1}(\mathbf{y})}{\Delta t}\ + \mathbf{u}^n \cdot \nabla_y\phi^n\right)\widehat{\phi}\ d\mathbf{y}\ dt \\
&\qquad + \int_\Omega \left[D_2\ \nabla_{\mathbf{y}}\phi^n \cdot \nabla_{\mathbf{y}}\widehat{\phi} + \tau_0\phi^n\ \left(\int_{\mathbb{S}^2\times\mathbb{R}_+} \psi^{n-1}\ dr d\eta\right)\widehat{\phi}\right]\ d\mathbf{y} = 0, \quad (4.13)
\end{aligned}$$

for any $\widehat{\phi} \in H^1$. Problem (4.12) is re-written as

$$a^n(\psi^n, \widehat{\psi}) = l_a^n(\widehat{\psi}), \text{ for any } \widehat{\psi} \in V_1 \quad (4.14)$$

with

$$a^n = a^{1n} + a^{2n}$$

where a^{1n}, a^{2n} are defined on $V \times V_1$ by

$$\begin{aligned}
a^{1n}(\varphi_1, \varphi_2) = &\int_{\Omega\times Q} A(r) D_1 \nabla_\eta\varphi_1 \cdot (\nabla_\eta\varphi_2 - 2\eta\varphi_2)\ d\mathbf{q}d\mathbf{y} \\
&- \int_{\Omega\times Q} A(r)\mathrm{P}_{\eta^\perp}\left(\nabla_{\mathbf{y}}\mathbf{u}^n\eta\right)\varphi_1 \cdot \nabla_\eta\varphi_2\ d\mathbf{q}d\mathbf{y} \\
&- \tau_0\int_{\Omega\times Q} \phi^{n-1}\varphi_1\left(\frac{\partial}{\partial r}\varphi_2 + \alpha\ \varphi_2\right)\ d\mathbf{q}d\mathbf{y} \\
&+ \int_{\Omega\times Q} g(\nabla_{\mathbf{y}}\mathbf{u}^n, \mathbf{u}^n, \eta) r\varphi_1\varphi_2\ d\mathbf{q}d\mathbf{y}
\end{aligned}$$

and

$$a^{2n}(\varphi_1, \varphi_2) = \frac{1}{\Delta t}\int_{\Omega\times Q} \varphi_1\varphi_2\ d\mathbf{q}d\mathbf{y},$$

respectively, and l_a^n is defined on L^2_α by

$$\begin{aligned} l_a^n(\varphi) = 2\int_{\Omega\times Q} g(\nabla_{\mathbf{y}}\mathbf{u}^n, \mathbf{u}^n, \eta)\left(\int_r^\infty \psi^{n-1}\, dr'\right)\varphi\, d\mathbf{q}d\mathbf{y} \\ + \frac{1}{\Delta t}\int_{\Omega\times Q} \psi^{n-1}\circ z_n\ \varphi\, d\mathbf{q}d\mathbf{y}. \end{aligned} \tag{4.15}$$

The problem (4.13) is re-written as

$$b^n(\phi^n, \widehat{\phi}) = l_b^n(\widehat{\phi}),\ \text{ for any } \widehat{\phi}\in H^1, \tag{4.16}$$

with b^n defined on $H^1\times H^1$ such that

$$\begin{aligned} b^n(\varphi_1,\varphi_2) = \int_\Omega \left(\frac{1}{\Delta t}\varphi_1\ \varphi_2\ + (\mathbf{u}^n\cdot\nabla_{\mathbf{y}}\varphi_1)\,\varphi_2 + D_2\ \nabla_{\mathbf{y}}\varphi_1\cdot\nabla_{\mathbf{y}}\varphi_2\right)d\mathbf{y} \\ + \int_\Omega \tau_0\varphi_1\ \varphi_2\ \left(\int_{\mathbb{S}^2\times\mathbb{R}_+}\psi^{n-1}\, drd\eta\right)\ d\mathbf{y}, \end{aligned}$$

and l_b^n defined on L^2 by

$$l_b^n(\varphi) = \frac{1}{\Delta t}\int_\Omega \phi^{n-1}\varphi\ d\mathbf{y}. \tag{4.17}$$

Lemma 4.2. *Let $N\in\mathbb{N}^*$, $\phi^0\in L^\infty(\Omega)$, $\phi^0\geq 0$ and $\psi^0\in L^2_\alpha$ such that*

$$0\leq\psi^0\leq C_0e^{-\alpha r}\ \ a.e\ in\ Q$$

with $C_0>0$ a constant.

Then there exist two sequences $\{\psi^n\}_{n=1}^N\subset V$ and $\{\phi^n\}_{n=1}^N\subset H^1(\Omega)$ satisfying (4.14) and (4.16).
Moreover, for Δt small enough, we have that:

$$0\leq\psi^n\leq C_\infty e^{-\alpha r}, \qquad \text{for every } n\in\{0,1,\dots,N\}, \tag{4.18a}$$

$$0\leq\phi^n\leq\|\phi^0\|_{L^\infty}, \qquad \text{for every } n\in\{0,1,\dots,N\}, \tag{4.18b}$$

and

$$\begin{aligned} \max_{n=0,\cdots N}\Bigg[\int_{\Omega\times Q}|\psi^n|^2\ d\mathbf{q}d\mathbf{y} + D_1\Delta t\sum_{n=1}^N\int_{\Omega\times Q}A(r)|\nabla_\eta\psi^n|^2\ d\mathbf{q}d\mathbf{y} \\ +2\underline{g}\Delta t\sum_{n=1}^N\int_{\Omega\times Q}r|\psi^n|^2\ d\mathbf{q}d\mathbf{y} + \sum_{n=1}^N\int_{\Omega\times Q}|\psi^n-\psi^{n-1}\circ z_n|^2\ d\mathbf{q}d\mathbf{y}\Bigg] \\ \leq 4e^{k_3T}\|\psi^0\|^2_{L^2_\alpha}, \end{aligned} \tag{4.19}$$

and

$$\max_{n=0,\cdots N}\left[\int_\Omega |\phi^n|^2\,d\mathbf{y}+\sum_{n=1}^N\int_\Omega|\phi^n-\phi^{n-1}|^2\,d\mathbf{y}+2D_2\Delta t\sum_{n=1}^N\int_\Omega|\nabla_{\mathbf{y}}\phi^n|^2\;d\mathbf{y}\right]$$
$$\leq 2\|\phi^0\|^2_{L^2(\Omega)},\quad (4.20)$$

where in the above we denoted

$$k_1=\frac{2\overline{g}}{\alpha},$$
$$k_2=\alpha\tau_0\|\phi^0\|_{L^\infty}+C_DC_A,$$
$$C_\infty=2C_0e^{(k_1+k_2)T},$$

and

$$k_3=\alpha\tau_0\|\phi^0\|_{L^\infty}+\frac{C_P^2C_A}{D_1}+4\bar{g}\alpha^{-3/2}C_\infty\sqrt{|\Omega||S_2|}.$$

(Recall C_D and C_A are given by equations (4.7) and (4.8)).

Proof of Lemma 4.2. Let us consider the sequence of numbers $\{C_n\}_{n=0}^N$ defined by induction as

$$C_n=\frac{1+k_1\Delta t}{1-k_2\Delta t}C_{n-1},\ \text{for every } n=1,\dots,N. \quad (4.21)$$

with C_0 as in the hypothesis of the Lemma.
We proceed by induction. Suppose that ψ^{n-1} and ϕ^{n-1} are defined as elements of V and $L^\infty(\Omega)$, respectively. Suppose also that

$$0\leq\psi^{n-1}\leq C_{n-1}e^{-\alpha r}, \quad (4.22a)$$
$$0\leq\phi^{n-1}\leq\|\phi^0\|_{L^\infty}. \quad (4.22b)$$

We shall prove the existence of $\psi^n\in V$ and $\phi^n\in H^1(\Omega)$ solutions of (4.14) and (4.16), respectively. We also prove that they satisfy

$$0\leq\psi^n\leq C_ne^{-\alpha r},$$
$$0\leq\phi^n\leq\|\phi^0\|_{L^\infty}.$$

The above inequalities give (4.18a) and (4.18b) since we have

$$C_n=C_0\left(\frac{1+k_1\Delta t}{1-k_2\Delta t}\right)^n\leq C_\infty$$

for Δt small enough.

Step 1. *Regularization and existence.*

We introduce a regularization of a^n, denoted a^n_ε defined on $V_1 \times V_1$,

$$a^n_\varepsilon(\varphi_1, \varphi_2) = \varepsilon \int_{\Omega\times Q} \frac{\partial}{\partial r}\varphi_1 \frac{\partial}{\partial r}\varphi_2 \; d\mathbf{q}d\mathbf{y} + a^n(\varphi_1, \varphi_2).$$

We shall first prove the existence of a sequence $(\psi^n_\varepsilon)_\varepsilon$ in V_1 solutions of

$$a^n_\varepsilon(\psi^n_\varepsilon, \widehat{\psi}) = l^n_a(\widehat{\psi}), \quad \text{for any } \widehat{\psi} \in V_1 \tag{4.23}$$

Clearly a^n_ε is bilinear and continuous on $V_1 \times V_1$. Next we prove the coercivity of a^n_ε. Indeed, let $\varphi \in V_1$ and we remark that

$$\int_{\mathbb{S}^2} 2\eta \cdot \nabla_\eta\varphi \; \varphi \; d\eta = \int_{\mathbb{S}^2} \eta \cdot \nabla_\eta\varphi^2 \; d\eta = 0$$

since $\nabla_\eta \cdot \eta = 2$ and $\eta \cdot \eta = 1$. One has

$$\int_{\mathbb{S}^2} |A(r)\mathrm{P}_{\eta^\perp}(\nabla_{\mathbf{y}}\mathbf{u}\; \eta)\, \varphi \cdot \nabla_\eta\varphi| \; \mathrm{d}\eta \le \frac{1}{2}\int_{\mathbb{S}^2} \left(\mathrm{D_1A(r)}|\nabla_\eta\varphi|^2 \; + \frac{\mathrm{C_P^2C_A}}{\mathrm{D_1}}\varphi^2\right) \; \mathrm{d}\eta.$$

Finally,

$$\tau_0 \int_{\mathbb{R}_+} \phi^{n-1}\varphi\frac{\partial}{\partial r}\varphi \; a(r)dr \le -\frac{1}{2}\alpha\tau_0 \int_{\mathbb{R}_+} \phi^{n-1}\varphi^2 \; a(r)dr. \tag{4.24}$$

We remark that this inequality can be proved by using a regularized sequence $(\varphi_m)_m$ that converges to φ in V_1 and the fact that the remaining term in the right-hand side of (4.24) can be dropped according to its appropriate sign. Then, invoking (4.22b) and the above remarks, it follows that

$$\begin{aligned} a^{1n}_\varepsilon(\varphi, \varphi) \ge \frac{D_1}{2}\int_{\Omega\times Q} A(r)|\nabla_\eta\varphi|^2 \; d\mathbf{q}d\mathbf{y} + \underline{g}\int_{\Omega\times Q} r\varphi^2 \; d\mathbf{q}d\mathbf{y} \\ - \frac{1}{2D_1}\left(\alpha\tau_0 D_1\|\phi^0\|_{L^\infty} + C_P^2C_A\right)\int_{\Omega\times Q}\varphi^2 \; d\mathbf{q}d\mathbf{y}, \end{aligned}$$

which in turn implies

$$\begin{aligned} a^n_\varepsilon(\varphi, \varphi) \ge \; & \varepsilon\int_{\Omega\times Q}\left|\frac{\partial}{\partial r}\varphi\right|^2 \; d\mathbf{q}d\mathbf{y} + \frac{D_1}{2}\int_{\Omega\times Q} A(r)|\nabla_\eta\varphi|^2 \; d\mathbf{q}d\mathbf{y} \\ & + \underline{g}\int_{\Omega\times Q} r\varphi^2 \; d\mathbf{q}d\mathbf{y} \\ & + \frac{1}{2D_1}\left(\frac{2D_1}{\Delta t} - \alpha\tau_0 D_1\|\phi^0\|_{L^\infty} - C_P^2C_A\right)\int_{\Omega\times Q}\varphi^2 \; d\mathbf{q}d\mathbf{y}, \end{aligned} \tag{4.25}$$

The coercivity of a^n_ϵ follows for Δt small enough.
Next, due to the inequality (4.22a), we have

$$\int_r^\infty \psi^{n-1} \, dr' \le \frac{C_{n-1}}{\alpha}$$

which implies that, for any $\varphi \in L^2_\alpha$,

$$\int_{\Omega\times Q} g(\nabla_{\mathbf{y}}\mathbf{u}^n, \mathbf{u}^n, \eta) \left(\int_r^\infty \psi^{n-1}\ dr'\right)\ |\varphi|\ d\mathbf{q}d\mathbf{y} \leq \frac{\bar{g}}{\alpha}\int_{\Omega\times Q} |\varphi|\ drd\eta d\mathbf{y}. \tag{4.26}$$

One also obtains

$$\int_{\Omega\times Q} \psi^{n-1}\circ z_n\ |\varphi|\ d\mathbf{q}d\mathbf{y} \leq C_{n-1}\int_{\Omega\times Q} |\varphi|\ drd\eta d\mathbf{y}. \tag{4.27}$$

We deduce that $l^n_a \in (L^2_\alpha)' \subset (V_1)'$ by the continuous embedding of L^2_α in L^1. Applying the Lax-Milgram theorem, for all $\varepsilon > 0$ there exists a unique $\psi^n_\varepsilon \in V_1$ solution of (4.23). Next we will prove the existence of solutions to (4.16). First, b^n is clearly a bilinear and continuous function on $H^1 \times H^1$. To prove its coercivity, let $\varphi \in H^1$. Since

$$\int_\Omega \mathbf{u}^n \cdot \nabla_{\mathbf{y}}\varphi\ \varphi = \frac{1}{2}\int_\Omega \mathbf{u}^n \cdot \nabla_{\mathbf{y}}\varphi^2 = 0 \tag{4.28}$$

we have

$$b^n(\varphi,\varphi) \geq \frac{1}{\Delta t}\int_\Omega \varphi^2\ d\mathbf{y} + D_2\int_\Omega |\nabla_{\mathbf{y}}\varphi|^2\ d\mathbf{y},$$

using the positivity of ψ^{n-1}, and thus b^n is coercive. Moreover, $l^n_b \in (H^1)'$ since $\phi^{n-1} \in L^\infty$. As a consequence of the Lax-Milgram theorem, there exists a unique $\phi^n \in H^1$ satifying (4.16).

Step 2. L^∞ - *Estimates*

To begin we first prove two estimates for ψ^n_ε: for its V-norm and for its derivative with respect to r. It follows from (4.25) and the continuity of l^n_a that there exists a constant $C > 0$, dependent of Δt, such that

$$\int_{\Omega\times Q} \left(A(r)|\nabla_\eta\psi^n_\varepsilon|^2 + (1+r)|\psi^n_\varepsilon|^2\right)\ d\mathbf{q}d\mathbf{y} \leq C,$$
$$\varepsilon\int_{\Omega\times Q} \left|\frac{\partial}{\partial r}\psi^n_\varepsilon\right|^2\ d\mathbf{q}d\mathbf{y} \leq C.$$

Next we prove the non-negativity of ψ^n_ε and ϕ^n. Let us denote $[\cdot]_+$ and $[\cdot]_-$ respectively the positive and negative part, both positive valued. Then, $\phi^n = [\phi^n]_+ - [\phi^n]_-$ and these two parts belong to H^1. We have

$$l^n_b([\phi^n]_-) = b^n(\phi^n, [\phi^n]_-) = -b^n([\phi^n]_-, [\phi^n]_-)$$

and invoking (4.17) and (4.22b), $l^n_b([\phi^n]_-) \geq 0$. Therefore

$$b^n([\phi^n]_-, [\phi^n]_-) \leq 0,$$

hence $\phi^n \geq 0$. Next, $\psi^n_\varepsilon = [\psi^n_\varepsilon]_+ - [\psi^n_\varepsilon]_-$, the positive and negative parts belong V_1, and

$$l^n_a([\psi^n_\varepsilon]_-) = a^n_\varepsilon(\psi^n_\varepsilon, [\psi^n_\varepsilon]_-) = -a^n_\varepsilon([\psi^n_\varepsilon]_-, [\psi^n_\varepsilon]_-),$$

Invoking (4.15) and (4.22a), $l_a^n([\psi_\varepsilon^n]_-) \geq 0$. Thus

$$a_\varepsilon^n([\psi_\varepsilon^n]_-, [\psi_\varepsilon^n]_-) \leq 0,$$

hence $\psi_\varepsilon^n \geq 0$. Let us now obtain L^∞ estimates . We have, according to (4.22b) and using the above notation, that

$$\begin{aligned} b^n([\phi^n - \|\phi^0\|_{L^\infty}]_+, [\phi^n - \|\phi^0\|_{L^\infty}]_+) \\ &= b^n(\phi^n - \|\phi^0\|_{L^\infty}, [\phi^n - \|\phi^0\|_{L^\infty}]_+) \\ &= b^n(\phi^n, [\phi^n - \|\phi^0\|_{L^\infty}]_+) - b^n(\|\phi^0\|_{L^\infty}, [\phi^n - \|\phi^0\|_{L^\infty}]_+) \\ &= l_b^n([\phi^n - \|\phi^0\|_{L^\infty}]_+) - b^n(\|\phi^0\|_{L^\infty}, [\phi^n - \|\phi^0\|_{L^\infty}]_+) \\ &\leq \frac{1}{\Delta t} \int_\Omega \left(\phi^{n-1} - \|\phi^0\|_{L^\infty}\right) [\phi^n - \|\phi^0\|_{L^\infty}]_+ \, d\mathbf{y}, \end{aligned}$$

Then by (4.22b)

$$b^n([\phi^n - \|\phi^0\|_{L^\infty}]_+, [\phi^n - \|\phi^0\|_{L^\infty}]_+) \leq 0,$$

hence $\phi^n \leq \|\phi^0\|_{L^\infty}$. Let C_n as defined in (4.21); then

$$\begin{aligned} a_\varepsilon^n([\psi_\varepsilon^n - C_n e^{-\alpha r}]_+, [\psi_\varepsilon^n - C_n e^{-\alpha r}]_+) \\ &= a_\varepsilon^n(\psi_\varepsilon^n - C_n e^{-\alpha r}, [\psi_\varepsilon^n - C_n e^{-\alpha r}]_+) \\ &= a_\varepsilon^n(\psi_\varepsilon^n, [\psi_\varepsilon^n - C_n e^{-\alpha r}]_+) - a_\varepsilon^n(C_n e^{-\alpha r}, [\psi_\varepsilon^n - C_n e^{-\alpha r}]_+) \\ &= l_a^n([\psi_\varepsilon^n - C_n e^{-\alpha r}]_+) - a_\varepsilon^n(C_n e^{-\alpha r}, [\psi_\varepsilon^n - C_n e^{-\alpha r}]_+). \end{aligned} \tag{4.29}$$

Next, for any $\varphi \in V_1$ positive,

$$\begin{aligned} a_\varepsilon^n(C_n e^{-\alpha r}, \varphi) = &- \varepsilon \int_{\Omega\times Q} \alpha C_n \frac{\partial}{\partial r}\varphi \; dr d\eta d\mathbf{y} \\ &- \int_{\Omega\times Q} C_n A(r) \mathrm{P}_{\eta^\perp}(\nabla_{\mathbf{y}} \mathbf{u}^n \eta) \cdot \nabla_\eta \varphi \; dr d\eta d\mathbf{y} \\ &- \int_{\Omega\times Q} C_n \tau_0 \phi^{n-1} \left(\frac{\partial}{\partial r}\varphi + \alpha \, \varphi \right) \; dr d\eta d\mathbf{y} \\ &+ \int_{\Omega\times Q} C_n g(\nabla_{\mathbf{y}} \mathbf{u}^n, \mathbf{u}^n, \eta) r\varphi dr d\eta d\mathbf{y} + C_n \frac{1}{\Delta t} \int_{\Omega\times Q} \varphi \; dr d\eta d\mathbf{y}. \end{aligned}$$

We remark that

$$\begin{aligned} \varepsilon \int_{\Omega\times Q} \alpha C_n \frac{\partial}{\partial r}\varphi \; dr d\eta d\mathbf{y} = -\varepsilon \int_{\Omega\times\mathbb{S}^2} \alpha C_n \varphi(r=0,\eta,\mathbf{y}) \; d\eta d\mathbf{y} \leq 0, \\ \int_{\Omega\times Q} C_n \tau_0 \phi^{n-1} \frac{\partial}{\partial r}\varphi \; dr d\eta d\mathbf{y} = -\int_{\Omega\times\mathbb{S}^2} C_n \tau_0 \phi^{n-1} \varphi(r=0,\eta,\mathbf{y}) \; d\eta d\mathbf{y} \leq 0. \end{aligned}$$

Then, by (4.7), (4.8), (4.22b) and the positivity of φ,

$$\begin{aligned} a_\varepsilon^n(C_n e^{-\alpha r}, \varphi) &\geq \int_{\Omega\times Q} C_n A(r) \nabla_\eta \cdot \left(\mathrm{P}_{\eta^\perp}(\nabla_{\mathbf{y}} \mathbf{u}^n \eta)\right) \varphi \; dr d\eta d\mathbf{y} \\ &\quad + C_n \left(\frac{1}{\Delta t} - \alpha\tau_0 \|\phi^0\|_{L^\infty}\right) \int_{\Omega\times Q} \varphi \; dr d\eta d\mathbf{y} \\ &\geq C_n \left(\frac{1}{\Delta t} - k_2\right) \int_{\Omega\times Q} \varphi \; dr d\eta d\mathbf{y}. \end{aligned} \tag{4.30}$$

Moreover, by (4.15), (4.26) and (4.27)

$$l_a^n(\varphi) \leq C_{n-1}\left(\frac{2\overline{g}}{\alpha}+\frac{1}{\Delta t}\right)\int_{\Omega\times Q}\varphi\ dr d\eta d\mathbf{y}. \tag{4.31}$$

Now, replacing φ by $[\psi_\varepsilon^n - C_n \mathrm{e}^{-\alpha \mathrm{r}}]_+$ and using (4.29) (4.30) and (4.31) one gets

$$\begin{aligned} a_\varepsilon^n([\psi_\varepsilon^n - C_n e^{-\alpha r}]_+, [\psi_\varepsilon^n - C_n e^{-\alpha r}]_+) \\ \leq \left[C_{n-1}\left(k_1+\frac{1}{\Delta t}\right) - C_n\left(\frac{1}{\Delta t}-k_2\right)\right]\int_{\Omega\times Q}\varphi\ dr d\eta d\mathbf{y}. \end{aligned}$$

Using now the particular form of C_n gives

$$a_\varepsilon^n([\psi_\varepsilon^n - C_n e^{-\alpha r}]_+, [\psi_\varepsilon^n - C_n e^{-\alpha r}]_+) \leq 0,$$

hence

$$\psi_\varepsilon^n \leq C_n e^{-\alpha r}. \tag{4.32}$$

Step 3. *Convergence and positivity*

The sequence $(\psi_\varepsilon^n)_\varepsilon$ obtained for all $\varepsilon > 0$ is uniformly bounded in V by (4.4.1), so it weakly converges to an element $\psi^n \in V$ up to a subsequence. Moreover, $\left(\varepsilon^{1/2}\frac{\partial}{\partial r}\psi_\varepsilon^n\right)_\varepsilon$ is bounded in L^2_α, then for $\varepsilon \to 0$, ψ^n solves (4.14).The positivity of ψ_ε^n yields the positivity of ψ^n. Moreover, by virtue of (4.32), ψ^n for $\varepsilon \to 0$, and inequalities (4.18a) are satisfied.

Step 4. *Additional estimates*

From (4.25), (4.15) and (4.18a) one gets

$$\begin{aligned} 0 = a_\varepsilon^n(\psi_\varepsilon^n, \psi_\varepsilon^n) - l_a^n(\psi_\varepsilon^n) \geq & \frac{D_1}{2}\int_{\Omega\times Q} A(r)|\nabla_\eta \psi_\varepsilon^n|^2\ d\mathbf{q}d\mathbf{y} \\ & + \underline{g}\int_{\Omega\times Q} r|\psi_\varepsilon^n|^2\ d\mathbf{q}d\mathbf{y} \\ & - \frac{k_3}{2}\int_{\Omega\times Q}|\psi_\varepsilon^n|^2\ d\mathbf{q}d\mathbf{y} \\ & + \frac{1}{\Delta t}\int_{\Omega\times Q}\left(\psi_\varepsilon^n - \psi^{n-1}\circ z_n\right)\psi_\varepsilon^n\ d\mathbf{q}d\mathbf{y}. \end{aligned}$$

Remarking that $2s_1(s_1-s_2) = s_1^2 + (s_1-s_2)^2 - s_2^2$ for any reals s_1, s_2, leads to

$$\begin{aligned} D_1\int_{\Omega\times Q} A(r)|\nabla_\eta\psi_\varepsilon^n|^2\ d\mathbf{q}d\mathbf{y} + 2\underline{g}\int_{\Omega\times Q} r|\psi_\varepsilon^n|^2\ d\mathbf{q}d\mathbf{y} \\ + \frac{1}{\Delta t}\int_{\Omega\times Q}\left[|\psi_\varepsilon^n|^2 + |\psi_\varepsilon^n - \psi^{n-1}\circ z_n|^2 - |\psi^{n-1}\circ z_n|^2\right]\ d\mathbf{q}d\mathbf{y} \\ \leq k_3\int_{\Omega\times Q}|\psi_\varepsilon^n|^2\ d\mathbf{q}d\mathbf{y}. \end{aligned}$$

Then, taking the lim inf for $\varepsilon \to 0$, multiplying by Δt and using the fact that $\int_\Omega |\psi^{n-1} \circ z_n|^2 = \int_\Omega |\psi^{n-1}|^2$, gives

$$D_1 \Delta t \int_{\Omega\times Q} A(r)|\nabla_\eta \psi^n|^2 \, d\mathbf{q}d\mathbf{y} + 2\underline{g}\Delta t \int_{\Omega\times Q} r|\psi^n|^2 \, d\mathbf{q}d\mathbf{y}$$
$$+ (1 - k_3\Delta t) \int_{\Omega\times Q} |\psi^n|^2 \, d\mathbf{q}d\mathbf{y} + \int_{\Omega\times Q} |\psi^n - \psi^{n-1} \circ z_n|^2 \, d\mathbf{q}d\mathbf{y}$$
$$\leq \int_{\Omega\times Q} |\psi^{n-1}|^2 \, d\mathbf{q}d\mathbf{y}.$$

Multiply the last inequality by $(1 - k_3\Delta t)^{n-1}$ and sum over n from 1 to N. Use the inequality

$$(1 - k_3\Delta t)^n \geq (1 - k_3\Delta t)^N \geq \frac{1}{2} e^{-k_3 T}$$

to get (4.19). Taking $\hat{\phi} = \phi^n$ in (4.13) and using (4.18b) and (4.28) we obtain

$$\frac{1}{2\Delta t} \int_\Omega \left(|\phi^n|^2 + |\phi^n - \phi^{n-1}|^2 - |\phi^{n-1}|^2 \right) \, d\mathbf{y} + D_2 \int_\Omega |\nabla_{\mathbf{y}} \phi^n|^2 \, d\mathbf{y} \leq 0$$

Summing over n from 1 to N produces (4.20), which ends the proof. □

4.4.2 Construction of a solution

We now define, for any N large enough, the following functions

$$\psi_N(\cdot, t) = \frac{t - t_{n-1}}{\Delta t} \psi^n(\cdot) + \frac{t_n - t}{\Delta t} \psi^{n-1}(\cdot), \quad t \in [t_{n-1}, t_n]$$

and

$$\psi_N^+(\cdot, t) = \psi^n(\cdot), \quad \psi_N^-(\cdot, t) = \psi^{n-1}(\cdot), \quad t \in (t_{n-1}, t_n]$$

for $n = 1, \ldots, N$.
We shall use analogous notations for ϕ_N and $\mathbf{u}_N$. Let $\widetilde{\psi} \in \mathcal{X}_1$, $\widetilde{\phi} \in \mathcal{X}_2$, both be test functions and set $\widehat{\psi} = \int_{t_{n-1}}^{t_n} \widetilde{\psi} \, dt$ and $\widehat{\phi} = \int_{t_{n-1}}^{t_n} \widetilde{\phi} \, dt$. It is clear that $\widehat{\psi} \in V_1$ and $\widehat{\phi} \in H^1(\Omega)$. Then

$$\int_{t_{n-1}}^{t_n} a^n(\psi^n, \widetilde{\psi}(\cdot, t)) \, dt = \int_{t_{n-1}}^{t_n} l_a^n(\widetilde{\psi}(\cdot, t)) \, dt,$$
$$\int_{t_{n-1}}^{t_n} b^n(\psi^n, \widetilde{\psi}(\cdot, t)) \, dt = \int_{t_{n-1}}^{t_n} l_b^n(\widetilde{\psi}(\cdot, t)) \, dt.$$

Adding these inequalities, we obtain, for any $\widetilde{\psi} \in \mathcal{X}_1$,

$$\begin{aligned}
&\int_0^T \int_{\Omega\times Q} \frac{\psi_N^+(r,\eta,\mathbf{y},t) - \psi_N^-(r,\eta,\mathbf{z}_N(\mathbf{y},t),t)}{\Delta t}\ \widetilde{\psi}(r,\eta,\mathbf{y},t)\ d\mathbf{q}d\mathbf{y} \\
&\quad + D_1 \int_0^T \int_{\Omega\times Q} A(r)\nabla_\eta \psi_N^+ \cdot \left(\nabla_\eta \widetilde{\psi} - 2\eta\widetilde{\psi}\right)\ d\mathbf{q}d\mathbf{y} \\
&\quad - \int_0^T \int_{\Omega\times Q} A(r)\mathrm{P}_{\eta^\perp}\left(\nabla_{\mathbf{y}}\mathbf{u}_N^+\eta\right)\psi_N^+ \cdot \nabla_\eta\widetilde{\psi}\ d\mathbf{q}d\mathbf{y} \\
&\quad + \int_0^T \int_{\Omega\times Q} \psi_N^+\left(g(\nabla_{\mathbf{y}}\mathbf{u}_N^+,\mathbf{u}_N^+,\eta)r\widetilde{\psi} - \tau_0\phi_N^-\left(\frac{\partial}{\partial r}\widetilde{\psi} + \alpha\widetilde{\psi}\right)\right)\ d\mathbf{q}d\mathbf{y} \\
&\qquad\qquad = 2\int_0^T \int_{\Omega\times Q} g(\nabla_{\mathbf{y}}\mathbf{u}_N^+,\mathbf{u}_N^+,\eta)\left(\int_r^\infty \psi_N^-\ dr'\right)\widetilde{\psi}\ d\mathbf{q}d\mathbf{y}, \quad (4.33)
\end{aligned}$$

where in the above,

$$\mathbf{x}_N(\mathbf{y},t) = x_n(\mathbf{y}) \text{ and } \mathbf{z}_N(\mathbf{y},t) = z_n(\mathbf{y}), \text{ for any } t \in (t_{n-1},t_n).$$

Proceeding likewise, for any $\widetilde{\phi} \in \mathcal{X}_2$,

$$\begin{aligned}
&\int_0^T \int_\Omega \frac{\phi_N^+(\mathbf{y},t) - \phi_N^-(\mathbf{y},t)}{\Delta t}\ \widetilde{\phi}(\mathbf{y},t)\ d\mathbf{y}dt + \int_0^T \int_\Omega \left(u_N^+ \cdot \nabla_y \phi_N^+\right)\widetilde{\phi}\ d\mathbf{y}dt \\
&+ \int_0^T \int_\Omega D_2\ \nabla_{\mathbf{y}}\phi_N^+ \cdot \nabla_{\mathbf{y}}\widetilde{\phi}\ d\mathbf{y}dt + \tau_0 \int_0^T \int_\Omega \phi_N^+\left(\int_{\mathbb{S}^2\times\mathbb{R}_+} \psi_N^-\ drd\eta\right)\widetilde{\phi}\ d\mathbf{y}dt \\
&\qquad\qquad = 0. \quad (4.34)
\end{aligned}$$

However, to evaluate the limit $\Delta t \to 0$, we need some additional convergence results about the approximations. First, let us define the maps,

$$\begin{aligned}
&\Lambda_1[\psi](\mathbf{y},t) = \int_{\mathbb{S}^2\times\mathbb{R}_+} \psi(r,\eta,\mathbf{y},t)\ drd\eta, \\
&\Lambda_2[\psi](r,\eta,\mathbf{y},t) = \int_r^\infty \psi(r',\eta,\mathbf{y},t)\ dr', \quad \text{for any } \psi \in L^2(0,T;L^2_\alpha).
\end{aligned} \quad (4.35)$$

We have the following lemma:

Lemma 4.3. *Let $\phi^0 \in L^\infty(\Omega)$, $\phi^0 \geq 0$ and $\psi^0 \in L^2_\alpha$ such that*

$$0 \leq \psi^0 \leq C_0 e^{-\alpha r},\ \textit{a.e in } Q,$$

with $C_0 > 0$ a constant. For $\{\psi_N\}_N$ and $\left\{\psi_N^\pm\right\}_N$, constructed by virtue of Lemma 4.2, there exists $\psi \in L^2(0,T;V) \cap L^\infty(0,T;L^2_\alpha)$, positive, such that, for $N \to +\infty$ we have the

following convergence, up to a subsequence of N:

$$\psi_N^{\pm} \rightharpoonup \psi \qquad *-\textit{weakly in } L^\infty(0,T;L^2_\alpha), \tag{4.36}$$
$$A^{1/2}\nabla_\eta \psi_N^{+} \rightharpoonup A^{1/2}\nabla_\eta \psi \qquad \textit{weakly in } L^2(0,T;L^2_\alpha), \tag{4.37}$$
$$r^{1/2}\psi_N^{+} \rightharpoonup r^{1/2}\psi \qquad \textit{weakly in } L^2(0,T;L^2_\alpha), \tag{4.38}$$
$$\Lambda_1[\psi_N^{-}] \rightharpoonup \Lambda_1[\psi] \qquad \textit{weakly in } L^2((0,T)\times\Omega), \tag{4.39}$$
$$\Lambda_2[\psi_N^{-}] \rightharpoonup \Lambda_2[\psi] \qquad \textit{weakly in } L^2(0,T;L^2_\alpha). \tag{4.40}$$

(where Λ_1 and Λ_2 are given by (4.35))

Proof of lemma 4.3. It is clear from (4.19) that

$$\psi_N^{+} \quad \text{is bounded in } \ L^2(0,T;V)$$

and

$$\psi_N^{\pm} \quad \text{is bounded in } \ L^\infty(0,T;L^2_\alpha). \tag{4.41}$$

We then deduce that

$$\psi_N^{-}\circ z_N \quad \text{is bounded in } \ L^\infty(0,T;L^2_\alpha).$$

From (4.19) one infers

$$\psi_N^{+} - \psi_N^{-}\circ z_N \to 0 \quad \text{in the norm of } \ L^2(0,T;L^2_\alpha).$$

Then there exists $\psi^+ \in L^2(0,T;V)\cap L^\infty(0,T;L^2_\alpha)$ and $\psi^- \in L^\infty(0,T;L^2_\alpha)$ such that, up to a subsequence in N we have

$$\psi_N^{+} \rightharpoonup \psi^{+} \quad \textit{weakly in } L^2(0,T;V)$$

$$\psi_N^{\pm} \rightharpoonup \psi^{\pm} \quad *-\textit{weakly in } L^\infty(0,T;L^2_\alpha),$$

and

$$\psi_N^{-}\circ z_N \rightharpoonup \psi^{+} \quad *-\textit{weakly in } L^\infty(0,T;L^2_\alpha).$$

On the other hand we have

$$\begin{aligned} x_n(\mathbf{y}) - \mathbf{y} &= \chi^n(t_n;t_{n-1},\mathbf{y}) - \chi^n(t_{n-1};t_{n-1},\mathbf{y}) \\ &= \Delta t\ \frac{\partial}{\partial t}\chi^n(\xi;t_{n-1},\mathbf{y}) \\ &= \Delta t\ \mathbf{u}^n(\chi^n(\xi;t_{n-1},\mathbf{y})). \end{aligned}$$

This implies

$$\|\mathbf{x}_N(\mathbf{y},t) - \mathbf{y}\|_{L^\infty(]0,T[\times\Omega)} \le\ \Delta t\ \|\mathbf{u}\|_{L^\infty(]0,T[\times\Omega)} \tag{4.42}$$

Now, for any $\widetilde{\psi} \in \mathcal{C}_0^\infty(Q \times \Omega \times]0,T[)$, with the help of (4.42) and (4.41), we obtain

$$\begin{aligned}
&\left| \int_0^T \int_{\Omega\times Q} \left[\psi_N^-(r,\eta,\mathbf{y},t) - \psi_N^-(r,\eta,\mathbf{z}_N(\mathbf{y},t),t) \right] \widetilde{\psi}(r,\eta,\mathbf{y},t)\ d\mathbf{q}d\mathbf{y}dt \right| \\
&= \left| \int_0^T \int_{\Omega\times Q} \psi_N^-(r,\eta,\mathbf{y},t) \left[\widetilde{\psi}(r,\eta,\mathbf{y},t) - \widetilde{\psi}(r,\eta,\mathbf{x}_N(\mathbf{y},t),t) \right]\ d\mathbf{q}d\mathbf{y}dt \right| \\
&\leq C\Delta t\, \|\mathbf{u}\|_{L^\infty([0,T]\times\Omega)}\, \|\widetilde{\psi}\|_{C^1}.
\end{aligned}$$

We deduce that $\psi_N^- - \psi_N^- \circ z_N \to 0$ in the sense of distributions $\mathcal{D}'(Q\times]0,T[)$. This leads to the conclusion that $\psi^+ = \psi^-$, and we denote by ψ the common value ψ^+ or ψ^-. Therefore (4.36), (4.37) and (4.38) are proved. Let now $\varphi \in L^2((0,T)\times\Omega)$

$$\begin{aligned}
&\int_0^T \int_\Omega \left(\Lambda_1 \psi_N^- - \Lambda_1 \psi \right) \varphi(\mathbf{y},t)\ d\mathbf{y}dt \\
&= \int_0^T \int_{\Omega\times Q} \psi_N^- \varphi e^{-\alpha r}\ d\mathbf{q}d\mathbf{y}dt - \int_0^T \int_{\Omega\times Q} \psi\varphi e^{-\alpha r}\ d\mathbf{q}d\mathbf{y}dt \\
&\to 0, \quad \text{as } N \to +\infty
\end{aligned}$$

since $\varphi e^{-\alpha r} \in L^2_\alpha$. Now, invoking (4.36), proves (4.39). Finally, let $\widetilde{\psi} \in L^2(0,T;L^2_\alpha)$ and with the help of (4.38) we get

$$\begin{aligned}
&\int_0^T \int_{\Omega\times Q} \left(\Lambda_2 \psi_N^+ - \Lambda_2 \psi \right) \widetilde{\psi}\ d\mathbf{q}d\mathbf{y}dt \\
&= \int_0^T \int_{\Omega\times Q} r\psi_N^+ \widetilde{\psi}\ d\mathbf{q}d\mathbf{y}dt - \int_0^T \int_{\Omega\times Q} r\psi\widetilde{\psi}\ d\mathbf{q}d\mathbf{y}dt \\
&\to 0, \quad \text{as } N \to +\infty.
\end{aligned}$$

Which proves (4.40). The positivity of ψ follows from the positivity of ψ^n for any n. This ends the proof. □

We now focus on the convergence of the ϕ_N sequence.

Lemma 4.4. *Let $\phi^0 \in L^\infty(\Omega)$, $\phi^0 \geq 0$ and $\psi^0 \in L^2_\alpha$ such that*

$$0 \leq \psi^0 \leq C_0 e^{-\alpha r} \text{ a.e in } Q,$$

with $C_0 > 0$ a constant. For $\{\phi_N\}_N$ and $\left\{\phi_N^\pm\right\}_N$, constructed by virtue of Lemma 4.2, there exists $\phi \in L^2(0,T;H^1) \cap L^\infty(0,T;L^2)$ positive such that we have the following convergence, up to a subsequence of N:

$$\nabla_{\mathbf{y}} \phi_N^+ \rightharpoonup \nabla_{\mathbf{y}} \phi \qquad \text{weakly } L^2(0,T;L^2) \tag{4.43}$$

$$\phi_N^\pm,\ \phi_N \to \phi \qquad \text{strongly } L^2(0,T;L^2(\Omega)) \tag{4.44}$$

Proof of lemma 4.4. From (4.20), we deduce that

$$\phi_N^+ \quad \text{is bounded in } \ L^2(0,T;H^1(\Omega)), \tag{4.45}$$

$$\phi_N^\pm \quad \text{is bounded in } \ L^\infty(0,T;L^2_\alpha)$$

and

$$\phi_N^- \quad \text{is bounded in } \ L^2(\delta,T;H^1(\Omega)) \quad \text{for any} \quad \delta \in]0,T[.$$

Since we have

$$\phi_N = \frac{t_n - t}{\Delta t}\phi_N^- + \frac{t - t_{n-1}}{\Delta t}\phi_N^+$$

we deduce that

$$\phi_N \quad \text{is bounded in } \ L^\infty(0,T;L^2_\alpha)$$

and

$$\phi_N \quad \text{is bounded in } \ L^2(\delta,T;H^1(\Omega)) \quad \text{for any} \quad \delta \in]0,T[.$$

It follows there exists a $\phi \in L^2(0,T;H^1) \cap L^\infty(0,T;L^2)$ such that (4.43) is satisfied. On the other hand, from the equality

$$\frac{\partial \phi_N}{\partial t} = \frac{\phi^n - \phi^{n-1}}{\Delta t} \quad \text{on} \quad [t_{n-1},\ t_n]$$

and from (4.13) we deduce that for any $\widehat{\phi} \in H^1(\Omega)$ we have

$$\int_\Omega \frac{\partial \phi_N}{\partial t}\widehat{\phi}\, d\mathbf{y} = -\int_\Omega u_N^+ \cdot \nabla_{\mathbf{y}}\phi_N^+ \widehat{\phi}\, d\mathbf{y} - D_2 \int_\Omega \nabla_{\mathbf{y}}\phi_N^+ \cdot \nabla_{\mathbf{y}}\widehat{\phi}\, d\mathbf{y} - \tau_0 \int_\Omega \phi_N^+ \left(\int_{\mathbb{S}^2 \times \mathbb{R}_+} \psi_N^-\, dr d\eta \right) \widehat{\phi}\, d\mathbf{y}$$

Using (4.45) and (4.41), gives

$$\frac{\partial \phi_N}{\partial t} \quad \text{is bounded in } \ L^2(0,T;(H^1(\Omega))').$$

Then, up to a subsequence of N, we have

$$\phi_N \to \phi \quad \text{strongly in } \ L^2(\delta,T;L^2(\Omega)), \quad \text{for any} \quad \delta \in]0,T[. \tag{4.46}$$

Let us now prove that

$$\phi_N \to \phi \quad \text{strongly in } L^2(0,T;L^2(\Omega)). \tag{4.47}$$

We fix $\varepsilon > 0$ and we have for any $\delta \in]0,T[$:

$$\int_0^T \|\phi_N - \phi\|^2_{L^2(\Omega)}\, dt = \int_0^\delta \|\phi_N - \phi\|^2_{L^2(\Omega)}\, dt + \int_\delta^T \|\phi_N - \phi\|^2_{L^2(\Omega)}\, dt$$
$$\leq 2C\delta + \int_\delta^T \|\phi_N - \phi\|^2_{L^2(\Omega)}\, dt$$

where C is an upper bound for $\|\phi_N\|_{L^\infty(0,T;L^2)}$ and $\|\phi\|_{L^\infty(0,T;L^2)}$. Now taking $\delta = \frac{\varepsilon}{4C}$ we obtain from (4.46) that for N large enough

$$\int_\delta^T \|\phi_N - \phi\|^2_{L^2(\Omega)}\, dt \leq \frac{\varepsilon}{2},$$

which proves (4.47). From (4.20) one gets

$$\phi_N^+ - \phi_N^- \to 0 \quad \text{strongly in } \ L^2(0,T;L^2(\Omega)).$$

Using the fact that

$$\phi_N - \phi_N^+ = \frac{t - t_n}{\Delta t}(\phi_N^+ - \phi_N^-)$$

and

$$\phi_N - \phi_N^- = \frac{t - t_{n-1}}{\Delta t}(\phi_N^+ - \phi_N^-)$$

leads to

$$\phi_N - \phi_N^\pm \to 0 \quad \text{strongly in } \ L^2(0,T;L^2(\Omega)).$$

This ends the proof. □

4.4.3 Final stage of the proof

In the following we let $N \to +\infty$ in (4.33) and (4.34) with $\widetilde{\psi} \in \mathcal{C}_c^\infty((-T,T) \times \overline{\Omega} \times \mathbb{S}^2 \times [0,+\infty))$ and $\widetilde{\phi} \in \mathcal{C}_c^\infty((-T,T) \times \overline{\Omega} \times \mathbb{S}^2 \times [0,+\infty))$, respectively. We now prove that ψ and ϕ given by Lemmas 4.3 and 4.4 satisfy the variational equalities (4.10) and (4.11), respectively. Since Δt is small enough, we have

$$\begin{aligned}
&\int_0^T \int_{\Omega\times Q} \frac{\psi_N^+(r,\eta,\mathbf{y},t) - \psi_N^-(r,\eta,\mathbf{z}_N(\mathbf{y},t),t)}{\Delta t}\ \widetilde{\psi}(r,\eta,\mathbf{y},t)\ d\mathbf{q}d\mathbf{y}dt \\
&= -\int_0^T \int_{\Omega\times Q} \psi_N^-(r,\eta,\mathbf{y},t) \frac{\widetilde{\psi}(r,\eta,\mathbf{x}_N(\mathbf{y},t),t) - \widetilde{\psi}(r,\eta,\mathbf{y},t-\Delta t)}{\Delta t}\ d\mathbf{q}d\mathbf{y}dt \qquad (4.48) \\
&\quad - \frac{1}{\Delta t}\int_0^{\Delta t} \int_{\Omega\times Q} \psi^0(r,\eta,\mathbf{y})\widetilde{\psi}(r,\eta,\mathbf{y},t-\Delta t)\ d\mathbf{q}d\mathbf{y}dt.
\end{aligned}$$

Smoothness of $\widetilde{\psi}$ entails

$$\frac{1}{\Delta t}\int_0^{\Delta t} \int_{\Omega\times Q} \psi^0(r,\eta,\mathbf{y})\widetilde{\psi}(r,\eta,\mathbf{y},t-\Delta t)\ d\mathbf{q}d\mathbf{y}dt \to \int_{\Omega\times Q} \psi^0\widetilde{\psi}(t=0)\ d\mathbf{q}d\mathbf{y}, \qquad (4.49)$$

and

$$\frac{\widetilde{\psi}(r,\eta,\mathbf{y},t) - \widetilde{\psi}(r,\eta,\mathbf{y},t-\Delta t)}{\Delta t} \to \frac{\partial}{\partial t}\widetilde{\psi}(r,\eta,\mathbf{y},t) \quad \textit{strongly in } L^2(0,T;L^2_\alpha). \qquad (4.50)$$

We also have

$$\frac{\widetilde{\psi}(r,\eta,\mathbf{x}_n(\mathbf{y}),t)-\widetilde{\psi}(r,\eta,\mathbf{y},t)}{\Delta t}=\nabla_y\widetilde{\psi}(r,\eta,\mathbf{y}+\theta_1(\mathbf{x}_n(\mathbf{y})-\mathbf{y}),t)\cdot\xi_N,$$

with $\theta_1\in]0,1[$ and

$$\xi_N=\frac{\mathbf{x}_n(\mathbf{y})-\mathbf{y}}{\Delta t}.$$

Since $\mathbf{x}_n(y)=\chi^n(t_{n-1},t_n,\mathbf{y})$ we have

$$\begin{aligned}\xi_N&=\frac{\chi^n(t_{n-1},t_n,\mathbf{y})-\chi^n(t_n,t_n,\mathbf{y})}{\Delta t}\\&=-\frac{\partial\chi^n}{\partial t}(t_{n-1}+\theta_2\Delta t,t_n,\mathbf{y})\\&=-\mathbf{u}^n(\chi^n(t_{n-1}+\theta_2\Delta t,t_n,\mathbf{y})),\end{aligned}$$

with $\theta_2\in]0,1[$. Then

$$\begin{aligned}&\frac{\widetilde{\psi}(r,\eta,\mathbf{x}_n(\mathbf{y}),t)-\widetilde{\psi}(r,\eta,\mathbf{y},t)}{\Delta t}\\&\qquad=-\nabla_y\widetilde{\psi}(r,\eta,\mathbf{y}+\theta_1(\mathbf{x}_n(\mathbf{y})-\mathbf{y}),t)\cdot\mathbf{u}^n(\chi^n(t_{n-1}+\theta_2\Delta t,t_n,\mathbf{y})).\end{aligned}\tag{4.51}$$

On the other hand, for any $s\in[t_{n-1},t_n]$

$$\begin{aligned}\chi^n(s;t_n,\mathbf{y})-\mathbf{y}&=\chi^n(s;t_n,\mathbf{y})-\chi^n(t_n;t_n,\mathbf{y}),\\&=\frac{\partial\chi^n}{\partial t}(t_n+\theta_3(s-t_n),t_n,\mathbf{y})(s-t_n),\\&=\mathbf{u}^n(\chi^n(t_n+\theta_3(s-t_n),t_n,\mathbf{y}))(s-t_n),\end{aligned}$$

with $\theta_3\in]0,1[$, then

$$|\chi^n(s;t_n,\mathbf{y})-\mathbf{y}|\le|s-t_n|\ \|\mathbf{u}\|_{L^\infty(\Omega\times]0,T[)}.\tag{4.52}$$

Then one deduces from (4.51) and (4.52):

$$\frac{\widetilde{\psi}(r,\eta,\mathbf{x}_N(\mathbf{y},t),t)-\widetilde{\psi}(r,\eta,\mathbf{y},t)}{\Delta t}\to-\mathbf{u}(t,\mathbf{y})\cdot\nabla_{\mathbf{y}}\widetilde{\psi}(r,\eta,\mathbf{y},t),\tag{4.53}$$

strongly in $L^2(0,T;L^2_\alpha)$. Next, from (4.48), (4.49), (4.50) and (4.53) one gets

$$\begin{aligned}&\int_0^T\int_{\Omega\times Q}\frac{\psi_N^+(r,\eta,\mathbf{y},t)-\psi_N^-(r,\eta,\mathbf{z}_N(\mathbf{y},t),t)}{\Delta t}\ \widetilde{\psi}(r,\eta,\mathbf{y},t)\ d\mathbf{q}d\mathbf{y}dt\\&\qquad\to-\int_0^T\int_{\Omega\times Q}\psi\left(\frac{\partial}{\partial t}\widetilde{\psi}+\mathbf{u}\cdot\nabla_{\mathbf{y}}\widetilde{\psi}\right)\ d\mathbf{q}d\mathbf{y}dt-\int_{\Omega\times Q}\psi^0\widetilde{\psi}(t=0)\ d\mathbf{q}d\mathbf{y}.\end{aligned}$$

Now, from the strong convergences

$$\begin{aligned}&\nabla_{\mathbf{y}}\mathbf{u}_N^+\to\nabla_{\mathbf{y}}\mathbf{u},\\&g(\nabla_{\mathbf{y}}\mathbf{u}_N^+,\mathbf{u}_N^+,\eta)\to g(\nabla_{\mathbf{y}}\mathbf{u},\mathbf{u},\eta),\end{aligned}$$

and the fact that

$$\phi_N^- \to \phi,$$

one easily calculates the limit in (4.33) and gets (4.10). Moreover,

$$\int_0^T \int_\Omega \frac{\phi_N^+(\mathbf{y},t) - \phi_N^-(\mathbf{y},t)}{\Delta t}\ \widetilde{\phi}(\mathbf{y},t)\ d\mathbf{y}dt \\ \to -\int_\Omega \psi^0 \widetilde{\psi}(t=0)\ d\mathbf{y} - \int_0^T \int_\Omega \phi \frac{\partial}{\partial t}\widetilde{\phi}\ d\mathbf{y}dt.$$

Calculating the limit in (4.34) easily leads to (4.11).

4.5 Conclusions

Understanding polymer dynamics under different experimental conditions is of importance for the laboratory biologists. In this work we studied the influence of an external velocity field on the polymer-fibrils fragmentation (scission) and lengthening process. To the best of our knowledge this type of study has never been taken into account in the mathematical modelling of this problem. And even if our approach is at its early stage of development, we managed to obtain a rather good generalization of the existing models using more realistic assumptions when adapted to the prion study.

In this work, we generalized the corresponding Fokker-Planck-Smoluchowski partial differential equation for rigid rods in order to account for the fragmentation/lengthening process adapted for prion proliferation. Moreover, we have introduced a set of two equations on monomers and polymers with a known flow. We prove existence and positivity of weak solutions to the system with assumptions on the rates and distribution kernel. The proof is based on variational formulation, a semi-discretization in time, and we obtain estimations which allow us to pass to the limit. To achieve this, we introduced a suitable functional framework (see section 4.3.2).

The matter of existence of solutions to the full system (*i.e.* considering the time dependence of monomers together with the Navier-Stokes equations given in section 4.2) will be adressed in a future work.

Appendix: Additionnal computations

Let $M \in \mathcal{M}_3(\mathbb{R})$, $\eta \in \mathbb{S}^2$, we shall compute in spherical coordinates according to the base $(e_\theta, e_\varphi, e_r)$

$$\nabla_\eta \cdot \mathrm{P}_{\eta^\perp} M\eta = \nabla_\eta \cdot M\eta - \nabla_\eta \cdot (M\eta \cdot \eta)\eta.$$

Note that in spherical coordinates, $\eta = e_r$ and for F a vector value function,

$$\nabla_\eta \cdot F = \partial_\theta F_\theta + \frac{\cos\theta}{\sin\theta} F_\theta + \frac{1}{\sin\theta}\partial_\varphi F_\varphi + 2F_r,$$

with $F_k = F \cdot e_k$, for $k = \theta, \varphi, r$. According to the derivative of the vector of the base, see Appendix II [169] and the fact that

$$\partial_k M e_r \cdot e_j = M \partial_k e_r \cdot e_j + M e_r \cdot \partial_k e_j,$$

assumed that $F = M e_r$, then

$$\nabla_\eta \cdot M e_r = M e_\theta \cdot e_\theta + M e_\varphi \cdot e_\varphi.$$

Next, take $F = (M e_r \cdot e_r) e_r$, it is clear that

$$F_\theta = (M e_r \cdot e_r)(e_r \cdot e_\theta) = 0, \text{ and } F_\varphi = (M e_r \cdot e_r)(e_r \cdot e_\varphi) = 0,$$

thus

$$\nabla_\eta \cdot (M e_r \cdot e_r) e_r = 2 M e_r \cdot e_r.$$

Finally,

$$\nabla_\eta \cdot \mathrm{P}_{\eta^\perp} M \eta = M e_\theta \cdot e_\theta + M e_\varphi \cdot e_\varphi - 2 M e_r \cdot e_r.$$

Chapter 5

Rod-like polymers under polymerization and fragmentation, from individual-discrete to population-continuous

Ce chapitre présente un modèle de polymères rigides avec fragmentation et élongation, soumis à un fluide. Nous présentons le point de vue individu-discret en écrivant les équations sur chaque polymères puis nous nous intéressons à un redimensionnement de ce problème pour obtenir un problème limite. Ce travail n'est pas encore abouti, il est issu d'une collaboration avec R. Yvinec.

5.1 Introduction

In this Chapter we are interested in Polymers under flow and particularly, biological polymers composed of proteins. In Chapter 4, an *ad hoc* model has been derived to describe polymerization and fragmentation of rod like polymers. This model takes its origin from biological experiments where polymers are studied under flow. The polymers under consideration are formed, for instance, by proteins aggregation. They look like rigid rod polymers thus the model was based on the theory developed in [23, 64] for rod-like polymers. This theory involves polymers with a fix length. But, our biological polymers are also subjected to polymerization (addition one by one of proteins) hence the length may increase. Moreover, these polymers can break-up into smaller pieces (fragmentation). A polymerization-fragmentation model has been used in [90] to model prion (protein responsible for several diseases) proliferation. The model in Chapter 4 combines both these

models: rigid-rod polymers under flow and polymerization-fragmentation, in order to propose a new brand model to study such polymers.

Here, we write a discrete and individual model which allows us to write equations for each polymer and monomer and their relative interactions *wrt* to the law of physics. Once the discrete model is established the aim is to justify the average equations of [47]. The next section discusses the method related to this approach.

5.2 Bibliographical review and comments

Our topic here is proving a limit theorem for a particular stochastic processes given by a discrete population model. The strategy is to describe our discrete population model using a point process (the empirical measure), and to prove its convergence under appropriate scaling and coefficient assumption to a measure that solve a limiting model. The convergence will holds in law, and the technique of convergence will use martingale techniques (we first show that a certain compacity condition holds, and then prove a unique limit is possible). Such ideas come back to [58, 111, 121, 122, 167, 181, 190, 204] among others. The interest of this approach are multiple.

- For a theoretical interest, this approach can be used to prove existence of solution of the limiting model. If one is able to find a particular discrete model, that possess a sequence of solution that converge, and such that the limit needs to solve the limiting model, then we have proved existence ([109, 163] in the context of aggregation-fragmentation model.)

- Second, such approach have been widely used to obtain accurate and fast algorithms of a fully non-linear continuous model, such as many of the variant of Poisson-McKean-Vlasov equations ([208]). For such approach, the convergence rate of the stochastic model is of importance to assess the validity of the approximation made ([36, 159])

- Third, in physical or biological context, this approach allows to prove the rigorous basis of a particular model. Indeed, in the discrete population model, one have to specify each reaction or evolution rules very properly. Then, according to the assumption on coefficient describing this evolution, along with a particular scaling (usually large population, or fast reaction rates and so on), one end up with a limiting model or another. Then the (sometimes) implicit assumptions of a continuous model are made explicit. One can also unify different model by relating each other with particular scaling ([115]).

- Finally, last but not least, this approach can be used to simplify models, when the discreteness make the model intractable analytically. One can then study several limiting behavior of a particular model.

Our main goal combines some of these interest. From a particular continuous model Chapter 4 (see also [67]), we wanted to give precise and rigorous justification based of

this model on physical laws. Also, we are looking to a formulation that could be easier to simulate numerically, as well as to derive analytical results. We ended up with a hybrid model, bewteen the fully discrete population model, which would have a too large population for any realistic values, and a fully continuous model, which do not captures stochastic effect.

We first review mean-field results in the context of aggregation-fragmentation models. Stochastic and finite number of particle model are sometimes called the direct simulation model, and its measure-valued stochastic process the direct simulation process. Pure aggregation model are usually named stochastic coalescent, or Marcus-Lushnikov model.

Pure-coagulation kernel model: The study of stochastic pure-coagulation model were originated by [100, 149, 150]

For an interesting survey of results on pure-coagulation model, see the very popular work of [1], which contains a wide variety of application, review available exact solutions, gelation phenomena, various example and types of coagulation kernel, and mean-field limit. This authors pose a certain number of interesting open problems related to these model.

In [163], the authors derive the fluid limit of the "stochastic coalescent" model, a stochastic formulation of the smoluchowski's coagulation equation, where each pair of particle of mass x and y can coagulate into a bigger particle of mass $x + y$, with coagulation rate kernel $K(x, y)$. The authors used such approach to derive a general result of existence of the mean-field smoluchowski model ($K(x, y) \leq \varphi(x)\varphi(y)$, with sub-linear function φ, and $\varphi(x)^{-1}\varphi(y)^{-1}K(x, y) \to 0$ as $(x, y) \to \infty$). The authors also provides a review and new result of uniqueness of the mean-field smoluchowski model for similar aggregation kernel, provided an extra assumption on the initial distribution of particle mass. Importantly, they also provide an example of an aggregation kernel for which uniqueness does not hold, by exhibiting two conservative solution of the same equation. Finally, in the special case of discrete mass particle, the author provide a bound of the convergence rate of the stochastic coalescent to the mean-field smoluchowski model. See also [77] for other results on well-posedness of smoluchowski's coagulation model, with homogeneous kernel and [36] for a convergence rate of the Marcus-Lushnikov model towards the smoluchowski's coagulation model, in Wasserstein distance (in $\frac{1}{\sqrt{n}}$) In [109], The authors used the stochastic formulation model to study the gelling phenomena of the smoluchowski's coagulation-fragmentation equation. In particular, they derived condition on coagulation kernel $K(x, y)$ and fragmentation kernel $F(x, y)$ to show the tightness of the stochastic coagulation-fragmentation model, and hence existence of solution of smoluchowski's coagulation-fragmentation equation. Their condition on the kernel involved $\lim_{x+y\to\infty} K(x, y)/xy = 0$ and there exists G such that $F(x, y) \leq G(x + y) \to 0$ with $lim_{x\to\infty}G(x) = 0$. Result on gelation phenomena involved minoration condition such as the existence of $M, \varepsilon > 0$, and $\varepsilon ij \leq K(i, j) \leq Mij$. Fluid limit results in the case where gelation occurs were recently derived in [76, 78] where the authors show that different limiting models are possible, namely the smoluchowski model and a modified version, named Flory's model.

Aggregation/Fragmentation field: [211, 212] The author consider a general pure fragmentation model (with example including binary fragmentation, homogeneous frag-

mentation). In particular, the author review condition on the fragmentation kernel so that the discrete stochastic model (and its deterministic counterpart) undergoes almost surely explosion in finite time, (a phenomena related to a non-conservation of mass and the creation of an infinite number of particles of mass 0, called "dust"). As in the pure aggregation model, these condition involved minoration condition, such as the fragmentation kernel blow-up sufficiently rapidly in 0. See also [11] for a review on analytical techniques to characterize such phenomena.

Review of results on **deterministic discrete aggregation-fragmentation** model, see [220].

Model with coagulation and diffusion: Coallision-Annihilating model (particle are killed as soon as they encounter another particle. the autors in [123] derived the mean-field kinetics equation on the particle number density, assuming that particle are smaller and smaller as they are present in a larger number. Particle undergo Brownian motion in $\mathbb{R}^3$, with constant diffusion (with respect to the scaling parameter). More recently, the author in [164] considered general Brownian-coagulation model, where particles undergo free diffusion and coagulate once they collide. Using specific scaling between radius and diffusivity of the particles, the authors derived the mean-field reaction-diffusion equation. Both studies mentioned above made use on result of waiting time of collision between, Brownian motion, and are then strongly dependent on the particular assumption on diffusion. See also [7, 94, 95, 117, 227] for recent spatially inhomogeneous model of coagulation particle system.[120] extended mean-field limit of a large number of coupled stochastic differential equation, driven by correlated Brownian noise. The macroscopic limit is still of McKean-Vlasov type but, contrary to the spatially uncorrelated noise, is shown to be a stochastic partial differential equation. They make use of general result of convergence of exchangeable systems of processes.

Deterministic discrete size system of coagulation-fragmentation with diffusion (infinite system of spatially structured pde) were looked by [129, 134, 225] where the authors derived existence results (for gelation phenomena, see [32, 63]), and for deterministic continuous size analog result, see [47, 62]

For a physical discussion on the validity of the protein aggregation and diffusion kinetics treated as rigid body, see [107] and for experiment on Brownian coagulation kinetics, see [26].

Cell population model: [13]. The authors considered a cell population with division infected by parasites (which act then as a structure variable for the cell population), and considered a limit model with a large number of parasites within a finite population of cells. It is possible to make an analogy of this model with polymerization-fragmentation model, considering polymer as cells an parasites as monomer. We will then make extensively used of the results in this paper, as we will also consider a limit where the small particules (monomer, parasites) are present in a large number, while the large particle (polymer, cells) are present in a finite number, and follows a stochastic fragmentation (or division) model. Other similar studies of host-parasite include [12, 157]

Evolution models: [38] In this works, the authors extended evolution population models (structured by a "trait" that undergoes mutation) with interaction (see [39, 80]) by including a space structure, namely a reflected diffusion in a bounded domain, and

obtained, in the large population limit, a nonlinear reaction-diffusion partial differential equation with Neumann's boundary condition. They prove then a law of large number, with boundedness and lipschitz assumption on birth and death rates as well as drift and diffusion coefficient to ensure well-posedness of the limiting model. We will make extensively used of this work in the next, as our initial stochastic model could be reformulated as a special case of their model. Note that similar to our case, drift and diffusion coefficient are independent of the scaling. Other works on evolution population model, with a slight different approach, see [93], where the authors identified in such model a slow component and a fast component, and used Kurt's averaging techniques (separation of time scales).

The limiting model can also be a delay deterministic equation, see the work of [158] in the context of age-structured population model.

For recent results on **convergence rate** of stochastic model towards their mean-field limit, see also [159] (using functional and semi-group approach). For Central-Limit theorem in the context of particular Kuramoto model (convergence of the flucutation): [146, 147]

Other approach: On the "Master" equation and its asymptotic relation to Partial Differential Equation, [185], the author used a more analytical approach, working with the particule densities evolution equation associated to the stochastic individual model, and exploiting the relation between finite-difference numerical scheme associated to the mean-field pde model. For similar approach on evolution models, see [37]

Comments on limit theorem when the limit is deterministic or not. If the limit is deterministic, the limit theorem will have a stronger result than convergence in law. Indeed, in such case, the limit will also holds in probability. Moreover, uniqueness need to be proved on solutions of a deterministic (pde) equation. When the limit is random, the convergence theorem will only holds in law, and we need to prove that uniqueness in law holds for the limit problem. This latter fact is usually done on the martingale problem, which have been more easy to handle for uniqueness property.

Some notations used through this paper:

t	time
Space	
Γ	bounded open set in $\mathbb{R}^3$
$\mathbb{S}^2$	Unit sphere in $\mathbb{R}^3$
Function Space	
$\mathcal{D}(\mathbb{R}_+, E)$	*càdlàg* E-valued functions
$\mathcal{C}^{k_1,\dots,k_n}(E_1 \times \cdots \times E_n)$	Continuous functions with k_i continuous derivatives according to the variable belongs to E_i, for all $i = 1, \dots, n$
$\mathcal{C}_b^{k_1,\dots,k_n}(E_1 \times \cdots \times E_n)$	idem with bounded functions and derivatives
Measure Space	
$\mathcal{M}(E)$	Measure on E
$\mathcal{M}_F(E)$	The space of finite measure
$\mathcal{M}_\delta(E)$	Finite sum of dirac measures
$\mathcal{M}^+(E)$	The cone of non-negative measure
Monomers	
i	labelled one single monomer
X_t^i	Center of mass in Γ of a single monomer
x	Continuous space variable in Γ
N_t^m	Number of monomer
Polymers	
j	Labelled one single polymer
Y_t^j	Center of mass in Γ of a single polymer
H_t^j	Orientation in $\mathbb{S}^2$ of a single polymer
R_t^j	Length in $\mathbb{N}^*$ of a single polymer
Z_t^j	(R_t^j, H_t^j, Y_t^j)
y	Continuous space variable in Γ
η	Continuous orientational variable in $\mathbb{S}^2$.
r	Continuous length variable in $\mathbb{R}_+$
z	(r, η, y)
N_t^p	Number of polymer
Others	
$u(x,t)$	$\mathbb{R}^3$-valued fluid velocity at $x \in \Gamma$

5.3 An individual and discrete length approach

We are concerned in modelling polymers under flow and particularly dilute solution of rigid rod polymers arising in biology, see [47]. Precisely, we will derive equations standing for polymers formed by protein aggregation and subject to fragmentation. The spatial domain of the problem will be denoted by Γ a bounded open set of $\mathbb{R}^3$, the time by $t \geq 0$ and the velocity field of the fluid by $u : \Gamma \times \mathbb{R}_+ \mapsto \mathbb{R}^3$, that is $u(x,t) \in \mathbb{R}^3$ is the velocity at point $x \in \Gamma$ and time $t \geq 0$. We assume incompressibility of the given fluid:

$$\nabla_x \cdot u(x,t) = 0, \quad \forall\, (x,t) \in \Gamma \times \mathbb{R}_+\,,$$

and impermeability of the boundary (Neumann type boundary condition):

$$\nabla_x u(x,t) \cdot \vec{n} = 0 \quad \forall\, (x,t) \in \partial\Gamma \times \mathbb{R}_+.$$

The polymer is described by the position of its center of mass $Y_t \in \Gamma$ at time t and a configurational variable $(R_t, H_t) \in \mathbb{R}^+ \times \mathbb{S}^2$, where $R_t > 0$ is the length of the polymer, while $H_t \in \mathbb{S}^2$ is its orientation. The monomers forming the polymer will belong to a certain type of proteins, thus seen as elementary particles. We assume that each polymer is assimilated to perfect rigid-rod with length R_t that can be regarded as the number of monomers (proteins) that compose it. We describe the motion of a free protein in the fluid by its position $X_t \in \Gamma$ at time $t \geq 0$. We assume that the free monomers are identical, and assimilated to perfect spheres of radius $a > 0$.

In this section we obtain a model of evolution and motion of the polymers and monomers inside the fluid. However, since it involves several mechanisms, let us first describe the four steps of the method, that will lead to the establishment of the different equations in the model.

- First we derive in subsection 5.3.1 the equation of motion of an individual free monomer;
- Next we get in subsection 5.3.2 equation of motion of an individual polymer. Both these equations are obtained thanks to general laws of Physics [23, 64].
- After that we need to model the elongation process of polymers in subsection 5.3.3. Indeed, to fit with the model introduce in [47] , we have to include in the model that such polymers formed of protein can lengthen: proteins (free monomers) aggregate at both ends of one polymer, successively one by one.
- Another mechanism is involved, a fragmentation process of the polymers, presented in subsection 5.3.4. Considering a finite population of monomers and polymers, these two last processes will be introduced in term of jump Markov processes.

We want to emphasize here that our model has the advantage of providing explicit equations for a single monomer and a single polymer. These are therefore the departing point in order to furnish a complete justification of future models. We will adopt the point

process approach to describe the whole discrete population in section 5.4. Then, we will use limit theorem and martingale technique to prove a limiting model when there are an infinity of monomers, but still a finite number of polymers, in section 5.5.

In the following we introduce the equations of the motion and configuration for monomers and polymers. As we use *white noise forces* for particles interactions with the fluid and jump Markov process for the elongation and fragmentation of the polymers, the unknown of the system will be given by in terms of stochastic processes. In order to defined them, we always refer to a stochastic process *wrt* the probability space $(\Omega, \mathcal{F}, P)$, sufficiently marge, that stands for the realizations.

5.3.1 Individual monomer motion

For this process, we naturally use the Langevin equation [124]. Namely, we consider one single monomer, represented by a microscopic rigid sphere of radius $a > 0$, moving in a fluid domain $\Gamma \subseteq \mathbb{R}^3$, itself moving with velocity $u \in \mathbb{R}^3$. The equation of motion of the monomer reads

$$m dV_t = -\xi \left(V_t - u(t, X_t)\right) dt + \sqrt{2k_B T \xi}\; dW_t^{(m)},$$

where m is the mass of the monomer and ξ is the drag constant, while $(V_t)_{t\geq 0} \subset \mathbb{R}^3$ and $(X_t)_{t\geq 0} \subset \mathbb{R}^3$ are two stochastic processes, corresponding respectively to its velocity and its position. $(W_t^{(m)})_{t\geq 0}$ is a standard 3-dimensional Wiener process with independent components and normal reflexive boundary [203], representing the interaction of the monomer with the surrounding fluid domain. The constant in front of the increments of the Wiener process follows the Nernst-Einstein relation with k_B the Boltzmann constant and T the temperature, see [64] .

Now, assuming that the time scale m/ξ tends to zero (see section 5.3.5), we approach the problem by the following stochastic differential equation (see [19, 24, 98] for more precise results)

$$dX_t = u(X_t, t)dt + \sqrt{2D}\; dW_t. \tag{5.1}$$

In the case of a spherical particle (the protein), the Einstein-Stokes equation leads to a diffusion coefficient

$$D = \frac{k_B T}{\xi} = \frac{k_B T}{6\pi\nu a},$$

in a fluid of viscosity ν and at small Reynolds number, where a is the radius of the sphere [64]. The generator of this process is denoted by L_m and defined as follow

$$L_m f = u \cdot \nabla f + D\Delta f, \quad \forall f \in D(L_m), \tag{5.2}$$

where $D(L_m)$ is the domain of the operator L_m. Note that function $f \in C^2(\overline{\Gamma})$ with vanishing normal derivatives belongs to $D(L_m)$ and are dense into $C(\overline{\Gamma})$, see [38]. We will then only consider such function on the next.

Now the motion of a single monomer is well described. We treat next the motion of a single polymer.

5.3.2 Individual polymer equations

Here, we establish the equation for the motion of a single polymer, represented as a rigid rod in the fluid domain Γ, with the same velocity field as above $u \in \mathbb{R}^3$. Since there is no more spherical symmetry of the object considered, we need to describe both the rotational motion and the translational motion. Moreover, for now, no lengthening or splitting of the polymer is considered, hence the length of the polymer is fixed equal to $R > 0$. Therefore, its evolution equation reduces simply to

$$dR_t \,=\, 0\,. \tag{5.3}$$

Rotational motion

The configuration of a polymer is given by its length and orientation. Since its length $R_t = R > 0$ is fixed, there is only its orientation, given by a stochastic process $(H_t)_{t\geq 0} \subset \mathbb{S}^2$ for which we need to write the evolution equation. The increments of the orientation are given by

$$dH_t = M_t \wedge H_t \; dt, \tag{5.4}$$

where $(M_t)_{t\geq 0}$ is the stochastic process giving the angular velocity of the polymer in $\mathbb{R}^3$, which satisfies the Langevin equation,

$$[J]dM_t = T \; dt + \sqrt{2k_BT\xi_r} \; dB_t, \tag{5.5}$$

where $(B_t)_{t\geq 0}$ is a standard 3-dimensional Wiener process with independent components, $[J]$ the moment of inertia, T the total torque and ξ_r the rotational friction coefficient [64]. Since we consider the polymer as a rigid rod, in the velocity field u, the torque T (for instance derived in [60, 64]) is given by

$$T = -\xi_r(M_t - H_t \wedge \nabla_x u(t, Y_t)H_t), \tag{5.6}$$

where the stochastic process $(Y_t)_t \subset \Gamma$ represents the position of the center of mass of the polymer, which equation of motion will be derived later. Moreover, the moment of inertia is given by:

$$[J] = j(I - H_t \otimes H_t) \qquad \text{with} \qquad j = \frac{mR^2}{12}\,,$$

where m is the mass of the rod. Then, as for the motion of one single monomer, we simplify equation (5.4) when assuming that $\frac{m}{\xi_r}$ tends to zero (see section 5.3.5). Thus, using (5.5) and (5.6), it yields

$$dH_t = -H_t \wedge \Big(H_t \wedge \nabla_x u(Y_t, t)H_t \; dt + \sqrt{2D_r} \; dB_t\Big)\,, \tag{5.7}$$

where the rotational diffusion coefficient D_r is defined by

$$D_r = \frac{2k_BT}{\xi_r} = \frac{3k_BT(\ln(L/b) - \gamma)}{\pi\nu L^3},$$

where $b = 2a$ the thickness of the polymer (a is the radius of the monomer) and $L = bR$ is the physical length of the polymers. Here, γ is a constant standing for a correction term, see [64].

Translational motion

Due to the nature of the polymer (rod), it feels an anysotropic translational friction, whose coordinates are denoted by $\xi_\perp$ and $\xi_{||}$, *i.e.* its perpendicular and parallel components respectively, *wrt* to the orientation H_t, see [64]. Let $(V_t)_{t\geq 0} \subset \mathbb{R}^3$ be the stochastic process governing the translational velocity of the center of mass of the polymer (and $(W_t^{(p)})_{t\geq 0}$ a standard 3-dimensional Wiener process with independent components. Thus, the perpendicular velocity $V_t^\perp = (I_3 - H_t \otimes H_t)\, V_t$ satisfies again a Langevin equation, namely

$$m dV_t^\perp = (I_3 - H_t \otimes H_t) \left(-\xi_\perp (V_t - u(t, Y_t))\ dt + \sqrt{2k_B T \xi_\perp}\ dW_t^{(p)} \right),$$

which is the projection of the dynamics onto the perpendicular space to H_t. Also, the parallel velocity $V_t^{||} = (H_t \otimes H_t)\, V_t$ satisfies

$$m dV_t^{||} = (H_t \otimes H_t) \left(-\xi_{||} (V_t - u(t, Y_t))\ dt + \sqrt{2k_B T \xi_{||}}\ dW_t^{(p)} \right).$$

As remarked in [64], drag coefficients satisfy $\xi_\perp = 2\xi_{||}$, we reduce again these equations by taking $m/\xi_\perp \to 0$ (see section 5.3.5). It leads to

$$\begin{cases} (I_3 - H_t \otimes H_t)\, V_t\ dt &= (I_3 - H_t \otimes H_t)\, u(t, Y_t)\ dt \\ & \quad + \sqrt{\frac{2k_B T}{\xi_\perp}}\, (I_3 - H_t \otimes H_t)\ dW_t^{(p)}, \\ (H_t \otimes H_t)\, V_t\ dt &= (H_t \otimes H_t)\, u(t, Y_t)\ dt \\ & \quad + \sqrt{\frac{2k_B T}{\xi_{||}}}\, (H_t \otimes H_t)\ dW_t^{(p)}. \end{cases}$$

Thus, for the position of the center of mass we get:

$$dY_t = u(Y_t, t)\ dt + \sqrt{2D_\perp}\, (I_3 - H_t \otimes H_t)\ dW_t^{(p)} + \sqrt{2D_{||}}\, (H_t \otimes H_t)\ dW_t^{(p)}, \quad (5.8)$$

with

$$D_{||} = \frac{k_B T}{\xi_{||}} = \frac{k_B T \ln(L/b)}{2\pi\nu L} \text{ and } D_\perp = \frac{1}{2} D_{||}.$$

Finally, the generator of the process $(R_t, H_t, Y_t)_{t\geq 0}$, denoted by L_p, is

$$L_p g = u \cdot \nabla_y g + \left[D_\perp \eta \otimes \eta + D_{||} (I_3 - \eta \otimes \eta) \right] \nabla_y \cdot \nabla_y g + \left(P_{\eta^\perp} \nabla_y u\ \eta - 4 D_r \eta \right) \cdot \nabla_\eta g + D_r \nabla_\eta \cdot \nabla_\eta g, \quad (5.9)$$

$$\forall g \in D(L_p).$$

where $D(L_P)$ is the domain of the operator L_P and η denotes the spherical variable. The contribution of the spherical motion to the generator is derived in appendix. Similarly, note $f \in C^{2,2}(\overline{\Gamma}, \mathbb{S}^2)$ with vanishing normal derivatives belongs to $D(L_p)$ and are dense into $C(\overline{\Gamma}, \mathbb{S}^2)$, [38]. We will then only consider such function on the next.

Next we treat the polymerization and fragmentation processes, which will be seen as discrete events in time, governed by jump Markov processes. Their descriptions will therefore introduce survivor functions, in order to model when these events happen (see [83, 155] for chemical justifications).

5.3.3 Elongation process

Let us consider first a single monomer, labelled by i, and a single polymer, labelled by j, in the fluid. As said before, they are characterized by a position $X^i \in \Gamma$ for the monomer (and a given volume constant *wrt* time), while it is a vector $Z^j = (R^j, H^j, Y^j) \in \mathbb{N} \times \mathbb{S}^2 \times \Gamma$ that holds for the polymer j, where R^j is its length, H^j its orientation and Y^j its position. This latter defines actually a given volume occupied by the polymer, and may change by the elongation process.

Then one can define a probability per unit of time that the monomer and the polymer will encounter and polymerize, depending on their relative position and on the size of the polymer:

$$\tau(X^i, Z^j).$$

Thus the survivor function associated to this will be

$$F^{ij}_{elong}(t) = 1 - exp(-\int_0^t \tau(X^i_s, Z^j_s)ds).$$

Let S^{ij}_{elong} be the stopping time corresponding to F^{ij}_{elong}. For all $t < S^{ij}_{elong}$, the motion of the monomer is governed by equation (5.1), while for the polymer it holds the three equations for the length (5.3), the orientation (5.7) and the translation of its center of mass (5.8).

At $t = S^{ij}_{elong}(w)$ ($w \in \Omega$ being "the chosen stochastic realization"), the process is stopped. The monomer is killed, and the polymer is changing through a deterministic transition:

$$Z^j(t^+) = Z^j(t^-) + \mathbf{e}_1, \tag{5.10}$$

where $\mathbf{e}_1 = (1, 0, 0)$. In other words, the length of the polymer increases of one monomer.

Remark 5.1. The assumption made here is that the polymerization process does not change the position of the center of mass of the polymer, neither its orientation. One can introduce non-local transition for the elongation.

Consider now a single polymer j in an environment of N^m_s monomers around *wrt* time s. For all $1 \leq i \leq N^m_s$, this polymer can interact with a monomer i. Because the monomers are present in a finite number, the stopping time for the polymer to elongate will simply be the minimum of all the stopping time of the elongation of the polymer

with each monomer. These events are supposed to be independent from each other. The survivor function associated to the minimum of these stopping times is then:

$$F^j_{elong}(t) = 1 - exp\left(-\int_0^t \sum_{i=1}^{M_s} \tau(X^i_s, Z^j_s)ds\right).$$

Similarly for a single monomer i with N^p_s polymers

$$F^i_{elong}(t) = 1 - exp\left(-\int_0^t \sum_{j=1}^{N^p_s} \tau(X^i_s, Z^j_s)ds\right).$$

Finally, for the whole population, the stopping time S_{elong} defined as the next elongation event is associate to the survivor function

$$F_{elong}(t) = 1 - exp\left(-\int_0^t \sum_{i=1}^{N^m_s}\sum_{j=1}^{N^p_s} \tau(X^i_s, Z^j_s)ds\right).$$

Hence, as said before, at time $t = S_{elong}(w)$, one monomer i is killed, so the number of monomers satisfies

$$N^m_{t^+} = N^m_{t^-} - 1. \tag{5.11}$$

5.3.4 Fragmentation process

One can use the same reasoning for the fragmentation process. We define a probability per unit of time for a polymer, labelled by j, to break up. This probability depends on its position and configuration given by $Z^j \in \mathbb{N} \times \mathbb{S}^2 \times \Gamma$ and is

$$\beta(Z^j)$$

Then for each polymer j, we can define a stopping time given by the survivor function

$$F^j_{frag}(t) = 1 - exp\left(-\int_0^t \beta(Z^j_s)ds\right).$$

At time $t = S^j_{frag}(w)$ the stopping time corresponding to F^j_{frag}, the polymer j is changing through the transition

$$Z^j_{t^+} = ([\theta R^j_{t^-}], H^j_{t^-}, Y^j_{t^-}), \tag{5.12}$$

and a new polymer is created

$$Z^{N_{t^+}}_{t^+} = ([(1-\theta) R^j_{t^-}], H^j_{t^-}, Y^j_{t^-}), \tag{5.13}$$

with the population of polymers increments by

$$N^p_{t^+} = N^p_{t^-} + 1. \tag{5.14}$$

The notation $[r]$ denotes the closest integer from r and $\theta \in (0,1)$ is chosen according to a probability density function k_0 satisfying the symmetry condition, namely

$$k_0(\theta) = k_0(1-\theta),\ \forall \theta \in (0,1),$$

and truncated upon the condition that

$$[\theta R^j_{t^-}] \geq R_0,$$
$$[(1-\theta) R^j_{t^-}] \geq R_0.$$

R_0 being a given critical length that ensures no polymers of size 0 is created.

Remark 5.2. The assumption made here is that the fragmentation does not change the orientation and the center of mass of the resulting polymers from the original one. Here again, the transition could involve non-local fragmentation. After the fragmentation process, the two resulting polymers wil evolve independently of each other according to Equations of motion (5.7)-(5.8), with independent brownian motion.

The stopping time S_{elong} defined as the next fragmentation event is associate to the survivor function

$$F_{elong}(t) = 1 - exp\left(- \int_0^t \sum_{j=1}^{N^p_s} \beta(Z^j_s) ds \right).$$

Finally, since elongation and fragmentation event are both independents we construct the survivor function of the whole system as

$$F(t) = 1 - exp\left(- \int_0^t \left(\sum_{i=1}^{N^m_s} \sum_{j=1}^{N^p_s} \tau(X^i_s, Z^j_s) + \sum_{j=1}^{N^p_s} \beta(Z^j_s) \right) ds \right).$$

5.3.5 Some necessary comments on the model

We can give an algorithmic point of view of the model. Let $t_k \geq 0$ be a given time with $(X^i_{t_k})_{i=1,\dots,N^m_{t_k}}$ the position of the monomers and $(R^j_{t_k}, H^j_{t_k}, Y^i_{t_k})_{i=1,\dots,N^p_{t_k}}$ the position-configuration of the polymers. Boundedness assumption on coefficient allows to simulate this stochastic process in an acceptance-reject manner, which we briefly recall below, see [38]. Simulation of brownian trajectories with reflexion conditions have been discussed in [140]. The algorithm is

i) Let $t_{k+1} > t_k$ be the next possible stopping time associated to the survivor function F.

ii) For all $t \in (t_k, t_{k+1})$ the motion of the monomers is given by (5.1) and the polymers are governed by equation (5.3) for the size, equation (5.7) for the orientation and (5.8) for the center of mass.

iii) If t_{k+1} is associated to an elongation event, the system changes following the transition (5.10) for the corresponding polymer that elongates and (5.11) for the monomers population.

iv) If t_{k+1} is associated to a fragmentation event, the system changes following the transition (5.12-5.13) for the two resulting polymers and (5.14) for the population of polymers.

v) If t_{k+1} is not associated to any event, the system does not change and no transition happens.

vi) We go back to step i).

Because all stochastic differential equations involved in the equation of motion of monomers and polymers have global existence and uniqueness property, this description ensures the existence and unicity of the solutions of this model up to the explosion time, that is the accummulation point of the jump times. (see next section)

The model describes above needs some comments:

- Neglecting the inertial effects in the motion of monomers and polymers will be justified later by the fact that the mass will be chosen converging to zero. For a model (without elongation-fragmentation) that take it into account we can refer to [60].
- The modelization of the brownian intensity is valid under low Reynolds number, thus the fluid model should be a Stokes flow.
- The brownian motion on the sphere is introduced here as a 3-dimensional Wiener process on the rotational velocity. It is interpreted as all the interaction with surrounding particles, in a different way than [23, 60, 64] where it is derived from a Brownian potential from a given *a priori* density of polymers.
- Due to the difference of order of size between monomers, polymers and the spatial domain, the fact that fragmentation and elongation do not change the center of mass of the polymer could be justified. But one could consider non-local elongation and fragmentation.
- The above choice of the repartition kernel (self-similarity and definition with a reference function k_0) is mainly made to simplify notation on the stochastic differential equations below. More general probability kernel $k(R, R')$ from a polymer of size R providing a polymer of size R' could be taken without any difficulties.

5.4 The measure-valued stochastic process

First of all, let us introduce some technical notations for this section. Consider E a measurable space, we denote by $\mathcal{M}_F(E)$ the set of finite measures on E equipped with

the topology of the weak convergence. Moreover, for any $\mu \in \mathcal{M}_F(E)$ and h a measurable bounded function on E, we write

$$\langle \mu, h \rangle_E = \int_E h(x)\mu(dx)$$

Also, we introduce the space

$$\mathcal{M}_\delta(E) := \left\{ \sum_{i=1}^{n} \delta_{x_i} : n \geq 0,\, (x_1, \ldots, x_n) \in E^n \right\}$$

that is the finite sum of Dirac masses which will be useful to describes the configuration of the system.

The last notation is $\mathcal{C}^{k_1,\ldots,k_n}(E_1 \times \cdots \times E_n)$ for the space of continuous functions with k_i continuous derivatives according to the variable belongs to E_i, for all $i = 1, \ldots, n$. Also if $\mathcal{C}$ is replace by $\mathcal{C}_b$, we consider bounded functions as well as all their derivatives.

5.4.1 The empirical measure

Our study focus on describing the evolution of the population of monomers and polymers. To that, we represent the population of monomers and polymers, respectively, with the following measures at time t:

$$\mu_t^m = \sum_{i=1}^{N_t^m} \delta_{X_t^i} \text{ and } \mu_t^p = \sum_{j=1}^{N_t^p} \delta_{Z_t^j}.$$

with $N_t^m = \langle \mu_t^m, \mathbf{1} \rangle$ the total number of monomers and $N_t^p = \langle \mu_t^p, \mathbf{1} \rangle$ of polymers. As the dynamic of the two populations is coupled, we introduce what we call the empirical measure of the system:

$$\mu_t = (\mu_t^m, \mu_t^p) \in \mathcal{M}_\delta(\Gamma) \times \mathcal{M}_\delta(\mathbb{N}^* \times \mathbb{S}^2 \times \Gamma). \tag{5.15}$$

This point of view define $(\mu_t)_{t \geq 0}$ as measure-valued stochastic process that entirely contains the information of the system. The aim of this section is thus to construct the stochastic differential equation of this process, that describes the evolution of our model.

For that, $\mathcal{M}_\delta(\Gamma) \times \mathcal{M}_\delta(\mathbb{N} \times \mathbb{S}^2 \times \Gamma)$ is equipped with the topology product. Until it is mentioned, h stands for a couple of functions

$$h = (f, g) \in \mathcal{C}_b^2(\Gamma) \times \mathcal{C}_b^{0,2,2}(\mathbb{N} \times \mathbb{S}^2 \times \Gamma)$$

with vanishing normal derivatives on $\partial\Gamma$ and ϕ a function

$$\phi \in \mathcal{C}_b^2(\mathbb{R}, \mathbb{R}).$$

Also, we denote by

$$\langle \mu, h \rangle = \langle \mu^m, f \rangle_\Gamma + \langle \mu^p, g \rangle_{\mathbb{N} \times \mathbb{S}^2 \times \Gamma}.$$

If no doubt remains, we drop the space on which act $\langle , \rangle$. Finally, for technical reason, the evolution is regarding with respect to *test functions* ϕ_h defines, for all measure $\mu \in \mathcal{M}_F$, by

$$\phi_h(\mu) = \phi(< \mu, h >). \tag{5.16}$$

These functions are know to be convergence determining on the space of finite measure, see [58].

5.4.2 Continuous motion

In order to derive the evolution of $(\mu_t)_{t\geq 0}$ the empirical measure product (5.15), we first focus on the continuous motion between to consecutive stopping time. For sake of clarity let us introduce two operators, first L be

$$Lh = (L_m f, L_p g), \tag{5.17}$$

where L_m and L_p are respectively given in equations (5.2) and (5.9), and A such that

$$\begin{aligned} Ah = \quad & \Big(D\nabla_x f^T \nabla_x f \,,\, \tfrac{1}{2}\left(\nabla_\eta g^T \mathcal{R}\right)\left(\mathcal{R}^T \nabla_\eta g\right) \\ & + \tfrac{1}{2}\left(\nabla_y g^T \mathcal{D}_{||}\right)\left(\mathcal{D}_{||}^T \nabla_y g\right) + \tfrac{1}{2}\left(\nabla_y g^T \mathcal{D}_{\perp}\right)\left(\mathcal{D}_{\perp}^T \nabla_y g\right) \Big), \end{aligned} \tag{5.18}$$

where $\mathcal{D}_\perp = \sqrt{2D_\perp}(I_3 - n \otimes n)$, $\mathcal{D}_{||} = \sqrt{2D_{||}} n \otimes n$ and $\mathcal{R} = -\sqrt{2D_r} n \wedge \cdot$. Now we are in position to introduce the following lemma which states the evolution of the empirical product measure between jump (stopping) time.

Lemma 5.1. *Let T_k and T_{k+1} be two consecutive jump time. We assume that μ_t is the empirical product measure defined by* (5.15)*. The evolution of μ_t with respect to the functions ϕ_h define in* (5.16) *is given, for any $s, t \in (T_k, T_{k+1})$, by*

$$\phi_h(\mu_t) = \phi_h(\mu_s) + \int_s^t \mathcal{L}_0 \phi_h(\mu_\sigma) d\sigma + M_{t,s}$$

where $M_{t,s}$ is a process starting in s and $\mathcal{L}_0$ defined by

$$\mathcal{L}_0 \phi_h(\mu) = \phi'(\langle \mu, h \rangle)\langle \mu, Lh \rangle + \phi''(\langle \mu, h \rangle)\langle \mu, Ah \rangle$$

with L and A respectively given in (5.17) *and* (5.18)*.*

This lemma is a straightforward consequence of Itô calculus. Indeed, between two jumping time, the number of monomers N_s^m and polymers N_s^p are constant. Moreover, the size of each polymer is constant thus from the SDE on the motion of the monomers (5.1) and its infinitesimal generator L_m defined in (5.2), together with the SDE on the motion of the polymers (5.8), their orientation (5.7) and the infinitesimal generator L_p defined in (5.9), so we get by computation of the Itô rules the above lemma. Futhermore,

the computation allow us to get the exact expression of the martingale $M_{t,s}$ which is decomposed as

$$M_{t,s} = M^m_{t,s} + M^p_{t,s}, \tag{5.19}$$

with $M^m_{t,s}$ and $M^p_{t,s}$ two processes given by

$$M^m_{t,s} = \int_s^t \phi'(\langle \mu_\sigma, h\rangle) \sum_{i=1}^{N^m_\sigma} \left(\sqrt{2D}\nabla f(X^i_\sigma) dW^{(m)i}_\sigma\right),$$

and

$$M^p_{t,s} = \int_s^t \phi'(\langle \mu_\sigma, h\rangle) \sum_{j=1}^{N^p_\sigma} \Bigg(\sqrt{2D_r}\nabla_\eta g(Z^j_\sigma) \cdot dB^j_\sigma \wedge H^j_\sigma + \nabla_y g(Z^j_\sigma) \cdot \left[\sqrt{2D_\perp}(I_3 - H^j_\sigma \otimes H^j_\sigma) + \sqrt{2D_{||}} H^j_\sigma \otimes H^j_\sigma\right] dW^{(p)j}_\sigma \Bigg).$$

We notice that $W^{(m)i}_s$, $W^{(p)j}_s$ and B^j_s are a family of 3-dimensional Wiener process with independent components corresponding to each monomers and polymers, respectively labelled by i and j.

5.4.3 The stochastic differential equation

In the previous section we write the evolution of the empirical measure between stopping times. The aim of this section is to describe the whole evolution of this measure with an SDE. To do that, we assume that we have a sequence $0 = T_0 < T_1 < T_2 < \cdots < T_N < T_{N+1}$ of consecutive stopping times and we suppose that the time t belongs to (T_N, T_{N+1}). Consequently, the empirical product measure μ_t satisfies, for any $t \in (T_N, T_{N+1})$

$$\phi_h(\mu_t) = \sum_{k=0}^{N-1} \left(\Delta\phi_h(\mu_{T_k}) + \int_{T_k}^{T^-_{k+1}} d\phi_h(\mu_s) \right) + \Delta\phi_h(\mu_{T_N}) + \int_{T_N}^t d\phi_h(\mu_s),$$

where $\Delta\phi_h(\mu_{T_k}) = \phi_h(\mu_{T_k}) - \phi_h(\mu_{T^-_k})$ and the convention $\mu_{0^-} = 0$. Consequently, remarking that the above equality is true for any sequence of stopping, from Lemma 5.1 we get the evolution of μ_t for any $t \geq 0$ given by

$$\phi_h(\mu_t) = \sum_{s \leq t} (\phi_h(\mu_{s^-} + \Delta\mu_s) - \phi_h(\mu_{s^-})) + \int_0^t \mathcal{L}_0\phi_h(\mu_s) ds + M^0_t \tag{5.20}$$

with $M^0_t := M_{t,0}$ where $M_{t,0}$ satisfies (5.19) and $\Delta\mu_s = \mu_s - \mu^-_s$. In order to defined the transition $\Delta\mu_s$ we introduce the following notation

Note 5.1. We use the purely notional maps S_m^i and S_p^j for all $i, j \in \mathbb{N}^*$, such that for $\mu = (\mu_m, \mu_p) \in \mathcal{M}_\delta(\Gamma) \times \mathcal{M}_\delta(\mathbb{N}^* \times \mathbb{S}^2 \times \Gamma)$

$$S_m^i(\mu) = X^i \text{ and } S_p^j(\mu) = (R^j, H^j, Y^i).$$

In order to have a consistent definition of these two maps, we refer to [39].

Let s be a stopping time with elongation event, where the monomer i elongate with the polymer j, the transition defines by (5.10-5.11) leads to

$$\Delta\mu_s = \Delta_1^{i,j}\mu_s := \left(-\delta_{S_m^i(\mu_{s^-})}\,,\, -\delta_{S_p^j(\mu_{s^-})} + \delta_{S_p^j(\mu_{s^-})+\mathbf{e}_1}\right). \tag{5.21}$$

That means formally: the monomer i is killed, the polymer i get a length incremented by one. Now, when s is a stopping time with a fragmentation event, where the polymer j breaks up, the transition defines by (5.14) and (5.12-5.13) leads to

$$\Delta\mu_s = \Delta_2^j\mu_s := \left(0\,,\, \delta_{\Theta(\theta,S_p^j(\mu_{s^-}))} + \delta_{\Theta(1-\theta,S_p^j(\mu_{s^-}))} - \delta_{S_p^j(\mu_{s^-})}\right) \tag{5.22}$$

where $\Theta(\theta, Z) = ([\theta R], H, Y)$ for all $Z = (R, H, Y) \in \mathbb{N}^* \times \mathbb{S}^2 \times \Gamma$. That means formally: a polymer j of size R breaks up into two new polymers of size $[\theta R]$ and $[(1-\theta)R]$. Nothing happens to the monomers. Finally, $\Delta\mu_s = (0, 0)$ for all non-jump time.

Following works of [39, 80], The transition events of elongation and fragmentation will be described in term of Poisson point measures. Let us defined them, together with the probabilistic objects of the model.

Definition 5.2 (Probabilistic objects)**.** Let $(\Omega, \mathcal{F}, P)$ a sufficiently large probability space. We defined on this space the two independent random Poisson point measures

i) The elongation point measure $Q^1(ds, di, dj, du)$ on $\mathbb{R}_+ \times \mathbb{N} \times \mathbb{N} \times \mathbb{R}_+$ with intensity

$$E\left[Q_1(ds, di, dj, du)\right] = dsdu(\sum_{k\geq 1}\delta_k(di))(\sum_{k\geq 1}\delta_k(dj))$$

ii) The fragmentation Poisson measure. $Q_2(ds, dj, d\theta, du)$ on $\mathbb{R}_+ \times \mathbb{N} \times (0, 1) \times \mathbb{R}_+$ with intensity

$$E\left[Q_2(ds, dj, d\theta, du)\right] = dsduk_0(\theta)d\theta(\sum_{k\geq 1}\delta_k(dj))$$

where ds and du are Lebesgue measure on $\mathbb{R}^+$, $d\theta$ is the Lebesgue measure on $(0, 1)$ and $\sum_{k\geq 1}\delta_k(di))$ is the counting measure on $\mathbb{N}$. Moreover, we define a family of 3-dimentionnal Wiener process with independent components (and independent of the Poisson measures), indexed by $i \in \mathbb{N}$ and $j \in \mathbb{N}$:

$$(W_t^{(m)i})_{t\geq 0},\ (W_t^{(p)j})_{t\geq 0}, \text{ and } (B_t^j)_{t\geq 0}$$

Finally, let $\mu_0 \in \mathcal{M}_\delta$ an initial random measure, independent of the above processes and the canonical filtration $(\mathcal{F}_t)_{t\geq 0}$ associated to these processes.

From (5.20) together with (5.21-5.22) and the probability objects given in Definition 5.2, we are able to state the discrete-individual polymer-flow model that is the SDE on $(\mu_t)_{t\geq 0}$ for the function ϕ_h that reads

$$\begin{aligned}
\phi_h(\mu_t) &= \phi_h(\mu_0) + \int_0^t \mathcal{L}_0\phi_h(\mu_s)ds \\
&+ \int_0^t \int_{\mathbb{N}\times\mathbb{N}\times\mathbb{R}_+} \left(\phi_h(\mu_{s^-} + \Delta_1^{i,j}\mu_s) - \phi_h(\mu_s^-)\right) \\
&\qquad \times \mathbf{1}_{u\leq \tau(S_m^i(\mu_{s^-}),S_p^j(\mu_{s^-}))}\mathbf{1}_{i\leq N_{s^-}^m, j\leq N_{s^-}^p} \\
&\qquad \times Q_1(ds,di,dj,du) \\
&+ \int_0^t \int_{\mathbb{N}\times(0,1)\times\mathbb{R}_+} \left(\phi_h(\mu_{s^-} + \Delta_2^j\mu_s) - \phi_h(\mu_s^-)\right) \\
&\qquad \times \mathbf{1}_{\Theta(\theta,S_p^j(\mu_{s^-}))\,,\,\Theta(1-\theta,S_p^j(\mu_{s^-}))\geq R_0} \\
&\qquad \times \mathbf{1}_{u\leq\beta(S_p^j(\mu_s))}\mathbf{1}_{j\leq N_{s^-}^p} \\
&\qquad \times Q_2(ds,dj,d\theta,du) \\
&+ M_t^0
\end{aligned} \tag{5.23}$$

where $\mathcal{L}_0$ is the generator of the piecewise continuous motion defined in Lemma 5.1 and $M_t^0 := M_{t,0}$ is the process given by (5.19). Now, we can compute the infinitesimal of the process that is:

Lemma 5.3 (Infinitesimal generator)**.** *The infinitesimal generator $\mathcal{L}$ associated to the SDE on $(\mu_t)_t$ for the function ϕ_h given by* (5.23) *is decomposed as follows*

$$\mathcal{L} = \mathcal{L}_0 + \mathcal{L}_1 + \mathcal{L}_2$$

where $\mathcal{L}_0$ is defined in Lemma 5.1 and

$$\begin{aligned}
\mathcal{L}_1\phi_h(\mu_t) &= \int_\Gamma \int_{\mathbb{N}\times\mathbb{S}^2\times\Gamma} \tau(x,z)\left(\phi_h(\mu_{s^-} + \Delta_1) - \phi_h(\mu_{s^-})\right) \\
&\qquad \times \mu_{s^-}^m(dx)\mu_{s^-}^p(dz),
\end{aligned}$$

with $\Delta_1(x,z) = (-\delta_x, -\delta_z + \delta_{z+\mathbf{e}_1})$ and

$$\begin{aligned}
\mathcal{L}_2\phi_h(\mu_t) &= \int_{\mathbb{N}\times\mathbb{S}^2\times\Gamma} \int_0^1 \beta(z)\left(\phi_h(\mu_{s^-} + \Delta_2) - \phi_h(\mu_{s^-})\right) \\
&\qquad \times \mathbf{1}_{[\theta r],[(1-\theta)r]>R_0} k_0(\theta)d\theta\mu_{s^-}^p(dz)
\end{aligned}$$

with $\Delta_2(z) = (0, \delta_{\Theta(\theta,z)} + \delta_{\Theta(1-\theta,z)} - \delta_z)$.

This lemma is obtained by Markov properties. Indeed, by taking expectation in the SDE (5.23) and the definition of the random Poisson point measure, we identify the generator ([39, 80]). Thus the evolution of the empirical measure μ_t can be re-written as

$$\phi_h(\mu_t) = \phi_h(\mu_0) + \int_0^t \mathcal{L}\phi_h(\mu_s)ds + M_t^{total}$$

where

$$M_t^{total} = M_t^0 + M_t^1 + M_t^2, \tag{5.24}$$

with $M_t^0 := M_{t,0}$ the process given by (5.19) and M_t^1, M_t^2 the compensated random Poisson measure that are for $k = 1, 2$:

$$\begin{aligned} M_t^1 &= \int_0^t \int_{\mathbb{N}\times\mathbb{N}\times\mathbb{R}_+} \cdots (Q_1(dsdidjdu) - E[Q_1(dsdidjdu)]) \\ M_t^2 &= \int_0^t \int_{\mathbb{N}\times(0,1)\times\mathbb{R}_+} \cdots (Q_2(dsdjd\theta du) - E[Q_2(dsdjd\theta du)]) \end{aligned}$$

with dots standing for the terms behind $Q_{k=1,2}$ in the SDE (5.23).

5.4.4 Existence, Uniqueness

In this section we study the well-posedness of the discrete-individual polymer-flow model (5.23). For that we assume the following hypothesis:

(H1) Let τ and β be continuous non-negative function, uniformly bounded respectively by $\overline{\tau} > 0$ and $\overline{\beta} > 0$, that is

$$\tau(x, z) \leq \overline{\tau} \text{ and } \beta(z) \leq \overline{\beta}, \quad \forall x \in \Gamma, \forall z \in \mathbb{N} \times \mathbb{S}^2 \times \Gamma.$$

(H2) We recall that $k_0 : (0, 1) \mapsto \mathbb{R}_+$ is a symmetrical probability density function, *i.e.*

$$\int_0^1 k_0(\theta)d\theta = 1 \text{ and } k_0(\theta) = k_0(1 - \theta), \forall \theta \in (0, 1).$$

In order to state of the problem we introduce the following definition of admissible solution. Solution are given in terms of a martingale problem. Its advantage relies on the fact that the limiting problem will be identified as a martingale problem.

Definition 5.4 (Admissible Solution)**.** Assuming that the probabilistic objects of Definition 5.2 are given. An admissible solution to the discrete-individual polymer-flow model (5.23) is a $(\mathcal{F}_t)_{t\geq 0}$-adapted measure-valued Markov process:

$$\mu = (\mu^m, \mu^p) \in \mathcal{D}\left([0, \infty), \mathcal{M}_\delta(\Gamma) \times \mathcal{M}_\delta(\mathbb{N}^* \times \mathbb{S}^2 \times \Gamma)\right),$$

such that, for all $\phi \in \mathcal{C}_b^2(\mathbb{R},\mathbb{R})$ and $h \in \mathcal{C}_b^2(\Gamma) \times \mathcal{C}_b^{0,2,2}(\mathbb{N}\times\mathbb{S}^2\times\Gamma)$,

$$\phi_h(\mu_t) - \phi_h(\mu_0) - \int_0^t \mathcal{L}\phi_h(\mu_s)ds, \tag{5.25}$$

is a $L^1 - (\mathcal{F}_t)_{t\geq 0}$ martingale starting in $t=0$ given by M_t^{total} defined in (5.24) and where $\mathcal{L}$ the infinitesimal generator derived in Lemma 5.3. Moreover, it satisfies

$$\int_\Gamma \mu_t^m(dx) + \int_{\mathbb{N}\times\mathbb{S}^2\times\Gamma} r\mu_t^p(dz) = \int_\Gamma \mu_0^m(dx) + \int_{\mathbb{N}\times\mathbb{S}^2\times\Gamma} r\mu_0^p(dz).$$

The last equation in the above definition stands for the mass balance of the system in the system. Indeed, since neither production, nor degradation of monomers and polymers is assumed, together with the impermeability condition at the boundary (Neumann type boundary condition on u), the system preserves the total number of monomers. Now, we are able to state the following proposition:

Proposition 5.5. *Assuming that the probabilistic objects of Definition 5.2 are given, hypothesis (H1-H2) are fulfilled, and*

$$E\left(\langle \mu_0, 1\rangle\right) < +\infty,$$

then there exists a unique admissible solution $(\mu_t)_{t\geq 0}$ to the discrete-individual polymer-flow model (5.23)*.*

Furthermore, if for some $\alpha \geq 1$,

$$E\left(\langle \mu_0, 1\rangle^\alpha\right) < +\infty,$$

then for any $T < \infty$,

$$E\left(\sup_{t\in[0,T]} \langle \mu_t, 1\rangle^\alpha\right) < +\infty$$

Proof. Following [39, 80], we only have to check the last point, and that the mass conservation holds. Indeed, we gave a constructive description of the stochastic process, based on the existence and uniqueness of equation of motion for individuals and on the Poisson measures. That the martingale property holds is a consequence of the generator identification above.

In order to prove the mass conservation, let $\phi = Id$ and $h = (1, \mathbf{r})$ with $\mathbf{r} : (r,\eta,y) \mapsto r$, then

$$\phi_h(\mu_t) := \int_\Gamma \mu_t^m(dx) + \int_{\mathbb{N}\times\mathbb{S}^2\times\Gamma} r\mu_t^p(dz).$$

In that case we have

$$\phi_h(\mu_{s^-} + \Delta_1^{i,j}\mu_s) - \phi_h(\mu_s^-) = \langle \Delta_1^{i,j}\mu_s, (1,\mathbf{r})\rangle = 0,$$

and

$$\phi_h(\mu_{s^-} + \Delta_2^{j}\mu_s) - \phi_h(\mu_s^-) = \langle \Delta_2^{j}\mu_s, (1,\mathbf{r})\rangle = 0.$$

Moreover,

$$\mathcal{L}_0\phi_h(\mu_s) = \langle \mu_{s^-}, (L_m 1, L_p \mathbf{r})\rangle = 0,$$

and $M_t^0 = 0$. Using the SDE (5.23) on the empirical measure, we get the mass conservation.

We now show that jump times do note accumulate, thanks to moment estimates. We note $\tau_n = \inf\{t \geq 0, \langle \mu_t, 1\rangle \geq n\}$. With Equation (5.23) and taking $\phi_h(\mu) = (\langle \mu, 1\rangle)^\alpha$ (and truncating ϕ with $(n+1)^\alpha$ to be more correct) we get, neglecting the negative terms,

$$\begin{aligned}\sup_{s\in[0,t\wedge\tau_n]} \langle \mu_s, 1\rangle^\alpha &\leq \langle \mu_0, 1\rangle^\alpha \\ &\quad + \int_0^{t\wedge\tau_n} \int_{\mathbb{N}\times(0,1)\times\mathbb{R}_+} [(\langle \mu_{s^-}, 1\rangle + 1)^\alpha - \langle \mu_{s^-}, 1\rangle^\alpha] \\ &\qquad \times \mathbf{1}_{u\leq\beta(S_p^j(\mu_{s^-}))}\mathbf{1}_{j\leq N_{s^-}^p} Q^2(ds, dj, d\theta, du)\end{aligned}$$

Using the standard estimates $(x+1)^\alpha - x^\alpha \leq C_\alpha(1 + x^{\alpha-1})$ for all $x \geq 0$ for some constant $C_\alpha > 0$, we deduce

$$\begin{aligned}\sup_{s\in[0,t\wedge\tau_n]} \langle \mu_s, 1\rangle^\alpha &\leq \langle \mu_0, 1\rangle^\alpha \\ &\quad + C_\alpha \int_0^{t\wedge\tau_n} \int_{\mathbb{N}\times(0,1)\times\mathbb{R}_+} \left[1 + \langle \mu_{s^-}, 1\rangle^{\alpha-1}\right] \\ &\qquad \times \mathbf{1}_{u\leq\beta(S_p^j(\mu_{s^-}))}\mathbf{1}_{j\leq N_{s^-}^p} Q^2(ds, dj, d\theta, du)\end{aligned}$$

Taking expectations, since $N_{s^-}^p = \langle \mu_{s^-}^p, 1\rangle$, β is bounded by $\overline{\beta}$ (*cf.* hypothesis (H1)) and $E[\langle \mu_0, 1\rangle^\alpha] < \infty$, we have, for some constant $C_\alpha := C_\alpha(\mu_0, \overline{\beta})$ (changing from line to line) depending on α, μ_0 and B

$$\begin{aligned}&E\Big[\sup_{s\in[0,t\wedge\tau_n]} \langle \mu_s, 1\rangle^\alpha\Big] \\ &\qquad \leq C_\alpha\left(1 + \int_0^{t\wedge\tau_n} E\left[\left(1 + \langle \mu_{s^-}, 1\rangle^{\alpha-1}\right)\langle \mu_{s^-}^p, 1\rangle\right] ds\right)\end{aligned}$$

Now remarking that $\langle \mu_{s^-}^p, 1\rangle \leq \langle \mu_{s^-}, 1\rangle$ and $\langle \mu_{s^-}, 1\rangle \leq \langle \mu_{s^-}, 1\rangle^\alpha$ since $\alpha \geq 1$ and $N_s^p \in \mathbb{N}$, we have

$$E\Big[\sup_{s\in[0,t\wedge\tau_n]} \langle \mu_s, 1\rangle^\alpha\Big] \leq C_\alpha\left(1 + 2\int_0^{t\wedge\tau_n} E\left[\langle \mu_{s^-}, 1\rangle^\alpha\right] ds\right)$$

Using first this inequality with $\alpha = 1$, and then for some $\alpha \geq 1$, and using Gronwall's lemma, we can conclude that

$$E\Big[\sup_{s\in[0,t\wedge\tau_n]} \langle \mu_s, 1\rangle^\alpha\Big] < C_\alpha(t) \tag{5.26}$$

Then the sequence τ_n needs to tends a.s to infinity. If not, we cand find $T_0 < \infty$ such that $\epsilon = P\left(\sup_n \tau_n < T_0\right) > 0$. This implies $E\Big[\sup_{s\in[0,T_0\wedge\tau_n]}\langle \mu_s, 1\rangle^\alpha\Big] \geq \epsilon n^\alpha$, which contradicts (5.26). So τ_n goes to infinity and we conclude by letting n to infinity in (5.26) thanks to Fatou lemma.

□

We will also need to derive our results to use ϕ unbounded and particularly some ϕ being like $x \mapsto x^\alpha$. For that we introduce the following corollary:

Corollary 5.6. *Assume (H1-H2) and for some $\alpha \geq 2$*

$$E\left(\langle \mu_0, 1\rangle^\alpha\right) < +\infty.$$

1. *If for all measurable functions*

$$\phi \in \mathcal{C}^2(\mathbb{R}, \mathbb{R}) \text{ and } h \in \mathcal{C}_b^2(\Gamma) \times \mathcal{C}_b^{0,2,2}(\mathbb{N} \times \mathbb{S}^2 \times \Gamma),$$

such that, for all $\mu \in \mathcal{M}_\delta(\Gamma) \times \mathcal{M}_\delta(\mathbb{N}^* \times \mathbb{S}^2 \times \Gamma)$

$$|\phi_h(\mu)| + |\mathcal{L}\phi_h| \leq C(1 + \langle \mu, 1\rangle^p),$$

2. *Or if*

$$\phi : x \mapsto x^\alpha \text{ and } h \in \mathcal{C}_b^2(\Gamma) \times \mathcal{C}_b^{0,2,2}(\mathbb{N} \times \mathbb{S}^2 \times \Gamma),$$

then the process

$$\phi_h(\mu_t) - \phi_h(\mu_0) - \int_0^t \mathcal{L}\phi_h(\mu_s) ds$$

is a $L^1 - (\mathcal{F}_t)_{t\geq 0}$ martingale starting from 0.

Proof. The first point is immediate thanks to proposition 5.5. For the second one, we'll use the conservation mass property to get a finner majoration. The only term that could be a problem is the one given by $\mathcal{L}_1$. Take $\phi(x) = x^\alpha$, so that

$$\begin{aligned}
|\, \mathcal{L}_1\phi_h(\mu_t)\,| &= \Big|\int_\Gamma \int_{\mathbb{N}\times\mathbb{S}^2\times\Gamma} \tau(x,z)\left(\phi_h(\mu_{s^-} + \Delta_1) - \phi_h(\mu_{s^-})\right) \\
&\qquad \times\ \mu_{s^-}^m(dx)\mu_{s^-}^p(dz)\Big| \\
&\leq \int_\Gamma \int_{\mathbb{N}\times\mathbb{S}^2\times\Gamma} \overline{\tau} C(h) \langle \mu_s, h\rangle^{\alpha-1} \mu_{s^-}^m(dx)\mu_{s^-}^p(dz) \\
&\leq \overline{\tau} C(h) t \sup_{[0,t]} \langle \mu_s, 1\rangle^{\alpha-1} \langle \mu_s^m, 1\rangle \langle \mu_s^p, 1\rangle \\
&\leq \overline{\tau} C(h) t \langle \mu_0^m, 1\rangle \sup_{[0,t]} \langle \mu_s, 1\rangle^{\alpha-1} \langle \mu_s^p, 1\rangle \\
&\leq \overline{\tau} C(h) t \langle \mu_0^m, 1\rangle \sup_{[0,t]} \langle \mu_s, 1\rangle^{\alpha}
\end{aligned}$$

where used the conservation of mass property in the last but one line. All other term are similarly bounded by $\sup_{[0,t]}\langle \mu_s, 1\rangle^\alpha$, so that proposition 5.5 allows to conclude. □

5.4.5 Coupled weak formulation and Martingale properties

The evolution of the empirical product measure, can be write in term of a system of two equations, one on the monomers measure and another on the polymers measure. We first remind some notations for this problem, the generator L is decomposed as follows

$$\mathcal{L} = \mathcal{L}^0 + \mathcal{L}^1 + \mathcal{L}^2$$

with $\mathcal{L}^0$ given in Lemma (5.1) and $\mathcal{L}^{k=1,2}$ in Lemma 5.3. The martingale is given by

$$M_t^{total} = M_t^0 + M_t^1 + M_t^2$$

with $M_t^0 := M_{t,0}$ given in (5.19) and $M_t^{k=1,2}$ from the compensated Poisson *wrt* $Q_{k=1,2}$.

Now we decomposed the martingale in several processes. First, taking $\phi = Id$ and $g = 0$ in the total martingale, we get

$$M_t^m := M_t^{total}(\phi = Id, g = 0) = M_t^{0,m} + M_t^{1,m} + M_t^{2,m}, \tag{5.27}$$

and then $f = 0$,

$$M_t^p := M_t^{total}(\phi = Id, f = 0) = M_t^{0,p} + M_t^{1,p} + M_t^{2,p}, \tag{5.28}$$

with $M_t^{i,m} := M_t^i(\phi = Id, g = 0)$ and $M_t^{i,p} := M_t^i(\phi = Id, f = 0)$ for $i = 0, 1, 2$. We also notice that

$$M_t^{total}(\phi = Id) = M_t^m + M_t^p.$$

We are now ready to state our system as a coupled system of two equations. Let us take $\phi = Id$ the identity function in (5.25), then we identify each equation by taking on one hand $h = (f, 0)$ and on the other hand $h = (0, g)$, together with the definition of $\mathcal{L}$ in Lemma 5.3 we get the *weak formulation*:

$$\left\{\begin{array}{rcl}
\langle \mu_t^m, f\rangle &=& \langle \mu_0^m, f\rangle + \displaystyle\int_0^t \langle \mu_t^m, L_m f\rangle ds \\
&& \displaystyle - \int_0^t \int_\Gamma \langle \mu_{s^-}^p, \tau(x,\cdot)\rangle f(x) \mu_{s^-}^m(dx) ds + M_t^m \\
\\
\langle \mu_t^p, g\rangle &=& \langle \mu_0^p, g\rangle + \displaystyle\int_0^t \langle \mu_t^p, L_p g\rangle ds \\
&& \displaystyle + \int_0^t \int_{\mathbb{N}\times\mathbb{S}^2\times\Gamma} \langle \mu_{s^-}^m, \tau(\cdot, z)\rangle \left(g(z + \mathbf{e}_1) - g(z)\right) \mu_{s^-}^p(dz) ds \\
&& \displaystyle - \int_0^t \int_{\mathbb{N}\times\mathbb{S}^2\times\Gamma} \int_0^1 \beta(z) \mathbf{1}_{[\theta r],[(1-\theta)r]>R_0} k_0(\theta) g(z) d\theta \mu_{s^-}^p(dz) ds \\
&& \displaystyle + 2\int_0^t \int_{\mathbb{N}\times\mathbb{S}^2\times\Gamma} \int_0^1 \beta(z) \mathbf{1}_{[\theta r],[(1-\theta)r]>R_0} k_0(\theta) g(\Theta(\theta, z)) d\theta \mu_{s^-}^p(dz) ds \\
&& + M_t^p
\end{array}\right. \tag{5.29}$$

We note that the integral with the factor 2 in front of it, is obtain by changing of variable and using (H2).

The next proposition state the quadratic variation of all these process.

Proposition 5.7. *Assume (H1-H2) and that*

$$E\left(\langle \mu_0, 1\rangle^2\right) < +\infty.$$

Then the process $M_t^{total}(\phi = Id) = M_t^m + M_t^p$ *defined in* (5.27) *and* (5.28) *is an* $L^2-(\mathcal{F}_t)_{t\geq 0}$ *martingale starting from* 0 *with quadratic variations:*

$$\langle M^{total}\rangle_t = \langle M^m\rangle_t + \langle M^p\rangle_t + \langle M^m, M^p\rangle_t$$

such that:

The quadratic variation of M^m *is*

$$\langle M^m\rangle_t = \langle M^{0,m}\rangle_t + \langle M^{1,m}\rangle_t,$$

with

$$\begin{aligned}\langle M^{0,m}\rangle_t &= 2D\int_0^t\int_\Gamma \mid \nabla f(x)\mid^2 \mu_s^m(dx)ds,\\ \langle M^{1,m}\rangle_t &= \int_0^t\int_\Gamma \langle \mu_s^p, \tau(x,\cdot)\rangle f^2(x)\mu_s^m(dx)ds.\end{aligned}$$

Then for M^p *it is*

$$\langle M^p\rangle_t = \langle M^{0,p}\rangle_t + \langle M^{1,p}\rangle_t + \langle M^{2,p}\rangle_t,$$

with

$$\begin{aligned}\langle M^{0,p}\rangle_t = \int_0^t\int_{\mathbb{N}\times\mathbb{S}^2\times\Gamma} &\Big(\Big(\nabla_n g^T\mathcal{R}\Big)\Big(\mathcal{R}^T\nabla_n g\Big)\\ &+\Big(\nabla_y g^T\mathcal{D}_{||}\Big)\Big(\mathcal{D}_{||}^T\nabla_y g\Big)+\Big(\nabla_y g^T\mathcal{D}_{\perp}\Big)\Big(\mathcal{D}_{\perp}^T\nabla_y g\Big)\Big)\mu_s^p(dz)ds,\\ \langle M^{1,p}\rangle_t = \int_0^t\int_{\mathbb{N}\times\mathbb{S}^2\times\Gamma} &\langle \mu_s^m, \tau(\cdot,z)\rangle\left(g(z+\mathbf{e}_1)-g(z)\right)^2\mu_s^p(dz)ds,\\ \langle M^{2,p}\rangle_t = \int_0^t\int_{\mathbb{N}\times\mathbb{S}^2\times\Gamma}\int_0^1 &\beta(z)\mathbf{1}_{[\theta r],[(1-\theta)r]>R_0}k_0(\theta)\\ &\times\ \left(g(\Theta(\theta,z))+g(\Theta(1-\theta,z))-g(z)\right)^2\mu_s^p(dz)d\theta ds.\end{aligned}$$

Finally the cross variation is

$$\begin{aligned}\langle M^m, M^p\rangle_t &= \langle M^{1,m}, M^{1,p}\rangle_t\\ &= -2\int_0^t\int_\Gamma\int_{\mathbb{N}\times\mathbb{S}^2\times\Gamma}\tau(x,z)f(x)\\ &\qquad\qquad\times\left(g(z+\mathbf{e}_1)-g(z)\right)\mu_s^m(dx)\mu_s^p(dz)ds.\end{aligned}$$

Proof. The proof is classical. Lets take $\phi(x) = x^2$, such that $\phi_h(\mu) = (\langle\mu, 1\rangle)^2$. With corollary 5.6 we get that

$$(\langle\mu_t, h\rangle)^2 - (\langle\mu_0, h\rangle)^2 - \int_0^t \mathcal{L}(\langle\mu_s, h\rangle)^2 ds$$

is a martingale. Then we use Itô formula to compute $(\langle\mu_t, h\rangle)^2$ from (5.29), which gives

$$(\langle\mu_t, h\rangle)^2 - (\langle\mu_0, h\rangle)^2 - 2\int_0^t(\langle\mu_s, h\rangle)d(\langle\mu_s, h\rangle) - \langle M_t^m + M_t^p\rangle_t$$

is a martingale. Now, when comparing these two expressions, it leads to the quadratic variations given in the proposition. The proof is left to the reader. □

Remark 5.3. We notice that all the cross variations which are not given in the proposition are in fact equal to zero.

5.5 Scaling equations and the limit problem

5.5.1 Infinite monomers approximation with large polymers

Let us introduce a parameter $n \in \mathbb{N}^*$ that will be discuss later. We consider a set of parameter

$$\tau^n \text{ and } \beta^n \text{ satisfying (H1)},$$

$$k_0^n \text{ satisfying (H2) and } R_0^n > 0,$$

that depends on this parameter n, thus $\mathcal{L}_1$ and $\mathcal{L}_2$ are changed in consequences, that leads to a generator denoted by $\tilde{\mathcal{L}}^n$ defined as in Lemma 5.3 but with rescaled parameters.

Remark 5.4. We note here that $\mathcal{L}^0$ is unchanged, indeed, we assume that the diffusion coefficients D, $D_\perp$, $D_{||}$ and D_r are constant. It seems to be a hard hypothesis but the scaling of these coefficients are currently not derived, maybe one could inspired by [64]. We believe that the mathematical analysis is similar when the diffusion is rescaled.

Now, we rescale the initial condition from this parameter, let $\tilde{\mu}_0^n \in \mathcal{M}_\delta(\Gamma) \times \mathcal{M}_\delta(\mathbb{N}^* \times \mathbb{S}^2 \times \Gamma)$ from a quantity M_0 of monomers, N_0 of polymers, such that

$$\tilde{\mu}_0^n = \left(\sum_{i=0}^{[nM_0]} \delta_{X_0^i}, \sum_{j=0}^{N_0} \delta_{\tilde{Z}_0^{i,n}} \right). \tag{5.30}$$

with $\tilde{Z}_0^{i,n} = (\tilde{R}_0^{j,n} = [nR_0^j], H_0^j, Y_0^j)$. These transformation is nothing but considering a large number of monomers and large size of polymers (in terms of numbers of monomers that forms them). For all $n \in \mathbb{N}^*$, we have a unique solution $\tilde{\mu}_t^n$ given by the Equation (5.23) where the coefficients (τ, β, k_0) and initial condition μ_0 are respectively replaced by (τ^n, β^n, k_0^n) and $\tilde{\mu}_0^n$. The aim of the scaling is now to study the problem when the mass (or the size) of one monomer is given by the parameter $1/n$.

Let us now rescale the solution for a large population of monomers by taking a mass of monomer in $1/n$, thus

$$\mu_t^n = \left(\frac{1}{n} \tilde{\mu}_t^{m,n}, \sum_{j=0}^{\tilde{N}_t^{p,n}} \delta_{Z_t^{i,n}} \right). \tag{5.31}$$

with $\tilde{N}_t^{p,n} = \langle \tilde{\mu}_t^{p,n}, 1 \rangle$ (idem for $\tilde{N}_t^{m,n}$) and

$$Z_t^{i,n} = (R_t^{j,n} = \tilde{R}_t^{j,n}/n, H_t^j, Y_t^j) \in \frac{1}{n}\mathbb{N}^* \times \mathbb{S}^2 \times \Gamma.$$

Remark 5.5. We notice that the size of the polymers (numbers of monomers that forms them) is rescaled from the size of the monomers, this suggests that the size will describe now a physical length.

Now, the rescaled empirical measure belongs to a different space that is for any $n \in \mathbb{N}^*$

$$\mu_t^n \in \mathcal{M}_\delta(\Gamma) \times \mathcal{M}_\delta(\frac{1}{n}\mathbb{N}^* \times \mathbb{S}^2 \times \Gamma) \hookrightarrow \mathcal{M}_\delta(\Gamma) \times \mathcal{M}_\delta(\mathbb{R}_+^* \times \mathbb{S}^2 \times \Gamma).$$

The injection is used to stay in a same state value for the stochastic processes μ_t^n.

From this scaling, we note several relations:

$$\begin{aligned}
\langle \tilde{\mu}_t^{m,n}, 1\rangle &= n\langle \mu_t^{m,n}, 1\rangle, \\
\langle \tilde{\mu}_t^{p,n}, 1\rangle &= \langle \mu_t^{p,n}, 1\rangle, \\
\langle \tilde{\mu}_t^{m,n}, \tau^n(\cdot, z)\rangle &= n\langle \mu_t^{m,n}, \tau^n(\cdot, z))\rangle, \\
\langle \tilde{\mu}_t^{p,n}, \tau^n(x, \cdot)\rangle &= \langle \mu_t^{p,n}, \tau^n(x, (n,1,1)\cdot)\rangle, \\
\langle \tilde{\mu}_t^{p,n}, \beta^n(\cdot)\rangle &= \langle \mu_t^{p,n}, \beta^n((n,1,1)\cdot)\rangle,
\end{aligned}$$

where $(n,1,1)\cdot(r,\eta,y) = (nr,\eta,y)$. The following proposition is a consequence of these relation and proposition 5.7

Proposition 5.8. *Assume that (τ^n, β^n) satisfy (H1), k_0^n satisfies (H2) and*

$$E\left(\langle \mu_0^n, 1\rangle^2\right) < +\infty.$$

Then the rescaled measure μ_t^n defined in (5.30) is solution, for all $f \in \mathcal{C}^2(\overline{\Gamma})$ and $g \in \mathcal{C}_b^{0,2,2}(\mathbb{R}_+ \times \mathbb{S}^2 \times \overline{\Gamma})$ (still with vanishing normal derivatives), of

$$\left\{\begin{aligned}
\langle \mu_t^{m,n}, f\rangle &= \langle \mu_0^{m,n}, f\rangle + \int_0^t \langle \mu_t^{m,n}, L_m f\rangle ds \\
&\quad - \int_0^t \int_\Gamma \langle \mu_{s^-}^{p,n}, \tau^n(x,(n,1,1)\cdot)\rangle f(x) \mu_{s^-}^{m,n}(dx) ds + M_t^{m,n} \\
\langle \mu_t^{p,n}, g\rangle &= \langle \mu_0^{p,n}, g\rangle + \int_0^t \langle \mu_t^{p,n}, L_p g\rangle ds \\
&\quad + \int_0^t \int_{\mathbb{R}_+\times\mathbb{S}^2\times\Gamma} n\langle \mu_{s^-}^{m,n}, \tau^n(\cdot,(n,1,1)\cdot z)\rangle \left(g(z+\frac{1}{n}\mathbf{e}_1) - g(z)\right) \mu_{s^-}^{p,n}(dz) ds \\
&\quad - \int_0^t \int_{\mathbb{R}_+\times\mathbb{S}^2\times\Gamma} \int_0^1 \beta^n((n,1,1)\cdot z) \mathbf{1}_{[\theta nr], [(1-\theta)nr] > R_0} k_0^n(\theta) g(z) d\theta \mu_{s^-}^{p,n}(dz) ds \\
&\quad + 2\int_0^t \int_{\mathbb{R}_+\times\mathbb{S}^2\times\Gamma} \int_0^1 \beta^n((n,1,1)\cdot z) \mathbf{1}_{[\theta nr], [(1-\theta)nr] > R_0} k_0^n(\theta) g(\Theta^n(\theta, z)) d\theta \mu_{s^-}^{p,n}(dz) ds \\
&\quad + M_t^{p,n}
\end{aligned}\right. \tag{5.32}$$

where $\Theta^n(\theta, Z) = ([\theta nR]/n, H, Y)$ and $M_t^{total,n} = M_t^{m,n} + M_t^{p,n}$ is a square integrable martingale starting at 0 with quadratic variations:

$$\langle M^{total,n}\rangle_t = \langle M^{m;n}\rangle_t + \langle M^{p,n}\rangle_t + \langle M^{m,n}, M^{p,n}\rangle_t$$

such that:

The quadratic variation of $M^{m,n}$ *is*

$$\langle M^{m,n}\rangle_t = \langle M^{0,m,n}\rangle_t + \langle M^{1,m,n}\rangle_t,$$

with

$$\begin{aligned}\langle M^{0,m,n}\rangle_t &= \frac{2D}{n}\int_0^t \mid \nabla f(x) \mid^2 \mu_s^{m,n}(dx)ds,\\ \langle M^{1,m,n}\rangle_t &= \frac{1}{n}\int_0^t\int_\Gamma \langle \mu_s^{p,n}, \tau^n(x,(n,1,1)\cdot)\rangle f^2(x)\mu_s^{m,n}(dx)ds.\end{aligned}$$

Then for $M^{p,n}$ *it is*

$$\langle M^{p,n}\rangle_t = \langle M^{0,p,n}\rangle_t + \langle M^{1,p,n}\rangle_t + \langle M^{2,p,n}\rangle_t,$$

with

$$\begin{aligned}\langle M^{0,p,n}\rangle_t &= \int_0^t\int_{\mathbb{R}_+\times\mathbb{S}^2\times\Gamma} \Big(\Big(\nabla_n g^T \mathcal{R}\Big)\Big(\mathcal{R}^T\nabla_n g\Big)\\ &\qquad + \Big(\nabla_y g^T \mathcal{D}_{||}\Big)\Big(\mathcal{D}_{||}^T\nabla_y g\Big) + \Big(\nabla_y g^T\mathcal{D}_\perp\Big)\Big(\mathcal{D}_\perp^T\nabla_y g\Big)\Big)\mu_s^{p,n}(dz)ds,\\ \langle M^{1,p,n}\rangle_t &= \int_0^t\int_{\mathbb{R}_+\times\mathbb{S}^2\times\Gamma} n\langle\mu_s^{m,n}, \tau^n(\cdot,(n,1,1)\cdot z)\rangle\left(g(z+\frac{1}{n}\mathbf{e}_1)-g(z)\right)^2\mu_s^{p,n}(dz)ds,\\ \langle M^{2,p,n}\rangle_t &= \int_0^t\int_{\mathbb{R}_+\times\mathbb{S}^2\times\Gamma}\int_0^1 \beta^n((n,1,1)\cdot z)\mathbf{1}_{[\theta nr],[(1-\theta)nr]>R_0}k_0^n(\theta)\\ &\qquad\times\left(g(\Theta^n(\theta,z))+g(\Theta^n(1-\theta,z))-g(z)\right)^2\mu_s^{p,n}(dz)d\theta ds.\end{aligned}$$

Finally the cross variation is

$$\begin{aligned}\langle M^{m,n}, M^{p,n}\rangle_t &= \langle M^{1,m,n}, M^{1,p,n}\rangle_t\\ &= -2\int_0^t\int_\Gamma\int_{\mathbb{R}_+\times\mathbb{S}^2\times\Gamma}\tau^n(x,(n,1,1)\cdot z)f(x)\\ &\qquad\times\left(g(z+\frac{1}{n}\mathbf{e}_1)-g(z)\right)\mu_s^{m,n}(dx)\mu_s^{p,n}(dz)ds.\end{aligned}$$

5.5.2 The limit problem

We now recall our assumptions and make the following mean-field specific scaling

(H1) Let τ and β be continuous non-negative function, uniformly bounded respectively by $\overline{\tau}>0$ and $\overline{\beta}>0$, that is

$$\tau(x,z)\le\overline{\tau} \text{ and } \beta(z)\le\overline{\beta},\quad \forall x\in\Gamma,\ \forall z\in\mathbb{N}\times\mathbb{S}^2\times\Gamma.$$

Moreover, τ belongs to $C_b^{0,1,0,0}(\Gamma\times\mathbb{R}_+^*\times\mathbb{S}^2\times\Gamma)$.

(H2) Let $k_0 : (0,1) \mapsto \mathbb{R}_+$ is a symmetrical probability density function, *i.e.*

$$\int_0^1 k_0(\theta)d\theta = 1 \text{ and } k_0(\theta) = k_0(1-\theta),\ \forall \theta \in (0,1).$$

(H3) Let τ^n, β^n, k_0^n and R_0^n defined by $\forall x \in \Gamma$, $\forall z \in \mathbb{N} \times \mathbb{S}^2 \times \Gamma$ and $\forall n \in \mathbb{N}$,

$$\begin{aligned} \tau^n(x,(n,1,1)\cdot z) &= \tau(x,z) \\ \beta^n((n,1,1)\cdot z) &= \beta(z) \\ k_0^n(\theta) &= k_0(\theta) \\ R_0^n &= R_0 \end{aligned}$$

(H4) μ_0^n converge in law and for the weak topology towards a couple (μ_0^m, μ_0^p) of non-negative measure where μ^n is a deterministic finite measure on Γ and μ_0^p a finite random measure in $\mathcal{M}_\delta(\mathbb{R}_+^* \times \mathbb{S}^2 \times \Gamma)$, and, for some $p \geq 2$)

$$\sup_n E\left(\langle \mu_0^n, 1\rangle^p\right) < \infty$$

Remark 5.6. In order to facilitate the following computation, the scaling in (H3) is taken equal but could be easily replace by strong limit in n.

Remark 5.7. Below we will state the limiting problem, using the same notation as for the **initial** problem of section 5.4, in particular for μ^m,μ^p, etc... We hope that no confusion will be made...

Under these assumptions we formally derive from (5.32) our *candidate* limit problem that is for any $f \in \mathcal{C}_b^2(\Gamma)$ and $g \in \mathcal{C}_b^{1,2,2}(\mathbb{R}_+ \times \mathbb{S}^2 \times \Gamma)$,

$$\left\{ \begin{aligned} \langle \mu_t^m, f\rangle &= \langle \mu_0^m, f\rangle + \int_0^t \langle \mu_t^m, L_m f\rangle ds \\ &\quad - \int_0^t \int_\Gamma \langle \mu_{s^-}^p, \tau(x,\cdot)\rangle f(x) \mu_{s^-}^m(dx)ds \\ \langle \mu_t^p, g\rangle &= \langle \mu_0^p, g\rangle + \int_0^t \langle \mu_t^p, L_p g\rangle ds \\ &\quad + \int_0^t \int_{\mathbb{R}_+\times\mathbb{S}^2\times\Gamma} \langle \mu_{s^-}^m, \tau(\cdot,z)\rangle \frac{\partial}{\partial r} g(z) \mu_{s^-}^p(dz)ds \\ &\quad - \int_0^t \int_{\mathbb{R}_+\times\mathbb{S}^2\times\Gamma} \beta(z) g(z) d\theta \mu_{s^-}^p(dz)ds \\ &\quad + 2\int_0^t \int_{\mathbb{R}_+\times\mathbb{S}^2\times\Gamma} \int_0^1 \beta(z) k_0(\theta) g(\theta r, \eta, y)) d\theta \mu_{s^-}^p(dz)ds \\ &\quad + \overline{M}_t^p \end{aligned} \right. \tag{5.33}$$

where $\overline{M}^p_t = \overline{M}^{0,p}_t + \overline{M}^{2,p}_t$ is a martingale with

$$\overline{M}^{0,p}_t = \int_0^t \sum_{j=1}^{N^p_s} \Big[\sqrt{2D_r}\nabla_n g(Z^j_s)\cdot dB^j_s \wedge H^j_s + \nabla_y g(Z^j_s)\cdot \Big[\sqrt{2D_\perp}(I_3 - H^j_s\otimes H^j_s) + \sqrt{2D_{||}} H^j_s \otimes H^j_s\Big] dW^{(p)j}_s \Big],$$

and

$$\begin{aligned}\overline{M}^{2,p}_t &= \int_0^t \int_{\mathbb{N}\times(0,1)\times\mathbb{R}_+} \Big(g(\Theta(\theta, Z^j_s)) + g(\Theta(1-\theta, Z^j_s)) - g(Z^j_s)\Big) \\ &\qquad \times \mathbf{1}_{u\le \beta^j_{s^-}} \mathbf{1}_{j\le N^p_{s^-}} \\ &\qquad \times \Big(Q_2(ds,dj,d\theta,du) - E[Q_2(ds,dj,d\theta,du)]\Big).\end{aligned}$$

Remark 5.8. The identification of the limit problem will be through the martingal problem associated to (5.33), which we now state below. As this martingal problem is very much similar to the one studies in section 5.4.4, we omit the justification.

Before proving a convergence theorem to this limit problem we first need a result on its well-posedness. It is the following lemma:

Lemma 5.9. *Let us assume (H1-H2) and $\mu_0 \in \mathcal{M}^+_F(\Gamma)\times\mathcal{M}^+_\delta(\mathbb{R}^*_+\times\mathbb{S}^2\times\Gamma)$. There exists at least one solution $(\mu_t)_{t\ge0}$ to the limit problem* (5.33) *such that*

$$\mu \in \mathcal{D}(0,T;\mathcal{M}^+_F(\Gamma)\times\mathcal{M}^+_F(\mathbb{R}^*_+\times\mathbb{S}^2\times\Gamma)).$$

Moreover, μ^p remains a point process, that is $\mu^p \in \mathcal{M}_\delta(\mathbb{R}^*_+\times\mathbb{S}^2\times\Gamma)$ for all $t\ge0$, and we have the following conservation, for any $t\ge0$

$$\langle \mu^m_t, \mathbf{1}\rangle + \langle \mu^p_t, \mathbf{r}\rangle = \langle \mu^m_0, \mathbf{1}\rangle + \langle \mu^p_0, \mathbf{r}\rangle,$$

and

$$\langle \mu^p_t, \mathbf{1}\rangle = \langle \mu^p_0, \mathbf{1}\rangle.$$

(where $\mathcal{M}^+$ denotes the cone of positive measures)

Proof. Let us consider an auxiliary problem: For any $h=(f,g)\in \mathcal{C}^0_b(\Gamma)\times\mathcal{C}^{1,0,0}_b(\mathbb{R}_+\times\mathbb{S}^2\times\Gamma)$ and $t\ge0$

$$\begin{aligned}\langle \mu^m_t, f\rangle &= \langle \mu^m_0, f\rangle - \int_0^t\int_\Gamma \langle \mu^p_s, \tau(x,\cdot)\rangle f(x)\mu^m_s(dx)ds \\ \langle \mu^p_t, g\rangle &= \langle \mu^p_0, g\rangle + \int_0^t \int_{\mathbb{R}_+\times\mathbb{S}^2\times\Gamma} \langle \mu^m_s, \tau(\cdot,z)\rangle \partial_r g(z)\mu^p_s(dz)ds\end{aligned} \tag{5.34}$$

This system involves, only, polymerization. We do not consider at this time spacial and rotational motion for sake of simplicity.

We consider through this proof that μ^0 is given such that,

$$\mu_0^m \in \mathcal{M}_F(\Gamma) \text{ a non-negative measure,}$$

and

$$\mu_0^p = \sum_{j=1}^{N^p} \delta_{(R_0^j, H_0^j, Y_0^j)} \in \mathcal{M}_\delta(\mathbb{R}_+^* \times \mathbb{S}^2 \times \Gamma), \text{ with } R_0^j > 0,\ H_0^j \in \mathbb{S}^2,\ Y_0^j \in \Gamma$$

where $N^p = \langle \mu_0^p, \mathbf{1} \rangle$. Hence, a solution to the problem (5.34) is given by a solution to

$$\begin{aligned} \langle \mu_t^m, f \rangle &= \langle \mu_0^m, f \rangle - \int_0^t \int_\Gamma \langle \mu_s^p, \tau(x, \cdot) \rangle f(x) \mu_s^m(dx) ds \\ R_t^j &= R_0^j + \int_0^t \langle \mu_s^m, \tau(\cdot, R_s^j) \rangle ds,\ j = 1, \ldots, N^p \end{aligned} \tag{5.35}$$

where $\mu_t^p = \sum_{j=1}^{N^p} \delta_{(R_t^j, H_0^j, Y_0^j)}$.

Let us defined S defined on $C(0, T; \mathcal{M}_F(\Gamma) \times \mathbb{R}_{N^p}$ such that $(\tilde{\mu}_t^m, (\tilde{R}_t^i)_i)_{t \geq 0}$ is given by

$$\begin{aligned} \langle \tilde{\mu}_t^m, f \rangle &= \langle \mu_0^m, f \rangle - \int_0^t \int_\Gamma \langle \mu_s^p, \tau(x, \cdot) \rangle f(x) \mu_s^m(dx) ds \\ \tilde{R}_t^j &= R_0^j + \int_0^t \langle \mu_s^m, \tau(\cdot, R_s^j) \rangle ds,\ j = 1, \ldots, N^p \end{aligned}$$

We equipped $C(0, T; \mathcal{M}_F(\Gamma) \times \mathbb{R}^{N^p})$ with the metric

$$d_\infty := \sup_{t \in (0,T)} \left(\varrho(\mu_t^m, \mu_t^{m\prime}) + \sup_{1 \leq j \leq N^p} |R_t^j - R_t^{j\prime}| \right)$$

where

$$\varrho(\mu^m, \mu^{m\prime}) := \sup_{f \in \mathcal{C}_b^0(\Gamma), \|f\|_{L^\infty} \leq 1} \int_\Gamma f(x)(\mu^m - \mu^{m\prime})(dx).$$

This metric makes $C(0, T; \mathcal{M}_F(\Gamma) \times \mathbb{R}_+^{*N^p})$ a complete space. We are know in position to state a Banach fixed point on S. First we considered the subset

$$\begin{aligned} \mathcal{K}_T = \Bigg\{ & (\mu^m, (R^j)_j) \in \mathcal{C}^0(0, T; \mathcal{M}_F(\Gamma) \times \mathbb{R}^{N^p}), \\ & \forall t \geq 0,\ \mu_t^m \text{ is a non-negative measure and } R_t^j > 0, \\ & \forall A \subset \mathcal{B}(\Gamma),\ \forall s \leq t,\ \mu_t^m(A) \leq \mu_s^m(A), \\ & \langle \mu_t^m, \mathbf{1} \rangle + \sum_{i=1}^{N^p} R_t^i = \rho_0 \Bigg\} \end{aligned}$$

This subset is a non-empty set since the measure 0 together with the sequence $R_t^i = \rho_0 / N^p$ belongs to $\mathcal{K}_T$. Moreover, S restricted to $\mathcal{K}_T$ remains into itself whenever T is small

enough, that is $S : \mathcal{K}_T \mapsto \mathcal{K}_T$. Indeed, non-negativeness of $\tilde{\mu}^m$ holds true when T is small enough (depending on τ, ρ_0 and N^p) and it is obvious that $\tilde{R}^j$ remains positive, for all j. The mass conservation is also obviously satisfied.

Now, let us take $(\mu^m, (R^j)_j)$ and $(\mu^{m\prime}, (R^{j\prime})_j)$ both in $C(0,T; \mathcal{M}_F(\Gamma) \times \mathbb{R}_+^{*N^p})$, from (5.35), we get

$$\left|R_t^j - R_t^{j\prime}\right| \leq \left|R_0^j - R_0^{j\prime}\right| + \int_0^t \left|\langle \mu_s^m - \mu_s^{m\prime}, \tau(\cdot, Z_t^j)\rangle\right| ds + \int_0^t \left|\langle \mu_s^m, \tau(\cdot, Z_s^j) - \tau(\cdot, Z_s^{j\prime})\rangle\right| ds \quad (5.36)$$

Moreover, for any $f \in \mathcal{C}_b^0(\Gamma)$

$$\left|\langle \mu_t^m - \mu_t^{m\prime}, f\rangle\right| \leq \int_0^t \int_\Gamma \left|\langle \mu_s^p - \mu_s^{p\prime}, \tau(x,\cdot)\rangle f(x) \mu_s^m(dx)\right| ds + \int_0^t \left|\int_\Gamma \langle \mu_s^{p\prime}, \tau(x,\cdot)\rangle f(x)(\mu_s^m - \mu_s^{m\prime})(dx)\right| ds \quad (5.37)$$

The aim of the following is to bound each terms in (5.36) and (5.37). For that, from (H1) we remark that for any $x \in \mathbb{R}_+^*$,

$$\begin{aligned} \left|\langle \mu_t^p - \mu_t^{p\prime}, \tau(x,\cdot)\rangle\right| &= \sum_{i=1}^{N^p} \left|\tau(x, Z_t^j) - \tau(x, Z_t^{j\prime})\right| \\ &\leq N^p \|\partial_r \tau\|_{L^\infty} \sup_{1\leq j\leq N^p} \left|R_t^j - R_t^{j\prime}\right|. \end{aligned} \quad (5.38)$$

Then, from (H1) for any $f \in \mathcal{C}_b^0(\Gamma)$, $x \mapsto \langle \mu_s^{p\prime}, \tau(x,\cdot)\rangle f(x)$ belongs to $\mathcal{C}_b^0(\Gamma)$ too, thus for any $f \in \mathcal{C}_b^0(\Gamma)$ with $\|f\|_{L^\infty} \leq 1$:

$$\int_\Gamma \langle \mu_s^{p\prime}, \tau(x,\cdot)\rangle f(x)(\mu_s^m - \mu_s^{m\prime})(dx) \leq N^p \|\tau\|_{L^\infty} \varrho(\mu_s^m, \mu_s^{m\prime}). \quad (5.39)$$

Hence, combining (5.37), (5.38), (5.39), there exist M depending on τ, ρ_0 and N^p such that for all $t \geq 0$

$$\varrho(\mu_t^m, \mu_t^{m\prime}) \leq M \int_0^t \left(\sup_{1\leq j\leq N^p} \left|R_s^j - R_s^{j\prime}\right| + \varrho(\mu_s^m, \mu_s^{m\prime})\right) ds. \quad (5.40)$$

Now, from (5.36) and (H1), there exist a constant still denoted by M (depending on the same parameters) such that for all $t \geq 0$

$$\sup_{1\leq j\leq N^p} \left|R_t^j - R_t^{j'}\right| \leq M \int_0^t \left(\sup_{1\leq j\leq N^p} \left|R_s^j - R_s^{j\prime}\right| + \varrho(\mu_s^m, \nu_s^m)\right) ds, \quad (5.41)$$

and thus combining (5.40) and (5.41), we get

$$\sup_{1\le j\le N^p}\left|R_t^j-R_t^{j'}\right|+\varrho(\mu_t^m,\mu_t^{m\prime})$$
$$\le 2M\int_0^t\left(\sup_{1\le j\le N^p}\left|R_s^j-R_s^{j\prime}\right|+\varrho(\mu_s^m,\mu_s^{m\prime})\right)ds. \quad (5.42)$$

Finally, when taking the $\sup_{(0,T)}$ in (5.42), it follows that S is a contaction with T small enough. Hence, there exists a unique solution to (5.35). Since the choice of T depends only on τ, ρ_0 and N^p, we are able to extend the solution on any interval $[0,T]$ with $T>0$. It follows that there exists at least one solution to the weak formulation (5.34). □

The extension of this proof (for the existence) with space motion does not pose any difficulties as long as each individual stochastic differential equation for polymers' displacement is well defined, and stay in a compact (which is ensured by boundary condition). The existence of the whole stochastic process defined by (5.33) follow then by similar calculation of the section 5.4.4 and moment estimates (see also [38, Prop 3.2] and [208, Prop 2.2.5]). For strong unicity, we refer as well to [208, Prop 2.2.6]

Let us define the following generator, for any $\phi_h(\mu)=\phi(\langle\mu,h\rangle)$ with $h\in\mathcal{C}_b^2(\Gamma)\times\mathcal{C}_b^{1,2,2}(\mathbb{R}_+\times\mathbb{S}^2\times\Gamma)$ and $\phi\in\mathcal{C}_b^2(\mathbb{R})$,

$$\mathcal{L}^\infty\phi_h=\mathcal{L}_0\phi_h+\mathcal{L}_1^\infty\phi_h+\mathcal{L}_2^\infty\phi_h \quad (5.43)$$

where $\mathcal{L}_0$ defined in Lemma 5.1, and $\mathcal{L}_1^\infty$ is associated to the deterministic elongation process, and reads

$$\mathcal{L}_1^\infty\phi_h=\phi'(\langle\mu,h\rangle)\langle\mu,\Big(-\langle\tau(x,.),\mu^p\rangle f(x),\langle\tau(.,z),\mu^m\rangle\frac{\partial g(z)}{\partial r}\Big)\rangle$$

and finally $\mathcal{L}_2^\infty$ is associated to the (random) fragmentation process on continuous-size polymer, and reads

$$\mathcal{L}_2^\infty\phi_h=\int_{\mathbb{R}_+\times\mathbb{S}^2\times\Gamma}\int_0^1\beta(z)\Big[\phi\big(\langle\mu,h\rangle+g(\Theta(\theta,z))+g(\Theta(1-\theta),z)-g(z)\big)-\phi\big(\langle\mu,h\rangle\big)\Big]k(\theta)d\theta\mu^p(dz)$$

We have the analogous property of corollary 5.6 and property 5.7:

Proposition 5.10. *Assume (H1-H2). Suppose $\mu_0\in\mathcal{M}_F^+(\Gamma)\times\mathcal{M}_\delta(\mathbb{R}^*\times\mathbb{S}^2\times\Gamma)$, such that $E\Big(\langle\mu_0,1\rangle^2\Big)<\infty$. Then*

1. *for any*
$$\phi\in\mathcal{C}^2(\mathbb{R},\mathbb{R}) \text{ and } h\in\mathcal{C}_b^2(\Gamma)\times\mathcal{C}_b^{1,2,2}(\mathbb{R}^+\times\mathbb{S}^2\times\Gamma),$$
such that, for all $\mu\in\mathcal{M}_F^+(\Gamma)\times\mathcal{M}_\delta(\mathbb{R}^*\times\mathbb{S}^2\times\Gamma)$
$$|\phi_h(\mu)|+|\mathcal{L}^\infty\phi_h|\le C(1+\langle\mu,1\rangle^p),$$

2. Or if

$$\phi : x \mapsto x^2 \text{ and } h \in \mathcal{C}_b^2(\Gamma) \times \mathcal{C}_b^{1,2,2}(\mathbb{R}^+ \times \mathbb{S}^2 \times \Gamma),$$

then the process

$$\phi_h(\mu_t) - \phi_h(\mu_0) - \int_0^t \mathcal{L}^\infty \phi_h(\mu_s) ds$$

is a $L^1 - (\mathcal{F}_t)_{t\geq 0}$ *martingale starting from* 0*. Moreover, with* $\phi = Id$*, this martingale is* $\overline{M}_t^p = \overline{M}_t^{0,p} + \overline{M}_t^{2,p}$ *defined in 5.33 and is an* $L^2 - (\mathcal{F}_t)_{t\geq 0}$ *martingale starting from* 0 *with quadratic variations:*

$$\langle \overline{M}^p \rangle_t = \langle \overline{M}^{0,p} \rangle_t + \langle \overline{M}^{2,p} \rangle_t$$

where

$$\begin{aligned}
\langle \overline{M}^{0,p} \rangle_t &= \int_0^t \int_{\mathbb{R}_+ \times \mathbb{S}^2 \times \Gamma} \Big(\left(\nabla_n g^T \mathcal{R} \right) \left(\mathcal{R}^T \nabla_n g \right) \\
&\qquad + \left(\nabla_y g^T \mathcal{D}_{||} \right) \left(\mathcal{D}_{||}^T \nabla_y g \right) + \left(\nabla_y g^T \mathcal{D}_{\perp} \right) \left(\mathcal{D}_{\perp}^T \nabla_y g \right) \Big) \mu_s^p(dz) ds, \\
\langle \overline{M}^{2,p} \rangle_t &= \int_0^t \int_{\mathbb{R}^+ \times \mathbb{S}^2 \times \Gamma} \int_0^1 \beta(z) \left(g(\Theta(\theta, z)) + g(\Theta(1-\theta, z)) - g(z) \right)^2 \mu_s^p(dz) d\theta ds.
\end{aligned}$$

5.5.3 Convergence theorem

Now we are in position to state the main result, the convergence of the rescaled solutions to the limit problem:

Theorem 5.11. *Under assumptions (H1-H4), let the sequence of process* $(\mu^n)_{n\geq 1}$ *given by* (5.32) *and the process* μ *given by* (5.33)*. Then*

$$\mu^n \xrightarrow[n\to+\infty]{Law} \mu \text{ in } \mathcal{D}([0,\infty), w - \mathcal{M}_F(\Gamma) \times \mathcal{M}_F(\mathbb{R}_+^* \times \mathbb{S}^2 \times \Gamma)),$$

(convergence in law, where the measure space is equipped with the topology of weak convergence)

Proof. The proof of the scaling result will follow similar lines as [13, 80]. We start with moment estimates, that comes directly from the study of the discrete process below. Then we shall prove that μ^n is tight in $\mathcal{M}_F(\Gamma) \times \mathcal{M}_F(\mathbb{R}_+^* \times \mathbb{S}^2 \times \Gamma)$ endowed with the topology of weak convergence. We will finally consider uniqueness of the limiting values of μ^n.

Step 1: Moment estimates Under our assumption,

$$\sup_n E\left(\sup_{t\in[0,T]} \langle \mu_t^n, 1 \rangle^2 \right) < +\infty$$

because similar estimates as in proposition 5.5 holds for μ_t^n with a constant that does not depends on n other that by $E\left(\langle \mu_0^n, 1\rangle^2\right)$.

Step 2: Tightness We first show that μ^n is tight in $\mathcal{M}_F(\Gamma) \times \mathcal{M}_F(\mathbb{R}_+ \times \mathbb{S}^2 \times \Gamma))$ endowed with the vague topology. For this, we need two things [70, Thm 9.1]

- prove that for all function h in a dense subset of $\mathcal{C}_b^0(\Gamma) \times \mathcal{C}_b^0(\mathbb{R}_+ \times \mathbb{S}^2 \times \Gamma)$, the sequences $\langle \mu^n, h \rangle$ are tight in $\mathcal{D}\big([0,T], \mathbb{R}\big)$, for any $T > 0$
- prove that the following compact containment condition holds: $\forall T > 0, \forall \varepsilon > 0, \exists K_{\varepsilon,T}$ compacts subset of $\mathcal{M}_F(\Gamma) \times \mathcal{M}_F(\mathbb{R}_+^* \times \mathbb{S}^2 \times \Gamma)$,

$$\inf_n \mathcal{P}\Big(\mu_n \in K_{\varepsilon,T}, \text{ for } t \in [0,T]\Big) \geq 1 - \varepsilon$$

For the tightness of $\langle \mu^n, h \rangle$, note that equations (5.32) gives us $\langle \mu^n, h \rangle$ as the sum of process with finite variation and a martingale. The advantage to prove tightness for $\langle \mu^n, h \rangle$ rather than μ^n directly is to have a stochastic process at values in a finite-dimensional space. We will then use Rebolledo criterion [111, Cor 2.3.3 p 41], together with Aldous criterion [106, Theorem 3.21, page 350].

Let $h \in \mathcal{C}^2(\overline{\Gamma}) \times \mathcal{C}_b^2(\mathbb{R}_+^* \times \mathbb{S}^2 \times \overline{\Gamma})$

$$\lim_{n\to\infty} \left(g(z + \frac{1}{n}\mathbf{e}_1) - g(z) \right) n = \frac{\partial g}{\partial r}(z),$$

and the limit is controlled, uniformly in n, by the second derivatives of g. Let us denotes $V_t^{i,m,n}$, $i = 0, 1$, $V_t^{i,p,n}$, $i = 0, 1, 2$ for the finite variation part of $\langle \mu^n, h \rangle$, with analogy to our martingale notation. Our assumption leads to the following estimates (note that all constant are different and depend on bound of coefficient and test functions as mentioned)

$$\begin{aligned}
|V_t^{0,m,n}| &\leq C(f,u)t \sup_{[0,t]} \langle \mu_s^{m,n}, 1 \rangle \\
|V_t^{1,m,n}| &\leq C(f,\overline{\tau})t \sup_{[0,t]} \langle \mu_s^{m,n}, 1 \rangle \langle \mu_s^{p,n}, 1 \rangle \\
|V_t^{0,p,n}| &\leq C(g,u)t \sup_{[0,t]} \langle \mu_s^{p,n}, 1 \rangle \\
|V_t^{1,p,n}| &\leq C(g,\overline{\tau})t \sup_{[0,t]} \langle \mu_s^{m,n}, 1 \rangle \langle \mu_s^{p,n}, 1 \rangle \\
|V_t^{2,p,n}| &\leq C(g,\overline{\beta})t \sup_{[0,t]} \langle \mu_s^{p,n}, 1 \rangle
\end{aligned}$$

which provides immediately, thanks to step 1,

$$\sup_n E\big(\sup_t \mid V_t^n \mid \big) < \infty$$

Using that

$$\begin{aligned}
\lim_{n\to\infty} n \left(g(z + \frac{1}{n}\mathbf{e}_1) - g(z) \right)^2 &= 0 \\
\lim_{n\to\infty} \left(g(z + \frac{1}{n}\mathbf{e}_1) - g(z) \right) &= 0
\end{aligned}$$

we obtain similarly

$$\begin{aligned}
\langle M^{0,m,n}\rangle_t &\leq \frac{C(f)}{n} t \sup_{[0,t]} \langle \mu_s^{m,n}, 1\rangle \\
\langle M^{1,m,n}\rangle_t &\leq \frac{C(f,\overline{\tau})}{n} t \sup_{[0,t]} \langle \mu_s^{m,n}, 1\rangle \langle \mu_s^{p,n}, 1\rangle \\
\langle M^{0,p,n}\rangle_t &\leq C(g) \sup_{[0,t]} \langle \mu_s^{p,n}, 1\rangle \\
\langle M^{1,p,n}\rangle_t &\leq \frac{C(g,\overline{\tau})}{n} t \sup_{[0,t]} \langle \mu_s^{m,n}, 1\rangle \langle \mu_s^{p,n}, 1\rangle \\
\langle M^{2,p,n}\rangle_t &\leq C(g,\overline{\beta}) t \sup_{[0,t]} \langle \mu_s^{p,n}, 1\rangle \\
|\langle M^{1,m,n}, M^{2,m,n}\rangle_t| &\leq \frac{C(f,g,\overline{\tau})}{n} t \sup_{[0,t]} \langle \mu_s^{m,n}, 1\rangle \langle \mu_s^{p,n}, 1\rangle
\end{aligned}$$

and so

$$\sup_n E\big(\sup_t \mid \langle M^{total,n}\rangle_t \mid \big) < \infty$$

Let $\delta > 0$ and let $((S_n, T_n) : n \in \mathbb{N})$ be a sequence of couples of stopping times such that $S_n \leq T_n \leq T$ and $T_n \leq S_n + \delta$. We prove in the same way

$$E\big(\mid V_{T_n}^n - V_{S_n}^n \mid \big) \leq C(h,T)\delta$$

and

$$E\big(\mid \langle M^{total,n}\rangle_{T_n} - \langle M^{total,n}\rangle_{S_n} \mid \big) \leq C(h,T)\delta$$

We proceed now to show that the compact containment condition holds. Recall that the sets $\mathcal{M}_N(K)$ of measures with mass bounded by N and support included in a compact K are compact. Taking $K = \overline{\Gamma} \times \mathbb{S}^2 \times [0,R]$, then μ^n is not in such compact either if

$$\{\exists t, \langle \mu_t^n, 1\rangle \geq N\}$$

or

$$\{\exists t, \langle \mu_t^{p,n}, r\rangle \geq R\}$$

The conservation of mass property shows that this last possibility does not occur for R sufficiently large (given by the initial mass), while for the first possibility,

$$P\{\exists t, \langle \mu_t^n, 1\rangle \geq N\} \leq \frac{1}{N} E\big(\sup_t \mid \langle \mu_t^n, 1\rangle \mid \big)$$

which is arbitrary small for large N.

Step 3: Identification of the limit Let us consider an adherence value μ and the subsequence (denoted again by) μ^n, such that μ^n converge in law towards μ in $\mathcal{D}([0,T], w-\mathcal{M}_F(\Gamma)\times\mathcal{M}_F(\mathbb{R}_+^*\times\mathbb{S}^2\times\Gamma))$. Let $h\in\mathcal{C}_b^2(\Gamma)\times\mathcal{C}_b^{1,2,2}(\mathbb{R}_+\times\mathbb{S}^2\times\Gamma)$. For $k\in\mathbb{N}^*$, let $0\le t_1<\cdots<t_k<s<t\le T$ and $\varphi_1,\cdots,\varphi_k\in\mathcal{C}_b(\mathcal{M}_F(\Gamma)\times\mathcal{M}_F(\mathbb{R}_+^*\times\mathbb{S}^2\times\Gamma),\mathbb{R})$. For $z\in\mathcal{D}([0,T],\mathcal{M}_F(\Gamma)\times\mathcal{M}_F(\mathbb{R}_+^*\times\mathbb{S}^2\times\Gamma))$, we defined

$$\Psi(z)=\varphi_1(z_{t_1})\cdots\varphi_k(z_{t_k})\Big[\langle z_t,h\rangle-\langle z_s,h\rangle-\int_s^t\mathcal{L}^\infty(\langle z_u,h\rangle)\Big]$$

where $\mathcal{L}^\infty$ is the generator defined in (5.43). Then $\mid E(\Psi(\mu))\mid\le A+B+C$, where

$$\begin{aligned}
A=&\mid E(\Psi(\mu))-E(\Psi(\mu_n))\mid\\
B=&\mid E(\Psi(\mu_n))-E(\varphi_1(\mu^n_{t_1})\cdots\varphi_k(\mu^n_{t_k})\Big[M_t^{total,n}-M_s^{total,n}\Big])\mid\\
C=&\mid E(\varphi_1(\mu^n_{t_1})\cdots\varphi_k(\mu^n_{t_k})\Big[M_t^{total,n}-M_s^{total,n}\Big])\mid
\end{aligned}$$

Since $M^{total,n}$ is a martingale, $C=0$. By convergence in distribution, A converges to 0 when $n\to\infty$. And

$$B\le C(\varphi)\mid\int_s^t\mathcal{L}^n(\langle\mu_\sigma,h\rangle)-\mathcal{L}^\infty(\langle\mu_\sigma,h\rangle)d\sigma\mid$$

which, from Taylor-Young formula, and moment estimates, goes to 0 as $n\to\infty$.

This proves that $E(\Psi(\mu))=0$ and hence $\langle\mu_t,h\rangle-\langle\mu_0,h\rangle-\int_0^t\mathcal{L}^\infty(\langle\mu_\sigma,h\rangle)$ is a martingale.

Step 4: Conclusion In the step 3, we have identified the adherence values of the sequence of processes μ^n as the solutions μ of the martingale problem associated with the limit generator $\mathcal{L}^\infty$. We refer to similar argument as in [13, Prop 2.2] to show that two processes of $\mathcal{D}([0,\infty),\mathcal{M}_F(\Gamma)\times\mathcal{M}_F(\mathbb{R}_+^*\times\mathbb{S}^2\times\Gamma))$ satisfying the martingale problem associated with $\mathcal{L}^\infty$ have the same distribution.

□

Appendix: Derivation of a Fokker-Planck equation on the sphere

The Fokker-Planck equation assiociate to a stochastic process on the sphere has been studied. In this case, the brownian on the sphere is defined as a projection on the tangent space to the sphere of a standard 3-dimensional Wiener process interpreted in Stratonovich. The Stratonovich calculus is necessary to conserve the process on the sphere du to the classical chain rules. Here we study a variant of this problem which is the Stratonovitch stochastic differential equation (SDE) on the stochastic process $(n_t)_{t\ge0}$ such that $n=(n_1,n_2,n_3)^T\in\mathbb{S}^2\subset\mathbb{R}^3$,

$$dn_t = -n_t \wedge (n_t \wedge H(n_t, t)dt + \sigma \circ dW_t)\,.$$

with W_t a standard 3-dimensional Wiener process. This could be re-write as

$$dn_t = P_{n_t^\perp} H(n_t, t)dt + \sigma \mathcal{R}_{n_t} \circ dW_t,$$

with $P_{n^\perp}$ the projection on the tangent space to n defined by $P_{n^\perp} X = n \wedge X \wedge n = X - (X \cdot n)n$, for any $X \in \mathbb{R}^3$. Moreover, $\mathcal{R}_n$ is the matrix associate to the right hand vectorial product by n, *i.e.*

$$\mathcal{R}_n = \begin{pmatrix} 0 & n_3 & -n_2 \\ -n_3 & 0 & n_1 \\ n_2 & -n_1 & 0 \end{pmatrix},$$

thus, $\mathcal{R}_n X = -n \wedge X = X \wedge n$, for any $X \in \mathbb{R}^3$. The coefficient of $\mathcal{R}_n$ can be seen in term of Levi-Civitas coefficient ϵ_{ijk},

$$g_{i,j} = (\mathcal{R}_n)_{i,j} = -\sum_{p=1}^{3} \epsilon_{ipj} n_p.$$

As described in [187], the link between the SDE and the Fokker-Planck equation, is given by the drift and diffusion coefficient, respectively $D_i^{(1)}$ and $D_{i,j}^{(2)}$. In Stratonovich, the drift is given by

$$\begin{aligned} D_i^{(1)} &= H_i - (H_i \cdot n)n + \frac{1}{2}\sigma^2 \sum_{k,j=1}^{3} g_{k,j} \frac{\partial}{\partial n_k} g_{i,j} \\ &= H_i - (H_i \cdot n)n - \sigma^2 n_i, \end{aligned}$$

since

$$\sum_{k,j=1}^{3} g_{k,j} \frac{\partial}{\partial n_k} g_{i,j} = \sum_{k,j=1}^{3} \left(\sum_{p=1}^{3} \epsilon_{kpj} n_p \right) \epsilon_{ikj} = \\ = -\sum_{p=1}^{3} \left(\sum_{k,j=1}^{3} \epsilon_{kjp} \epsilon_{kji} \right) n_p = \sum_{p=1}^{3} 2\delta_{i,p} n_p.$$

The diffusion is given by

$$D_{i,j}^{(2)} = \frac{1}{2}\sigma^2 \sum_{k=1}^{3} g_{i,k} g_{j,k} = \frac{1}{2}\sigma^2 \left(|n|^2 \delta_{i,j} - n_i n_j \right),$$

since

$$\sum_{p,l=1}^{3} \left(\sum_{k=1}^{3} \epsilon_{ipk} \epsilon_{jlk} \right) n_p n_l = \sum_{p,l=1}^{3} \left(\delta_{i,j} \delta_{p,l} - \delta_{i,l} \delta_{p,j} \right) n_p n_l.$$

The Fokker-Planck operator is given by,

$$L^+ f = -\sum_{i=1}^{3} \frac{\partial}{\partial n_i} D_i^{(1)} f + \sum_{i,j=1}^{3} \frac{\partial^2}{\partial n_i \partial n_j} D_{i,j}^{(2)} f.$$

while its adjoint also called the backward Kolmogorov operator is

$$L^- f = \sum_{i=1}^{3} D_i^{(1)} \frac{\partial}{\partial n_i} f + \sum_{i,j=1}^{3} D_{i,j}^{(2)} \frac{\partial^2}{\partial n_i \partial n_j} f.$$

The Fokker-Planck equation on $\rho := \rho(n,t)$ the probability distribution may be written as follows,

$$\frac{\partial}{\partial t}\rho = L^+ \rho. \tag{5.44}$$

Thus, writing the Fokker-Planck equation (5.44) as a continuity equation leads to

$$\frac{\partial}{\partial t}\rho = -\sum_{i=1}^{3} \frac{\partial}{\partial n_i} \left[\left(D_i^{(1)} - \sum_{j=1}^{3} \frac{\partial}{\partial n_j} D_{i,j}^{(2)} - \sum_{j=1}^{3} D_{i,j}^{(2)} \frac{\partial}{\partial n_j} \right) \rho \right]$$

Remarking that $D_i^{(1)} - \sum_{j=1}^{3} \frac{\partial}{\partial n_j} D_{i,j}^{(2)} = H_i - (H_i \cdot n)n$, thus equation (5.44) is equivalent to

$$\frac{\partial}{\partial t}\rho = -\nabla \cdot \left(P_{n^\perp} H(n,t)\rho - \frac{1}{2}\sigma^2 \left(|n|^2 I_3 - n \otimes n \right) \nabla \rho \right),$$

Let ∇_n and $\nabla_n \cdot$ be, respectively, the gradient and divergence on the sphere in spherical coordinates, *i.e.* for any F vector valued function

$$\nabla_n \cdot F = \frac{1}{\sin(\theta)} \frac{\partial}{\partial \theta} \sin(\theta) F_\theta + \frac{1}{\sin(\theta)} \frac{\partial}{\partial \varphi} F_\varphi + 2F_r,$$

and f scalar valued function

$$\nabla_n f = e_\theta \frac{\partial}{\partial \theta} f + \frac{1}{\sin(\theta)} e_\varphi \frac{\partial}{\partial \varphi} f.$$

Noting that $\left(|n|^2 I_3 - n \otimes n \right) \nabla = \nabla_n$, the equation reads now

$$\frac{\partial}{\partial t}\rho = -\nabla_n \cdot \left(P_{n^\perp} H(n,t)\rho - \frac{1}{2}\sigma^2 \nabla_n \rho \right).$$

Chapter 6

A numerical scheme for rod-like polymers with fragmentation and monomers lengthening

Dans ce chapitre on propose un schéma numérique permettant de simuler les équations de Fokker-Planck-smoluchowski pour des polymères rigides avec polymérisation-fragmentation introduitent au Chapitre 4. Nous considérons le cas d'un écoulement de cisaillement linéaire. Le schéma consite à développer la solution en la variable d'orientation, selon les harmoniques sphériques. On obtient un système de polymérisation-fragmentation sur chaque coefficients spectraux. Celui-ci est approché par une méthode des caractéristiques en la variable de taille. On donne quelques résultats de simulations et d'erreur numériques.

6.1 Introduction

This present chapter deals with the simulation of dilute polymeric liquids and more particularly with the model introduced and analysed in the chapter 4. This latter describes the dynamics of the configurational distribution of rod-like polymers with monomer addition and fragmentation submitted to a flow. This problem is relevant for biological polymers, especially when polymers consist of proteins, like, for instance, prions protein forming rigid rod polymers during *in vivo* experiments. Chapter 4 provide a complete description of the model and its application to prions. Succinctly, we assume a fluid surrounding monomers and polymers. Each polymer has a length, related to the mass of monomers that forms it, that increases by addition of monomers one after another at its both ends. A polymer can split into two new polymers and the stress induced by the flow modifies the sensitivity to a polymer to break. Moreover, polymers move according to their angle

and position due to the flow. The key ingredient to study polymeric liquids is the stress tensor induced by polymers onto the fluid. The cornerstone, to compute this stress, is the probability of the configurational distribution equation on polymers which is of a Fokker-Planck-Smoluchowsky equation. This latter has to be coupled with the monomer density, which drives the polymer lengthening. Here, we propose a numerical scheme to approach the configurational density in the case of a steady shear flow. Other type of flows have been studied in similar problems, for instance a planar flow in [42], and could be developed in a similar way as presented in this chapter.

The second section of this chapter is dedicated to the introduction of the equations and to the reduction of the system from three dimensions to one in space. In the third section, a numerical scheme is developed, combining a decomposition in spherical harmonics and a semi-lagrangian method. Finally, the fourth section is devoted to numerical experiments.

6.2 Equation being at stake

6.2.1 The system studied

Let $\Omega \subset \mathbb{R}^3$ be a bounded open set standing for the flow-domain and $u(\cdot, t) \in \mathbb{R}^3$ a given incompressible velocity field on Ω at time $t \geq 0$. The configurational distribution of polymers is given by the function $\psi(r, \eta, y, t)$ where $r \in \mathbb{R}_+$ stands for the length of polymers, $\eta \in \mathbb{S}^2$ its orientation and $y \in \Omega$ the position in the flow-domain. On the other hand, the problem takes into account the monomer density given by $\phi(y, t)$ at $y \in \Omega$. Polymers lengthen and split at non-negative rates, respectively denoted by τ and β. The polymerisation rate τ depends on the local concentration ϕ of monomers, on the size r, the orientation η and eventually on the flow u. The fragmentation rate β depends on the size r, the orientation η and the gradient of the flow ∇u induced on the polymer. Moreover, when it splits at a size r, the two new polymers are of size r' and $r - r'$ with a probability given by a kernel κ.
Thus, from chapter 4 equation (4.2) on polymer reads now for ψ

$$\frac{\partial}{\partial t}\psi + (u \cdot \nabla_y)\,\psi + \mathcal{R}[\nabla u](\psi) + \mathcal{L}[\nabla u, u, \phi](\psi) = 0, \tag{6.1}$$

on $\mathbb{R}_+ \times \mathbb{S}^2 \times \Omega$ and $t > 0$. The rotational motion operator, $\mathcal{R}$, is defined by

$$\mathcal{R}[\nabla u](\psi) = -\nabla_\eta \cdot \Big(D\nabla_\eta \psi - \mathrm{P}_{\eta^\perp}(\nabla u\ \eta)\psi \Big),$$

where $D > 0$ stands for the rotational diffusion constant, $\nabla_\eta \cdot$ and ∇_η are respectively the divergence and the gradient on the sphere. The projection to the tangent space on the sphere at η satisfies $\mathrm{P}_{\eta^\perp}(z) = z - (z \cdot \eta)\eta$, for any $z \in \mathbb{R}^3$. Then, the lengthening-fragmentation process operator, $\mathcal{L}$, follows

$$\mathcal{L}[\nabla u, u, \phi](\psi) = \frac{\partial}{\partial r}(\tau(\phi, r, \eta, u)\psi) + \beta(r, \eta, \nabla u)\psi + \\ - 2\int_r^\infty \beta(r', \eta, \nabla u)\kappa(r, r')\psi(t, y, r', \eta)\ dr',$$

where the size distribution kernel $\kappa : \mathbb{R}_+ \times \mathbb{R}_+ \mapsto \mathbb{R}_+$ must observe the following property,

$$\kappa(r', r) = 0, \text{ if } r' > r,$$
$$\kappa(r', r) = \kappa(r - r', r),$$

and

$$\int_0^r \kappa(r', r)\ dr' = 1,$$

to be consistent with the fact that a polymer splits into two new polymers and with the mass conservation after scission.
In this chapter, in order to assume a shear flow, the boundary condition on ψ have to take into account that the flow u does not satisfy $u \cdot n = 0$ on the entire boundary. Thus we have to consider the in-flow part of the boundary $\Gamma = \partial\Omega$, defined by

$$\Gamma_{in} = \{y \in \Gamma : u \cdot n < 0\},$$

where n is the outward normal vector to the boundary. We complete equation (6.1) with the boundary conditions

$$\psi = \psi_{in} \text{ over } \Gamma_{in} \quad \text{and} \quad \psi(r, \eta, y, t)\big|_{r=0} = 0,$$

at any time $t \geq 0$, with ψ_{in} a given data. Initial condition at time $t = 0$, where ψ^0 is a given function, such that

$$\psi(r, \eta, y, t)\big|_{t=0} = \psi^0(r, \eta, y).$$

Let us now introduce the density equation of free monomers in Ω, as in chapter 4 equation (4.4), it reads

$$\frac{\partial}{\partial t}\phi + (u \cdot \nabla_y)\,\phi - d\Delta_y\phi = -\int_{\mathbb{S}^2 \times \mathbb{R}_+} \tau(\phi, r, \eta, u)\psi\ dr d\eta, \tag{6.2}$$

on Ω and $t > 0$ with $d > 0$ the diffusion constant. The source term takes into account the polymerization of monomers into polymers. This equation is completed by the boundary conditions

$$\phi = \phi_{in} \text{ over } \Gamma_{in} \quad \text{and} \quad \nabla_y\phi \cdot \vec{n} = 0 \text{ over } \Gamma \backslash \Gamma_{in},$$

at any time $t \geq 0$, where ϕ_{in} is given. Finally, initial condition reads

$$\phi(y, t)\big|_{t=0} = \phi^0(y),$$

with ϕ^0 a given data.

6.2.2 Space reduction

Let us reduce the problem (6.1)-(6.2) to a 1-dimensional problem in space. For that purpose, we consider a stationary shear flow given by the velocity field $u(y) = (\gamma y_2, 0, 0)^T$ in $\Omega = (0, L_1) \times (0, L_2) \times (0, L_3)$ with $L_1, L_2, L_3 > 0$ and the shear rate $\gamma > 0$, see Figure 6.1. The jacobian matrix of u is a constant matrix denoted by M_γ such that

$$M_\gamma := \nabla u(y) = \begin{pmatrix} 0 & \gamma & 0 \\ 0 & 0 & 0 \\ 0 & 0 & 0 \end{pmatrix}.$$

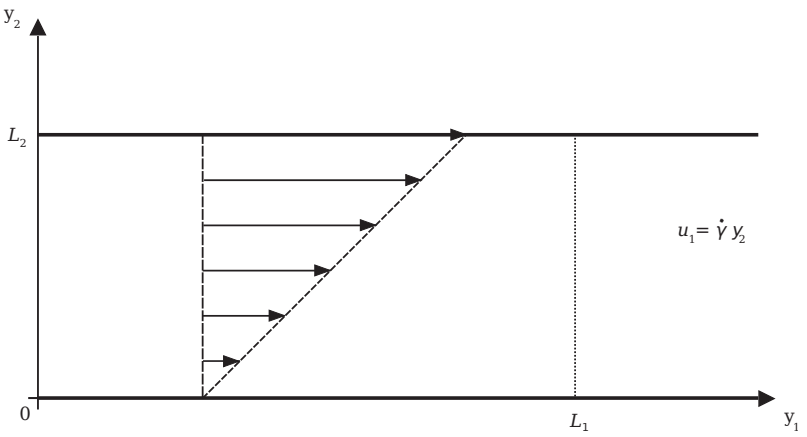

Figure 6.1: Shear flow. Intersection with the plane $y_3 = c \in (0, L_3)$.

This shear flow suggests to find solutions depending only on the second component of y. For that purpose, we consider an alternative problem on $\psi(r, \eta, x, t)$ the configurational density of polymer at $x \in (0, X)$ and $\phi(x, t)$ the density of monomer, with $X > 0$ the size of the one-dimensional physical space. With respect to this density, taking $v_\gamma(x) = (\gamma x, 0, 0)^T$, we are interested in the following equations on polymers,

$$\frac{\partial}{\partial t}\psi + \mathcal{R}[M_\gamma](\psi) + \mathcal{L}[M_\gamma, v_\gamma, \phi](\psi) = 0, \tag{6.3}$$

on $\mathbb{R}_+ \times \mathbb{S}^2 \times (0, X)$ and $t > 0$. Meanwhile, the monomer density satisfies

$$\frac{\partial}{\partial t}\phi - d\frac{\partial^2}{\partial x^2}\phi = -\int_{\mathbb{R}_+ \times \mathbb{S}^2} \tau(\phi, r, \eta, v_\gamma)\psi \; dr d\eta, \tag{6.4}$$

on $(0, X)$ and $t > 0$. These equations are complete with the boundary conditions

$$\frac{\partial}{\partial x}\phi(x, t)\big|_{x=0,X} = 0 \text{ and } \psi(r, \eta, x, t)\big|_{r=0} = 0, \tag{6.5}$$

at any time $t \geq 0$, with initial conditions

$$\psi(r, \eta, x, t)\big|_{t=0} = \psi^0(r, \eta, x) \text{ and } \phi(x, t)\big|_{t=0} = \phi^0(x), \tag{6.6}$$

where ψ^0 and ϕ^0 are given.

A solution of this reduced equations can be seen as a solution of the above mentioned problem. Indeed, one can construct a solution of the original problem by taking appropriate ψ_{in} and ϕ_{in} solutions of the 1-dimensional problem with respect to the same initial conditions.

6.3 Approximation of the solution

In this section we discretize the problem (6.3)-(6.4) with boundary conditions (6.5) and initial value (6.6) to approach numerically the solution. First a spectral method, used for instance in [42], is developed according to the spherical variable leading to a system of partial differential equations on spectral coefficients. The resulting equations consist of a polymerization-fragmentation system, with variable the length r and x considered as a parameter. The latter is solved thanks to a semi-lagrangian method.

6.3.1 Spectral method on the sphere

The spectral method consists in defining an orthonormal basis on square integrable functions on $\mathbb{S}^2$, and a convenient one is the spherical harmonics, eigenvectors of the laplacian on the sphere. To do that, let P_l^m be the associated Legendre polynomial of degree $l \geq 0$ and order $0 \leq m \leq l$. Real spherical harmonics, denoted by $S_{p,l,m}$, for $p = 0, 1$ and $p \leq m \leq l$, are defined as follows

$$S_{p,l,m}(\theta, \phi) = P_l^m\left(cos(\theta)\right) cos(m\varphi - p\pi/2),$$

for any $\theta \in (0, \pi)$ and $\phi \in (0, 2\pi)$. We use a second notation for the normalized real spherical harmonics, $Y_{p,l,m} = N_{l,m} S_{p,l,m}$, with

$$N_{l,m} = \sqrt{\frac{(2l+1)(l-m)!}{2\pi(1+\delta_{m0})(l+m)!}},$$

such that

$$\int_{\mathbb{S}^2} Y_{p,l,m} Y_{q,k,j} \; d\eta = \delta_{(p,l,m),(q,k,j)}. \tag{6.7}$$

Then, we approximate the configurational probability density ψ in terms of spherical harmonics by

$$\psi_L = \sum_{p=0}^{1} \sum_{l=0}^{L} \sum_{m=p}^{2l} \alpha_{p,l,m}(r, x, t) Y_{p,2l,m}(\eta)$$

with harmonics of even order in l at each point $x \in (0, X)$. Indeed, there is no way to identify a polymer of orientation η and $-\eta$, thus we are interested in even harmonics, that are satisfied if and only if l is even.
In order to simplify some notations we define two subsets of $\mathbb{N}^2$,

$$\mathcal{N}_p = \{(k, j) : k \geq 0 \text{ and } p \leq m \leq l\},$$

for relevant spectral coefficients and

$$\mathcal{M}_{l,m} = \{(k,j) : |k-l| \leq 2 \text{ and } |j-m| \leq 2\},$$

Spherical harmonics satisfy two properties of interest in our study. First, as mentioned, they are eigenvectors of the laplacian on the sphere,

$$-\Delta_\eta Y_{p,l,m} = l(l+1) Y_{p,l,m}.$$

when $(l,m) \in \mathcal{N}_p$ for $p = 0, 1$. Second, for a shear flow, we have

$$\nabla_\eta \cdot \left(\mathrm{P}_{\eta^\perp}(M_\gamma \eta) Y_{p,l,m} \right) = (-1)^{1-p} \gamma \sum_{(k,j) \in \mathcal{N}_{1-p} \cap \mathcal{M}_{l,m}} \frac{N_{l,m}}{N_{k,j}} \, a_{lk}^{mj} \, Y_{1-p,k,j}.$$

This is obtained using table 14.4-1 in [23], specified in table 6.1 for the definition of coefficients a_{lk}^{mj}. The goal is to write a system of equations on the $\alpha_{p,l,m}$, for that we assume that ψ_L is a solution of (6.3). For a sake of simplicity, we assume that β and τ are independent of η. Moreover, τ is taken independent of v_γ, thus we deal with $\beta(r) \equiv \beta(r, \eta, M_\gamma)$, forgetting M_γ to be more concise since it is a constant matrix, and $\tau(\phi, r) \equiv \tau(\phi, r, \eta, v_\gamma)$. After replacing the solution ψ_L in equation on polymers, multiplying by $Y_{p,2l,m}$ for any relevant $(2l, m) \in \mathcal{N}_p$ with $p = 0, 1$ and integrating over $\mathbb{S}^2$, this leads to a coupled system on $\alpha_{p,l,m}$ with $p = 0, 1$, $0 \leq l \leq L$ and $p \leq m \leq 2l$,

$$\frac{\partial}{\partial t}\alpha_{p,l,m} + \tau(\phi, r)\frac{\partial}{\partial r}\alpha_{p,l,m} + f_l(\phi, r)\alpha_{p,l,m} + \gamma G_{p,l,m}(\boldsymbol{\alpha}) = 2\int_r^\infty \beta(r')\kappa(r, r')\alpha_{p,l,m}(r', x, t) \, dt, \quad (6.8)$$

with $f_l(\phi, r) = 2l(2l+1)D + \beta(r) + \frac{\partial}{\partial r}\tau(\phi, r)$. Moreover, $\boldsymbol{\alpha}$ corresponds to the vector of components $\alpha_{p,l,m}$ and

$$G_{p,l,m}(\boldsymbol{\alpha}) = \sum_{p'=0}^{1} \sum_{l'=0}^{L} \sum_{m'=p'}^{2l'} G_{(p,l,m);(p',l',m')} \alpha_{p',l',m'}. \quad (6.9)$$

where coefficients $G_{(p,l,m);(p',l',m')}$ are derived in the Appendix. On the other hand, equation on the approach density of monomers ϕ_L, reads now

$$\frac{\partial}{\partial t}\phi_L - d\frac{\partial^2}{\partial x^2}\phi_L = -2\sqrt{\pi}\int_{\mathbb{R}_+} \tau(\phi, r)\alpha_{0,0,0}(r, x, t) \, dr, \quad (6.10)$$

since,

$$\int_{\mathbb{S}^2} Y_{p,l,m} d\eta = \begin{cases} 2\sqrt{\pi} & \text{if } (p,l,m) = (0,0,0), \\ 0 & \text{else.} \end{cases}$$

In the following section, we formulate a semi-lagrangian method to solve the system on $\alpha_{p,l,m}$.

$$
\begin{aligned}
a_{l,l-2}^{m,m-2} &= \frac{(l-2)(l+m)(l+m-1)(l+m-2)(l+m-3)(1-\delta_{m0})}{4(2l+1)(2l-1)} \\
a_{l,l}^{m,m-2} &= \frac{3(l+m)(l+m-1)(l-m+1)(l-m+2)(1-\delta_{m0})}{4(2l-1)(2l+3)} \\
a_{l,l+2}^{m,m-2} &= -\frac{(l+3)(l-m+1)(l-m+2)(l-m+3)(l-m+4)(1-\delta_{m0})}{4(2l+1)(2l+3)} \\
a_{l,l}^{m,m} &= -\frac{m}{2} \\
a_{l,l-2}^{m,m+2} &= -\frac{(l-2)(1+\delta_{m0})}{4(2l+1)(2l-1)} \\
a_{l,l}^{m,m+2} &= -\frac{3(1+\delta_{m0})}{4(2l-1)(2l+3)} \\
a_{l,l+2}^{m,m+2} &= \frac{(l+3)(1+\delta_{m0})}{4(2l+1)(2l+3)}
\end{aligned}
$$

All other $a_{l,l'}^{m,m'}$ are zero

Table 6.1: Tabulation of the $a_{l,l'}^{m,m'}$ from table 14-4.1 in [23].

6.3.2 Integration along the characteristics curves

The approximation with the spectral method on the sphere leads to a system of $(2L+1)(L+1)$ differential equations on each $\alpha_{p,l,m}$ with $p = 0, 1$ and $l = 0, \ldots, L$ and $m = p, \ldots, 2l$ where each equation on $\mathbb{R}_+ \times \mathbb{S}^2 \times (0, X)$ is given by (6.8). This system is of course coupled to the monomers equation (6.10). The method used is similar to the one developed in [5, 6] by O. Angulo *et al.* First, let $R_{max} > 0$ and approximate the system with a finite size on $r \in (0, R_{max})$. Equations on $\alpha_{p,l,m}$ read now,

$$
\begin{aligned}
\frac{\partial}{\partial t}\alpha_{p,l,m} + \tau(\phi, r)\frac{\partial}{\partial r}\alpha_{p,l,m} + f_l(\phi, r)\alpha_{p,l,m} + \gamma G_{p,l,m}(\boldsymbol{\alpha}) \\
= 2\int_r^{R_{max}} \beta(r')\kappa(r, r')\alpha_{p,l,m}(r', x, t)\, dt,
\end{aligned}
$$

over $(0, R_{max}) \times (0, X)$ and $t \geq 0$.
Let $R(t; t_0, r_0, x)$ be the characteristic curve starting in r_0 at time t_0 with $x \in (0, X)$ solution of the problem

$$
\begin{cases}
\dfrac{d}{dt}R(t; t_0, r_0, x) = \tau\left(\phi(x, t), R(t; t_0, r_0, x)\right), & \text{for } t > t_0, \\
R(t_0; t_0, r_0, x) = r_0.
\end{cases}
$$

We define the solution along the characteristic starting at (t_0, r_0) by $\tilde{\alpha}_{p,l,m}(x,t;t_0,r_0) = \alpha_{p,l,m}(R(t;t_0,r_0,x),x,t)$ satisfying

$$\frac{d}{dt}\tilde{\alpha}_{p,l,m} = 2\int_{R(t;t_0,r_0,x)}^{R_{max}} \beta(r')\kappa(R(t;t_0,r_0,x),r')\alpha_{p,l,m}(r',x,t)\,dr' - \\ - f_l(\phi(x,t),R(t;t_0,r_0,x))\tilde{\alpha}_{p,l,m} - \dot{\gamma}G_{p,l,m}(\tilde{\boldsymbol{\alpha}}), \quad (6.11)$$

such that $\tilde{\alpha}_{p,l,m}(x,t_0;t_0,r_0) = \alpha_{p,l,m}(r_0,x,t_0)$. Noticing again that x is a parameter, the system has to be solved for any $x \in (0,X)$.

6.3.3 Numerical scheme

Here we give the method to solve the reformulated problem (6.11) coupled with (6.10). First, let $L > 0$ be the fixed order of approximation over the spherical harmonics. Then, let us discretize the space by $X_i = i\Delta x$, $i = 0 \dots I$ with $\Delta x = X/I$ and the size by $R_j = j\Delta r$, $j = 0 \dots J$ with $\Delta r = R_{max}/J$. Now we assume that the numerical approximation of the solution is known at time t_n and denote by P_i^n the approximation of $\frac{1}{\Delta x}\int_{X_{i-1}}^{X_i}\phi(x,t_n)dx$ and $A_{p,l,m;i;j}^n$ of $\alpha_{p,l,m}(R_j, X_{i-1/2}, t_n)$ where $X_{i\pm1/2} = (i \pm 1/2)\Delta x$. It is now possible to compute $A_{p,l,m;j;i}^{n+1}$ and P_i^{n+1} for any $(l,m) \in \mathcal{N}_p$ for $p = 0, 1$, $i = 1, \dots, I$ and $j = 0, \dots, J$. First, we determine the next time $t_{n+1} = t_n + \Delta t_n$ with the time step

$$\Delta t_n = \frac{\Delta r}{\max_{\substack{0\le j\le J\\ 1\le i\le I}} \tau(P_i^n, R_j)}.$$

As the space variable x is taking as a parameter for the polymers equation, we fix the size by choosing $i \in (1, \dots, I)$ and forgetting the notation i to be concise, we now compute the $A_{p,l,m;j}^{n+1}$ (keeping in mind that it is at point $X_{i-1/2}$). We define S_j^n the size such that (S_j^n, t_n) and (R_j, t_{n+1}) be numerically on the same characteristic curve, given by

$$S_0^n = 0 \text{ and } S_j^n = R_j - \Delta t_n \tau(P_i^n, R_j)\ 1 \le j \le J.$$

It is necessary to interpolate the solution at time t_n onto the points S_j^n denoted by $B_{p,l,m;j}^n$ and it is given by a linear interpolation,

$$B_{p,l,m;j}^n = A_{p,l,m;j-1}^n + (S_j^n - R_{j-1})\frac{A_{p,l,m;j}^n - A_{p,l,m;j-1}^n}{\Delta r},\ 1 \le j \le J,$$

and let $B_{p,l,m;0}^n = A_{p,l,m;0}^n$. Let us define the trapezoidal rule by

$$E(A_{p,l,m;j}^n, A_{p,l,m;q}^n) = \frac{R_q - R_j}{2}(A_{p,l,m;j}^n + A_{p,l,m;q}^n).$$

and

$$E(B_{p,l,m;j}^n, A_{p,l,m;q}^n) = \frac{R_q - S_j^n}{2}(B_{p,l,m;j}^n + A_{p,l,m;q}^n).$$

Finally, we obtain the $A^{n+1}_{p,l,m;j}$ by discretization of (6.11)

$$\begin{aligned} A^{n+1}_{p,l,m;j} =& B^n_{p,l,m;j} - \Delta t_n f_l(P^n_i, R_j) A^{n+1}_{p,l,m;j} - \gamma \Delta t_n G_{p,l,m}(\mathbf{B}^n_j) \\ &+ 2\Delta t_n \beta(S^n_{j+1/2}) \kappa(S^n_j, S^n_{j+1/2}) E(B^n_{p,l,m;j}, A^n_{p,l,m;j}) \\ &+ 2\Delta t_n \sum_{q=j}^{J-1} \beta(R_{q+1/2}) \kappa(S^n_j, R_{q+1/2}) E(A^n_{p,l,m;q}, A^n_{p,l,m;q+1}), \end{aligned}$$

for $1 \leq j \leq J-1$ with $R_{j+1/2} = (j+1/2)\Delta r$, $S^n_{j+1/2} = (S^n_j + R_j)/2$, and $\mathbf{B}^n_j$ is vector of all the $B^n_{p,l,m;j}$. Furthermore,

$$A^{n+1}_{p,l,m;J} = B^n_{p,l,m;J} - \Delta t_n f_l(P^n_i, R_J) A^{n+1}_{p,l,m;J} - \gamma \Delta t_n G_{p,l,m}(\mathbf{B}^n_J)$$

and $A^{n+1}_{p,l,m;0} = 0$. We do that for any space point $X_{i-1/2}$ with $i = 1, \ldots, I$. We have to end with P^{n+1}_i, solving

$$(I - \Delta t_n M)\, P^{n+1} = K^n,$$

where M is the Neumann diffusion matrix and K^n is given by approaching the source terms in (6.10), given by

$$K^n_i = P^n_i - 2\sqrt{\pi}\Delta t_n \sum_{j=0}^{J-1} \tau(P^n_i, R_{j+1/2}) E(A^{n+1}_{0,0,0;i;j}, A^{n+1}_{0,0,0;i;j+1}).$$

This completes the method to solve the approximate problem.

6.4 Numerical experiments

In this section, we propose a numerical convergence analysis and some simulations. In order to analyse the convergence of the scheme let us define some technical tools and notations. First for the monomer density we denote by $\phi_{\Delta x}$ the approximation of the solution with a space discretization $X_i = i\Delta x$, $i = 0, \ldots, I$. The ℓ^2-norm is given by

$$||\phi_{\Delta x}(\cdot, T)||_{\ell^2(0,I)} = \sum_{i=1}^{I} P^N_i \Delta x, \tag{6.12}$$

where N is the last time step such that $t_N = T$. We now define the relative error by

$$E_\phi(\Delta x) = \frac{||\phi_{\Delta x}(\cdot, T) - \phi_{2\Delta x}(\cdot, T)||_{\ell^2}}{||\phi_{2\Delta x}(\cdot, T)||_{\ell^2}}.$$

and the order,

$$O_\phi(\Delta x) = \frac{\log\left(E_\phi(2\Delta x)/E_\phi(\Delta x)\right)}{\log 2}.$$

This is the definition used to compute the order of convergence in space on the solution ϕ.

Second, we compute the convergence in size according to the solution ψ, the configurational probability density of polymers. Let $\psi_{\Delta r}$ be the approximation of ψ with a size discretization $R_j = j\Delta r$, $j = 0, \cdots, J$. A generalized Parseval theorem gives

$$||f||^2_{L^2(\mathbb{S}^2)} = \sum_{p=0}^{1} \sum_{l=0}^{\infty} \sum_{m=p}^{l} |f_{p,l,m}|^2,$$

when

$$f = \sum_{p=0}^{1} \sum_{l=0}^{\infty} \sum_{m=p}^{l} f_{p,l,m} Y_{p,l,m}.$$

This follows from orthogonality of the spherical harmonics. Now, we are able to use the following norm

$$||\psi_{\Delta r}(\cdot, T)||_{\ell^\infty(\ell_2)} = \max_{j=0,\ldots,J} \left[\left(\sum_{i=1}^{I} \sum_{p=0}^{1} \sum_{l=0}^{L} \sum_{m=p}^{2l} |A^N_{p,l,m;i;j}|^2 \Delta x \right)^{1/2} \right] \tag{6.13}$$

where N is the last time step such that $t_N = T$. The relative error is given by

$$E_\psi(\Delta r) = \frac{||\psi_{\Delta r}(\cdot, T) - \psi_{2\Delta r}(\cdot, T)||_{\ell^\infty(\ell^2)}}{||\psi_{2\Delta r}(\cdot, T)||_{\ell^\infty(\ell^2)}}.$$

This is the relative error used to compute the order of convergence O_ψ defined as in (6.4).

For numerical simulations, we have chosen particular coefficients, as in [90] when applied to prions proliferation. The fragmentation rate is assumed to be linear in r, thus $\beta(r) = \beta_0 r$ with $\beta_0 > 0$. The polymerization rate is chosen to be a constant mass action, *i.e.* $\tau(\phi, r) = \tau_0 \phi$, with $\tau_0 > 0$. The parameters use in our simulations are given in table 6.2 and the initial conditions have been taken as below

$$\psi^0(r, \eta, x) = 4.0 \; e^{-\frac{(x-0.4)^2 + (r-0.4)^2}{0.01}},$$

that is uniformly distributed in η and

$$\phi^0(x) = 0.5 + 0.5 \; e^{-\frac{(x-0.5)^2}{0.5}}.$$

Parameter	Value	Parameter	Value
τ_0	0.01	β_0	0.05
γ	0.1	D	0.01
d	0.001	X	1
R_{max}	1	T	10

Table 6.2: Parameters use for simulations

The results on numerical convergence, with the method presented here, are shown in table 6.3 and 6.4. The order of convergence according to the space on ϕ is 2 (see table 6.3) meanwhile the one in size is 1 (see table 6.4). These results are obtained numerically using the above definition of relative error and order of convergence. This suggests that the method developed here provides good results to solve numerically the non-linear problem coupling the configurational density of polymers and the density of monomers.

Δx	Norm ℓ^2	Relative error E_ϕ	Order O_ϕ
1/10	$939.61 \cdot 10^{-3}$	—	—
1/20	$939.83 \cdot 10^{-3}$	$2.64 \cdot 10^{-3}$	—
1/40	$939.26 \cdot 10^{-3}$	$6.60 \cdot 10^{-4}$	1.999
1/80	$939.12 \cdot 10^{-3}$	$1.63 \cdot 10^{-4}$	2.021
1/160	$939.08 \cdot 10^{-3}$	$4.05 \cdot 10^{-5}$	2.005
1/320	$939.07 \cdot 10^{-3}$	$1.01 \cdot 10^{-5}$	2.001
1/640	$939.07 \cdot 10^{-3}$	$2.53 \cdot 10^{-6}$	2.001

Table 6.3: Convergence analysis according to x on ϕ. We use a degree of spherical harmonics $L = 7$ and a discretization in size given by $J = 100$. The error and order are given by the norm (6.12).

Δr	Norm $\ell^\infty(\ell^2)$	Relative error E_ψ	Order 0_ψ
1/20	1.3910	—	—
1/40	1.4055	$8.80 \cdot 10^{-2}$	—
1/80	1.4215	$4.57 \cdot 10^{-2}$	0.95
1/160	1.4261	$2.06 \cdot 10^{-2}$	1.15
1/320	1.4278	$9.54 \cdot 10^{-3}$	1.11
1/640	1.4284	$4.78 \cdot 10^{-3}$	1.00
1/1280	1.4286	$2.35 \cdot 10^{-3}$	1.02
1/2560	1.4287	$1.17 \cdot 10^{-3}$	1.01

Table 6.4: Convergence analysis according to r on ψ. We use a degree of spherical harmonics $L = 4$ and a discretization in space given by $I = 20$. The error and order are given by the norm (6.13).

We finish by showing simulations resulting from the solver. Figure 6.2 represents the density of monomers and the mass of polymers according to x defined by the map,

$$x \mapsto \int_{\mathbb{R}_+ \times \mathbb{S}^2} r\psi_L \, dr d\eta,$$

at both, initial conditions and final time ($T = 0$).
Figure 6.3 represents the size distribution of polymers at time T, given by the map

$$r \mapsto \int_{\Omega \times \mathbb{S}^2} \psi_L \, d\eta dx. \tag{6.14}$$

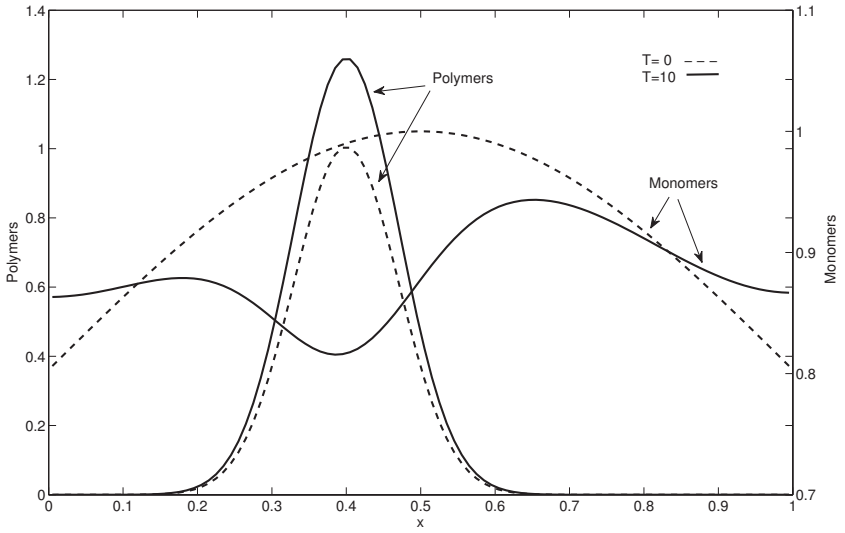

Figure 6.2: Mass of polymers and density of monomers according to th space variable x.

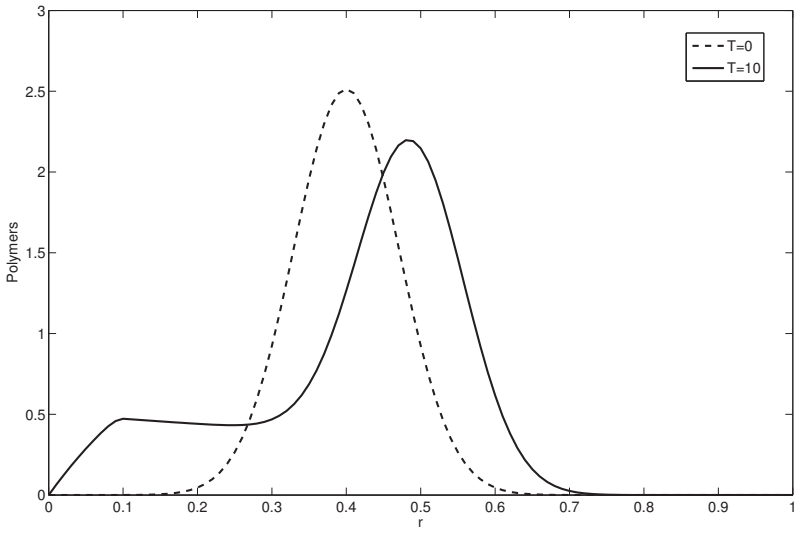

Figure 6.3: Size distribution of polymer, integrate over the sphere and the space.

Meanwhile, figure 6.4 is the configurational probability density of polymers at a point (x_0, r_0) and time T,

$$\eta \mapsto \psi_L(r_0, \eta, x_0, T)$$

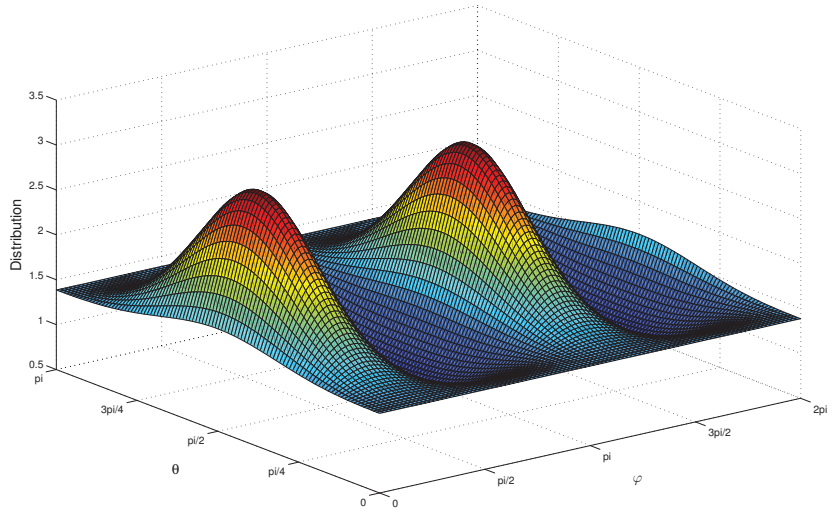

Figure 6.4: Probability configuration of polymers at $x = 0.4$ and $r = 0.4$ for $\theta \in (0, \pi)$ and $\varphi \in (0, 2\pi)$.

These figures give an idea of how the solutions behave. Indeed, the fragmentation leads to smaller polymers when some of them grow since the right hand side of the size distribution move to the right on figure 6.3 meanwhile the density of monomers decrease, see figure 6.2. Figure 6.4 shows that the shear flow tends to orientate the polymers in a dominant direction by virtue of the rotational motion. These data obtained with our method have to be confronted to experimental data. Indeed, the solver proposed here provide an algorithm that is ready to compared macroscopic data obtained experimentally, like size distribution and space distribution, to the model.

6.5 Discussion

In this chapter, we propose a new numerical method to solve efficiently the non-linear problem introduced in chapter 4 on fragmentation of rod-like polymers with addition of monomers. The details of the method were given, using spherical harmonics decomposition and a semi-lagrangian integration. We proved that the resulting solver have a numerical convergence and we shown some simulations on the behaviour of the solutions. The results obtained here indicate that this method should be taken into account as a numerical approach of this new problem. This is a first step ahead to understand the configurational probability density of such polymers and then to analyse the stress tensor induced on the flow. Future work will be dedicated to extend the solver to more general coefficients.

Appendix: Computation of the rotational motion

Here we derive the term involving in the system of partial differential equations for the spherical rotation. Multiplying equation (6.3.1) by $Y_{p,2l,m}$ and integrating over $\mathbb{S}^2$, leads to

$$\begin{aligned}
&\int_{\mathbb{S}^2} \nabla_\eta \cdot \Big(\mathrm{P}_{\eta^\perp}(M_\gamma \eta)\psi_L\Big) Y_{p,2l,m}\, d\eta \\
&= \gamma \sum_{p'=0}^{1} \sum_{l'=0}^{L} \sum_{m'=p'}^{2l'} \alpha_{p',l',m'} \int_{\mathbb{S}^2} \nabla_\eta \cdot \Big(\mathrm{P}_{\eta^\perp}(M_\gamma \eta) Y_{p',2l',m'}\Big) Y_{p,2l,m}\, d\eta \\
&= \gamma \sum_{p'=0}^{1} \sum_{l'=0}^{L} \sum_{m'=p'}^{2l'} \left((-1)^{1-p'} \sum_{(k,j)\in \mathcal{N}_{1-p'} \cap \mathcal{M}_{2l',m'}} \frac{N_{2l',m'}}{N_{k,j}} a_{2l'k}^{m'j} \delta_{(1-p',k,j);(p,2l,m)} \right) \alpha_{p',l',m'}
\end{aligned}$$

Now, let us define

$$G_{(p,l,m);(p',l',m')} = (-1)^p \delta_{1-p',p} \frac{N_{2l',m'}}{N_{2l,m}} a_{2l'2l}^{m'm}, \tag{6.15}$$

thus,

$$\int_{\mathbb{S}^2} \nabla_\eta \cdot \Big(\mathrm{P}_{\eta^\perp}(M_\gamma \eta)\psi_L\Big) Y_{p,2l,m}\, d\eta = \gamma \sum_{p'=0}^{1} \sum_{l'=0}^{L} \sum_{m'=p'}^{2l'} G_{(p,l,m);(p',l',m')} \alpha_{p',l',m'}.$$

The term introduced in (6.15) is used in the spectral decomposition to define (6.9).

Part III

Modélisation de la maladie d'Alzheimer

Chapter 7

Alzheimer's disease, analysis of a mathematical model including the role of the prion protein.

Dans ce chapitre, nous étudions un modèle qui représente l'évolution de la maladie d'Alzheimer. Celui-ci inclut le rôle de la protéine prion et notamment son implication dans la perte de mémoire. Nous utilisons une équation de transport pour la densité de plaques amyloides, structurée en taille, et trois équations différentielles pour les concentrations d'oligomères Aβ,de protéines PrP^Cet le complexe Aβ-×-PrP^C. De récentes découvertes suggèrent que ce dernier serait l'agent toxique pour les neurones, responsable de la perte de mémoire. Nous démontrons l'existence et l'unicité des solutions de ce modèle, ainsi que des résultats sur la convergence vers un équilibre sous différentes hypothèses du coefficient de polymérisation des plaques. Ce travail est issu d'une collaboration avec M. Helal.

7.1 Introduction

Alzheimer's disease (AD) is the most widespread age-related dementia with an estimation of about 35.6 million people worldwide being affected in 2009, as reported by the World Alzheimer Report 2010 [224]. By the 2050's, it is predicted three or four times more people living with AD. Dementia is a syndrome that affects memory, thinking, behaviour and ability to perform activities. Apart from social side-effects for patients, another notable consequence of AD is its cost, valued at $422 billions in 2009 [224]. Considering this situation, the stake being so much important to understand and cure Alzheimer disease that research is very prolific and recent findings in AD imply cellular prion protein (PrP^C) into the memory impairment [84, 126].

The pathogenesis of AD is related to a gradual build-up of β-amyloid (Aβ) plaques

in the brain [96]. β-amyloid are formed from the Aβ peptides obtained from the APP protein cleaved at a bad position. There exist different forms of β-amyloid , from soluble monomers to insoluble fibrillar aggregates [143, 144, 210, 215]. It has been revealed that the toxicity depends on the size of the structure and recent evidences suggest that oligomers (small aggregates) play a key role in memory impairment rather than Aβ plaques (larger aggregates) formed in the brain [195]. More specifically, β-amyloid oligomers cause spatial memory impairment *via* synaptic toxicity onto neurons. This phenomenon seems to be induced by a membrane receptor and there are some evidence that this rogue is the PrP^C, proteins responsible for Creutzfeldt-Jacob disease, [165]. Indeed, there is a high affinity between $PrP^C$and Aβ oligomers, moreover the prion proteins has also been identified as an APP regulator which confirms that both are highly related. It could be expected from this a new therapeutic target to recover memory in AD, or at least stopping the memory depletion.

Our objectives here is to introduce and study a brand new *in vivo* evolution model of AD mediates by PrP^C. To the best of our knowledge, indeed no model such as the one proposed here has ever been set-up. There exists some models specifically design for Alzheimer's disease and their treatment, such the one in [56, 57]. Nevertheless, the Prion protein has not been taken into account. The model study here could be a departing point to design novel treatments.

This chapter is organized as follows. We present the model in section 7.2, and provide a well-posedness result in the particular case where β-amyloid are formed at a constant rate. Then, the third section is dedicated to a theoretical study of our model in a more general context with power law rate of polymerization, *i.e.* the polymerization or build-up rate depends on the size. Finally, in the fourth section we propose a numerical scheme for the system and test it in particular cases.

7.2 The model

7.2.1 A model for β-amyloid and PrP^C

The model deals with four different species. First, the concentration of Aβ oligmers conisting of aggregates of few Aβ peptides, then the concentration of the PrP^Cprotein, third we have the concentration of the complex formed from one Aβ oligomer binding onto one PrP^C protein. These quantities are soluble and their concentration will be described in terms of ordinary differential equations. Finally we have the insoluble β-amyloid plaques described by a density according to their size. The size will be an abstract variable that could be the volume of the aggregate. To summarize we have

- $f(t,x) \geq 0$: the density of Aβ plaques of size x at time t,
- $u(t) \geq 0$: the concentration of soluble Aβ oligomers (unbounded oligomers) at time t,
- $p(t) \geq 0$: the concentration of soluble cellular prion proteins PrP^C at time t,

- $b(t) \geq 0$: the concentration of Aβ-×-PrP^Ccomplex (bounded oligomers) at time t.

Amyloids are formed from the clustering of Aβ oligomers. The rate of agglomeration depends on the concentration of soluble oligomers and the structure of the amyloid which is linked to its size. Actually, it consists to a mass action between plaques and oligomers at a non-negative rate given by $\rho(x)$ where x is the size of the plaque. Actually this size accounts for the mass of Aβ oligmers that form the polymer. We assume that the mass of one oligomer is given by a small parameter $\varepsilon > 0$. Thus the number of oligomers in a plaque of mass $x > 0$ is x/ε which justifies that we assume the size of the plaques to be continuous. Moreover, amyloids have a critical size

$$x_0 = \varepsilon n > 0,$$

where $n \in \mathbb{N}^*$ is the number of oligomers in the critical plaque. The amyloids are prone to be damaged at a non-negative rate μ, possibly depending on the size x of the plaques. All the parameters for Aβ oligomers, $PrP^C$and complex, as production, binding and degradation rate are non-negative and described in table 7.1.

Parameter/Variable	Definition	Unit
t	Time	days
x	Length of β-amyloid fibrils	–
x_0	Critical mass of β-amyloid plaques	–
n	Number of oligomers in a plaque of size x_0	–
ε	Mass of one oligomer	–
λ_u	Source of Aβ oligomers	days^{-1}
γ_u	Degradation rate of Aβ oligomers	days^{-1}
λ_p	Source of PrP^C	days^{-1}
γ_p	Degradation rate of PrP^C	days^{-1}
τ	Binding rate of Aβ oligomers onto PrP^C	days^{-1}
σ	Unbinding rate of Aβ-×-PrP^C	days^{-1}
δ	Degradation rate of Aβ-×-PrP^C	days^{-1}
$\rho(x)$	Conversion rate of oligomers into a fibril	$(\text{SAF/sq})^{-1}\cdot\text{days}^{-1}$
$\mu(x)$	Degradation rate of a fibril	days^{-1}

Table 7.1: Parameters description of the model

Then, writing evolution equations for these four quantities, we get for any $t > 0$

$$\begin{cases} \dfrac{\partial}{\partial t} f(x,t) + u(t) \dfrac{\partial}{\partial x}\big[\rho(x) f(x,t)\big] = -\mu(x) f(x,t), \quad \text{over } (x_0, +\infty) & (7.1) \\ \dot{u} = \lambda_u - \gamma_u u - \tau u p + \sigma b - nN(u) - \dfrac{1}{\varepsilon} u \displaystyle\int_{x_0}^{+\infty} \rho(x) f(x,t) dx, & (7.2) \\ \dot{p} = \lambda_p - \gamma_p p - \tau u p + \sigma b, & (7.3) \\ \dot{b} = \tau u p - (\sigma + \delta) b. & (7.4) \end{cases}$$

The term N accounts for the formation rate of a new β-amyloid plaque with size x_0 from the Aβ oligomers. In order to balance this term, we add the boundary condition

$$u(t)\rho(x_0) f(x_0, t) = N(u(t)), \quad \text{for any } t \geq 0. \tag{7.5}$$

The integral in the right-hand side of equation (7.2) is the total polymerization with parameters $1/\varepsilon$ since $\mathrm{d}x/\varepsilon$ counts the number of oligomers into a unit of length $\mathrm{d}x$. Finally, the problem is completed with non-negative initial data

$$f(x, t = 0) = f^0(x) \geq 0, \ \forall x \geq x_0, \tag{7.6}$$

and,

$$u(t = 0) = u_0 \geq 0, \ p(t = 0) = p_0 \geq 0 \text{ and } b(t = 0) = b_0 \geq 0. \tag{7.7}$$

where f_0, u_0, p_0 and b_0 are given data.

7.2.2 An associated ODE system

In this section we are interested in a constant polymerization and degradation rate, *i.e* independent of the structure of the plaque involved in the process, so we assume that

$$\rho(x) := \rho \text{ and } \mu(x) := \mu,$$

are positive constants. Moreover, without loss of generality we let $\varepsilon = 1$ even if it means to rescale the equations. Then we assume a pre-equilibrium hypothesis for the formation of β-amyloid plaques, as done in [178] for filament formation, thus we let

$$N(u) = \alpha u^n.$$

The formation rate is given by $\alpha > 0$ and the number of oligomers necessary to form a new plaque is an integer, $n \geq 1$. Doing these assumptions we are able to closed the system (7.1-7.4) with respect to (7.5) into a system of four differential equations. Indeed, integrating (7.1) over $(x_0, +\infty)$ we get formally an equation over the quantity of amyloids at time $t \geq 0$

$$A(t) = \int_{x_0}^{+\infty} f(x,t) dx.$$

This method has already been employed on prion model in first approximation in [90]. Now the problem reads

$$\begin{cases} \dot{A} = \alpha u^n - \mu A, \\ \dot{u} = \lambda_u - \gamma_u u - \tau u p + \sigma b - \alpha n u^n - \rho u A, \\ \dot{p} = \lambda_p - \gamma_p p - \tau u p + \sigma b, \\ \dot{b} = \tau u p - (\sigma + \delta) b. \end{cases} \tag{7.8}$$

The mass of β-amyloid plaques is given by $M(t) = \int_{x_0}^{+\infty} x f(x,t) dx$ which satisfies an equation (formal integration of (7.1)) that can be solved independently since

$$\dot{M} = n\alpha u^n + \rho u A - \mu M. \tag{7.9}$$

Notice that initial conditions for A and M are given by $A_0 = \int_{x_0}^{+\infty} f0(x) dx$ and $M_0 = \int_{x_0}^{+\infty} x f0(x) dx$, while the ones on u, p and b are unchanged.

The next section is devoted to the analysis of the system (7.8).

7.2.3 Well-posedness and stability of the ODE system

We first state, in the following proposition, existence and uniqueness of a global solution to the system (7.8) which derived from classic argument on differential equations.

Proposition 7.1 (Well-posedness)**.** *Assume that λ_u, λ_p, γ_u, γ_p, τ, σ, δ, ρ and μ positive, moreover, let $n \geq 1$ be an integer. For any $(A_0, u_0, p_0, b_0) \in \mathbb{R}^4_+$ there exists a unique non-negative bounded solution (A, u, p, b) to the system (7.8) defined for all time $t > 0$,* i.e *the solution A, u, p and b belong to $\mathcal{C}^1_b(\mathbb{R}_+)$ and remains in the stable subset*

$$S = \left\{ (A, u, p, b) \in \mathbb{R}^4 : 0 \leq nA + u + p + 2b \leq nA_0 + u_0 + p_0 + 2b_0 + \frac{\lambda}{m} \right\} \tag{7.10}$$

with $\lambda = \lambda_u + \lambda_p$ and $m = \min\{\mu, \gamma_u, \gamma_p, \delta\}$. Furthermore, let $M(t = 0) = M_0 \geq 0$, then there exist a unique non-negative solution M to (7.9), defined for all time $t > 0$.

Proof. Let $F : \mathbb{R}^4 \mapsto \mathbb{R}^4$, given by

$$F(A, u, p, b) = \begin{pmatrix} F_1 := \alpha u^n - \mu A \\ F_2 := \lambda_u - \gamma_u u - \tau u p + \sigma b - \alpha n u^n - \rho u A \\ F_3 := \lambda_p - \gamma_p p - \tau u p + \sigma b \\ F_4 := \tau u p - (\sigma + \delta) b \end{pmatrix}.$$

F is obviously $\mathcal{C}^1$ and locally Lipschitz on $\mathbb{R}^4$. Moreover, if $(A, u, p, b) \in \mathbb{R}^4_+$, $F_1 \geq 0$ when $A = 0$, $F_2 \geq 0$ when $u = 0$, $F_3 \geq 0$ when $p = 0$ and $F_4 \geq 0$ when $b = 0$, thus the solution remains in $\mathbb{R}^4_+$. Finally, remarking that

$$\frac{d}{dt}(nA + u + p + 2b) \leq \lambda - m(nA + u + p + 2b),$$

with $\lambda = \lambda_u + \lambda_p$ and $m = \min\{\mu, \gamma_u, \gamma_p, \delta\} > 0$, Gronwall's lemma ensures that

$$nA(t) + u(t) + p(t) + 2b(t) \leq nA_0 + u_0 + p_0 + 2b_0 + \frac{\lambda}{m}.$$

This provides the global existence of a unique non-negative bounded solution (A, u, p, b). We get straightforward the result on the mass M. □

We are interested in the steady state to get the asymptotic of the problem (7.8). It is to compute A_∞, u_∞, p_∞, b_∞ solving the problem

$$\begin{cases} \mu A_\infty - \alpha {u_\infty}^n = 0 & (7.11) \\ \lambda_u - \gamma_u u_\infty - \tau u_\infty p_\infty + \sigma b_\infty - \alpha n {u_\infty}^n - \rho u_\infty A_\infty = 0 & (7.12) \\ \lambda_p - \gamma_p p_\infty - \tau u_\infty p_\infty + \sigma b_\infty = 0 & (7.13) \\ \tau u_\infty p_\infty - (\delta + \sigma) b_\infty = 0 & (7.14) \end{cases}$$

From the structure of the second equation, we cannot give an explicit steady state to this problem. To get u_∞ we have to solve an algebraic equation which involves a polynomial of degree n. However we can prove that it exists, and u_∞ is given implicitly. The next proposition states it and establish a local stability.

Theorem 7.2 (Linear stability)**.** *Under hypothesis of proposition 7.1. There exists a unique positive steady state A_∞, u_∞, p_∞ and b_∞ to* (7.8) *with*

$$A_\infty = \frac{\alpha}{\mu} u_\infty^n, \quad p_\infty = \frac{\lambda_p}{\tau^* u_\infty + \gamma_p}, \quad b_\infty = \frac{1}{\sigma} \frac{\lambda_p(\tau - \tau^*)}{\tau^* u_\infty + \gamma_p} u_\infty,$$

where $\tau^* = \tau(1 - \sigma/(\delta + \sigma))$ and u_∞ is the unique positive root of Q, defined by

$$Q(x) = \gamma_p \lambda_u + ax - P(x), \ \forall x \geq 0$$

with $a = \tau^*(\lambda_u - \lambda_p) - \gamma_u \gamma_p$ and

$$P(x) = \tau^* \gamma_u x^2 + \alpha \gamma_p n x^n + (\alpha \tau^* n + \rho \gamma_p \frac{\alpha}{\mu}) x^{n+1} + \rho \tau^* \frac{\alpha}{\mu} x^{n+2}$$

Moreover, this equilibrium is locally linearly asymptotically stable.

Proof. First, equation (7.11) gives A_∞ with respect to u_∞. Then combining (7.14) and (7.14) we get p_∞ and b_∞ function of u_∞. Now replacing p_∞ and b_∞ in (7.12) we get u_∞ as the root of Q. We get straightforward that Q has a unique positive root. Indeed it is the intersection between a line and a monotone polynomial on the half plan. Now, let us linearise the system in A_∞, u_∞, p_∞ and b_∞. Let $X = (A, u, p, b)^T$ the linearised system reads

$$\frac{d}{dt} X = DX,$$

such that

$$D = \begin{pmatrix} -\mu & \alpha n {u_\infty}^{n-1} & 0 & 0 \\ -\rho u_\infty & \gamma_u - \tau p_\infty - \alpha n^2 {u_\infty}^{n-1} - \rho A_\infty & -\tau u_\infty & \sigma \\ 0 & -\tau p_\infty & -(\gamma_p + \tau u_\infty) & \sigma \\ 0 & \tau p_\infty & \tau u_\infty & -(\sigma + \delta) \end{pmatrix}.$$

The characteristic polynomial is of the form

$$P(\lambda) = \lambda^4 + a_1\lambda^3 + a_2\lambda^2 + a_3\lambda + a_4,$$

with the $a_i > 0$, $i = 1 \dots 4$ given in appendix. Moreover it satisfies

$$a_1 a_2 a_3 > a_3^2 + a_1^2 a_4.$$

Then, according to the Routh-Hurwitz Criteria (see [2, Th. 4.4, page 150]), all the roots of the characterisic polynomial P are negative or have negative real part, thus the equilibrium is locally asymptotically stable. □

To go further, we give a conditional global stability result when no nucleation is considered, *i.e.* $\alpha = 0$.

Proposition 7.3 (Global stability)**.** *Assume that $\alpha = 0$. Under the condition*

$$\left(1 + 2\frac{\delta + \gamma_u}{\sigma}\right) > \frac{\delta}{2\gamma_p} > \frac{\gamma_p}{\sigma},$$

the unique equilibrium given by

$$A_\infty = 0, \quad p_\infty = \frac{\lambda_p}{\tau^* u_\infty + \gamma_p}, \quad b_\infty = \frac{1}{\sigma}\frac{\lambda_p(\tau - \tau^*)}{\tau^* u_\infty + \gamma_p} u_\infty,$$

and u_∞ be the unique positive root of $Q(x) = \gamma_p\lambda_u + ax - \tau^*\lambda_u x^2$, with $a = \tau^*(\lambda_u - \lambda_p) - \gamma_u\gamma_p$, is globally asymptotically stable in the stable subset defined in (7.10)*.*

Proof. The proof is given by a Lyapounov function Φ stated in appendix. It is positive when the condition above is fulfilled and its derivative along the solution to the system (7.8) is negative definite. Thus, from the LaSalle's invariance principle we get that the equilibrium of (7.8) is globally asymptotically stable. □

7.3 The case of a power law polymerization rate

In the previous section, we investigated the case when the degradation rate and the polymerization rate of an amyloid are constants. The equations can be reduced to an ODE system that can be analysed using classical tools on ODE. This kind of coefficients are not always physically relevant. Because of that we study here the case when $\rho(x) \sim x^\theta$ and in the following we restrict our analysis to $\theta \in (0, 1)$. We will see that we are able to obtain a result of existence and uniqueness of solution for this more general case.

The last subsection will be devoted to a brief analysis of the long time behaviour of this solution. Indeed, this asymptotic will be obtained almost for free, thanks in particular to the stability analysis performed in subsection 7.2.3, as well as a stability estimate given by proposition 7.10 hereafter.

7.3.1 Hypothesis and main result

We are interested in non-negative solutions to the system (7.1-7.4) with the boundary condition (7.5), completed by initial data (7.6) and (7.7). Moreover, we require the solution searched to preserve the total mass of β-amyloid : this is biologically relevant. Hence the solution f will be sought in the natural space $L^1(x_0, +\infty; xdx)$, since xdx measures the mass at any time.

Let us present now exactly the mathematical assumptions we make, in order both to ensure that system (7.1-7.4) is biologically relevant and to allow its theoretical study.

$$\text{(H1)} \quad \left| \begin{array}{l} f_0 \in L^1(x_0, +\infty; xdx) \\ \text{and,} \\ f_0 \geq 0, \ a.e.\ x > x_0. \end{array} \right.$$

$$\text{(H2)} \quad \left| \begin{array}{l} \rho \geq 0\,, \ \text{ and } \ \rho \in W^{2,\infty}([x_0, \infty)) \\ \text{and,} \\ \mu \geq 0\,, \ \text{ and } \ \mu \in W^{1,\infty}([x_0, \infty)). \end{array} \right.$$

$$\text{(H3)} \quad \left| \begin{array}{l} N \geq 0\,, \ N \in W^{1,\infty}_{loc}(\mathbb{R}_+) \\ \text{and } \ N(0) = 0. \end{array} \right.$$

$$\text{(H4)} \quad \left| \ \lambda_u,\ \gamma_u,\ \lambda_p,\ \gamma_p,\ \tau,\ \sigma,\ \delta \ > \ 0. \right.$$

Some comments on the hypothesis:

- Note that (H2) implies there exists a constant $C > 0$ such that $\rho(x) \leq Cx$, with for example, $C = 2\|\rho'\|_{L^\infty} + \rho(x_0)/x_0$. Indeed for any $x \geq x_0$, it holds

$$\rho(x) \leq \|\rho'\|_{L^\infty}(x + x_0) + \rho(x_0) \leq \left(2\|\rho'\|_{L^\infty} + \frac{\rho(x_0)}{x_0}\right) x.$$

  We remark that this kind of regularity of the rate ρ contains the power laws $\rho(x) \sim x^\theta$ with $\theta \in (0; 1)$. It will also be crucial to perform estimates in the next subsection.

- Moreover hypothesis (H3) implies there exists a constant $K_M > 0$ such that $N(w) \leq K_M w$ for any $w \in (0, M)$. This will also be used in the computations of the next subsection.

- Finally, non negativity of the parameters of table 7.1, that is hypothesis (H4), is a natural assumption, regarding their biological meaning.

Before stating our existence result, we now introduce the definition of what will be called a solution to system (7.1-7.4).

Definition 7.4. Consider a function $f0$ satisfying (H1) and u_0, p_0, b_0 be three non-negative real data. Assume ρ, μ, N and all the parameters of table 7.1 verify assumptions (H2) to (H4), and let $T > 0$. Then a quadruplet (f, u, p, b) of non-negative functions is said to be a *solution* on the interval $(0, T)$ to the system (7.1-7.4) with the boundary condition (7.5) and the initial data (7.6) and (7.7), if it satisfies, for any $\varphi \in \mathcal{D}'([0,T] \times [x_0, +\infty))$ and $t \in (0, T)$

$$\int_{x_0}^{+\infty} f(x,t)\varphi(x,t)dx = \int_{x_0}^{+\infty} f0(x)\varphi(x,0)dx + \int_0^t N(u(s))\varphi(x_0,s)ds + \int_0^t \int_{x_0}^{+\infty} f(x,s)\left[\frac{\partial}{\partial t}\varphi(x,s) + u(s)\rho(x)\frac{\partial}{\partial x}\varphi(x,s) - \mu(x)\varphi(x,s)\right] dxds,$$

and,

$$u(t) = u_0 + \int_0^t \left[\lambda_u - \gamma_u u - \tau up + \sigma b - x_0 N(u) - u\int_{x_0}^{+\infty} \rho(x) f(x,s)dx\right], ds$$

$$p(t) = p_0 + \int_0^t \left[\lambda_p - \gamma_p p - \tau up + \sigma b\right] ds,$$

$$b(t) = b_0 + \int_0^t \left[\tau up - (\sigma + \delta)b\right] ds,$$

with the regularity:

$$f \in L^\infty\left(0, T; L^1\left(x_0, +\infty; xdx\right)\right) \text{ and } u, p, b \text{ belong to } C^0(0,T).$$

We are now able to state the well-posedness result.

Theorem 7.5 (Main result)**.** *Let $f0$ be a non-negative function satisfying (H1), u_0, p_0 and b_0 be non-negative real numbers, and assume hypothesis (H2) to (H4). Let $T > 0$, then there exists a unique non-negative solution (f, u, p, b) to (7.1-7.4) with* (7.5) *and initial conditions given by* (7.6) *and* (7.7)*, in the sense of definition 7.4, such that*

$$f \in C^0\left([0,T], L^1(x_0, +\infty; x^r dx)\right), \quad \forall r \in [0,1].$$

and,

$$u, p, b \in C_b^1(0,T).$$

The proof of the theorem 7.5 is decomposed into two part. First, we study under hypothesis (H1) to (H3) and in subsection 7.3.2, when $u \in \mathcal{C}_b^0(\mathbb{R}_+)$ is a given non-negative data, the initial boundary value problem

$$\begin{cases} \dfrac{\partial}{\partial t} f(x,t) + u(t)\dfrac{\partial}{\partial x}\left[\rho(x)f(x,t)\right] = -\mu(x)f(x,t) \text{ on } (x_0, +\infty) \times \mathbb{R}_+, & (7.15) \\ u(t)\rho(x_0)f(x_0,t) = N(u(t)), \quad \forall t \geq 0, & (7.16) \\ f(x,0) = f0(x), \quad \forall x \geq x_0. & (7.17) \end{cases}$$

Namely, we prove in the next subsection the following proposition:

Proposition 7.6. *Consider $u \in \mathcal{C}_b^0(\mathbb{R}_+)$ a given function, $f0$ satisfying (H1) and assume hypothesis (H2) to (H3). Let $T > 0$, then there exists a unique non-negative solution f to (7.15-7.17) in the sense of distributions, such that*

$$f \in C^0\left([0,T], L^1(x_0, +\infty; x^r dx)\right), \quad \forall r \in [0,1].$$

The proof is in the spirit of [50] for the Lifshitz-Slyozov equation. It consists in a mild formulation (definition with the characteristic) which is proved to be the unique solution in the sense of the distributions with the additional requirement to be continuous in time into $L^1(xdx)$ space.

The second step of the proof of theorem 7.5 is performed in subsection 7.3.3. Precisely, once we have the existence of a unique density f when u is a given data we are able to construct the operator

$$S : C^0([0,T])^3 \mapsto C^0([0,T])^3, (u,p,b) \mapsto (\tilde{u}, \tilde{p}, \tilde{b}) = S(u,p,b), \tag{7.18}$$

defined by

$$\begin{aligned}
\tilde{u} &= u_0 + \int_0^t \left[\lambda_u - \gamma_u u - \tau u p + \sigma b - x_0 N(u) - u \int_{x_0}^{+\infty} \rho(x) f(x,s) dx\right] ds, \\
\tilde{p} &= p_0 + \int_0^t \left[\lambda_p - \gamma_p p - \tau u p + \sigma b\right] ds, \\
\tilde{b} &= b_0 + \int_0^t \left[\tau u p - (\sigma + \delta) b\right] ds,
\end{aligned}$$

where f is the unique solution associated to u given by proposition 7.6. Thus, theorem 7.5 is finally proved in subsection 7.3.3 thanks to the Banach fixed point theorem applied to the operator S.

7.3.2 Existence of a solution to the autonomous problem

This section is devoted to the proof of proposition 7.6. Thus, in the following, we let $u \in \mathcal{C}_b^0(\mathbb{R}_+)$ a given function and we use the notations

$$a(x,t) = u(t)\rho(x) \text{ and } b(x,t) = -u(t)\rho'(x), \ \forall (x,t) \in [x_0, +\infty) \times \mathbb{R}_+.$$

From (H2) and remarking that $\rho(x) \leq Cx$, we get that for any $t > 0$

$$a(t,x) \leq Ax, \text{ for } x > x_0, \tag{7.19}$$

$$|a(t,x) - a(t,y)| \leq A|x-y|, \text{ for } x, y > x_0, \tag{7.20}$$

$$|b(t,x)| \leq B, \tag{7.21}$$

where $A = \max\left(C\|u\|_{L^\infty}, \|u\|_{L^\infty}\|\rho'\|_{L^\infty}\right)$ and $B = \|u\|_{L^\infty}\|\rho'\|_{L^\infty(x_0,+\infty)}$. In order to establish the mild formulation of the problem, we define the characteristic which reaches $x \geq x_0$ at time $t \geq 0$, that is the solution to

$$\begin{cases} \dfrac{d}{ds} X(s;x,t) = a(t, X(s;x,t)), \\ X(t;x,t) = x. \end{cases} \tag{7.22}$$

From property (7.20), their exist a unique characteristic which reach (x,t). It is important to note that it makes sense as long as $X(s;x,t) \geq x_0$. Thus, we define the starting time of the characteristic as follows

$$s_0(x,t) := \inf\{s \in [0,t] : X(s;x,t) \geq x_0\}.$$

The characteristic will be defined for any time $s \geq s_0$ and takes its origin from the initial or the boundary condition respectively if $s_0 = 0$ or $s_0 > 0$. We recall the classical properties for the characteristics,

$$\begin{cases} X(s;X(\sigma;x,t),\sigma) = X(s;x,t) \\ J(s;x,t) := \dfrac{\partial}{\partial x}X(s;x,t) = \exp\left(\displaystyle\int_s^t b(\sigma, X(\sigma;x,t))d\sigma\right) \\ \dfrac{\partial}{\partial t}X(s;x,t) = -a(t,x)J(s;x,t). \end{cases}$$

Also, remarking that $s_0(X(t;x_0,0),t) = 0$, then by monotonicity and continuity of X for any $t > 0$, we get

$$x \in (x_0, X(t;x_0,0)) \iff s_0(x,t) \in (0,t).$$

and for any $x \in (x_0, X(t;x_0,0))$ we have $X(s_0(x,t);x,t) = x_0$, it follows that

$$I(x,t) := -\frac{\partial}{\partial x}s_0(x,t) = J(s_0(x,t);x,t)/a(s_0(x,t),x_0), \quad \forall x \in (x_0, X(t;x_0,0)).$$

Regarding the derivative of $f(s, X(s;x,t))$ in s, and integrating over (s_0,t) we obtain the mild formulation of the problem. The mild solution is defined *a.e.* $(x,t) \in (x_0,+\infty)\times\mathbb{R}_+$ by

$$f(x,t) = \begin{cases} f0(X(0;x,t))J(0;x,t)\exp\left(-\int_0^t \mu(X(\sigma;x,t))d\sigma\right), & x \geq X(t;x_0,0) \\ N(u(s_0(x,t)))I(x,t)\exp\left(-\int_{s_0(x,t)}^t \mu(X(\sigma;x,t))d\sigma\right), & x \in (x_0, X(t;x_0,0)). \end{cases} \tag{7.23}$$

It infers from the formulation (7.23) that *a.e* $(x,t) \in [x_0,+\infty)\times\mathbb{R}_+$, f is non-negative since J and I are non-negative, and $f0$ satisfies (H1). We recall some useful properties that are derived in [50, Lemma 1].

Lemma 7.7. *Let $u \in \mathcal{C}_b^0(\mathbb{R}_+)$ be a given data and assume that (H2) holds true. Then for any $x \geq x_0$ and $t > 0$, as long as the characteristic curves $s \mapsto X(s;x,t)$ defined in* (7.22) *exists* i.e. *$s \geq s_0(x,t)$, we have*

$$\begin{aligned} &\text{for } s_1 \leq s_2,\ X(s_1;x,t) \leq X(s_2;x,t) \leq X(s_1;x,t)e^{A(s_2-s_1)} \\ &\text{if } x_n \to +\infty,\ \text{then for all } t \geq s \geq 0,\ X(s;x,t) \to +\infty \\ &\text{for } s \geq t,\ X(s;x,t) \leq xe^{A(s-t)} \end{aligned}$$

Proof. We refer to [50, Lemma 1], were the result follows from the fact that for any $x \geq x_0$, $t > 0$ and $s_0(x,t) \leq s_1 \leq s_2$, we have

$$\begin{aligned} x_0 \leq X(s_2;x,t) &= X(s_1;x,t) + \int_{s_1}^{s_2} a(s, X(s;x,t))ds \\ &\leq X(s_1;x,t) + A\int_{s_1}^{s_2} X(s;x,t)ds \end{aligned}$$

where A is given by (7.19). □

In the sequel we will repeatedly refer to the changes of variables,

$$y = X(0;x,t) \text{ over } x \in (X(t,x_0,0),+\infty), \text{ with Jacobian } J(0;x,t),$$

and

$$s = s_0(x,t) \text{ over } x \in (x_0, X(t;x_0,0)), \text{ with Jacobian } -I(x,t).$$

The first one is a $\mathcal{C}^1$ - diffeomorphism from $(X(t,x_0,0),+\infty)$ into $(x_0,+\infty)$, and the second from $(x_0, X(t;x_0,0))$ into $(0,t)$. Integrating f defined by (7.23) over $(0,R)$ with $R > X(t;x_0,0)$, using the change of variable above and with the help of lemma 7.7, taking the limit $R \to +\infty$ we get

$$\begin{aligned} \int_{x_0}^{+\infty} x|f(t,x)|dx &\leq \int_{x_0}^{+\infty} X(t;y,0)|f^0(y)|dy + \int_0^t X(t;s,x_0)|N(u(s))|ds \\ &\leq e^{At}\left(\int_{x_0}^{+\infty} y|f^0(y)|dy + \int_0^t x_0|N(u(s))|ds\right) \end{aligned} \tag{7.24}$$

when splitting the integral into two parts and using both the previous changes of variables. We conclude that for any $T > 0$, $f \in L^\infty\left(0,T;L^1(x_0,+\infty;xdx)\right)$ and therefore in $L^\infty\left(0,T;L^1(x_0,+\infty;x^r dx)\right)$, for any $r \in [0,1]$. In the lemma right after we claim that f defined by (7.23) is a weak solution.

Lemma 7.8. *Let f be the mild solution defined by* (7.23)*, then for any $t > 0$*

$$\begin{aligned} \int_{x_0}^{+\infty} f(x,t)\varphi(x,t)dx &= \int_{x_0}^{+\infty} f^0(x)\varphi(x,0)dx + \int_0^t N(u(s))\varphi(x_0,s)ds \\ &+ \int_0^t \int_{x_0}^{+\infty} f(x,s)\left[\frac{\partial}{\partial t}\varphi(x,s)u(s)\rho(x)\frac{\partial}{\partial x}\varphi(x,s) - \mu(x)\varphi(x,s)\right]dxds \end{aligned}$$

for all $\varphi \in \mathcal{D}'([0,T]\times[x_0,+\infty))$.

Proof. Since f belongs to $f \in L^\infty\left(0,T;L^1(x_0,+\infty;xdx)\right)$, it is possible to multiply the mild solution f against a test function $\varphi \in \mathcal{D}'([0,T]\times[x_0,+\infty))$ and integrate over $(x_0,+\infty)$, then

$$\begin{aligned} \int_{x_0}^{+\infty} f(x,t)\varphi(x,t)dx &= \int_{x_0}^{+\infty} f0(y)\varphi(X(t;y,0))e^{-\int_0^t \mu(X(\sigma;y,0))d\sigma}dy \\ &- \int_0^t N(u(s))\varphi(X(t;x_0,s),t)e^{-\int_s^t \mu(X(\sigma;x_0,s))d\sigma}ds \end{aligned} \tag{7.25}$$

by the same change of variable made above for (7.24). Furthermore, we have

$$\begin{aligned}\int_0^t \int_{x_0}^{X(s;x_0,0)} & f(x,s)\left[\partial_t\varphi(x,s)+a(s,x)\partial_x\varphi(x,s)-\mu(x)\varphi(x,s)\right]dxds \\ &= \int_0^t\int_{x^0}^{+\infty} f^0(x)\frac{d}{ds}\left(\varphi(X(s;x,0),s)e^{-\int_0^s \mu(X(\sigma;x,0))d\sigma}\right)dyds \\ &= \int_{x_0}^{+\infty} f^0(x)\varphi(X(t;x,0),t)e^{-\int_0^t \mu(X(\sigma;y,0))d\sigma}dx - \int_{x_0}^{+\infty} f0(x)\varphi(x,0)dx\end{aligned} \tag{7.26}$$

still using the change of variable mentioned above and

$$\begin{aligned}\int_0^t \int_{X(s;x_0,0)}^{\infty} & f(x,s)\left[\partial_t\varphi(x,s)+a(s,x)\partial_x\varphi(x,s)-\mu(x)\varphi(x,s)\right]dxds \\ &= -\int_0^t\int_0^s N(u(z))\frac{d}{ds}\left(\varphi(X(s;x_0,z),s)e^{-\int_z^s \mu(X(\sigma;x_0,z))d\sigma}\right)dzds \\ &= -\int_0^t N(u(s))\varphi(X(t;x_0,s),t)e^{-\int_s^t \mu(X(\sigma;x_0,s))d\sigma}dzds - \int_0^t N(u(s))\varphi(x_0,s)ds\end{aligned} \tag{7.27}$$

Finally, combining (7.25), (7.26) and (7.27) we obtain that f is a weak solution. □

The aim of the following is to state that the moments of f less than 1 are continuous in time.

Lemma 7.9. *Consider hypothesis (H1) to (H3). Let f be the mild solution given by* (7.23)*. Then for any $T>0$,*

$$f\in C^0\left([0,T],L^1(x_0,+\infty;x^r dx)\right),\quad \forall r\in[0,1].$$

Proof. Let $T>0$ and $r\in[0,1]$, since $f\in L^\infty_{loc}\left(\mathbb{R}_+,L^1(x_0,+\infty;x^r dx)\right)$, we have for any $t>0$ and $\delta t>0$ such that $t+\delta t\le T$

$$\int_{x_0}^{+\infty} x^r\left|f(x,t+\delta t)-f(x,t)\right|dx = I_1+I_2+I_3,$$

where

$$\begin{aligned}I_1 &= \int_{x_0}^{X(t;x_0,0)} x^r\left|f(x,t+\delta t)-f(x,t)\right|dx,\\ I_2 &= \int_{X(t;x_0,0)}^{X(t+\delta t;x_0,0)} x^r\left|f(x,t+\delta t)-f(x,t)\right|dx,\\ I_3 &= \int_{X(t+\delta t;x_0,0)}^{+\infty} x^r\left|f(x,t+\delta t)-f(x,t)\right|dx.\end{aligned}$$

The aim is to prove that each term goes to zero when δt goes to zero. We first bound I_3, that can be written from the initial condition since $x\ge X(t+\delta t;x_0,0)\ge X(t;x_0,0)$, as

follows

$$I_3 = \int_{X(t+\delta t;x_0,0)}^{+\infty} x^r \Big| f0(X(0;x,t+\delta t))J(0;x,t+\delta t)e^{-\int_0^{t+\delta t}\mu(X(\sigma;x,t+\delta t))d\sigma} \\ -f0(X(0;x,t))|J(0;x,t)e^{-\int_0^t \mu(X(\sigma;x,t))d\sigma}\Big| dx.$$

Let $f^{0,\varepsilon}$ be $\mathcal{C}_0^\infty$ with compact support $supp(f^{0,\varepsilon}) \subset (0, R_\varepsilon)$ converging in $L^1([x_0,+\infty), xdx)$ to $f0$. We write I_3 as follows

$$I_3 = I_3^1 + I_3^2 + I_3^3, \tag{7.28}$$

where

$$I_3^1 = \int_{X(t+\delta t;x_0,0)}^{+\infty} x^r |f0(X(0;x,t+\delta t)) - f^{0,\varepsilon}(X(0;x,t+\delta t))|J(0;x,t+\delta t)e^{-\int_0^{t+\delta t}\mu(X(\sigma;x,t+\delta t))d\sigma}dx,$$

$$I_3^2 = \int_{X(t+\delta t;x_0,0)}^{+\infty} x^r \Big| f^{0,\varepsilon}(X(0;x,t+\delta t))J(0;x,t+\delta t)e^{-\int_0^{t+\delta t}\mu(X(\sigma;x,t+\delta t))d\sigma} \\ -f^{0,\varepsilon}(X(0;x,t))J(0;x,t)e^{-\int_0^t \mu(X(\sigma;x,t))d\sigma}\Big| dx,$$

$$I_3^3 = \int_{X(t+\delta t;x_0,0)}^{+\infty} x^r |f^{0,\varepsilon}(X(0;x,t)) - f^0(X(0;x,t))|J(0;x,t)e^{-\int_0^t \mu(X(\sigma;x,t))d\sigma}dx.$$

Dropping the exponential term when bounding by one and doing the change of variable $y = X(0;x,t+\delta t)$ in I_3^1 and $y = X(0;x,t)$ in I_3^3, we get

$$I_3^1 + I_3^3 \le 2e^{AT}\int_{x_0}^{+\infty} y^r |f0(y) - f^{0,\varepsilon}(y)|dy = C_3^1(T,\varepsilon), \tag{7.29}$$

with the help of lemma 7.7. Let us bound now I_3^2 by

$$I_3^2 \le \int_{X(t+\delta t;x_0,0)}^{+\infty} x^r |f^{0,\varepsilon}(X(0;x,t+\delta t)) - f^{0,\varepsilon}(X(0;x,t))|J(0;x,t+\delta t)dx \\ + \int_{X(t+\delta t;x_0,0)}^{+\infty} x^r f^{0,\varepsilon}(X(0;x,t))|J(0;x,t+\delta t) - J(0;x,t)|dx \\ + \int_{X(t+\delta t;x_0,0)}^{+\infty} x^r f^{0,\varepsilon}(X(0;x,t))J(0;x,t)|e^{-\int_0^{t+\delta t}\mu(X(\sigma;x,t+\delta t))d\sigma} - e^{-\int_0^t \mu(X(\sigma;x,t))d\sigma}|dx$$

and we denote each integrals by J_3^1 to J_3^3, respectively. Remarking that $J(0,x,t) \le e^{BT}$ since (7.21) and

$$J_3^1 \le e^{BT}\|f^{0,\varepsilon}\|_{L^\infty}\int_{X(t+\delta t;x_0,0)}^{C_\varepsilon} x^r |X(0;x,t+\delta t) - X(0;x,t)|dx \\ \le \delta t e^{BT}\|f^{0,\varepsilon}\|_{L^\infty}\int_{X(t+\delta t;x_0,0)}^{C_\varepsilon} x^r \sup_{s\in[t,t+\delta t]}\Big|\frac{\partial}{\partial t}X(0;x,s)\Big| dx \\ \le \delta t A e^{2BT}\|f^{0,\varepsilon}\|_{L^\infty}\int_{x_0}^{C_\varepsilon} x^{r+1}dx, \tag{7.30}$$

where C_ε depends on T, A and R_ε *i.e.* the compact support of $f^{0,\varepsilon}$. Then

$$J_3^2 \leq e^{BT}\|f^{0,\varepsilon}\|_{L^\infty}\int_{X(t+\delta t;x_0,0)}^{R_\varepsilon} x^r|e^{G(t,\delta t,x)}-1|dx$$

with

$$\begin{aligned}|G(t,\delta t,x)| &= |\int_0^{t+\delta t} b(\sigma,X(\sigma;x,t+\delta t))d\sigma - \int_0^t b(\sigma,X(\sigma;x,t))d\sigma| \\ &\leq \int_0^{t+\delta t}|\rho'(X(\sigma;x,t+\delta t))-\rho'(X(\sigma;x,t))|u(\sigma)d\sigma + \int_t^{t+\delta t}|b(\sigma,X(\sigma;x,t))|d\sigma.\end{aligned}$$

Thus, with (7.19) and (7.21),

$$\begin{aligned}|G(t,\delta t,x)| &\leq K\|u\|_{L^\infty}\int_0^T |X(\sigma;x,t+\delta t)-X(\sigma;x,t)|d\sigma + \delta tB \\ &\leq \delta tK\|u\|_{L^\infty}\int_0^T \sup_{s\in[t,t+\delta t]}\left|\frac{\partial}{\partial t}X(\sigma;x,s)\right|d\sigma + \delta tB \\ &\leq \delta t\left(K\|u\|_{L^\infty}ATe^{BT}x + B\right)\end{aligned}$$

where K is the lipchitz constant of ρ'. Since $x \leq R_\varepsilon$, let $C_G(T,\varepsilon) = K\|u\|_{L^\infty}ATe^{BT}R_\varepsilon + B$, and remarking that if $|x| \leq y$, then

$$|e^x - 1| \leq |e^y - 1| + |e^{-y} - 1|,$$

thus we get

$$J_3^2 \leq e^{BT}\|f^{0,\varepsilon}\|_{L^\infty}\left(|e^{\delta tC_G(T,\varepsilon)}-1| + |e^{-\delta tC_G(T,\varepsilon)}-1|\right)\int_{x_0}^{R_\varepsilon} x^r dx \tag{7.31}$$

For J_3^3, since μ is non-negative,

$$J_3^3 \leq e^{BT}\|f^{0,\varepsilon}\|_{L^\infty}\int_{X(t+\delta t;x_0,0)}^{R_\varepsilon} x^r\left|e^{-\left(\int_0^{t+\delta t}\mu(X(\sigma;x,t+\delta t))d\sigma - \int_0^t \mu(X(\sigma;x,t))d\sigma\right)}-1\right|dx$$

Exactly as above,

$$|\int_0^{t+\delta t}\mu(X(\sigma;x,t+\delta t))d\sigma - \int_0^t \mu(X(\sigma;x,t))d\sigma| \leq \delta tMATe^{BT}x + \delta t\|\mu\|_{L^\infty}$$

with M the lipschitz constant of μ, and then denoting by $C_M(T,\varepsilon) = MATe^{BT}R_\varepsilon + \|\mu\|_{L^\infty}$, we get

$$J_3^3 \leq e^{BT}\|f^{0,\varepsilon}\|_{L^\infty}\left(|e^{\delta tC_M(T,\varepsilon)}-1| + |e^{-\delta tC_M(T,\varepsilon)}-1|\right)\int_{x_0}^{R_\varepsilon} x^r dx \tag{7.32}$$

From estimations (7.29), (7.30), (7.31) and (7.32) we can conclude that for any $\varepsilon > 0$,

$$I_3(\delta t) \leq C_3^1(T,\varepsilon) + C_3^2(T,\delta t,\varepsilon), \tag{7.33}$$

with $\lim_{\varepsilon\to 0} C_3^1(T,\varepsilon) = 0$ and $\lim_{\delta t\to 0} C_3^2(T,\delta t,\varepsilon) = 0$.

Concerning I_1, f can be written from the boundary condition. Let u^ε be $\mathcal{C}_0^\infty$ such that

$$u^\varepsilon \longrightarrow u, \text{ uniformly on } [0,T].$$

Then we write I_1 as follows

$$\begin{aligned} I_1 \leq & \int_{x_0}^{X(t+\delta t;x_0,0)} x^r |N(u(s_0(x,t+\delta t)) - N(u^\varepsilon(s_0(x,t+\delta t))| I(x,t+\delta t) dx \\ & + \int_{x_0}^{X(t;x_0,0)} x^r \Big| N(u^\varepsilon(s_0(x,t+\delta t)) I(x,t+\delta t) e^{-\int_{s_0(x,t+\delta t)}^t \mu(X(\sigma;x,t+\delta t))d\sigma} \\ & \qquad - N(u^\varepsilon(s_0(x,t)) I(x,t) e^{-\int_{s_0(x,t)}^t \mu(X(\sigma;x,t))d\sigma} \Big| dx \\ & + \int_{x_0}^{X(t;x_0,0)} x^r |N(u(s_0(x,t)) - N(u^\varepsilon(s_0(x,t))| I(x,t) dx \end{aligned}$$

With the help of (H3) we get similarly to I_3 that there exist two constant $C_1^1(T,\varepsilon)$ and $C_1^2(T,\delta t,\varepsilon)$

$$I_1(\delta t) \leq C_1^1(T,\varepsilon) + C_1^2(T,\delta t,\varepsilon), \tag{7.34}$$

with $\lim_{\varepsilon\to 0} C_1^1(T,\varepsilon) = 0$ and $\lim_{\delta t\to 0} C_1^2(T,\delta t,\varepsilon) = 0$.

Finally, we deal with I_2. It is a mixed of the two forms of f,

$$\begin{aligned} I_2 = \int_{X(t;x_0,0)}^{X(t+\delta t;x_0,0)} x^r \Big| & N(u(s_0(x,t+\delta t))) I(x,t+\delta t) e^{-\int_{s_0(x,t+\delta t)}^{t+\delta t} \mu(X(\sigma;x,t+\delta t))d\sigma} \\ & - f0(X(0;x,t)) J(0;x,t) e^{-\int_{s_0(x,t)}^t \mu(X(\sigma;x,t))d\sigma} \Big| dx \end{aligned}$$

Using the lipschitz constant of N denoted by K_N, from the definition of I and with the help of lemma 7.7, we get

$$\begin{aligned} I_2 \leq & \, x_0^r e^{(rA+B)T} K_N \, |X(t+\delta t;x_0,0) - X(t;x_0,0)| \\ & + x_0^r e^{rAT} \int_{X(t;x_0,0)}^{X(t+\delta t;x_0,0)} |f0(X(0;x,t)) J(0;x,t)| \, dx \end{aligned}$$

Still using the regularization $f^{0,\varepsilon}$ of $f0$, there exist two constant $C_2^1(T,\varepsilon)$ and $C_2^2(T,\delta t,\varepsilon)$ such that for any $\varepsilon > 0$,

$$I_2(\delta t) \leq C_2^1(T,\varepsilon) + C_2^2(T,\delta t,\varepsilon), \tag{7.35}$$

with $\lim_{\varepsilon\to 0} C_2^1(T,\varepsilon) = 0$ and $\lim_{\delta t\to 0} C_2^2(T,\delta t,\varepsilon) = 0$. To conclude, gathering from (7.33), (7.34) and (7.35), we get for any $\varepsilon > 0$ and $\delta t > 0$,

$$\int_{x_0}^{+\infty} x^r |f(x,t+\delta t) - f(x,t)| dx \leq C^1(T,\varepsilon) + C^2(T,\delta t,\varepsilon),$$

where $C^1(T,\varepsilon)$ and $C^2(T,\delta t,\varepsilon)$ are two constants such that $\lim_{\varepsilon\to 0} C^1(T,\varepsilon) = 0$ and $\lim_{\delta t\to 0} C^2(T,\delta t,\varepsilon) = 0$. Noticing that the proof remains the same when δt is negative, taking the lim sup in δt we get

$$0 \leq \limsup_{\delta t\to 0} \int_{x_0}^{+\infty} x^r |f(x,t+\delta t) - f(x,t)| dx \leq C^1(T,\varepsilon), \text{ for any } \varepsilon > 0,$$

The proof is ended when taking the limit ε goes to zero that leads to $f \in \mathcal{C}^0([0,T], L^1([x_0,+\infty), x^r dr)$ for all $r \in [0,1]$. □

We finish this section with a useful estimate for the uniqueness investigation.

Proposition 7.10. *Let u_1, $u_2 \in \mathcal{C}_b^0(\mathbb{R}_+)$ be two given functions and $T > 0$. Let f_1 and f_2 be two mild solutions to (7.15)-(7.17), associated respectively to the velocity and initial data u_1 f_1^0 and u_2, f_2^0, that is given by formula (7.23). Then, for any $t \in (0,T)$*

$$\begin{aligned}\int_{x_0}^{+\infty} x\,|f_1(x,t) - f_2(x,t)|\,dx \;&\leq \int_{x_0}^{+\infty} x\left|f_1^0(x) - f_2^0(x)\right| dx \\ &\quad - \int_0^t \int_{x_0}^{+\infty} \mu(x) x\,|f_1(x,s) - f_2(x,s)|\,dxds \\ &\quad + A_1 \int_0^t \int_{x_0}^{+\infty} x\,|f_1(x,s) - f_2(x,s)|\,dxds \\ &\quad + \int_0^t \left(K_{1,2} + C\|f_2(s)\|_{L^1(xdx)}\right)|u_1(s) - u_2(s)|\,ds,\end{aligned}$$

where A_1 is given by (7.19) for u_1 and $K_{1,2}$ is the lipschitz constant of N on $[0,R]$ with $R = \max(\|u_1\|_{L^\infty(0,T)}, \|u_2\|_{L^\infty(0,T)})$. Finally $C > 0$ denotes the constant such that $\rho(x) < Cx$.

Proof. This estimation is obtained from classical argument of approximation. Indeed, let $h = f_1 - f_2$ thus

$$\begin{aligned}\int_{x_0}^{+\infty} h(x,t)\varphi(x,t)dx &= \int_{x_0}^{+\infty} h_0(x)\varphi(x,0)dx + \int_0^t \left(N(u_1(s)) - N(u_2(s))\right)\varphi(x_0,s)ds \\ &\quad + \int_0^t \int_{x_0}^{+\infty} h(x,s)\left[\frac{\partial}{\partial t}\varphi(x,s) + a_1(s,x)\frac{\partial}{\partial x}\varphi(x,s) - \mu(x)\varphi(x,s)\right]dxds \\ &\quad + \int_0^t \int_{x_0}^{+\infty} \left(a_1(s,x) - a_2(s,x)\right) f_2(x,s)\frac{\partial}{\partial x}\varphi(x,s)dxds.\end{aligned}$$

Let h_ε be a regularization of h and S_δ a regularization of the *Sign* function. Let us take $\varphi(x,s) = S_\delta(h_\varepsilon(s,x))g(x)$ with $g \in \mathcal{C}_c^\infty([x_0,+\infty))$. Then passing to the limit $\delta \to 0$ and

then $\varepsilon \to 0$, we get

$$\int_{x_0}^{+\infty} |h(x,t)|g(x)dx = \int_{x_0}^{+\infty} |h_0(x)|g(x)dx + \int_0^t |N(u_1(s)) - N(u_2(s)))\, Sign(h_0(x_0))g(x_0)ds$$
$$+ \int_0^t \int_{x_0}^{+\infty} |h(x,s)| \left[a_1(s,x)\frac{\partial}{\partial x}g(x) - \mu(x)g(x) \right] dxds$$
$$+ \int_0^t \int_{x_0}^{+\infty} (a_1(s,x) - a_2(s,x))\, f_2(x,s) Sign(h(s,x))\frac{\partial}{\partial x}g(x)dxds.$$

Finally, we approach the identity function with a regularized function $\eta_R \in \mathcal{C}_c^\infty([x_0, +\infty))$ such that $\eta_R(x) = x$ over $(0, R)$, then passing to the limit $R \to +\infty$ ends the proof.

□

We get straightforward from proposition 7.8 that f defined by (7.23) is a weak solution and the only one from 7.10. Indeed, getting $u_1 = u_2$ and $f_1^0 = f_2^0$ in proposition 7.10 leads to the uniqueness. Finally, proposition 7.9 provide the continuity in time of the moments with order less or equal to one. This concludes the proof of proposition 7.6

7.3.3 Proof of the main result

In this section we prove the main result theorem 7.5, we first study the operator S in (7.18).

Lemma 7.11. *Consider hypothesis (H2) to (H4). Let u_0, p_0 and b_0 be non-negative real numbers accounting for initial data, and $f0$ satisfying (H1). Let $M > 0$ large enough such that $u_0, p_0, b_0 < M/2$ and define*

$$X_M = \left\{ (u,p,b) \in \mathcal{C}^0([0,T])^3 : 0 \le u,p,b \le M \right\}$$

where $\mathcal{C}^0([0,T])^3$ is equipped with the uniform norm. Then, there exists $T > 0$ such that

$$S : X_M \mapsto X_M, \text{ is a contraction.}$$

Proof. Let M sufficiently large such that $\max(u_0, p_0, b_0) < M/2$, and $T > 0$ small enough such that

$$(\gamma_u + \tau M + \sigma + x_0 C_1(M) + C_2(M,T))MT \le M/2, \tag{7.36}$$
$$(\gamma_p + \tau M)MT \le M/2, \tag{7.37}$$
$$(\sigma + \delta)MT \le M/2, \tag{7.38}$$

and,

$$(\lambda_u + \sigma M)T \le M/2, \tag{7.39}$$
$$(\lambda_p + \sigma M)T \le M/2, \tag{7.40}$$
$$\tau M^2 T \le M/2, \tag{7.41}$$

where $C_1(M)$ is the lipschitz constant of N on $(0, M)$ and

$$C_2(M,T) = Ce^{MCT}\left(\|f0\|_{L^1(xdx)} + C_1(M)MT\right) \tag{7.42}$$

where C is the constant such that on $\rho(x) \leq Cx$, see (7.24). This assumptions ensure that for any $(u,p,b) \in X_M$, then $S(u,p,b) \in X_M$, *i.e* the solution remains bounded by M and non-negative. It remains to prove that S is a contraction. Let (u_1,p_1,b_1) and (u_2,p_2,b_2) belong to X_M. Then

$$\begin{aligned}|\tilde{u}_1 - \tilde{u}_2|_\infty \leq \gamma_u T|u_1-u_2|_\infty + \tau T|u_1p_1 - u_2p_2|_\infty + \sigma T|b_1-b_2|_\infty + x_0TC_1(M)|u_1-u_2|_\infty \\ + T\sup_{t\in[0,T]}\left|u1\int_{x_0}^{+\infty}\rho(x)f_1(x,s)dx - u2\int_{x_0}^{+\infty}\rho(x)f_2(x,s)dx\right| \end{aligned} \tag{7.43}$$

Remarking that,

$$|u_1p_1 - u_2p_2|_\infty \leq M|u_1-u_2|_\infty + M|p_1-p_2|_\infty \tag{7.44}$$

and

$$\begin{aligned}\sup_{t\in[0,T]}\left|u1\int_{x_0}^{+\infty}\rho(x)f_1(x,s)dx - u2\int_{x_0}^{+\infty}\rho(x)f_2(x,s)dx\right| \\ \leq C_2(M,T)|u_1-u_2| + CM\sup_{t\in[0,T]}\left|\int_{x_0}^{+\infty}x|f_1(x,t)-f_2(x,t)|dx\right| \end{aligned} \tag{7.45}$$

and from proposition 7.10,

$$\sup_{t\in[0,T]}\left|\int_{x_0}^{+\infty}x|f_1(x,t)-f_2(x,t)|dx\right| \leq T\left(C_1(M) + CC_2(M,T)\right)|u_1-u_2|_\infty \tag{7.46}$$

We do the same to bound $|\tilde{p}_1 - \tilde{p}_2|_\infty$ and $|\tilde{b}_1 - \tilde{b}_2|_\infty$. It infers that there exists a constant $C(M,T)$ depending only on M and T such that

$$|(\tilde{u}_1,\tilde{p}_1,\tilde{b}_1) - (\tilde{u}_2,\tilde{p}_2,\tilde{b}_2)|_\infty \leq C(M,T)T|(u_1,p_1,b_1) - (u_2,p_2,b_2)|_\infty \tag{7.47}$$

with $C(M,T)T \to 0$, when T goes to 0. Hence, if T is small enough such that $C(M,T)T < 1$, then S is a contraction. □

Now, with the help of proposition 7.11, we have a local non-negative solution on an interval of time $[0,T]$ which is unique when it is ensured that the solution (u,p,b) remain bounded by the constant M. The solution satisfy $f \in C^0(0,T;L^1(xdx))$ and $u,p,b \in C^0(0,T)$. Futhermore from (H3), N is continuous and from (H2), $\rho(x) \leq Cx$ where C is a positive constant, thus $\rho f \in C^0(0,T;L^1(dx))$. We conclude that u,p and b defined in definition 7.4 have continuous derivatives.

Now we remark that the solutions satisfies on $[0,T]$

$$\begin{aligned}\frac{\mathrm{d}}{\mathrm{d}t}(u+p+2b) &= \lambda_u + \lambda_p - \gamma_u u - \gamma_p p - \delta 2b - nN(u) - \frac{1}{\varepsilon}u\int_{x_0}^{+\infty}\rho(x)f(x,t)dx \\ &\leq \lambda - m(u+p+2b)\end{aligned}$$

with $m = \min(\gamma_u, \gamma_p, \delta)$ and $\lambda = \lambda_u + \lambda_p$. Using Gronwall's lemma, the solutions remain bounded, at any time by, namely

$$u + p + 2b \leq u_0 + p_0 + 2b_0 + \frac{\lambda}{m}. \tag{7.48}$$

From this global bound on u, p and b, we can construct the solution on any interval of time $[0, T]$, $[T, 2T]$, *etc.* This ends the proof of the theorem.

We just obtained a global in time existence of solution. Therefore we question in the next subsection the long time behaviour of this solution, as well as a possible estimate of the rate of convergence towards some equilibrium. It is the subject of the next subsection.

7.3.4 Asymptotic profile and equilibrium.

Since we aim at investigating the long time behaviour of the solution (f, u, p, b) to (7.1-7.7), we start by considering the steady formulation of (7.1). Namely, assume that ρ and μ satisfy (H2). Let $u_\infty > 0$, then we are interested in f_∞, verifying for all x in $(x_0, +\infty)$,

$$\begin{cases} \dfrac{d}{dx} f_\infty(x) & = -\dfrac{\mu(x) + u_\infty \rho'(x)}{u_\infty \rho(x)} f_\infty(x), \\ u_\infty \rho(x_0) f_\infty(x_0) & = N(u_\infty). \end{cases} \tag{7.49}$$

If $\inf_{x \in [x_0, +\infty)} \rho(x) > 0$ it follows from (H2) that the flow is globally lipschitz. Thus, there exists a unique solution $f_\infty \in \mathcal{C}^0([x_0, \infty))$, to (7.49). Actually, this solution is given explicitly by,

$$f_\infty(x) = \frac{N(u_\infty)}{u_\infty \rho(x)} \exp\left(- \int_{x_0}^{x} \frac{\mu(y)}{u_\infty \rho(y)} dy \right). \tag{7.50}$$

It appears that $f_\infty \in L^1(xdx)$, so we can define rigorously

$$F(u_\infty) := \int_{x_0}^{\infty} \rho(x) f_\infty(x) dx,$$

where the dependency with respect to u_∞ is contained in the function f_∞. Note that if ρ is assumed to be constant as in the first part of the chapter, we have $F(u_\infty) = \rho\, A_\infty$, where A_∞ is the quantity of amyloids, defined in subsection 7.2.2. Hence, as in the stability analysis of the ODE model, we are now interested in solving the following system. We search $(u_\infty, p_\infty, b_\infty)$, satisfying

$$\lambda_u - \gamma_u u_\infty - \tau u_\infty p_\infty + \sigma b_\infty - x_0 N(u_\infty) - u_\infty F(u_\infty) = 0, \tag{7.51}$$

$$\lambda_p - \gamma_p p_\infty - \tau u_\infty p_\infty + \sigma b_\infty = 0, \tag{7.52}$$

$$b \tau u_\infty p_\infty - (\sigma + \delta) b_\infty = 0, \tag{7.53}$$

If there exist a solution to the above system, we get the equilibrium of problem (7.1-7.4), as done in subsection 7.2.2, on the ODE model. Indeed, we can prove the following proposition.

Proposition 7.12. *Let (f, u, p, b) be the solution to the problem (7.1-7.7). Assume that $(u_\infty, p_\infty, b_\infty)$ is a triplet of non negative numbers, solution to (7.51-7.53), where $f_\infty \in L^1([x_0, +\infty))$ is given by* (7.50)*. Moreover, we suppose that there exists $\lambda > 0$ such that*

$$|u(t) - u_\infty| e^{\lambda t} \to_{t\to+\infty} 0. \tag{7.54}$$

Then, f tends, when t goes to $+\infty$, to the function f_∞ in the following sense:

$$\int_{x_0}^{+\infty} x\,|f(x,t) - f_\infty(x)|\,dx \to_{t\to+\infty} 0, \tag{7.55}$$

and the convergence rate is exponential.

Proof. It is a straightforward consequence of proposition 7.10, applied to $f_1 = f$ and $f_2 = f_\infty$. The exponential rate of convergence comes from equation (7.54). □

7.4 Numerical scheme

In this section we propose a numerical method to discretize system (7.1-7.7), and some test cases in order to validate numerically our model. We chose the framework of finite volume schemes.

We introduce a uniform grid of points $(x_{i+1/2})_{i\in\mathbb{N}}$, discretizing the space domain $(x_0, +\infty)$, given by:

$$x_{1/2} = x_0 = \varepsilon\, n\,, \quad x_{i+1/2} = i\Delta x + x_0\,,\ i \geq 1\,,$$

where Δx is the space step. Let us also define the centers of the space cells:

$$x_i \,=\, (i - 1/2)\Delta x + x_0\,,\ i \geq 1\,.$$

We first focus on the space discretization of the problem in the next subsection, before dealing with the fully discretization in subsection 7.4.2. The space step Δx will then be linked to the time step through a CFL stability condition. Finally we propose a test cases in subsection 7.4.3.

7.4.1 Semi discrete in space scheme.

As usual in the finite volume framework, we introduce a sequence $(f_i)_{i\in\mathbb{N}}$ of approximations of the averages of f through each space cell $(x_{i-1/2}, x_{i+1/2})$, for $i \in \mathbb{N}^*$, that is

$$f_i(t) \sim \frac{1}{\Delta x}\int_{x_{i-1/2}}^{x_{i+1/2}} f(x,t)dx, \text{ for any } i \geq 1,$$

while the boundary condition (7.5) is taken into account by defining the function $f_0(t)$ such that,

$$u(t)\rho(x_0)f_0(t) = N(u(t)).$$

After integration of (7.1) over $(x_{i-1/2}, x_{i+1/2})$, we get, by applying an upwind scheme (since u and ρ are non negative), for all $i \geq 1$

$$\frac{d}{dt} f_i + u(t) \frac{\rho_{i+1/2} f_i(t) - \rho_{i-1/2} f_{i-1}(t)}{\Delta x} = -\mu_i f_i(t), \tag{7.56}$$

where for all $i \geq 0$:

$$\begin{cases} \rho_{i\pm 1/2} = \rho\left(x_{i\pm 1/2}\right), \\ \mu_i = \mu(x_i). \end{cases}$$

The total rate of polymerization into amyloid, $F(t) = \int_{x_0}^{+\infty} \rho(x) f(x,t) dx$ is approached by

$$\mathcal{F}(t) \, = \sum_{i \geq 0} \Delta x \, \rho_{i+1/2} f_i(t).$$

7.4.2 Fully discrete scheme.

We now provide a complete discretization of (7.1)-(7.7), using an explicit time discretization. Let $(t^n) = (n\,\Delta t)_{n \in \mathbb{N}}$ be the time discretization, where the time step Δt is chosen such that the following CFL condition is satisfied:

$$\begin{cases} C_1 \, \overline{\rho} \dfrac{\Delta t}{\Delta x} \, \leq \, 1, \\ \tau C_1 \Delta t \, \leq \, 1, \\ \sigma \Delta t \leq 1, \\ (\tau C_2 + n K_1 + \dfrac{\overline{\rho}}{\varepsilon} C_3) \Delta t \, \leq \, 1, \end{cases} \tag{7.57}$$

where the constants depend on the parameters of the system and will be precised right after, in order for our scheme to be stable and preserve the positivity of the solution.

The initial condition of our scheme is chosen as, for any $i \geq 1$:

$$\begin{cases} f_i^0 \, = \, \dfrac{1}{\Delta x} \displaystyle\int_{x_{i-1/2}}^{x_{i+1/2}} f^0(x) \, dx, \\ u^0 = u_0, \; p^0 = p_0, \; b^0 = b_0, \end{cases} \tag{7.58}$$

where f^0, u_0, p_0 and b_0 are the initial data of the continuous problem.

Let $T > 0$ and $N \in \mathbb{N}$ such that $N = T/\Delta t$. Then we construct an approximate

solution to (7.1)-(7.7) on $(x_0;+\infty)\times(0,T)$, as

$$\begin{cases} f_{app}(x,t) \;=\; \displaystyle\sum_{i\geq 1}\sum_{n=0}^{N-1} f_i^n\, 1_{[x_{i-1/2},x_{i+1/2})}(x)\, 1_{[t^n,t^{n+1})}(t)\,, \\ u_{app}(t) \;=\; \displaystyle\sum_{n=0}^{N-1} u^n\, 1_{[t^n,t^{n+1})}(t)\,, \\ p_{app}(t) \;=\; \displaystyle\sum_{n=0}^{N-1} p^n\, 1_{[t^n,t^{n+1})}(t)\,, \\ b_{app}(t) \;=\; \displaystyle\sum_{n=0}^{N-1} b^n\, 1_{[t^n,t^{n+1})}(t)\,, \end{cases}$$

where the sequences f_i^n, u^n, p^n and b^n are given below, using an explicit Euler scheme in time. Namely, the scheme reads, for all $n\geq 0$, for all $i\geq 1$:

$$(1+\Delta t\mu_i)f_i^{n+1} = f_i^n - u^n\frac{\Delta t}{\Delta x}\left(\rho_{i+1/2}f_i^n - \rho_{i-1/2}f_{i-1}^n\right), \tag{7.59}$$

such that the boundary condition is satisfied at time t^n:

$$u^n\rho_{1/2}f_0^n = N(u^n).$$

Meanwhile, the other sequences are given by

$$\begin{cases} (1+\gamma_u\Delta t)u^{n+1} &= u^n + \Delta t\left(\lambda_u - \tau u^n p^n + \sigma b^n - nN(u^n) - \dfrac{1}{\varepsilon}u^n F^n\right), \\ (1+\gamma_p\Delta t)p^{n+1} &= p^n + \Delta t\left(\lambda_p - \tau u^n p^n + \sigma b^n\right), \\ (1+\delta\Delta t)b^{n+1} &= b^n + \Delta t\left(\tau u^n p^n - \sigma b^n\right), \end{cases} \tag{7.60}$$

where

$$F^n \;=\; \sum_{i\geq 0}\Delta x\,\rho_{i+1/2}f_i^n$$

is the total rate of amyloid at time t^n.

7.4.3 Stability condition and conservation of positivity.

Since we look for physically relevant solutions, we need at least to check the non-negativity of the approximate solution $(f_{app}, u_{app}, p_{app}, b_{app})$. We will see here that this requirement will impose the CFL conditions (7.57).

Let us define the mass of oligomers at time t^n,

$$\psi^n = \frac{1}{\varepsilon}\sum_{i\geq 1} x_{i-1/2}f_i^n + u^n + b^n,$$

and the mass of prion proteins at time t^n,

$$\varphi^n = p^n + b^n.$$

Then, we can define the constants involved in (7.57). First, a bound for the total number of oligomers may be

$$C_1 = \psi^0 + \frac{\lambda_u}{a_1}, \tag{7.61}$$

where $a^1 = \min(\underline{\mu}, \gamma_u, \delta) > 0$, with $\underline{\mu} = \inf_{x>0} \mu(x) > 0$.

Second, a bound for the total number of prion proteins can be given by:

$$C_2 = \varphi^0 + \frac{\lambda_p}{a_2}, \tag{7.62}$$

where $a_2 = \min(\gamma_p, \delta) > 0$.

Finally, we can define a bound for the total number of amyloids, by

$$C_3 = \sum_{i\geq 1} f_i^0 + \frac{K_1 C_1}{\underline{\mu}}. \tag{7.63}$$

where

$$K_1 = \sup_{u\in(0,C_1)} N(u)/u. \tag{7.64}$$

We are now able to state a stability result on our scheme.

Lemma 7.13. *Let $T > 0$, let Δx, Δt be the space and time step, satisfying conditions* (7.57)*, where*

$$\overline{\rho} \geq \sup_{x\in(x_0,\infty)} \rho(x)\,.$$

Assume that the initial conditions (7.58) *are non negative. Then the sequences (f_i^n), (u^n), (p^n) (b^n), given by the scheme* (7.59)-(7.60)*, are well defined and there exists a constant C_0 (depending on initial data and parameters) such that for all $i \geq 1$, for any n in $\{0, \ldots, N\}$:*

$$0 < u^n,\ p^n, b^n < C_0\,, \quad f_i^n > 0\,, \quad \text{and} \ \sum_{i\geq 1} f_i^n \Delta x < C_0. \tag{7.65}$$

Proof. From the non negativity of the initial data, it holds

$$\psi^0 < C_1\,, \quad \varphi^0 < C_2\,, \quad \text{and} \ \sum_{i\geq 1} f_i^0 < C_3, \tag{7.66}$$

so that the lemma is verified at time t^0. Now we proceed somehow by induction. Suppose that (7.66) holds true at time t^n, then, by applying the scheme, and using the conditions (7.57), we get straightforward

$$(1 + a_1\Delta t)\psi^{n+1} \leq \psi^n + \lambda_u \Delta t \leq \psi^0 + \frac{1 + a_1\Delta t}{a_1}\lambda_u$$

thus, $\psi^{n+1} < C_1$. Similarly, we have $\varphi^{n+1} < C_2$. Finally, from (7.59) and the non-negativity, we have

$$(1 + \underline{\mu}\Delta t) \sum_{i \geq 1} f_i^{n+1} \Delta x \leq \sum_{i \geq 1} f_i^n \Delta x + \Delta t K_1 C_1$$

and thus $\sum_{i \geq 1} f_i^{n+1} \Delta x < C_3$. This ends the proof, since $C_0 = \max(C_1, C_2, C_3)$ □

7.4.4 Propositions of test cases

Let $\varepsilon = \rho_0 = \mu = \lambda_u = \lambda_p = \gamma_u = \gamma_p = \delta = \sigma = \tau = 1$, $n = 2$ (the number of oligomers to form an amyloid) and $\theta = 1/2$. Moreover we use the following nucleation rate

$$N(u) = u^2. \tag{7.67}$$

Thus $K = \sup_{u \in (0,C)} N(u)/u = C$. The equilibrium of p and b in function of $\overline{u}$ are given by

$$p_\infty = \frac{2}{u_\infty + 2} \quad \text{and} \quad b = \frac{u_\infty}{2 + u_\infty}, \tag{7.68}$$

while

$$f_\infty(x) = u_\infty \, x^{-1/2} \exp\left(-\frac{2}{u_\infty}(x^{1/2} - 2^{1/2}) \right), \text{ for any } x > 2. \tag{7.69}$$

Thus,

$$\int_2^{+\infty} x^{1/2} f_\infty(x) dx = \frac{1}{2}(2\sqrt{2} + u_\infty) u_\infty^2 \tag{7.70}$$

and hence, u_∞ solves

$$4 - 4z - 10z^2 - 4(\sqrt{2} + 1)z^3 - 2(\sqrt{2} + 1)z^4 - z^5 = 0. \tag{7.71}$$

There exist a unique positive root in $(0, 1)$ which provides u_∞.

Appendix

A Characteristic polynomials of the linearised ODE system

Here we give the coefficient a_i, $i = 1, \ldots, 4$ for the characteristic polynomial of the linearised system in proposition 7.2. They are:

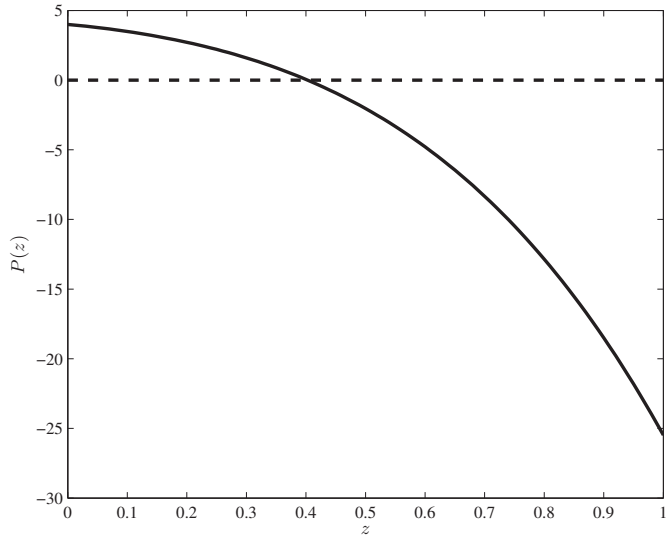

Figure 7.1: Graph of the polynomial $P(z) = 4 - 4z - 10z^2 - 4(\sqrt{2}+1)z^3 - 2(\sqrt{2}+1)z^4 - z^5$ on $(0,1)$ in full line. The intersection with the zero axe in dash line is the steady state u_∞.

$$
\begin{aligned}
a_1 &= \left(\mu + \gamma_u + \tau\frac{\lambda_p}{\tau^*\bar{u} + \gamma_p} + \alpha n^2 \bar{u}^{n-1} + \rho\frac{\alpha}{\mu}\bar{u}^n + \gamma_p + \tau\bar{u} + \sigma + \delta\right),\\
a_2 &= \left(\mu + \gamma_u + \alpha n^2 \bar{u}^{n-1} + \rho\frac{\alpha}{\mu}\bar{u}^n\right)(\gamma_p + \tau\bar{u} + \sigma + \delta) + \gamma_p\sigma + (\gamma_p + \tau\bar{u})\delta\\
&\quad + \mu\left(\gamma_u + \tau\frac{\lambda_p}{\tau^*\bar{u} + \gamma_p} + \alpha n^2 \bar{u}^{n-1} + \rho\frac{\alpha}{\mu}\bar{u}^n\right) + \rho\alpha n\bar{u}^n + \tau(\gamma_p + \delta)\frac{\lambda_p}{\tau^*\bar{u} + \gamma_p},\\
a_3 &= \left(\mu + \gamma_u + \alpha n^2 \bar{u}^{n-1} + \rho\frac{\alpha}{\mu}\bar{u}^n\right)(\gamma_p\sigma + (\gamma_p + \tau\bar{u})\delta) + (\gamma_p\delta + (\gamma_p + \delta)\mu)\tau\frac{\lambda_p}{\tau^*\bar{u} + \gamma_p}\\
&\quad + \left\{\mu\left(\gamma_u + \alpha n^2 \bar{u}^{n-1} + \rho\frac{\alpha}{\mu}\bar{u}^n\right) + \rho\alpha n\bar{u}^n\right\}(\gamma_p + \tau\bar{u} + \sigma + \delta),\\
a_4 &= \mu\gamma_p\delta\tau\frac{\lambda_p}{\tau^*\bar{u} + \gamma_p} + \left\{\mu\left(\gamma_u + \alpha n^2 \bar{u}^{n-1} + \rho\frac{\alpha}{\mu}\bar{u}^n\right) + \rho\alpha n\bar{u}^n\right\}(\gamma_p\sigma + (\gamma_p + \tau\bar{u})\delta).
\end{aligned}
$$

B Lyapunov function

In order to derived the global stability in proposition 7.3 we consider Liapunov to the system (7.8) be the function

$$\begin{aligned}\Phi =&\frac{1}{2}\left(\frac{2\gamma_p}{\delta}\right)s_1\theta_1^2+\frac{1}{2}\left(1+2\frac{\delta+\gamma_u+\rho(A_\infty+\theta_1)}{\sigma}\right)\theta_2^2+\frac{1}{2}\left(\frac{2\gamma_p}{\delta}\right)\theta_3^2+\frac{1}{2}\left(\frac{\sigma}{\gamma_p}\right)\theta_4^2\\&+\left(\frac{\rho p_\infty}{\gamma_u+\rho A_\infty+\mu}\right)\theta_1\theta_2+\theta_1\theta_3+\theta_2\theta_3\\&+\left(\frac{\rho p_\infty}{\gamma_u+\rho A_\infty+\mu}+1+\frac{\rho}{\tau}\right)\theta_1\theta_4+2\theta_2\theta_4+\left(\frac{2\gamma_p}{\delta}\right)\theta_3\theta_4,\end{aligned}$$

where $\theta_1 = A - A_\infty$, $\theta_2 = u - u_\infty$, $\theta_3 = p - p_\infty$, $\theta_4 = b - b_\infty$, with $s_1 = \max(T_1, T_2)$ such that

$$\begin{aligned}T_1 =& \frac{\rho^2\delta u_\infty^2(1+2\frac{1+\delta}{\sigma})}{8\mu\gamma_p}+\frac{(\gamma_p+\mu)^2(\frac{\delta}{2\gamma_p})^2}{4\gamma_p\mu}\\&+\frac{[(\delta+\mu)(\frac{\rho p_\infty}{\gamma_u+\rho A_\infty+\mu}+1)+(\sigma+\delta+\mu)\frac{\rho}{\tau}+2\rho u_\infty]^2}{8\mu\sigma}\end{aligned}$$

and,

$$\begin{aligned}T_2 =&\frac{\left(\frac{\delta}{2\gamma_p}\right)^2\left(\frac{\rho p_\infty}{\gamma_u+\rho A_\infty+\mu}\right)^2\left(\frac{2\sigma+\delta}{2\gamma_p}\right)}{\left(1+2\frac{\delta+\gamma_u}{\sigma}-\frac{\delta}{2\gamma_p}\right)\left(\frac{\delta}{2\gamma_p}\frac{\sigma}{\gamma_p}-1\right)}+\frac{\left(\frac{\delta}{2\gamma_p}\right)^2\left(\frac{\rho p_\infty}{\gamma_u+\rho A_\infty+\mu}\right)\left[2+4\frac{\rho}{\tau}\frac{\delta+\gamma_u}{\sigma}\right]}{\left(1+2\frac{\delta+\gamma_u}{\sigma}-\frac{\delta}{2\gamma_p}\right)\left(\frac{\delta}{2\gamma_p}\frac{\sigma}{\gamma_p}-1\right)}\\&+\frac{\left(\frac{\delta}{2\gamma_p}\right)^3\left[\frac{\rho}{\tau}\left(2+\frac{\rho}{\tau}\right)+\frac{\sigma}{\gamma_p}+2\frac{\delta+\gamma_u}{\gamma_p}\right]}{\left(1+2\frac{\delta+\gamma_u}{\sigma}-\frac{\delta}{2\gamma_p}\right)\left(\frac{\delta}{2\gamma_p}\frac{\sigma}{\gamma_p}-1\right)}+\frac{\left(\frac{\delta}{2\gamma_p}\right)^2\left(1+\frac{\rho}{\tau}\right)\left[1+2\frac{\delta+\gamma_u}{\sigma}\right]\frac{\rho}{\tau}}{\left(1+2\frac{\delta+\gamma_u}{\sigma}-\frac{\delta}{2\gamma_p}\right)\left(\frac{\delta}{2\gamma_p}\frac{\sigma}{\gamma_p}-1\right)}\\&+\left(\frac{\delta}{2\gamma_p}\right)\left(\frac{\rho p_\infty}{\gamma_u+\rho A_\infty+\mu}\right)^2\left(\frac{1}{1+2\frac{\delta+\gamma_u}{\sigma}}\right)+\frac{\left(1+2\frac{\delta+\gamma_u}{\sigma}\right)\left(\frac{\delta}{2\gamma_p}\right)^2}{\left(1+2\frac{\delta+\gamma_u}{\sigma}-\frac{\delta}{2\gamma_p}\right)}.\end{aligned}\tag{7.72}$$

This Lyapunov function Φ is positive when $\left(1+2\frac{\delta+\gamma_u}{\sigma}\right) > \frac{\delta}{2\gamma_p} > \frac{\gamma_p}{\sigma}$. Its derivative along the solutions to the system (7.8) is

$$\begin{aligned}\dot\Phi =&-\left(\mu s_1+\rho u\frac{\rho\frac{\delta}{2\gamma_p}p_\infty}{\gamma_u+\rho A_\infty+\mu}\right)\theta_1^2-\rho u_\infty\left(1+2\frac{\gamma_u+\rho(A_\infty+\theta_1)+\delta}{\sigma}\right)\left(\frac{\delta}{2\gamma_p}\right)\theta_1\theta_2\\&-\left(\frac{2(\gamma_u+\rho(A_\infty+\theta_1)+\tau p)(\gamma_u+\rho(A_\infty+\theta_1)+\delta)}{\sigma}+\gamma_u+\rho(A_\infty+\theta_1)\right)\left(\frac{\delta}{2\gamma_p}\right)\theta_2^2\\&-\left((\delta+\mu)\left(\frac{\rho p_\infty}{\gamma_u+\rho A_\infty+\mu}+1\right)+(\sigma+\delta+\mu)\frac{\rho}{\tau}+2\rho u_\infty\right)\left(\frac{\delta}{2\gamma_p}\right)\theta_1\theta_4\\&-\left(\frac{\delta\tau u}{2\gamma_p}+\gamma_p\right)\theta_3^2-\delta\left(\frac{\sigma}{\gamma_p}\frac{\delta}{2\gamma_p}\right)\theta_4^2-(\gamma_p+\mu)\left(\frac{\delta}{2\gamma_p}\right)\theta_1\theta_3\end{aligned}$$

$\dot\Phi$ is non-positive. Furthermore, $\dot\Phi = 0$ if and only if $\theta_1 = \theta_2 = \theta_3 = \theta_4 = 0$.

Bibliography

[1] D. J. Aldous. Deterministic and stochastic models for coalescence (aggregation and coagulation): a review of the mean-field theory for probabilists. *Bernoulli*, 5(1):3–48, 1999.

[2] L. J. S. Allen. *An Introduction to Mathematical Biology*. Prentice Hall, 2006.

[3] M.-T. Alvarez-Martinez, P. Fontes, V. Zomosa-Signoret, J.-D. Arnaud, E. Hingant, L. Pujo-Menjouet, and J.-P. Liautard. Dynamics of polymerization shed light on the mechanisms that lead to multiple amyloid structures of the prion protein. *Biochimica et Biophysica Acta (BBA) - Proteins & Proteomics*, 1814(10):1305–17, Oct. 2011.

[4] M. T. Alvarez-Martinez, J. Torrent, R. Lange, J.-M. Verdier, C. Balny, and J.-P. Liautard. Optimized overproduction, purification, characterization and high-pressure sensitivity of the prion protein in the native (PrPC-like) or amyloid (PrPSc-like) conformation. *Biochimica et Biophysica Acta (BBA) - Proteins & Proteomics*, 1645(2):228–240, Feb. 2003.

[5] O. Angulo, J. López-Marcos, and M. López-Marcos. A semi-Lagrangian method for a cell population model in a dynamical environment. *Mathematical and Computer Modelling*, Dec. 2011.

[6] O. Angulo and J. C. López-Marcos. Numerical integration of a size-structured cell population model in an environment of changing substrate concentration. In *Proceedings of the International Conference 2003 (ICCMSE 2003) - Computational Methods in Sciences and Engineering*, pages 28–32, 2003.

[7] I. Armendáriz. Brownian coagulation and a version of Smoluchowski's equation on the circle. *The Annals of Applied Probability*, 20(2):660–695, 2010.

[8] J. M. Ball and J. Carr. Asymptotic behaviour of solutions to the Becker-Döring equations for arbitrary initial data. *Proceedings of the Royal Society of Edinburgh: Section A Mathematics*, 108(1-2):109–116, 1988.

[9] J. M. Ball and J. Carr. The discrete coagulation-fragmentation equations: Existence, uniqueness, and density conservation. *Journal of Statistical Physics*, 61(1-2):203–234, Oct. 1990.

[10] J. M. Ball, J. Carr, and O. Penrose. The Becker-Döring Cluster Equations: Basic Properties and Asymptotic Behaviour of Solutions. *Communications in Mathematical Physics*, 104(4):657–692, 1986.

[11] J. Banasiak. Shattering and non-uniqueness in fragmentation models: an analytic approach. *Physica D*, 222:63–72, 2006.

[12] V. Bansaye, J.-F. Delmas, L. Marsalle, and V. C. Tran. Limit theorems for Markov processes indexed by continuous time Galton-Watson trees. *Annals of Applied Probability*, 21(6):2263–2314, 2011.

[13] V. Bansaye and V. C. Tran. Branching Feller diffusion for cell division with parasite infection. *ALEA*, 8:81–127, 2011.

[14] J. W. Barrett and E. Süli. Existence of global weak solutions to Fokker-Planck and Navier-Stokes-Fokker-Planck equations in kinetic models of dilute polymers. *Discrete and Continuous Dynamical Systems - Series S*, 3(3):371–408, 2010.

[15] J. W. Barrett and E. Süli. Existence and equilibration of global weak solutions to kinetic models for dilute polymers I: Finitely extensible nonlinear bead-srping chains. *Mathematical Models and Methods in Applied Sciences*, 21(6):1211–89, 2011.

[16] I. V. Baskakov and O. V. Bocharova. In vitro conversion of mammalian prion protein into amyloid fibrils displays unusual features. *Biochemistry*, 44(7):2339–48, Feb. 2005.

[17] P. Beauvais. *Les maladies à prion*. Flammarion, 2005.

[18] R. Becker and W. Döring. Kinetische Behandlung der Keimbildung in übersättigten Dämpfen. *Annalen der Physik*, 416(8):719–752, 1935.

[19] N. Berglund and B. Gentz. *Noise-Induced Phenomena in Slow-Fast Dynamical Systems,A Sample-Paths Approach*. Springer, 2006.

[20] R. A. Bessen, D. A. Kocisko, G. J. Raymond, S. Nandan, P. T. Lansbury, and B. Caughey. Non-genetic propagation of strain-specific properties of scrapie prion protein. *Nature*, 375(6533):698–700, June 1995.

[21] G. Bhak, J.-H. Lee, J.-S. Hahn, and S. R. Paik. Granular assembly of alpha-synuclein leading to the accelerated amyloid fibril formation with shear stress. *PloS One*, 4(1):e4177, Jan. 2009.

[22] J. Billingham. On modelling the formation of micelles in the presence of a slow influx of monomer. *The Quarterly Journal of Mechanics and Applied Mathematics*, 53(2):285–297, May 2000.

[23] R. B. Bird, C. F. Curtiss, R. C. Armstrong, and O. Hassager. *Dynamics of Polymeric Liquids, vol. 2: Kinetic theory*. Wiley, New York, 1987.

[24] N. N. Borodin. A Limit Theorem for Solutions of Differential Equations with Random Right-Hand Side. *Theory of Probability and its Applications*, 22(3):482, 1978.

[25] J.-P. Bourgade and F. Filbet. Convergence of a finite volume scheme for coagulation-fragmentation equations. *Mathematics of Computation*, 77(262):851–882, 2008.

[26] M. Bowen. Temporal evolution of the cluster size distribution during brownian coagulation. *Journal of Colloid and Interface Science*, 105(2):617–627, 1985.

[27] J. A. Cañizo. Convergence to Equilibrium for the Discrete Coagulation-Fragmentation Equations with Detailed Balance. *Journal of Statistical Physics*, 129(1):1–26, Aug. 2007.

[28] V. Calvez, M. Doumic, and P. Gabriel. Self-similarity in a general aggregation–fragmentation problem. Application to fitness analysis. *Journal de Mathématiques Pures et Appliquées*, Jan. 2012.

[29] V. Calvez, N. Lenuzza, M. Doumic, J.-P. Deslys, F. Mouthon, and B. Perthame. Journal of Biological Dynamics. *Journal of Biological Dynamics*, 4(1):28–42, 2010.

[30] V. Calvez, N. Lenuzza, M. Doumic, J.-P. Deslys, F. Mouthon, and B. Perthame. Prion dynamics with size dependency–strain phenomena. *Journal of Biological Dynamics*, 4(1):28–42, Jan. 2010.

[31] V. Calvez, N. Lenuzza, D. Oelz, J.-P. Deslys, P. Laurent, F. Mouthon, and B. Perthame. Size distribution dependence of prion aggregates infectivity. *Mathematical biosciences*, 217(1):88–99, Jan. 2009.

[32] J. A. Canizo, L. Desvillettes, and K. Fellner. Absence of Gelation for Models of Coagulation-Fragmentation with Degenerate Diffusion. *Preprint*, ?

[33] J. Castilla, P. Saá, C. Hetz, and C. Soto. In vitro generation of infectious scrapie prions. *Cell*, 121(2):195–206, Apr. 2005.

[34] B. Caughey and G. S. Baron. Prions and their partners in crime. *Nature*, 443(7113):803–810, Oct. 2006.

[35] B. Caughey, G. S. Baron, B. Chesebro, and M. Jeffrey. Getting a grip on prions: oligomers, amyloids, and pathological membrane interactions. *Annual Review of Biochemistry*, 78:177–204, Jan. 2009.

[36] E. Cepeda and N. Fournier. Smoluchowski's equation: rate of convergence of the Marcus-Lushnikov process. *Stochastic Processes and their Applications*, 121(6):1–34, 2011.

[37] F. A. C. C. Chalub and M. O. Souza. From discrete to continuous evolution models: A unifying approach to drift-diffusion and replicator dynamics. *Theoretical Population Biology*, 76(4):268–277, 2009.

[38] N. Champagnat. Invasion and adaptive evolution for individual-based spatially structured populations. *Journal of Mathematical Biology*, 55(2):147–188, 2007.

[39] N. Champagnat, R. Ferrière, and S. Méléard. Individual-based probabilistic models of adaptive evolution and various scaling approximations. *Progress in Probability*, 59:75–113, 2005.

[40] N. Champagnat, R. Ferrière, and S. Méléard. Individual-based probabilistic models of adaptive evolution and various scaling approximations. *Progress in Probability*, 59:75–114, 2008.

[41] E. Chatani, Y.-H. Lee, H. Yagi, Y. Yoshimura, H. Naiki, and Y. Goto. Ultrasonication-dependent production and breakdown lead to minimum-sized amyloid fibrils. *Proceedings of the National Academy of Sciences of the United States of America*, 106(27):11119–24, July 2009.

[42] C. Chauvière and A. Lozinski. Simulation of complex viscoelastic flows using the Fokker–Planck equation: 3D FENE model. *Journal of Non-Newtonian Fluid Mechanics*, 122(1-3):201–214, Sept. 2004.

[43] S. Chen, F. A. Ferrone, and R. Wetzel. Huntington's disease age-of-onset linked to polyglutamine aggregation nucleation. *Proceedings of the National Academy of Sciences of the United States of America*, 99(18):11884–9, Sept. 2002.

[44] P. Chien, J. S. Weissman, and A. H. DePace. Emerging principles of conformation-based prion inheritance. *Annual Review of Biochemistry*, 73:617–56, Jan. 2004.

[45] F. Chiti and C. M. Dobson. Protein misfolding, functional amyloid, and human disease. *Annual Review of Biochemistry*, 75:333–66, July 2006.

[46] C. Chothia and J. Janin. Principles of protein-protein recognition. *Nature*, 256(5520):705–708, Aug. 1975.

[47] I. S. Ciuperca, E. Hingant, L. I. Palade, and L. Pujo-Menjouet. Fragmentation and monomer lengthening of rod-like polymers, a relevant model for prion proliferation. *Discrete and Continuous Dynamical Systems - Series B*, 17(3):775–799, Jan. 2012.

[48] D. W. Colby, K. Giles, G. Legname, H. Wille, I. V. Baskakov, S. J. DeArmond, and S. B. Prusiner. Design and construction of diverse mammalian prion strains. *Proceedings of the National Academy of Sciences of the United States of America*, 106(48):20417–22, Dec. 2009.

[49] J.-F. Collet and T. Goudon. Lifshitz-Slyozov equations: The model with encounters. *Transport Theory and Statistical Physics*, 28(6):545–573, Oct. 1999.

[50] J.-F. Collet and T. Goudon. On solutions of the Lifshitz-Slyozov model. *Nonlinearity*, 13(4):1239–1262, July 2000.

[51] J. F. Collet and F. Poupaud. Existence of solutions to coagulation-fragmentation systems with diffusion. *Transport Theory and Statistical Physics*, 25(3-5):503–513, Apr. 1996.

[52] J. Collinge and A. R. Clarke. A general model of prion strains and their pathogenicity. *Science*, 318(5852):930–6, Nov. 2007.

[53] J. Collinge, K. C. Sidle, J. Meads, J. Ironside, and A. F. Hill. Molecular analysis of prion strain variation and the aetiology of 'new variant' CJD. *Nature*, 383(6602):685–90, Oct. 1996.

[54] S. R. Collins, A. Douglass, R. D. Vale, and J. S. Weissman. Mechanism of prion propagation: amyloid growth occurs by monomer addition. *PLoS Biology*, 2(10):e321, Oct. 2004.

[55] J. H. Come, P. E. Fraser, and P. T. Lansbury. A kinetic model for amyloid formation in the prion diseases: importance of seeding. *Proceedings of the National Academy of Sciences of the United States of America*, 90(13):5959–63, 1993.

[56] D. L. Craft, L. M. Wein, and S. D. J. The Impact of Novel Treatments on Aβ Burden in Alzheimer's Disease: Insights from A Mathematical Model. In M. L. Brandeau, F. Sainfort, and W. P. Pierskalla, editors, *Operations Research and Health Care*, volume 70 of *International Series in Operations Research & Management Science*, pages 839–865. Kluwer Academic Publishers, Boston, 2005.

[57] D. L. Craft, L. M. Wein, and D. J. Selkoe. A mathematical model of the impact of novel treatments on the A beta burden in the Alzheimer's brain, CSF and plasma. *Bulletin of mathematical biology*, 64(5):1011–31, Sept. 2002.

[58] D. Dawson, B. Maisonneuve, and J. Spencer. *Measure-valued markov processes*, volume 1541. Ecole d'été de Probabilités de Saint-Flour XXI - 1991 Springer Berlin / Heidelberg, 1993.

[59] P. Degond, M. Lemou, and M. Picasso. Viscoelastic fluid models derived from kinetic equations for polymers. *SIAM Journal on Applied Mathematics*, 62(5):1501–1519, 2002.

[60] P. Degond and H. Liu. Kinetic models for polymers with inertial effects. *Networks and Heterogeneous Media*, 4(4):625–647, Oct. 2009.

[61] N. R. Deleault, B. T. Harris, J. R. Rees, and S. Supattapone. Formation of native prions from minimal components in vitro. *Proceedings of the National Academy of Sciences of the United States of America*, 104(23):9741–6, June 2007.

[62] L. Desvillettes and K. Fellner. Large Time Asymptotics for a Continuous Coagulation-Fragmentation Model with Degenerate Size-Dependent Diffusion. *SIAM Journal on Mathematical Analysis*, 41(6):2315, 2010.

[63] L. Desvillettes, K. Fellner, and J. A. Canizo. Regularity and mass conservation for discrete coagulation-fragmentation equations with diffusion. *Annales de l'Institut Henri Poincare (C) Non Linear Analysis*, 27(2):639–654, 2010.

[64] M. Doi and S. F. Edwards. The Theory of Polymer Dynamics, 1986.

[65] M. Doumic, T. Goudon, and T. Lepoutre. Scaling limit of a discrete prion dynamics model. *Communications in Mathematical Sciences*, 7(4):839–865, Dec. 2009.

[66] M. Doumic and L. M. Tine. Estimating the Division Rate for the Growth-Fragmentation Equation. *Journal of Mathematical Biology*, To appear, 2012.

[67] L. Edelstein-keshet and G. B. Ermentrout. Models for spatial polymerization dynamics of rod-like polymers. *Journal of Mathematical Biology*, 40:64–96, 2000.

[68] H. Engler, J. Prüss, and G. F. Webb. Analysis of a model for the dynamics of prions II. *Journal of Mathematical Analysis and Applications*, 324(1):98–117, Dec. 2006.

[69] W. P. Esler, E. R. Stimson, J. M. Jennings, H. V. Vinters, J. R. Ghilardi, J. P. Lee, P. W. Mantyh, and J. E. Maggio. Alzheimer's Disease Amyloid Propagation by a Template-Dependent Dock-Lock Mechanism †. *Biochemistry*, 39(21):6288–6295, May 2000.

[70] S. N. Ethier and T. G. Kurtz. *Markov Processes: Characterization and Convergence*. Wiley Interscience, 2005.

[71] K. C. Evans, E. P. Berger, C.-G. Cho, K. H. Weisgraber, and P. T. Lansbury. Apolipoprotein E is a kinetic but not a thermodynamic inhibitor of amyloid formation: implications for the pathogenesis and treatment of Alzheimer disease. *Proceedings of the National Academy of Sciences of the United States of America*, 92(3):763–767, Jan. 1995.

[72] J. Falsig, K. P. Nilsson, T. P. J. Knowles, and A. Aguzzi. Chemical and biophysical insights into the propagation of prion strains. *HFSP journal*, 2(6):332–41, Dec. 2008.

[73] M. Fändrich. Absolute correlation between lag time and growth rate in the spontaneous formation of several amyloid-like aggregates and fibrils. *Journal of Molecular Biology*, 365(5):1266–70, Feb. 2007.

[74] F. Ferrone. Analysis of protein aggregation kinetics. *Methods in Enzymology*, 309:256–274, 1999.

[75] F. Filbet. An asymptotically stable scheme for diffusive coagulation-fragmentation models. *Communications in Mathematical Sciences*, 6(2):257–280, June 2008.

[76] N. Fournier and J.-S. Giet. Convergence of the Marcus-Lushnikov process. *Methodology and Computing in Applied Probability*, 6(2):219–231, 2004.

[77] N. Fournier and P. Laurençot. Well-posedness of Smoluchowski's coagulation equation for a class of homogeneous kernels. *Journal of Functional Analysis*, 233(2):351–379, 2006.

[78] N. Fournier and P. Laurençot. Marcus-Lushnikov processes, Smoluchowski's and Flory's models. *Stochastic Processes and their Applications*, 119(1):167–189, 2009.

[79] N. Fournier and S. Méléard. A microscopic probabilistic description of a locally regulated population and macroscopic approximations. *The Annals of Applied Probability*, 14(4):1880–1919, Nov. 2004.

[80] N. Fournier and S. Mischler. Exponential trend to equilibrium for discrete coagulation equations with strong fragmentation and without a balance condition. *Proceedings of the Royal Society A: Mathematical, Physical and Engineering Sciences*, 460(2049):2477–2486, Sept. 2004.

[81] P. Gabriel. *Équations de transport-fragmentation et applications aux maladies à prions*. PhD thesis, Université Pierre et Marie Curie, June 2011.

[82] D. C. Gajdusek. Kuru and Creutzfeldt-Jakob disease. Experimental models of non-inflammatory degenerative slow virus disease of the central nervous system. *Annals of Clinical Research*, 5(5):254–261, 1973.

[83] D. T. Gillespie. Concerning the validity of the Stochastic approach to Chemical Kinetics. *Journal of Statistical Physics*, 16(3):331–318, 1977.

[84] D. A. Gimbel, H. B. Nygaard, E. E. Coffey, E. C. Gunther, J. Laurén, Z. a. Gimbel, and S. M. Strittmatter. Memory impairment in transgenic Alzheimer mice requires cellular prion protein. *The Journal of Neuroscience*, 30(18):6367–74, May 2010.

[85] M. Gobbi, L. Colombo, M. Morbin, G. Mazzoleni, E. Accardo, M. Vanoni, E. Del Favero, L. Cantù, D. A. Kirschner, C. Manzoni, M. Beeg, P. Ceci, P. Ubezio, G. Forloni, F. Tagliavini, and M. Salmona. Gerstmann-Sträussler-Scheinker disease amyloid protein polymerizes according to the "dock-and-lock" model. *The Journal of Biological Chemistry*, 281(2):843–9, Jan. 2006.

[86] C. S. Goldsbury, G. J. Cooper, K. N. Goldie, S. A. Müller, E. L. Saafi, W. T. Gruijters, M. P. Misur, A. Engel, U. Aebi, and J. Kistler. Polymorphic fibrillar assembly of human amylin. *Journal of Structural Biology*, 119(1):17–27, June 1997.

[87] R. F. Goldstein and L. Stryer. Cooperative polymerization reactions. Analytical approximations, numerical examples, and experimental strategy. *Biophysical journal*, 50(4):583–99, Oct. 1986.

[88] W. S. Gosal, I. J. Morten, E. W. Hewitt, D. A. Smith, N. H. Thomson, and S. E. Radford. Competing pathways determine fibril morphology in the self-assembly of beta2-microglobulin into amyloid. *Journal of Molecular Biology*, 351(4):850–64, Aug. 2005.

[89] J. D. Green, C. Goldsbury, J. Kistler, G. J. S. Cooper, and U. Aebi. Human amylin oligomer growth and fibril elongation define two distinct phases in amyloid formation. *The Journal of Biological Chemistry*, 279(13):12206–12, Mar. 2004.

[90] M. L. Greer, L. Pujo-Menjouet, and G. F. Webb. A mathematical analysis of the dynamics of prion proliferation. *Journal of Theoretical Biology*, 242(3):598–606, Oct. 2006.

[91] M. L. Greer, P. van den Driessche, L. Wang, and G. F. Webb. Effects of General Incidence and Polymer Joining on Nucleated Polymerization in a Model of Prion Proliferation. *SIAM Journal on Applied Mathematics*, 68(1):154, 2007.

[92] J. S. Griffith. Nature of the Scrapie Agent: Self-replication and Scrapie. *Nature*, 215(5105):1043–1044, Sept. 1967.

[93] A. Gupta, J. A. J. Metz, and V. C. Tran. A new proof for the convergence of an individual based model to the Trait substitution sequence. *preprint*, 2012.

[94] A. Hammond and F. Rezakhanlou. Kinetic Limit for a System of Coagulating Planar Brownian Particles. *Journal of Statistical Physics*, pages 1–45, 2006.

[95] A. Hammond and F. Rezakhanlou. The Kinetic Limit of a System of Coagulating Brownian Particles. *Archive for Rational Mechanics and Analysis*, 185(1):1–67, 2007.

[96] J. Hardy and D. J. Selkoe. The amyloid hypothesis of Alzheimer's disease: progress and problems on the road to therapeutics. *Science*, 297(5580):353–6, July 2002.

[97] J. D. Harper and P. T. Lansbury. Models of amyloid seeding in Alzheimer's disease and scrapie: mechanistic truths and physiological consequences of the time-dependent solubility of amyloid proteins. *Annual Review of Biochemistry*, 66:385–407, Jan. 1997.

[98] R. Z. Has'minskii. On Stochastic Processes Defined by Differential Equations with a Small Parameter. *Theory of Probability and its Applications*, 11(2):211, 1966.

[99] E. M. Hendriks, M. H. Ernst, and R. M. Ziff. Coagulation equations with gelation. *Journal of Statistical Physics*, 31(3):519–563, June 1983.

[100] E. M. Hendriks, J. L. Spouge, M. Eibl, and M. Schreckenberg. Exact Solutions for Random Coagulation Processe. *Z. Phys. B*, V:219–227, 1985.

[101] J. Hofrichter, P. D. Ross, and W. A. Eaton. Kinetics and Mechanism of Deoxyhemoglobin S Gelation: A New Approach to Understanding Sickle Cell Disease. *Proceedings of the National Academy of Sciences of the United States of America*, 71(12):4864–68, Dec. 1974.

[102] D.-P. Hong and A. L. Fink. Independent heterologous fibrillation of insulin and its B-chain peptide. *Biochemistry*, 44(50):16701–9, Dec. 2005.

[103] P. Hortschansky, V. Schroeckh, T. Christopeit, G. Zandomeneghi, and M. Fändrich. The aggregation kinetics of Alzheimer's beta-amyloid peptide is controlled by stochastic nucleation. *Protein Science*, 14(7):1753–9, July 2005.

[104] R. Huilgol and N. Phan-Thien. *Fluid mechanics of viscoelasticity: general principles, constitutive modelling, analytical and numerical techniques*. Elsevier, Amsterdam, 1997.

[105] P.-E. Jabin and B. Niethammer. On the rate of convergence to equilibrium in the Becker–Döring equations. *Journal of Differential Equations*, 191(2):518–543, July 2003.

[106] J. Jacod and A. N. Shiryaev. *Limit theorems for stochastic processes*. Springer, 1987.

[107] J. Janin. The Kinetics of Protein-Protein Recognition. *Proteins*, 161:153–161, 1997.

[108] J. T. Jarrett and P. T. Lansbury. Seeding "one-dimensional crystallization" of amyloid: A pathogenic mechanism in Alzheimer's disease and scrapie? *Cell*, 73(6):1055–1058, June 1993.

[109] I. Jeon. Existence of Gelling Solutions for Coagulation- Fragmentation Equations. *Communications in Mathematical Physics*, 567:541–567, 1998.

[110] J. L. Jiménez, G. Tennent, M. Pepys, and H. R. Saibil. Structural diversity of ex vivo amyloid fibrils studied by cryo-electron microscopy. *Journal of Molecular Biology*, 311(2):241–7, Aug. 2001.

[111] A. Joffe and M. Metivier. Weak convergence of sequences of semimartingales with applications to multitype branching processes. *Advances in Applied Probability*, 18(1):20–65, 1986.

[112] B. Jourdain, T. Lelièvre, and C. Le Bris. Existence of solution for a micro–macro model of polymeric fluid: the FENE model. *Journal of Functional Analysis*, 209(1):162–193, Apr. 2004.

[113] J. W. Kelly. The alternative conformations of amyloidogenic proteins and their multi-step assembly pathways. *Current Opinion in Structural Biology*, 8(1):101–6, Feb. 1998.

[114] R. H. Kimberlin. Scrapie Agent: Prions or Virinos. *Nature*, 297(5862):107–108, 1982.

[115] M. Kimmel and O. Arino. Comparison of approaches to modeling of cell population dynamics. *SIAM Journal on Applied Mathematics*, 53(5):1480–1504, 1993.

[116] J. G. Kirkwood. *Macromolecules*. Gordon and Breach, New York, 1967.

[117] C. Klingenberg, K. Oeslchlager, and S. Grosskinskya. A Rigorous Derivation of Smoluchowski's Equation in the Moderate Limit. *Stoch. An. Appl.*, 22:1–19, 2006.

[118] T. P. J. Knowles, C. A. Waudby, G. L. Devlin, S. I. A. Cohen, A. Aguzzi, M. Vendruscolo, E. M. Terentjev, M. E. Welland, and C. M. Dobson. An analytical solution to the kinetics of breakable filament assembly. *Science*, 326(5959):1533–7, Dec. 2009.

[119] A. N. Kolmogorov and S. V. Fomin. *Introductory real analysis*. Dover Publications Inc., New York, 1975.

[120] P. M. Kotelenez and T. G. Kurtz. Macroscopic limits for stochastic partial differential equations of McKean–Vlasov type. *Probability Theory and Related Fields*, 146(1-2):189–222, 2008.

[121] T. G. Kurtz. Solutions of Ordinary Differential Equations as Limits of Pure Jump Markov Processes. *Journal of applied Probability*, 7(1):49–58, 1970.

[122] T. G. Kurtz. *Approximation of population processes*. CBMS-NSF Regional Conference Series in Applied Mathematics, SIAM., 1991.

[123] R. Lang and N. X. Xanh. Smoluchowski's Theory of Coagulation in Colloids Holds Rigorously in the Boltzmann-Grad-Limit. *Z. Wahrscheinlichkeitstheorie verw. Gebiete*, 54:227–280, 1980.

[124] P. Langevin. On the Theory of Brownian Motion. *C. R. Acad. Sci.*, 146:530–533, 1908.

[125] P. T. Lansbury and B. Caughey. The chemistry of scrapie infection: implications of the 'ice 9' metaphor. *Chemistry & Biology*, 2(1):1–5, Jan. 1995.

[126] J. Laurén, D. A. Gimbel, H. B. Nygaard, J. W. Gilbert, and S. M. Strittmatter. Cellular prion protein mediates impairment of synaptic plasticity by amyloid-beta oligomers. *Nature*, 457(7233):1128–32, Feb. 2009.

[127] P. Laurençot. On a Class of Continuous Coagulation-Fragmentation Equations. *Journal of Differential Equations*, 167(2):245–274, Nov. 2000.

[128] P. Laurençot. The lifshitz slyozov equation with encounters. *Mathematical Models and Methods in Applied Sciences*, 11(4):731–748, 2001.

[129] P. Laurençot. The discrete coagulation equations with multiple fragmentation. *Proceedings of the Edinburgh Mathematical Society. Series II*, 45(1):67–82, Feb. 2002.

[130] P. Laurençot. The Lifshitz–Slyozov–Wagner equation with conserved total volume. *SIAM Journal on Mathematical Analysis*, 34(2):257–272, 2002.

[131] P. Laurençot and S. Mischler. From the Becker–Döring to the Lifshitz–Slyozov–Wagner Equations. *Journal of Statistical Physics*, 106(5-6):957–991, 2002.

[132] P. Laurençot and C. Walker. Well-posedness for a model of prion proliferation dynamics. *Journal of Evolution Equations*, 7(2):241–264, Oct. 2007.

[133] P. Laurencot. Weak solutions to the Lifshitz-Slyozov-Wagner equation. *Indiana University Mathematics Journal*, 50(3), 2001.

[134] P. Laurencot and D. Wrzosek. The Becker Doring Model with Diffusion II. Long Time Behavior. *Journal of differential equations*, 148:268–291, 1998.

[135] C.-C. Lee, A. Nayak, A. Sethuraman, G. Belfort, and G. J. McRae. A three-stage kinetic model of amyloid fibrillation. *Biophysical Journal*, 92(10):3448–58, May 2007.

[136] C.-C. Lee, Y. Sun, and H. W. Huang. Membrane-mediated peptide conformation change from alpha-monomers to beta-aggregates. *Biophysical Journal*, 98(10):2236–45, May 2010.

[137] G. Legname, I. V. Baskakov, H.-O. B. Nguyen, D. Riesner, F. E. Cohen, S. J. DeArmond, and S. B. Prusiner. Synthetic mammalian prions. *Science*, 305(5684):673–6, July 2004.

[138] T. Lelievre. *Modèles multi-échelles pour les fluides viscoélastiques*. PhD thesis, Ecole Nationale des Ponts et Chaussées, June 2004.

[139] N. Lenuzza. *Modélisation de la réplications des Prions : Implication de la dépendance en taille des agrégats de PrP et de l'hétérogénéité des populations cellulaires*. Thèse de doctorat, Ecole Centrale Paris, Oct. 2009.

[140] D. Lépingle. Euler scheme for reflected stochastic differential equations. *Mathematics and Computers in Simulation*, 38(1-3):119–126, 1995.

[141] J.-P. Liautard. Are prions misfolded molecular chaperones? *FEBS Letters*, 294(3):155–157, Dec. 1991.

[142] I. Lifshitz and V. Slyozov. The kinetics of precipitation from supersaturated solid solutions. *Journal of Physics and Chemistry of Solids*, 19(1-2):35–50, Apr. 1961.

[143] A. Lomakin. On the nucleation and growth of amyloid beta -protein fibrils: Detection of nuclei and quantitation of rate constants. *Proceedings of the National Academy of Sciences*, 93(3):1125–1129, Feb. 1996.

[144] A. Lomakin. Kinetic theory of fibrillogenesis of amyloid beta -protein. *Proceedings of the National Academy of Sciences*, 94(15):7942–7947, July 1997.

[145] A. Lomakin, D. S. Chung, G. B. Benedek, D. A. Kirschner, and D. B. Teplow. On the nucleation and growth of amyloid beta-protein fibrils: detection of nuclei and quantitation of rate constants. *Proceedings of the National Academy of Sciences of the United States of America*, 93(3):1125–9, Feb. 1996.

[146] E. Luçon. Quenched limits and fluctuations of the empirical measure for plane rotators in random media. *Electronic Journal of Probability*, 16:792–829, 2011.

[147] E. Luçon. Large time asymptotics for the fluctuation SPDE in the kuramoto synchronization model. *preprint*, pages 1–39, 2012.

[148] T. Lührs, R. Zahn, and K. Wüthrich. Amyloid formation by recombinant full-length prion proteins in phospholipid bicelle solutions. *Journal of Molecular Biology*, 357(3):833–41, Mar. 2006.

[149] A. A. Lushnikov. Coagulation in Finite Systems. *Journal of Colloid and Interface Science*, 65(2):—-, 1978.

[150] A. H. Marcus. Stochastic Coalescence. *Technometrics*, 10(1):133–143, 1968.

[151] J. Masel, N. Genoud, and A. Aguzzi. Efficient inhibition of prion replication by PrP-Fc(2) suggests that the prion is a PrP(Sc) oligomer. *Journal of Molecular Biology*, 345(5):1243–51, Feb. 2005.

[152] J. Masel and V. A. Jansen. The measured level of prion infectivity varies in a predictable way according to the aggregation state of the infectious agent. *Biochimica et Biophysica Acta (BBA) - Molecular Basis of Disease*, 1535(2):164–173, Feb. 2001.

[153] J. Masel, V. A. Jansen, and M. A. Nowak. Quantifying the kinetic parameters of prion replication. *Biophysical Chemistry*, 77(2-3):139–152, Mar. 1999.

[154] J. A. McCammon. Protein dynamics. *Reports on Progress in Physics*, 47(1):1–46, Jan. 1984.

[155] D. A. McQuarrie. Stochastic Approach to Chemical Kinetics. *Journal of Applied Probability*, 4(3):413–478, 1967.

[156] J. Meinhardt, C. Sachse, P. Hortschansky, N. Grigorieff, and M. Fändrich. Abeta(1-40) fibril polymorphism implies diverse interaction patterns in amyloid fibrils. *Journal of Molecular Biology*, 386(3):869–77, Feb. 2009.

[157] S. Méléard and S. Roelly. A host-parasite multilevel interacting process and continuous approximations. *Preprint*, pages 1–31, Jan. 2011.

[158] Metz J A J and V. C. Tran. Daphnias: from the individual based model to the large population equation. *preprint*, 2012.

[159] S. Mischler, C. Mouhot, and B. Wennberg. A new approach to quantitative chaos propagation estimates for drift, diffusion and jump processes. *preprint*, pages 1–45, 2011.

[160] M. Morillas, W. Swietnicki, P. Gambetti, and W. K. Surewicz. Membrane Environment Alters the Conformational Structure of the Recombinant Human Prion Protein. *Journal of Biological Chemistry*, 274(52):36859–65, Dec. 1999.

[161] A. M. Morris, M. A. Watzky, and R. G. Finke. Protein aggregation kinetics, mechanism, and curve-fitting: a review of the literature. *Biochimica et Biophysica Acta (BBA) - Proteins & Proteomics*, 1794(3):375–97, Mar. 2009.

[162] J. J. Neu, J. A. Cañizo, and L. L. Bonilla. Three eras of micellization. *Physical Review E*, 66(6), Dec. 2002.

[163] J. R. Norris. Smoluchowski's coagulation equation: uniqueness, nonuniqueness, and a hydrodynamic limit for stochastic coalescent. *The Annals of Applied Probability*, 9(1):78–109, 1999.

[164] J. R. Norris. Brownian coagulation. *Communications in Mathematical Sciences*, Suppl. iss(1):93–101, 2004.

[165] H. B. Nygaard and S. M. Strittmatter. Cellular Prion Protein Mediates the Toxicity of -Amyloid Oligomers: Implications for Alzheimer Disease. *Archives of Neurology*, 66(11):1325–1328, Nov. 2009.

[166] E. P. O'Brien, Y. Okamoto, J. E. Straub, B. R. Brooks, and D. Thirumalai. Thermodynamic perspective on the dock-lock growth mechanism of amyloid fibrils. *The Journal of Physical Chemistry B*, 113(43):14421–30, Oct. 2009.

[167] K. Oelschlager. A Martingale Approach to the Law of Large Numbers for Weakly Interacting Stochastic processes. *The Annals of Applied Probability*, 12(2):458–479, 1984.

[168] F. Oosawa and M. Kasai. A theory of linear and helical aggregations of macromolecules. *Journal of molecular biology*, 4:10–21, Jan. 1962.

[169] F. Otto and A. E. Tzavaras. Continuity of Velocity Gradients in Suspensions of Rod–like Molecules. *Communications in Mathematical Physics*, 277(3):729–758, Nov. 2008.

[170] S. B. Padrick and A. D. Miranker. Islet Amyloid: Phase Partitioning and Secondary Nucleation Are Central to the Mechanism of Fibrillogenesis †. *Biochemistry*, 41(14):4694–4703, Apr. 2002.

[171] J. S. Pedersen and D. E. Otzen. Amyloid-a state in many guises: survival of the fittest fibril fold. *Protein Science*, 17(1):2–10, Jan. 2008.

[172] J. S. n. Pedersen, D. Dikov, J. L. Flink, H. A. Hjuler, G. Christiansen, and D. E. Otzen. The changing face of glucagon fibrillation: structural polymorphism and conformational imprinting. *Journal of Molecular Biology*, 355(3):501–23, Jan. 2006.

[173] D. Peretz, R. Williamson, G. Legname, Y. Matsunaga, J. Vergara, D. R. Burton, S. J. DeArmond, S. B. Prusiner, and M. R. Scott. A Change in the Conformation of Prions Accompanies the Emergence of a New Prion Strain. *Neuron*, 34(6):921–932, June 2002.

[174] T. T. Perkins, D. E. Smith, and S. Chu. Single Polymer Dynamics in an Elongational Flow. *Science*, 276(5321):2016–2021, June 1997.

[175] B. Perthame. *Transport equations in biology*. Birkhäuser, 2007.

[176] A. T. Petkova, R. D. Leapman, Z. Guo, W.-M. Yau, M. P. Mattson, and R. Tycko. Self-propagating, molecular-level polymorphism in Alzheimer's beta-amyloid fibrils. *Science*, 307(5707):262–5, Jan. 2005.

[177] G. W. Platt, K. E. Routledge, S. W. Homans, and S. E. Radford. Fibril growth kinetics reveal a region of beta2-microglobulin important for nucleation and elongation of aggregation. *Journal of Molecular Biology*, 378(1):251–63, Apr. 2008.

[178] S. Portet and J. Arino. An in vivo intermediate filament assembly model. *Mathematical Biosciences and Engineering*, 6(1):117–134, Jan. 2009.

[179] E. T. Powers and D. L. Powers. The kinetics of nucleated polymerizations at high concentrations: amyloid fibril formation near and above the "supercritical concentration". *Biophysical journal*, 91(1):122–32, July 2006.

[180] E. T. Powers and D. L. Powers. Mechanisms of protein fibril formation: nucleated polymerization with competing off-pathway aggregation. *Biophysical Journal*, 94(2):379–91, Jan. 2008.

[181] Y. V. Prokhorov. Convergence of random processes and limit theorems in probability theory. *theory of Probability and its application*, I(2), 1956.

[182] S. B. Prusiner. Novel proteinaceous infectious particles cause scrapie. *Science*, 216(4542):136–44, Apr. 1982.

[183] S. B. Prusiner. Prions. *Proceedings of the National Academy of Sciences of the United States of America*, 95(23):13363–83, Nov. 1998.

[184] J. Prüss, L. Pujo-Menjouet, G. F. Webb, and R. Zacher. Analysis of a model for the dynamics of prions. *Discrete and Continuous Dynamical Systems - Series B*, 6(1):225–235, Jan. 2006.

[185] C. Reichert. Laws of large numbers for mesoscopic stochastic models of reacting and diffusing particles. *preprint*, 2012.

[186] E. Rhoades, J. Agarwal, and A. Gafni. Aggregation of an amyloidogenic fragment of human islet amyloid polypeptide. *Biochimica et Biophysica Acta (BBA) - Protein Structure and Molecular Enzymology*, 1476(2):230–238, Feb. 2000.

[187] H. Risken. *The Fokker-Planck Equation: Methods of Solutions and Applications*. Springer Verlag, 1996.

[188] C. Ritter, M.-L. Maddelein, A. B. Siemer, T. Lührs, M. Ernst, B. H. Meier, S. J. Saupe, and R. Riek. Correlation of structural elements and infectivity of the HET-s prion. *Nature*, 435(7043):844–8, June 2005.

[189] D. Robert and B. Vian. *Eléments de biologie cellulaire*. Doin Editions, 2004.

[190] S. Roelly and A. Rouault. Construction et propriétés de martingales des branchements spatiaux interactifs. *International statistical review*, 58(2):173–189, 1990.

[191] R. Sabaté, U. Baxa, L. Benkemoun, N. Sánchez de Groot, B. Coulary-Salin, M.-L. Maddelein, L. Malato, S. Ventura, A. C. Steven, and S. J. Saupe. Prion and non-prion amyloids of the HET-s prion forming domain. *Journal of Molecular Biology*, 370(4):768–83, July 2007.

[192] R. Sabaté and J. Estelrich. Evidence of the existence of micelles in the fibrillogenesis of beta-amyloid peptide. *The Journal of Physical Chemistry B*, 109(21):11027–32, June 2005.

[193] N. Sanghera and T. J. T. Pinheiro. Binding of prion protein to lipid membranes and implications for prion conversion. *Journal of Molecular Biology*, 315(5):1241–56, Feb. 2002.

[194] T. Scheibel, A. S. Kowal, J. D. Bloom, and S. L. Lindquist. Bidirectional amyloid fiber growth for a yeast prion determinant. *Current Biology*, 11(5):366–369, Mar. 2001.

[195] D. J. Selkoe. Soluble oligomers of the amyloid beta-protein impair synaptic plasticity and behavior. *Behavioural brain research*, 192(1):106–13, Sept. 2008.

[196] T. R. Serio, A. G. Cashikar, A. S. Kowal, G. J. Sawicki, J. J. Moslehi, L. Serpell, M. F. Arnsdorf, and S. L. Lindquist. Nucleated Conformational Conversion and the Replication of Conformational Information by a Prion Determinant. *Science*, 289(5483):1317–1321, Aug. 2000.

[197] G. Simonett and C. Walker. On the solvability of a mathematical model for prion proliferation. *Journal of Mathematical Analysis and Applications*, 324(1):580–603, Dec. 2006.

[198] M. Slemrod. Trend to equilibrium in the Becker-Doring cluster equations. *Nonlinearity*, 2(3):429–443, Aug. 1989.

[199] D. E. Smith, H. P. Babcock, and S. Chu. Single-Polymer Dynamics in Steady Shear Flow. *Science*, 283(5408):1724–1727, Mar. 1999.

[200] C. Soto, L. Estrada, and J. Castilla. Amyloids, prions and the inherent infectious nature of misfolded protein aggregates. *Trends in Biochemical Sciences*, 31(3):150–5, Mar. 2006.

[201] P. O. Souillac, V. N. Uversky, and A. L. Fink. Structural transformations of oligomeric intermediates in the fibrillation of the immunoglobulin light chain LEN. *Biochemistry*, 42(26):8094–104, July 2003.

[202] I. W. Stewart and E. Meister. A global existence theorem for the general coagulation-fragmentation equation with unbounded kernels. *Mathematical Methods in the Applied Sciences*, 11(5):627–648, Sept. 1989.

[203] D. W. Stroock and S. R. S. Varadhan. Diffusion processes with boundary conditions. *Communications on Pure and Applied Mathematics*, 24(2):147–225, 1971.

[204] A.-S. Sznitman. Topics in Propagation of Chaos. 1987.

[205] M. Tanaka, S. R. Collins, B. H. Toyama, and J. S. Weissman. The physical basis of how prion conformations determine strain phenotypes. *Nature*, 442(7102):585–9, Aug. 2006.

[206] G. C. Telling, P. Parchi, S. J. DeArmond, P. Cortelli, P. Montagna, R. Gabizon, J. Mastrianni, E. Lugaresi, P. Gambetti, and S. B. Prusiner. Evidence for the Conformation of the Pathologic Isoform of the Prion Protein Enciphering and Propagating Prion Diversity. *Science*, 274(5295):2079–2082, Dec. 1996.

[207] P. R. ten Wolde and D. Frenkel. Homogeneous nucleation and the Ostwald step rule. *Physical Chemistry Chemical Physics*, 1(9):2191–2196, 1999.

[208] V. C. Tran. Modèles particulaires stochastiques pour des problèmes d'évolution adaptative et pour l'approximation de solutions statistiques. Technical report, 2006.

[209] H.-H. G. Tsai, J.-B. Lee, S.-S. Tseng, X.-A. Pan, and Y.-C. Shih. Folding and membrane insertion of amyloid-beta (25-35) peptide and its mutants: Implications for aggregation and neurotoxicity. *Proteins: Structure, Function, and Bioinformatics*, 78(8):1909–25, 2010.

[210] B. Urbanc, L. Cruz, S. V. Buldyrev, S. Havlin, M. C. Irizarry, H. E. Stanley, and B. T. Hyman. Dynamics of plaque formation in Alzheimer's disease. *Biophysical journal*, 76(3):1330–4, Mar. 1999.

[211] W. Wagner. Explosion phenomena in stochastic coagulation-fragmentation models. *The Annals of Applied Probability*, 15(3):2081–2112, 2005.

[212] W. Wagner. Random and deterministic fragmentation models. *Monte Carlo Methods and Applications*, 16(3-4):399–420, 2010.

[213] C. Walker. Prion proliferation with unbounded polymerization rates. In *Sixth Mississippi State Conference on Differential Equations and Computational Simulations - Electronic Journal of Differential Equations, Conference 15*, pages 387–397, 2007.

[214] J. Wall and A. Solomon. Flow cytometric characterization of amyloid fibrils. *Methods in Enzymology*, 309:460–466, 1999.

[215] D. M. Walsh. Amyloid-beta Protein Fibrillogenesis. Detection of a protofibrillar intermediate. *Journal of Biological Chemistry*, 272(35):22364–22372, Aug. 1997.

[216] F. Wang, X. Wang, and J. Ma. Conversion of bacterially expressed recombinant prion protein. *Methods*, 53(3):208–13, Mar. 2011.

[217] F. Wang, X. Wang, C.-G. Yuan, and J. Ma. Generating a prion with bacterially expressed recombinant prion protein. *Science*, 327(5969):1132–5, Feb. 2010.

[218] F. Wang, F. Yang, Y. Hu, X. Wang, X. Wang, C. Jin, and J. Ma. Lipid interaction converts prion protein to a PrPSc-like proteinase K-resistant conformation under physiological conditions. *Biochemistry*, 46(23):7045–53, June 2007.

[219] F. Wang, S. Yin, X. Wang, L. Zha, M.-S. Sy, and J. Ma. Role of the highly conserved middle region of prion protein (PrP) in PrP-lipid interaction. *Biochemistry*, 49(37):8169–76, Sept. 2010.

[220] J. A. D. Wattis. An introduction to mathematical models of coagulation-fragmentation processes: a discrete deterministic mean-field approach. *Physica D: Nonlinear Phenomena*, 222(1-2):1–20, 2006.

[221] R. Wetzel. Kinetics and thermodynamics of amyloid fibril assembly. *Accounts of Chemical Research*, 39(9):671–9, Sept. 2006.

[222] H. Wille, W. Bian, M. McDonald, A. Kendall, D. W. Colby, L. Bloch, J. Ollesch, A. L. Borovinskiy, F. E. Cohen, S. B. Prusiner, and G. Stubbs. Natural and synthetic prion structure from X-ray fiber diffraction. *Proceedings of the National Academy of Sciences of the United States of America*, 106(40):16990–5, Oct. 2009.

[223] J. J. W. Wiltzius, M. Landau, R. Nelson, M. R. Sawaya, M. I. Apostol, L. Goldschmidt, A. B. Soriaga, D. Cascio, K. Rajashankar, and D. Eisenberg. Molecular mechanisms for protein-encoded inheritance. *Nature Structural & Molecular Biology*, 16(9):973–8, Sept. 2009.

[224] A. Wimo and M. Prince. World Alzheimer Report 2010: The global economic impact of dementia. Technical report, Alzheimer's Disease International, 2010.

[225] D. Wrzosek. Existence of solutions for the discrete coagulation-fragmentation model with diffusion. *Topological Methods in Nonlinear analysis*, 9(558):279–296, 1997.

[226] D. Wrzosek. Mass-conserving solutions to the discrete coagulation–fragmentation model with diffusion. *Nonlinear Analysis: Theory, Methods & Applications*, 49(3):297–314, Apr. 2002.

[227] M. R. Yaghouti, C. S. Faculty, F. Rezakhanlou, and A. Hammond. Coagulation, Diffusion and the Continuous Smoluchowski Equation. *Stochastic Processes and their Applications*, 119(9):3042–80, 2009.

[228] L. Zhu, X.-J. Zhang, L.-Y. Wang, J.-M. Zhou, and S. Perrett. Relationship Between Stability of Folding Intermediates and Amyloid Formation for the Yeast Prion Ure2p: A Quantitative Analysis of the Effects of pH and Buffer System. *Journal of Molecular Biology*, 328(1):235–254, Apr. 2003.

[229] V. Zomosa-Signoret, J.-D. Arnaud, P. Fontes, M.-T. Alvarez-Martinez, and J.-P. Liautard. Physiological role of the cellular prion protein. *Veterinary Research*, 39(4):09, Nov. 2007.